



GRIGORE T. POPA UNIVERSITY OF
MEDICINE AND PHARMACY IASI

**Molecular mechanisms of human diseases
in the framework of autophagy and
immunobiology**

Habilitation Thesis

MARIANA PAVEL-TANASĂ, MD, PhD

Senior Lecturer

2023

Contents

SUMMARY	1
REZUMAT	3
SECTION I. OVERVIEW OF ACADEMIC CAREER: TEACHING, MEDICAL AND RESEARCH ACTIVITIES.....	5
Chapter 1: The molecular mechanisms of autophagy in health and disease.....	10
1.1. State of art.....	10
1.2. Autophagy-cancer interlink.....	14
1.2.1. Alpha catenins: the interlink between autophagy and cancer cell proliferation and survival	15
1.2.1.1. Introduction.....	15
1.2.1.2. Aim	15
1.2.1.3. Materials and methods	15
1.2.1.4. Results.....	20
1.2.1.5. Discussions	37
1.2.2. Dynamic mathematical models explain the autophagy-YAP1 signalling crosstalk: the balance between multiple forward and feedback paths dictates the cell fate.....	38
1.2.2.1. Introduction.....	38
1.2.2.2. Aim	40
1.2.2.3. Methods	40
1.2.2.4. Results.....	42
1.2.2.5. Discussions	55
1.2.3. Crosstalk between autophagy and other intracellular transduction pathways perturbed in cancers: forward and feedback paths.....	56
1.2.3.1. Introduction.....	56
1.2.3.2. Aim	58
1.2.3.3. Results.....	58
1.2.3.4. Concluding remarks and open questions	63
1.3. Autophagy and neurodegeneration interlink.....	64
1.3.1. Polyglutamine tracts regulate beclin 1-dependent autophagy in neurodegenerative diseases.....	65
1.3.1.1. Introduction.....	65
1.3.1.2. Aim	65
1.3.1.3. Materials and methods	66
1.3.1.4. Results.....	68
1.3.1.5. Discussions	74
1.4. Autophagy and ageing	76
1.4.1. Therapeutic potential of autophagy in ageing	77
1.4.2. The role of vinexin-YAP/TAZ axis in promoting the autophagic brain decline.....	78
1.4.2.1. Introduction.....	78
1.4.2.2. Aim	78
1.4.2.3. Materials and methods	78
1.4.2.4. Results.....	81
1.4.2.5. Discussions	92
Chapter 2: The molecular mechanisms of immune system regulation in health and disease.....	95
2.1. The landscape of immune cells in haematological malignancies.....	95

2.1.1. State of art.....	95
2.1.2. Characterisation of MHC-II antigen presentation machinery and immune checkpoint ligands profile in AML	97
2.1.2.1. Introduction.....	97
2.1.2.2. Aim	97
2.1.2.3. Materials and methods	98
2.1.2.4. Results.....	98
2.1.2.5. Discussions	104
2.1.3. Immune checkpoint receptor expression and T cell maturation profile in AML.....	106
2.1.3.1. Introduction.....	106
2.1.3.2. Aim	106
2.1.3.3. Materials and methods	107
2.1.3.4. Results.....	107
2.1.3.5. Discussions	112
2.1.4. NK cell maturation profile in MDS and AML.....	114
2.1.4.1. Introduction.....	114
2.1.4.2. Aim	115
2.1.4.3. Materials and methods	115
2.1.4.4. Results.....	118
2.1.4.5. Discussions	124
2.2. Biological consequences of targeted immune therapy in solid tumours.....	126
2.2.1. State of art.....	126
2.2.2. Off-target effects of monoclonal antibodies-based therapy in metastatic colorectal cancer	127
2.2.2.1. Introduction.....	127
2.2.2.2. Aim	128
2.2.2.3. Materials and methods	128
2.2.2.4. Results.....	129
2.2.2.5. Discussions	135
2.3. The role of humoral immunity in COVID-19 and other inflammatory diseases.....	137
2.3.1. State of art.....	137
2.3.2. The role of adipokines and vitamin D in mediating the age-related antibody immune responses following dual anti-SARS-coV-2 vaccination.....	139
2.3.2.1. Introduction.....	139
2.3.2.2. Aim	139
2.3.2.3. Materials and methods	140
2.3.2.4. Results.....	141
2.3.2.5. Discussions	154
SECTION II. FUTURE DIRECTIONS IN TEACHING, MEDICAL AND SCIENTIFIC ACTIVITIES	157
Perspectives in the teaching and medical activities.....	157
Perspectives in the scientific activities.....	158
Final remarks	162
SECTION III. REFERENCES	163

ABBREVIATION LIST:

AMPK: AMP-dependent protein kinase

ATG: autophagy gene

BM: bone marrow

CALCOCO2: Calcium Binding And Coiled-Coil Domain 2

CBC: complete blood count

CI: confidence interval

CM: central memory

CRC: colorectal cancer

CRP: c-reactive protein

CTLA-4: Cytotoxic T lymphocyte Antigen 4

ECD: evolutionary conserved domain

ECM: extracellular matrix

ELN: European Leukemia Net

EM: effector memory

ERGIC: ER-Golgi intermediate compartment

FOXO3: forkhead box O3

HTT: huntingtin

ICOS: Inducible T cell Co-Stimulator

IF: immunofluorescence

LIR: LC3-interacting protein

MCP-1: monocyte chemoattractant protein-1

MHC: major histocompatibility complex

MITF: microphthalmia-associated transcription factor

mTORC1: mammalian target of rapamycin complex 1

N: naïve

NBR1: Neighbor of BRCA1 gene 1

NK: natural killer cell

OPTN: optineurin

OS: overall survival

PAI-1: plasminogen activator inhibitor 1
PBS: phosphate buffered saline
PD-1: Programmed-Death 1
PD-L1: Programmed-Death Ligand 1
PFA: paraformaldehyde
PFS: progression-free survival
pMECs: primary mammary epithelial cells
pMEFs: primary mouse embryonic fibroblasts
PVDF: polyvinylidene fluoride
qRT-PCR: quantitative reverse transcriptase PCR
RBD: region binding domain
RR: response rate
SCA3: spinocerebellar ataxia type 3
SD: standard deviation
SEM: standard error of the mean
SILAC: Stable isotope labelling by amino acids in cell culture
SQSTM1: Sequestosome 1
TAX1BP1: Tax1-binding protein 1
TFEB: transcription factor EB
TOLLIP: Toll-interacting protein
UBD: ubiquitin-binding domain
ULK1/2: unc-51 like autophagy activating kinase 1
VAMP: vesicle associated membrane protein
VCP: vasolin-containing protein
VEGF: Vascular Endothelial Growth Factor
WB: western blot
WIPI2: WD Repeat Domain, Phosphoinositide Interacting 2
WWTR1/ TAZ: WW Domain Containing Transcription Regulator 1
YAP1: Yes1 Associated Transcriptional Regulator
ZKSCAN3: zinc-finger protein with KRAB and SCAN domains 3

SUMMARY

The present habilitation thesis summarises the most significant professional, academic and most importantly, the scientific achievements from my post-doctoral period (2016-2023) and outlines some of the research directions that I intend to pursue further.

The thesis is structured based on the guidelines recommended and approved by the National Council for Attestation of Titles, Diplomas and Certificates (CNATDCU) in 3 main sections with corresponding subsections as follows:

- **Section I** – describes the most relevant professional, academic and scientific achievements during the post-doctoral period.
- **Section II** – outlines the perspectives for future academic and research directions.
- **Section III** – indicates the list of bibliographic references cited in this thesis.

Section I. In this section, I included the most significant scientific results of my personal contributions and structured them in two main chapters, each with three subchapters.

Chapter I focuses on one of the most remarkable part of my postdoctoral scientific contribution, in the field of autophagy. Part of the results included here were performed in collaboration with scientists from the University of Cambridge and are a follow-up of the research study conducted for my PhD thesis, entitled *Actin cytoskeleton modulators reveal novel roles for autophagy in health and disease* and completed in March 2016.

Subchapter 1 details the molecular mechanisms of autophagy we identified to be linked to cancer. More precisely, the presented studies outline the role of autophagy in regulating the activity of YAP/TAZ co-transcriptional factors, often mutated and overexpressed in a variety of cancers and point out the dynamics of autophagy process in controlling cell proliferation and survival in different cancer cell lines and at distinct time-points. Here we managed to generate a dynamic mathematical model based on differential equations that reveals the strength of various feedback and forward loops characterising the complex autophagy-YAP/TAZ axis. Nevertheless, other intracellular signalling pathways that monitor cell proliferation and survival may be dissected *via* similar applied mathematical models.

Subchapter 2 details the molecular mechanisms of autophagy we identified to be linked to neurodegeneration. The included **Nature** study describe the role of ataxin 3 in interacting with Beclin-1 (a key component of autophagy machinery) *via* its polyQ domain, and thus, promoting deubiquitination of Beclin-1 and preventing its degradation by proteasome. As a result, reduced ataxin-3 activity or ataxin3/Beclin-1 interaction causes intracellular depletion of Beclin-1 which directly impairs autophagy. N-terminal fragments of HTT containing expanded polyQ domains are found in the brains of Huntington disease patients and cause toxicity in cells and in Huntington disease mouse models. Here we found that, full-length mutant HTT binds Beclin-1 and competes for Beclin-1 binding with ataxin3, and consequently, fibroblasts from Huntington disease patients have impaired autophagy.

Subchapter 3 details the molecular mechanisms of autophagy we identified to be linked to ageing. The results presented here were a follow-up of the data achieved in subchapter 1. Shortly, we identified that increased *SORBS3* expression, via inhibiting YAP/TAZ activity, is an important contributor to autophagic decline in mammalian brain ageing.

My personal contributions to this research were published in prestigious ISI journals: *Nature* (IF 41.577), *Nature Communications* (IF 17.694), *Neuron* (IF 14.319), *Cell Death and Differentiation* (IF 12.073), *Autophagy* (IF 13.391), *Journal of Molecular Biology* (IF 5.469), *Bioessays* (IF 4.653), *FEBS Journal* (IF 4.530).

Chapter II focuses on detailing the postdoctoral research performed within the Laboratory of Immunology and together with collaborators from the Department of Haematology, Oncology, Cardiology, Microbiology etc. from *Grigore T. Popa* University of Medicine and Pharmacy of Iasi. The studies included in this chapter are centred by the role of immune cells and molecules in mediating various pathologies, from cancer to infections.

Subchapter 1 details the research contribution conducted in the field of haematological malignancies. More precisely we investigated the correlation between the expression of molecules involved in antigen presentation and various immune checkpoint ligand/receptors with poor clinical outcome in acute myeloid leukaemia (AML) cases. We also investigated the KIR expression on NK cells of myelodysplastic syndrome (MDS) or AML cases compared to healthy controls, and were able to conclude that, in our study, MDS did not appear to represent a smooth transitional stage towards malignancy, but rather a decisive step in the evolution of the immune response while struggling to choose an efficient path for fighting cancer cells.

Subchapter 2 details the personal contribution given to the study of immune responses in solid tumours, while investigating the side-effects consequently to the use of monoclonal antibody-based therapies. More precisely, we found that the development of proteinuria during the first-line treatment with bevacizumab and chemotherapy in patients with metastatic colorectal cancer was an independent prognostic factor for overall survival, and correlated with a better clinical outcome.

Subchapter 3 explores the main findings of the study investigating the humoral immune responses achieved following vaccination anti-SARS-CoV-2. Here we were able to show that adipokine serum levels, and not vitamin D, correlate with the magnitude of humoral immune responses after dual vaccination, but only in younger individuals than 60 years old. The older vaccinated individuals showed reduced anti-SARS-CoV-2 antibody titres irrespective of their infection status or adipokine serum levels.

My personal contributions to this research were published in prestigious ISI journals, such as: *Frontiers of Immunology* (IF 8.787), *Frontiers of Oncology* (IF 6.244), *Immunobiology* (IF 3.152) *Current Oncology* (IF 3.109), *Vaccines* (IF 4.961).

Section II. This section covers the future research projects I intend to develop. Firstly, I am planning to continue and finish the current projects, and then, start new promising ones. One research direction will investigate the role of autophagy in regulating the expression of various plasma membrane molecules involved in controlling the activity of various immune cells (e.g., peripheral blood lymphocytes) in the context of both haematological and solid cancers. Another research direction would involve studying the role of mechanical cues in facilitating cytokine secretion and production by both immune and cancer cells.

Section III. This section comprises the list of bibliographic references used to conduct this thesis.

REZUMAT

Această teză de abilitare cuprinde cele mai semnificative realizări profesionale, academice și, cel mai important, științifice din perioada mea post-doctorală (2016-2023) și conturează câteva dintre direcțiile de cercetare pe care intenționez să le investighez în continuare.

Teza este structurată, conform ghidurilor recomandate și aprobate de Consiliul Național de Atestare a Titlurilor, Diplomelor și Certificatelor (CNATDCU) în 3 secțiuni principale cu subsecțiuni, după cum urmează:

- **Secțiunea I** – descrie cele mai relevante realizări profesionale, academice și științifice din perioada post-doctorală.
- **Secțiunea II** – conturează perspectivele viitoarelor direcții academice și de cercetare.
- **Secțiunea III** – indică lista referințelor bibliografice citate în această teză.

Secțiunea I. În această secțiune am inclus cele mai semnificative rezultate științifice ale contribuțiilor personale și le-am structurat în două capitole principale, fiecare cu 3 subcapitole.

Capitolul I se concentrează pe contribuțiile mele științifice postdoctorale cele mai remarcabile din domeniul autofagiei. O parte din rezultatele incluse aici au fost realizate în colaborare cu oameni de știință de la Universitatea din Cambridge și sunt, în parte, o continuare a studiului de cercetare efectuat pentru teza mea de doctorat intitulată *Modulatori ai citoscheletului de actină dezvoltă roluri noi pentru autofagie în sănătate și boală* și finalizată în martie 2016. Capitolul I cuprinde la rândul său 3 subcapitole.

Subcapitolul 1 detaliază mecanismele moleculare ale autofagiei relevante în contextul cancerului. Mai precis, studiile prezentate subliniază rolul autofagiei în reglarea activității factorilor co-transcripționali YAP/TAZ, adesea supraexpresați într-o varietate de cancere și subliniază dinamica procesului de autofagie în controlul proliferației și supraviețuirii celulare în diferite linii celulare și la perioade de timp distincte. Astfel, am reușit să generăm modele matematice bazate pe ecuații diferențiale dependente de timp care dezvoltă importanța diferitelor bucle de feedback care caracterizează complexitatea axei autofagie-YAP/TAZ. Mai mult, și alte căi de semnalizare intracelulară, care monitorizează proliferația și supraviețuirea celulară, pot fi disecate prin modele matematice similare.

Subcapitolul 2 detaliază mecanismele moleculare ale autofagiei în relație cu bolile neurodegenerative. Studiul publicat în *Nature* descrie rolul ataxinei-3 în interacțiunea sa cu Beclin-1 (o componentă cheie a procesului de autofagie) prin intermediul domeniului său poliQ ce favorizează deubiquitinarea moleculei Beclin-1, împiedicând astfel degradarea acesteia de către proteazom. Ca urmare, activitatea redusă a ataxinei-3 sau scăderea interacțiunii dintre ataxina-3 și Beclin-1 duce la scăderea nivelului intracelular de Beclin-1, ceea ce conduce la reducerea procesului de autofagie. Fragmentele N-terminale ale HTT care conțin domeniul poliQ extinse se găsesc în creierul pacienților cu boala Huntington și provoacă toxicitate în celule și în modelele murine de boală. Aici am arătat că molecula HTT mutantă poate lega Beclin-1, concurând pentru legarea la Beclin-1 cu ataxina-3 și, în consecință, fibroblastele de la pacienții cu boala Huntington (caracterizați de HTT mutant) au procesul autofagic afectat.

Subcapitolul 3 detaliază mecanismele moleculare ale autofagiei în relație cu procesul de îmbătrânire. Rezultatele prezentate aici au fost o continuare a rezultatelor detaliate în subcapitolul 1. Pe scurt am identificat că expresia moleculei SORBS3 este crescută cu înaintarea în vârstă și contribuie la declinul autofagic prin inhibarea activității YAP/TAZ.

Contribuțiile mele personale la această cercetare au fost publicate în reviste prestigioase ISI, precum: *Nature* (IF 41.577), *Nature Communications* (IF 17.694), *Neuron* (IF 14.319), *Cell Death and Differentiation* (IF 12.073), *Autophagy* (IF 13.391), *Journal of Molecular Biology* (IF 5.469), *Bioessays* (IF 4.653), *FEBS Journal* (IF 4.530).

Capitolul II se concentrează pe detalierea cercetărilor postdoctorale efectuate împreună cu cercetători din cadrul Laboratorului de Imunologie și din cadrul Departamentelor de Hematologie, Oncologie, Cardiologie, Microbiologie etc. de la Universitatea de Medicină și Farmacie Grigore T. Popa din Iași. Studiile incluse în acest capitol sunt centrate pe rolul celulelor și moleculelor imune în mediarea diferitelor patologii, de la cancer la infecții.

Subcapitolul 1 detaliază rezultatele cercetării științifice efectuate în domeniul afecțiunilor maligne hematologice. Mai precis, am investigat corelația dintre expresia moleculelor implicate în prezentarea antigenică și a diversilor liganzi/receptori de reglare imună cu prognosticul clinic în leucemia acută mieloidă (LAM). De asemenea, am investigat expresia receptorilor KIR pe celulele NK în cazurile de sindrom mielodisplazic (SMD) sau LAM și am putut concluziona că, în studiul nostru, SMD nu pare să reprezinte o etapă de tranziție lină spre malignitate, ci mai degrabă un pas decisiv în evoluția răspunsului imun în căutarea unei căi eficiente de combatere a celulelor canceroase.

Subcapitolul 2 detaliază contribuția personală din studiului răspunsurilor imune la cazurile cu tumori solide, și anume investigarea efectele secundare ale utilizării terapiilor bazate pe anticorpi monoclonali. Astfel, am constatat că dezvoltarea proteinuriei în timpul tratamentului de primă linie cu bevacizumab și chimioterapie în cazul pacienților cu cancer colorectal metastatic a fost un factor de prognostic independent pentru supraviețuirea globală.

Subcapitolul 3 explorează principalele rezultate ale studiului ce a avut ca scop investigarea răspunsurilor imune umorale obținute în urma vaccinării anti-SARS-CoV-2. Aici am putut arăta că amploarea răspunsurilor imune umorale după vaccinare se corelează cu nivelurile serice ale adipokinelor, dar nu al vitaminei D, la indivizii mai tineri de 60 de ani.

Contribuțiile mele personale la această cercetare au fost publicate în reviste prestigioase ISI, precum: *Frontiers of Immunology* (IF 8.787), *Frontiers of Oncology* (IF 6.244), *Immunobiology* (IF 3.152) *Current Oncology* (IF 3.109), *Vaccines* (IF 4.961).

Secțiunea II. Această secțiune acoperă viitoarele proiecte de cercetare pe care intenționez să le dezvolt. În primul rând, plănuiesc să continui și să termin proiectele actuale, apoi să încep altele noi promițătoare. O primă direcție de cercetare va investiga rolul autofagiei în reglarea expresiei diferitelor molecule de la nivelul membranei plasmatică implicate în reglarea activității celulelor immune (ex. limfocitele periferice) în contextul cancerelor hematologice și solide. O altă direcție de cercetare ar implica studiul rolului stimulilor mecanici în controlul secreției și producției de citokine, atât de către celulele imune, cât și de cele canceroase.

Secțiunea III. Această secțiune cuprinde lista referințelor bibliografice citate în teză.

SECTION I. OVERVIEW OF ACADEMIC CAREER: TEACHING, MEDICAL AND RESEARCH ACTIVITIES

Introduction

I feel privileged to have chosen an academic path that gives me tremendous happiness and fulfilment by merging two noble and rewarding professions, medical doctor and teaching. It is important for both professions to have the up-to-date knowledge and understand the developments of diagnostics methods that considerably increased during the past decade along with the general technological expansion, in order to provide to medical students and forming doctors the right environment for intellectual growth. Thus, the research activities are mandatory for improving in both directions and shaping the key characteristics required for a successful flourishing academic career: intrinsic scientific curiosity, accuracy, dedication, responsibility and hard work.

The habilitation thesis reviews the main accomplishments for the three main axes that define my academic career (teaching, medical practice and training, scientific activities), outlining the main key milestones achieved during my postdoctoral time which form the foundation for my future development.

Teaching activities

The technology and information virtualization have spectacularly developed over the past 20 years. As a result, access to information, often unprocessed and unverified, has become extremely easy, challenging the scientific documentation skill, ability to concentrate and frequently the will for individual work among many young students. In this context, the role of the teacher, especially in the first years of the undergraduate cycle, is to correctly identify the potential initial shortcomings and guide them to overcome any difficulties in order to reach the level required for proper understanding of clinical pathology, deepened especially in the second part of the study cycle. In addition to this training component, our role also involves the transmission to future doctors of the system of educational, ethical and moral values, such as fairness, seriousness, devotion, mutual respect, responsibility, promoted by the *Grigore T. Popa* University of Medicine and Pharmacy from Iasi. Moreover, a successful academic should align to the new modern European teaching and examination methods, in a training environment that promotes mobility, professional development and career advancement.

My professional path was set with my initial decision to pursue studying medicine at the University of Medicine and Pharmacy *Grigore T. Popa* of Iasi (graduating in 2011), but also physics-informatics at the “Alexandru Ioan Cuza” University of Iasi (graduating from bachelor studies in 2008 and master’s in 2010). This complex university training allowed me to gain a multidisciplinary background which helped me to adapt and understand the rapid technological breakout of laboratory diagnosis methods and succeed in my PhD (October 2011 – March 2016). After completing my PhD studies in Medicine and one-year postdoctoral grant at the University of Cambridge and the Cambridge Institute for Medical Research, Great Britain, I started my teaching activities as a Lecturer (Assistant Professor) of Immunology at the University, Faculty of Medicine in 2017, under the guidance of true personalities in the field. Four years later I gained through contest a Senior Lecturer position in Immunology. During this time, I had the pleasure to teach the fundamentals of immunology to the second-year medical students during our laboratory classes in both Romanian and English for the General Medicine, Dental Medicine and General Nursing Sections and conducted lectures and final examinations for students enrolled in the General Medicine or General Nursing Sections.

During this time, I also had the chance to instruct several generations of young doctors from the Medical Laboratory and Clinical Microbiology specialisations by continuously guiding their daily duties and explaining them the practical techniques and principles for the laboratory analyses routinely investigated in the Laboratory of Immunology of *St Spiridon* Emergency County Hospital of Iasi coordinated by Prof. Petru Cianga. I also encouraged the forming doctors to develop their scientific skills by tutoring and coordinating them in various research projects and actively involving them in preparing and communicating the scientific results at various national medical laboratory conferences.

Immunology is one of the most complex research fields at the interface between molecular/cellular biology, physiology, microbiology, pathology and modern therapeutics. Moreover, immunology (and implicitly molecular/cellular biology) is a dynamic field, in continuous formation, with still many unknowns intensively studied by research groups in all prestigious international universities. In this context, it is mandatory to structure and select the key immunological concepts which are fundamentals for the 2nd year medical students in their journey to become successful doctors, and explain them in conjunction with the knowledge that they gained from the other preclinical courses, in order to integrate the new information with what they have already studied. Therefore, during my teaching hours I always start by drawing and presenting them simplified diagrams and illustrations, which are gaining more details as we advance in our immunological theory, this allowing me to configure together with the students the backbone of immunology. Importantly, I am also actively involved in preparing and evaluating the partial, final and recovery tests, as the evaluation process is fundamental in any academic act.

Since the beginning of my teaching activity, my interest focussed on improving my teaching methodology, by understanding how memory is formed and how new information is integrated with the existed one. To achieve this, I participated and graduated both modules (initial and advanced) of the Psycho-pedagogy Course organized for the training of teaching staff by the Pedagogic Department of the Faculty of Psychology and Educational Sciences at the *Alexandru Ioan Cuza* University of Iasi. This one-year course facilitated the acquisition of high-quality information in the field of education and communication, and apart from helping me in preparing the seminar/ laboratory hours and lectures and supervising bachelor's degree thesis, it also helped me to improve my disseminations skills during various national and international conferences. Thus, I actively participated to numerous scientific events, either as an invited lecturer or discussing the research data through posters and oral presentations. I also communicated my scientific knowledge by participating as a co-author, together with my collaborators from the University of Cambridge, in writing a book chapter entitled *Neurodegenerative diseases and autophagy* in the volume *The Molecular and Cellular Basis of Neurodegenerative Diseases* edited by Michael S. Wolfe and published by **Academic Press** in 2018.

Apart from the teaching and students' guiding duties, the academic position also implies organizational attributes. Thus, I have always positively responded to the requests of the department, faculty and university to participate as member in commissions of admission, residency or academic evaluation. In the meanwhile, I was asked and accepted to be a member in the several doctoral tutorial commissions, which familiarized me with the process of PhD supervision, thus, gaining a good experience for becoming a PhD coordinator.

Medical activities

My medical activities started since my time spent at the University of Cambridge, when I received the Honorary Clinical Fellowship at the Addenbrooke's University Hospital in the Department of Medical Genetics for almost one year. In January 2017 I started my residency

programme in the specialty of Laboratory Medicine, and completed it by becoming a specialist at the end of 2020 (specialist exam 10.00, OMS nr. 2160/18.12.2020), with a major in immunology and molecular biology. After becoming a specialist, I received integration at the *St Spiridon* Emergency County Hospital of Iasi in February 2021. During this time, I participated to numerous national medical laboratory and flow-cytometry workshops, conferences and training courses in order to update my knowledge in the field which is fast evolving and improve my practical abilities and skills which are mandatory for my chosen laboratory-based profession. Nevertheless, it is important to reach a certain threshold of knowledge in a specific field in order to understand the difficulty level of any information thought to the students/ medical residents, and be able to dissect and present it in a gradual manner.

Recently, I have been participated to numerous trainings for the use of the state-of-the-art equipment acquired by the Laboratory of Immunology coordinated by Prof. Petru Cianga through the Operational Program for Competitiveness 2014-2020, Axis 1, under POC/448/1/1 Research infrastructure projects for 527 public R&D institutions/universities "Multidisciplinary medical research-development platform 528 in the NE region" CENEMED, mySMIS code 127606: Bionano Saphyr Optical Genome Mapping System, Leica DM6B Fully Automated Upright Microscope System, FACS Aria III flow-cytometer, MiSeq next generation sequencing system, Digital Droplet PCR. For improving the operating skills required for working for the FACS Aria III flow-cytometer, I participated in December 2022 for one-week hands-on intensive training course organised by BD Biosciences in Erembodegem, Belgium.

Research activities

Scientific research is a fundamental part of one's academic career in a university striving for excellence in education at undergraduate and postgraduate levels.

I started my research activity since I was an undergraduate student, while studying the potential role of hyperthermia induced by magnetic nanoparticles in treating solid cancers. This research was supervised by Prof. Alexandru Stancu and involved the generation of computational-based numerical models for studying the heat distribution generated by magnetic nanoparticles in the presence of an applied magnetic field in various tumour tissues characterised by distinct stiffness and plasticity. The research was part of several national PN-II grants (parteneriate: NanoBioDet, HiFi, PCC2) and conducted to the publication of 4 ISI articles as first author in 2008-2011. In 2008 I had the chance to have a personal contribution to a prestigious international conference INTERMAG organised at Madrid, Spain. During this time, I also participated to two research summer internships earned through competition as part of the EPFL (École Polytechnique Fédérale de Lausanne) Summer Research Programme in 2008 (conducting a research projects investigating by bioinformatics analysis based on Hidden Markov Models, the transcription factors regulating the circadian rhythm in mice, under the coordination of Prof. Felix Naef) and UCAM (University of Cambridge) Amgen Scholars Programme (working on RNA-seq and ChIP-seq genome-wide studies of various subpopulations of differentiated Th cells under the supervision of Dr. Sarah Teichmann at the Laboratory of Molecular Biology). In 2011 I was admitted as a PhD student and a FP7 Marie-Curie Early Career Researcher (part of the TreatPolyQ ITN) at the University of Cambridge, studying under the supervision of Prof. David Rubinsztein, in his laboratory at the Cambridge Institute of Medical Research, the roles of autophagy in health and disease, focusing on two main research directions: neurodegeneration and cancer. As part of the TreatPolyQ ITN, I was appointed a second supervisor, the Nobel Laureate Aaron Ciechanover from the Technion – Israel Institute of Technology. It was during this time when I gained an extensive experience

in PCR and RT-PCR, nucleic acid extraction, primary cell culture (primary neurons, mammary epithelial cells), lentiviral transduction and siRNA/ plasmid transfection, immunofluorescence and confocal microscopy, westernblotting and immunoprecipitation, ChIP and promoter analysis, and quantitative proteomics using SILAC (stable-isotope labelling by amino acids in cell culture) and published two Nature Communications scientific papers and one book chapter. Also, as a PhD student, I won through competition the British Council Researcher Link Travel Grant (as part of a partnership programme between UK and South Korea) for studying the role of proteasome inhibitors and activators on autophagy regulation.

My postdoctoral experience started immediately after completing the PhD studies and submitting the thesis in March 2016, continuing to work in the laboratory of Prof. David Rubinsztein, while supervising PhD students and conducting various scientific projects, which resulted in publishing one NATURE original research paper, one Neuron review and other 2 papers in Autophagy and FEBS Journal. It is worth mentioning that the Neuron article encompassed more than 650 citations in the ISI Thomson Reuters system.

While returning as an academic at the *Grigore T Popa* University of Medicine and Pharmacy, I continued my postdoctoral course and conducted an extensive and diverse research work. First, I was **project director** for 2 CNCS-UEFISCDI financed research grants won through national competition, such as KirPhagy [PN-III-P1-1.1-PD-2019-0733](#) (3rd place in the Biology/ Life Sciences category, title: *The role of autophagy in coordinating the KIR-dependent NK homeostasis and its implications in hematologic malignancies*), STIFFMAG [PN-III-P1-1.1-PD-2016-1291](#) (1st place in the Physics category, title: *Mechanical analysis of tissue stiffness and plasticity in the context of magnetic fluid hyperthermia therapy*), and the [L'Oréal – UNESCO for Women in Science 2019 Fellowship](#) for the Life Sciences category (title: *The role of autophagy in natural killer cells homeostasis and its implications in female infertility*). Those projects reinforced the collaboration with the University of Cambridge and involved 2 mobility research projects in March 2018 and August 2019. At this point I consider important to mention that I am an associated external researcher at the University of Cambridge since January 2017. To further increase the international visibility of UMF Iasi and to extend collaborations with other international/ national universities I applied for and won the position in the Romanian management committee of the COST Action CA20140 - CorEuStem: The European Network for Stem Cell Core Facilities (CorEuStem).

Additionally, I contributed as a **member** in two other research grants, a national CCNCS-UEFISCDI project [PN-III-P2-2.1-PED-2021-3003](#) (BioHySkin no. 613PED/2022, title: *3d bio-inspired hybrid architectures for deep thickness skin repair and regeneration*) and an internal UMF Iasi grant (no. 9990/2022, title: *Correlation between frailty and immune senescence in patients with advanced non-small cell lung cancer starting checkpoint inhibitors therapy*) in the Health and Longevity Medicine category. It is also important to mention that I participated as a member of the evaluation team regarding the awarding of the public procurement contract for the supply of molecular biology and genetic equipment within the implementation of the CENEMED project.

I consider that the valuable research work can be conducted only in research groups where scientific rigour, hard work and team collaboration is promoted. From this perspective, I had the chance to work with wonderful research teams from UMF Iasi and University of Cambridge and define a successful multidisciplinary collaboration between various departments (Immunology, Microbiology, Infectious Diseases, Gastroenterology, Endocrinology, Internal Medicine/ Nephrology, and Cardiology departments) which resulted in the publication of scientific papers in prestigious ISI journals and disseminations of results at national and international conferences and meetings.

In summary, the overall international visibility of my research is reflected by the following indexes:

- Clarivate Analytics Web of Science Hirsch-Index: 12
- Total number of citations without self-citations: 1412
- In extenso ISI scientific articles: 30 (of which 9 were published in ISI journals with impact factor > 10: one article in *NATURE*, 4 articles in *Nature Communications*, one article in *Neuron*, one article in *Cell Death and Differentiation* and 2 articles in *Autophagy*)
- In extenso ISI scientific articles as main author (first or corresponding): 16
- In extenso IDB scientific papers: 1
- Book chapters published by prestigious publishing houses: 2

At this point I would like to mention that my research contribution received national recognition as reflected by the “Science and Engineering Early Researcher Rada Mihalcea” Mention Award in 2018 and the “L’Oréal – UNESCO for Women in Science 2019 Life Sciences” Award.

A successful career in academia requires continuous dedication, training and improvement, which are complemented by a good capacity to disseminate the results and knowledge to both students and general scientific community. All the aforementioned achievements constitute the foundation for further research activities from which early career researchers should benefit.

Chapter 1: The molecular mechanisms of autophagy in health and disease

1.1. State of art

1.1.1. Autophagy cell biology

Macroautophagy (henceforth autophagy) is a major intracytoplasmic protein degradation pathway whereby cytoplasmic contents are delivered to the lysosome for degradation by double-membraned vesicles called autophagosomes. It should be differentiated from other pathways that will not be considered in this review, like chaperone-mediated autophagy and microautophagy, where substrates are directly translocated into the lysosome without vesicular transport. The first morphologically characteristic structure in autophagy is the double-membraned cup-shaped autophagosome precursor called the phagophore that engulfs substrates as its edges extend. After the phagophore edges close, the completed autophagosomes traffic along microtubules towards the microtubule organising centre where the lysosomes are clustered to enable autophagosome-lysosome fusions, which lead to the degradation of the autophagic contents. Autophagy is regulated by a series of proteins including the so-called ATG proteins (Djajadikerta et al., 2020; Fleming et al., 2022).

Autophagy was initially characterized as a bulk and non-selective degradation pathway induced by nutrient deprivation. However, more recent studies made clear that autophagy also contributes to intracellular homeostasis in non-starved cells by selectively degrading cargo material, such as aggregate-prone proteins, including those causing many neurodegenerative conditions (aggrephagy), damaged mitochondria (mitophagy), excess peroxisomes (pexophagy) and invading pathogens (xenophagy) (Stolz et al., 2014). In the classic example, aggregates of aberrantly folded proteins are tagged with ubiquitin chains, which are recognized by ubiquitin-binding domain (UBD)-containing receptors, such as p62/SQSTM1, NBR1, optineurin (OPTN), TAX1BP1, NDP52/CALCOCO2, TOLLIP and RPN10 (Khaminets et al., 2016; Stolz et al., 2014). These receptors also contain LIR (LC3-interacting region) motifs in their sequence capable of recognizing the key autophagosome-associated protein, LC3. Thus, these receptors serve as bridge between ubiquitinated cargo and autophagosomes, and enhance the incorporation of cargo to autophagosomes for subsequent lysosomal degradation (Bjorkoy et al., 2005; Pankiv et al., 2007).

1.1.2. Key autophagy regulators

Autophagy activation in response to the primordial stimuli of nutrient deprivation and/or low cellular energy levels is mediated by signalling pathways that converge on ULK1/2 (mammalian homologs of the *C. elegans* uncoordinated-51 kinase). ULK1/2 form a complex with ATG13, ATG101 and FIP200. Nutrients and growth factor availability and levels of AMP/ATP (which reflect the energetic status of the cell) are sensed by mammalian target of rapamycin complex 1 (mTORC1) and AMP-dependent protein kinase (AMPK), respectively, which, in turn, oppositely regulate the ULK1/2 complex through a series of phosphorylation events. For instance, activation of AMPK by AMP-allosteric binding and phosphorylation of Thr172 promotes autophagy by directly activating ULK1 through phosphorylation of Ser 317 and Ser77 under glucose deprivation (Kim et al., 2011a), or Ser 555 under amino acid starvation and mitophagy (Egan et al., 2011). On the other hand, in media replete of amino acids (sensed by the Rag-Ragulator complex) and growth factors (that activate receptor tyrosine kinases and the PI3K/AKT pathway), mTORC1 is activated, which inhibits autophagy by binding to the ULK1 complex (via Raptor-ULK1 interaction) and phosphorylating both ATG13 and ULK1 (at Ser 757), thereby suppressing ULK1 kinase activity and preventing interaction between

ULK1 and AMPK (Ganley et al., 2009; Hosokawa et al., 2009b; Jung et al., 2009; Laplante and Sabatini, 2012).

Activation of the ULK complex is required for the recruitment of the class III PI 3-kinase, VPS34, to the phagophore initiation sites where VPS34 forms phosphatidylinositol 3-phosphate (PI3P), while in a complex VPS15, ATG14 and Beclin 1. The exact function of PI3P in autophagy is still unclear; however, it appears to aid the recruitment of WIPI proteins to the phagophore membrane, which, in turn, control the recruitment of crucial downstream autophagic proteins (e.g., ATG16L1 by WIPI2) dictate where the phagophores form (Dooley et al., 2014).

The ATG12 and ATG8/LC3 ubiquitin-like conjugation systems are then required for sustaining the expansion of the phagophore. In the first system, ATG12 is conjugated to ATG5, in a reaction that involves ATG7 and ATG10 (E1-like and E2-like enzymes, respectively), which in turn binds noncovalently to ATG16L1. This complex (ATG12-ATG5-ATG16L1) associates with pre-autophagosomal membranes enabling their elongation by assisting in the recruitment of LC3. However, before this can happen, LC3 has to be processed by the cysteine protease ATG4 that cleaves the C-terminus of LC3 exposing a Gly residue (LC3-I form). This cleavage is crucial for LC3-I conjugation to phosphatidylethanolamine (PE), by a mechanism dependent on ATG7, ATG3 and ATG12-ATG5-ATG16L1 (E1-like, E2-like and E3-like enzymes, respectively), leading to the formation of LC3-II, which gets tightly associated with autophagosomal membranes. This cascade of reactions then sustains extension of the phagophore edges and its closure, and fusion with lysosomes (Bento et al., 2016a).

Extension of the phagophore is also assisted by mATG9, the only identified multi-pass transmembrane protein among the core ATG proteins. This protein has been shown to localize to the *trans*-Golgi network and the endocytic compartment, including early endosomes, late endosomes and recycling endosomes, and is postulated to aid in the supply of lipid-bilayers to the nascent phagophore, enabling its further elongation, until it has to be closed to fully form the autophagosome (Bento et al., 2016a). This late stage, where the outer and the inner membranes of the pre-autophagosomal structure become separate entities, is poorly understood, but ATG2 in combination with WIPI1 appear to regulate autophagosome closure (Velikkakath et al., 2012), a process likely involving membrane fission/scission type events akin to the genesis of multivesicular bodies by ESCRT-mediated membrane budding (Knorr et al., 2015).

The sources of autophagosome membranes is an area of active investigation. Endoplasmic reticulum (ER), Golgi and *trans-Golgi* network, mitochondria, plasma membrane and endosomal compartments have all been suggested as possible sources of phagophore-membranes (Bento et al., 2016a). The ER emerged as one of the possible sources of membrane for pre-autophagosomes not only because isolation membranes were observed cradled within a subdomain of the ER and interconnected with it (Axe et al., 2008; Hayashi-Nishino et al., 2009), but also because ATG14- and ATG5-positive isolation membranes were found in close proximity to a subdomain of the ER in contact with mitochondria during starvation (Hamasaki et al., 2013). Post-Golgi tubulo-vesicular compartments undergoing remodelling and homotypic fusion (Guo et al., 2012; Orsi et al., 2012; Young et al., 2006), and the ER-Golgi intermediate compartment (ERGIC) have also been considered as pre-autophagosomal membrane sources (Ge et al., 2013; Ge et al., 2014), where the ERGIC was specifically observed to bud LC3-lipidation active vesicles that may serve as a docking platform for autophagosome biogenesis and expansion (Ge et al., 2013; Ge et al., 2014).

The plasma membrane and the endocytic compartments are also suggested as membrane sources for early autophagosomal-precursor structures. Clathrin-dependent endocytosis has been implicated in this process by delivering ATG16L1 and mATG9 to recycling endosomes (via different routes and involving VAMP3-dependent membrane fusion events), which leads

to the formation of early autophagosomal structures and mature autophagosomes (Moreau et al., 2011; Puri et al., 2013; Ravikumar et al., 2010a). Overexpression of the recycling endosome proteins TBC1D14 (a Rab11-effector) or PX-containing SNX18 were shown to induce accumulation of mATG9 and ATG16L1, respectively, along with other autophagic proteins (e.g., ULK1 and LC3) in this compartment (Knaevelsrud et al., 2013; Lamb et al., 2016; Longatti et al., 2012), reinforcing the possible role of recycling endosome as an important phagophore-membrane source.

1.1.3. Transcriptional regulation of autophagy

In addition to phosphorylation, discussed above, autophagy is also regulated at the transcriptional level. mTORC1, apart from regulating the ULK1/2 complex, also connects the lysosome nutrient-sensing machinery to the transcriptional regulation of autophagy genes via transcription factor EB (TFEB) (Settembre et al., 2012). In resting cells, phosphorylation of TFEB by active mTORC1 induces TFEB binding to 14-3-3 proteins and therefore TFEB retention in the cytosol (Roczniak-Ferguson et al., 2012; Settembre et al., 2011). However, under starvation and consequent mTORC1 inactivation, TFEB is no longer phosphorylated and translocates to the nucleus, where it binds to CLEAR consensus sequences in promoters of target genes and induces their transcription. Among these genes, many are directly related to the lysosome and autophagy (e.g. lysosomal hydrolases, vATPase subunits, ATG proteins) and thus TFEB appears to coordinately regulate autophagic and lysosomal activities (Sardiello et al., 2009; Settembre et al., 2011). ZKSCAN3 (zinc-finger protein with KRAB and SCAN domains 3) is a transcriptional repressor of autophagy that appears to oppose TFEB. ZKSCAN3 silencing enhances autophagosome and lysosomal biogenesis, and mTORC1 inhibition induces its accumulation in the cytosol (Chauhan et al., 2013). Now, more than 20 other transcription factors have been linked to transcriptional regulation of autophagy upon a wide range of stimuli (Fullgrabe et al., 2014). For instance, microphthalmia-associated transcription factor (MITF) (which belongs to the same family of proteins as TFEB) (Martina et al., 2014), p53 (Kenzelmann Broz and Attardi, 2013) and forkhead box O3 (FOXO3) (Mammucari et al., 2007) were shown to transactivate ATG genes.

1.1.4. Physiological relevance of autophagy

The physiological relevance of autophagy is related to the normal turnover of the cellular components and the clearance of misfolded long-lived proteins or damaged organelles. (Ashkenazi et al., 2017b; Menzies et al., 2017a; Pavel and Rubinsztein, 2013) Under stress conditions, such as starvation or oxidative stress, autophagy is upregulated to degrade dispensable macromolecules and restore nutrient balance. (Singh and Cuervo, 2011) In addition to its role in cellular homeostasis in both basal and stress conditions, by controlling the levels of various intracellular proteins, the autophagy pathway and its direct or indirect regulators are connected to many physiological and pathological conditions. First, autophagy is essential for life, starting with the early steps of embryogenesis. Autophagy activity is required in many steps of development, from fecundation and implantation through to organ development and survival during the neonatal starvation period (Hara et al., 2006; Komatsu et al., 2006; Mizushima and Levine, 2010; Tsukamoto et al., 2008). Recent studies have also reported that autophagy modulates stem cell development and neurogenesis by monitoring the degradation of Notch, the master transcriptional regulator of stem cell lineage (Wu et al., 2016). Additionally, it is worth mentioning its involvement in lifespan extension, aging, senescence, immunity, and defence against pathogens (Bandyopadhyay and Cuervo, 2007; Massey et al., 2006). Changes in the autophagic balance (too much or too little autophagy) have been broadly associated with cancer, heart diseases, gastrointestinal disorders and mainly with

neurodegenerative diseases (Ravikumar et al., 2010b; Sridhar et al., 2012). The great interest in autophagy over the last decade has led to a better understanding of the importance of this process in neurons, where aggregate-prone proteins accumulate and form toxic inclusions that impair the normal neuronal functioning (Ravikumar et al., 2002). Defects in different stages of autophagy translate into various neurodegenerative pathologies (Garcia-Arencibia et al., 2010; Klionsky, 2006; Winslow and Rubinsztein, 2008).

In this direction I aimed to understand how autophagy is perturbed in various physio- and pathological conditions, like cancer, neurodegeneration and ageing, by identifying the underlying cellular mechanisms, and the impact of autophagy modulation (either genetically or chemically) on the evolution of those conditions.

This research direction has been achieved by publishing the following scientific articles:

ISI ARTICLES

- **Autophagy and cancer**

Mariana Pavel*, So Jung Park*, Rebecca A. Frake, Sung Min Son, Marco M. Manni, Carla F. Bento, Maurizio Renna, Thomas Ricketts, Fiona M. Menzies, Radu Tanasa, David C. Rubinsztein. *α -Catenin levels determine direction of YAP/TAZ response to autophagy perturbation*, *Nature Communications* 2021; 12: 1703. **IF: 17.694**
<https://doi.org/10.1038/s41467-021-21882-1> (* equal contribution)

Mariana Pavel*, So Jung Park*, Radu Tanasa*, David C. Rubinsztein. *Cell type-specific YAP1-WWTR1/TAZ transcriptional responses after autophagy perturbations are determined by levels of α -catenins (CTNNA1 and CTNNA3)*, *Autophagy* 2021; 17(7): 1788-1790. **IF: 13.391**
<https://doi.org/10.1080/15548627.2021.1934273> (* equal contribution)

Mariana Pavel, Radu Tanasa, So Jung Park, Rubinsztein DC. *The complexity of biological control systems: An autophagy case study*. *Bioessays* 2022; 44(3): e2100224. **IF: 4.653**
<https://doi.org/10.1002/bies.202100224>.

Mariana Pavel, Maurizio Renna, So Jung Park, Fiona M. Menzies, Thomas Ricketts, Jens Füllgrabe, Avraham Ashkenazi, Rebecca A. Frake, Alejandro Carnicer Lombarte, Carla F. Bento, Kristian Franze, David C. Rubinsztein. *Contact inhibition controls cell survival and proliferation via YAP/TAZ-autophagy axis*, *Nature Communications* 2018; 9: 2961. **IF: 11.878**
<https://doi.org/10.1038/s41467-018-05388-x>

- **Autophagy and neurodegeneration**

Alvin Djajadikerta*, Swati Keshri*, **Mariana Pavel***, Ryan Prestil*, Laura Ryan*, David C. Rubinsztein. *Autophagy induction as a therapeutic strategy for neurodegenerative diseases*, *Journal of Molecular Biology* 2020; 432(8):2799-2821. **IF: 5.469**
<https://doi.org/10.1016/j.jmb.2019.12.035>. (* equal contribution)

Avraham Ashkenazi, Carla F. Bento, Thomas Ricketts, Mariella Vicinanza, Farah Siddiqi, **Mariana Pavel**, Ferdinando Squitieri, Maarten C. Hardenberg, Sara Imarisio, Fiona M. Menzies, David C. Rubinsztein. *Polyglutamine tracts regulate beclin 1-dependent autophagy*, *NATURE* 2017; 545:108-111. **IF: 41.577**
<https://dx.doi.org/10.1038/nature22078>.

Avraham Ashkenazi, Carla F. Bento, Thomas Ricketts, Mariella Vicinanza, Farah Siddiqi, **Mariana Pavel**, Ferdinando Squitieri, Maarten C. Hardenberg, Sara Imarisio, Fiona M. Menzies, David C. Rubinsztein. *Polyglutamine tracts regulate autophagy*, **Autophagy** 2017; 13(9):1613-1614. **IF: 11.100**
<https://doi.org/10.1080/15548627.2017.1336278>.

Fiona Menzies*, Angeleen Fleming*, Andrea Caricasole*, Carla Bento*, Steven Andrews*, Avraham Ashkenazi*, Jens Fullgrabe*, Anne Jackson*, Maria Jimenez-Sanchez*, Cansu Karabiyik*, Floriana Licitra*, Ana LopezRamirez*, **Mariana Pavel***, Claudia Puri*, Maurizio Renna*, Thoma Ricketts*, Lars Schlotawa*, Mariella Vicinanza*, Hyeran Won*, Ye Zhu*, John Skidmore*, David C. Rubinsztein. *Autophagy in neuronal health and disease*, **Neuron** 2017; 93(5):1015-1034. **IF: 14.319**
<https://dx.doi.org/10.1016/j.neuron.2017.01.022> (* equal contribution)

Mariana Pavel and David C. Rubinsztein, *Mammalian autophagy and the plasma membrane* (State-of-the-Art review), **FEBS Journal** 2017; 284(5): 672-679. **IF: 4.530**
<https://doi.org/10.1111/febs.13931>

- **Autophagy and ageing**

Park SJ, Frake RA, Karabiyik C, Son SM, Siddiqi FH, Bento CF, Sterk P, Vicinanza M, **Pavel Mariana**, Rubinsztein DC. *Vinexin contributes to autophagic decline in brain ageing across species*. **Cell Death and Differentiation** 2022; 29(5): 1055-1070. **IF: 12.073**
<https://doi.org/10.1038/s41418-021-00903-y>

BDI ARTICLES

Cansu Karabiyik, Rebecca A. Frake, So Jung Park, **Mariana Pavel**, David C. Rubinsztein. *Autophagy in ageing and ageing-related neurodegenerative diseases*. **Ageing and Neurodegenerative Diseases** 2021; 1:2
<https://doi.org/10.20517/and.2021.05>

BOOK CHAPTER

Angeleen Fleming, Mariella Vicinanza, Maurizio Renna, Claudia Puri, Thomas Ricketts, Jens Füllgrabe, Ana Lopez, Sarah M. de Jager, Avraham Ashkenazi, **Mariana Pavel**, Floriana Licitra, Andrea Caricasole, Stephen P. Andrews, John Skidmore, David C. Rubinsztein. *Chapter 11 – Neurodegenerative Diseases and Autophagy*. In: *The Molecular and Cellular Basis of Neurodegenerative Diseases. Underlying Mechanisms* (Editor: Michael S. Wolfe) **Academic Press** 2018; 299-343. ISBN 978-0-12-811304-2
<https://doi.org/10.1016/B978-0-12-811304-2.00011-0>

1.2. Autophagy-cancer interlink

The implication of autophagy in cancer evolution, from malignant cell transformation towards cell migration and metastasis is highly controversial, as contradictory results are reported for each distinct step in the malignization process, but also for each cancer type. Indeed, autophagy may act as a *tumour suppressor*, by preventing the tumour initiation, or it can promote *tumour progression*, by enabling the cancer cells to survive during metabolic stress, invade and metastasize and finally resist apoptotic insults triggered by cytostatic agents – reviewed in (Kenific and Debnath, 2015; Rubinsztein et al., 2012; White, 2012, 2015). Thus, it is unclear whether autophagy inhibition is *beneficial* or *damaging* in cancers, and much of

the controversy rises mainly from the general expectation that all cancers should react in the same direction, possibly to various extent, when autophagy is perturbed.

1.2.1. Alpha catenins: the interlink between autophagy and cancer cell proliferation and survival

1.2.1.1. Introduction

The identity and status of cells is commonly depicted using static “omics” profiles: epigenomic, transcriptomic, proteomic or metabolomic (Mincarelli et al., 2018; Rangarajan and Izard, 2013; Stadhouders et al., 2019; Yadav et al., 2018). Changes in cellular identity play an important role in promoting diseases, including cancers, inflammatory conditions and neurodegeneration, and identifying the factors regulating these cell identity switches might provide novel therapeutic opportunities (Comet et al., 2016; Young et al., 2018). However, it is not well understood how such static hallmarks change over time and convert into dynamic responses to external or internal perturbations that ultimately determine cellular functions.

Since certain effectors of critical signalling pathways are autophagy substrates, we expected that autophagy inhibition in different cell types would cause signaling responses in the same directions but possibly with differing amplitudes according to cell type. Those various reaction amplitudes would most likely result either from different starting levels of the effector proteins or varying baseline autophagic flux in distinct cell types. However, recent literature suggests that autophagy compromise may cause opposite effects in different cell lines (e.g. either activating (Lee et al., 2018; Wang et al., 2019) or inhibiting (Chen et al., 2019b) YAP/TAZ co-transcriptional regulators of the Hippo pathway) via unrelated mechanisms.

1.2.1.2. Aim

As YAP/TAZ are oncogenes that regulate critical processes including cell growth, cell size and resistance to apoptosis, we aimed to identify the mechanisms that cause opposite effects on YAP/TAZ activity in different cell lines upon the same autophagic stimulus.

1.2.1.3. Materials and methods

Antibodies

The following primary antibodies used for western blot (WB) and immunofluorescence (IF): rabbit polyclonal anti-ATG7 (ab52472, WB 1:1000, IF 1:200 dilution), rabbit monoclonal anti-ATG10 (ab124711, WB 1:1000), mouse monoclonal anti-BrdU (ab8152, IF 1:200), rat monoclonal anti-BrdU (ab6326, IF 1:100), mouse monoclonal anti-GAPDH (ab8245, WB 1:5000), goat polyclonal anti-GFP (ab5450, IF 1:200), rabbit polyclonal anti-GFP (ab6556, WB 1:1000), rabbit monoclonal anti-LC3 (ab192890, WB 1:1000), rabbit monoclonal anti-CTNNA3 (ab184916, WB 1:1000) from Abcam. Mouse monoclonal anti-LC3 (clone 5F10, Nanotools, IF 1:200), mouse monoclonal anti-YAP/TAZ (63.7) (sc-101199, Santa Cruz Biotechnology, IF 1:100), goat polyclonal anti-LaminB (M-20) (sc-6217, Santa Cruz Biotechnology, WB 1:100), mouse monoclonal anti-LAMP1 (ab25630, IF: 1:100), rabbit monoclonal anti-S6 Ribosomal Protein (5G10) (no. 2217, Cell Signaling, WB 1:1000), rabbit monoclonal anti- α -E-catenin (anti-CTNNA1) (no. 3236, Cell Signaling, WB 1:1000), rabbit monoclonal anti-MLC2 (no. 8505, Cell signaling, WB 1:1000), normal rabbit IgG (no. 2729S, Cell Signaling), rabbit polyclonal anti-ATG16L1 (no. 8089, Cell Signaling, IF 1:200), rabbit

anti-ATG16L1 (PM040, MBL, WB 1:1000), mouse anti-Flag M2 (F3165, Sigma-Aldrich, WB: 1:2000). The secondary antibodies used for IF were conjugated to Alexa Fluor 488, 568, 594 or 647 (Invitrogen). The horseradish peroxidase (HRP)-conjugated secondary antibodies used for western-blotting were: anti-mouse (NA931V, GE Healthcare), anti-rabbit (NA934V, GE Healthcare) and anti-goat (no. 611620, Invitrogen-Life Technologies); the following LICOR secondary antibodies were used: anti-mouse 680 and anti-rabbit 800. F-actin staining was detected with Phalloidin-Alexa Fluor 546 (A22283, Invitrogen-Life Technologies) and 488 (A12379, Invitrogen-Life Technologies).

Plasmids and siRNAs

The following constructs were used in this study: 8XGTIIC-luciferase (no. 34615, Addgene)(Dupont et al., 2011a), pCMV-Renilla Luciferase (E2261, Promega), empty mEmerald-C1 (no. 54734, Addgene), mEmerald-Alpha1-Catenin-C-18 (no. 53982, Addgene), GFP-YAP (no. 17843, Addgene). The mRFP-LC3 construct was kindly provided by Dr. Tamotsu Yoshimori (Osaka University, Japan). Alpha1-Catenin which was amplified from mEmerald-Alpha1-Catenin-C-18 was cloned into pFlag-CMV-5a expression vector (E7523, Sigma-Aldrich) using EcoRI and Sall restriction enzyme sites (pFlag-CTNNA1). Pre-designed siRNAs (On-Target plus SMART pool and/or set of deconvoluted oligos) targeting Control (D-001810-10), ATG7 (L-020112-00), ATG10 (L-019426-01), ATG16L1 (L-021033-01), CTNNA1 (L-010505-00) and CTNNA3 (L-020300-00) were purchased from Dharmacon ThermoScientific.

Mutagenesis

CTNNA1 mutants (Y419A-V422A, F511D-V514D, Y619A-I622A, L879A-F900A or Y419A-V422A- L879A-F900A) were generated using the Quickchange site-directed mutagenesis kit (Agilent Technologies, cat# 200514) according to manufacturer's instructions. Mutagenesis primers were designed using web-based QuikChange Primer Design program (Agilent Technologies). PCR products were incubated with DpnI restriction enzyme for 1 h and then mixed with XL-10 Gold-competent cells. After transformation, DNA was prepared from colonies and sequenced by Genewiz (UK). After establishing a CTNNA1 Y419A-V422A mutant, CTNNA1 mutant (CTNNA1 Y419AV422A) was used to generate a CTNNA1 Y419A-V422A- L879A-F900A using mutagenesis primers for L897A-F900A.

Reagents

Bafilomycin A1 (Millipore) was dissolved with dimethyl sulphoxide (DMSO, Sigma-Aldrich) and used at either 400 nM for 4-6 h or 200 nM overnight. SMER28 was dissolved with DMSO and used at either 20 μ M or 50 μ M for 24 h. VPS34-IN1 (Vps34 Inhibitor, no. 532628, Calbiochem) was resuspended in DMSO and used at a concentration of 1 μ M for 24 h. All control conditions without BafA1, SMER28 or VPS34-IN1 received an equivalent volume of DMSO as the compounds. Tat-Beclin1 L11S Peptide (Tat-scrambled control, NBP-49887) and Tat-Beclin1 D11 Autophagy Inducing Peptide (Retrainverso form, NBP-49888) were obtained from Novus Biologicals. Both peptides were dissolved with distilled water (DW) and used at 20 μ M concentration for 48 h. Trehalose (D-(+)-Trehalose dihydrate, no. T9351, Sigma-Aldrich) was dissolved with DW and used at 100 mM for 24 h.

Cell culture

MCF10A cells were obtained from Horizon (no. HD PAR-058) and were cultured in DMEM:F12 (D6421, Sigma-Aldrich) media containing 5% horse serum (H1270, Sigma-Aldrich), 2 mM L-glutamine (G7513, Sigma-Aldrich) and 100 U/ml penicillin-streptomycin (P0781, Sigma-Aldrich) and supplemented with 0.1 μ g/ml cholera toxin (C8052, Sigma-Aldrich), 20 ng/ml hEGF (E9644, Sigma-Aldrich), 10 μ g/ml insulin (I9278, Sigma-Aldrich), 0.5 μ g/ml hydrocortisone (H0135, Sigma-Aldrich), as previously reported(Pavel et al., 2018a).

Human cervical epithelium (HeLa) cells, human embryonic kidney 293T (HEK293T) cells, human breast cancer MCF7 cells, and human hepatocytes THLE-2 cells were obtained from American Type of Cell Collection (ATCC, USA) and human lung carcinoma A549 cells were kindly provided by Dr. F. Buss (University of Cambridge, UK). HeLa cells, HEK293T, MCF7 and A549 cells were cultured in DMEM (D6546, Sigma-Aldrich) containing 10% fetal bovine serum (FBS, F7524, Sigma-Aldrich), 100 U/ml penicillin-streptomycin (P0781, Sigma-Aldrich), 2 mM L-glutamine (G7513, Sigma-Aldrich). THLE2 cells were cultured in Bronchial Epithelial Cell Growth Medium (BEGM) supplemented with Bullet kit (BEGM Bullet Kit; CC3170, Lonza/Clonetics Corporation) added extra 5 ng/mL EGF, 70 ng/mL Phosphoethanolamine and 10% fetal bovine serum. Human liver carcinoma HepG2 cells were purchased from European Collection of Authenticated Cell Cultures and cells were grown in RPMI-1640 (R0883 Sigma-Aldrich) containing 10% FBS (F7524, Sigma-Aldrich), 100 U/ml penicillin-streptomycin (P0781, Sigma-Aldrich), 2 mM L-glutamine (G7513, Sigma-Aldrich). All the cell lines were incubated at 37⁰ C and 5% CO₂, humidified atmosphere and were tested for mycoplasma contamination every two weeks.

Stable Isotope Labeling by Amino Acids in Cell Culture (SILAC)-based quantitative proteomics

HeLa cells were grown in SILAC DMEM medium (88364, ThermoFisher Scientific) supplemented with 10% dialyzed fetal calf serum (FCS) (26400, ThermoFisher Scientific), 100 U/ml penicillin-streptomycin (P0781, Sigma-Aldrich). Media was supplemented with either light (Arg 0, Lys 0, Sigma-Aldrich), medium (Arg 6, Lys 4, Cambridge Isotope Laboratories, Andover, MA) or heavy (Arg 10, Lys 8, Cambridge Isotope Laboratories, Andover, MA) amino acids at 50 mg/L and l-proline at 280 mg/L. The cells were kept in culture for 6 days before treatment with BafA1 (200nM, 24 h). The cells were then washed twice in PBS, collected in LoBind microcentrifuge tubes (0030122356, Eppendorf) and lysed in 200 µl of lysis buffer (2% SDS, 100 mM Tris/HCl pH 7.5, 1x Roche protease inhibitor cocktail) for 5 min at RT. The samples were sonicated 10 x 10 s bursts of medium-high power (on a Diagenode Bioruptor) to shear DNA, centrifuged at 16000 xg for 5 min and equal amount of either M/L (DMSO/ BafA1) or H/M (DMSO/ BafA1) cell lysates were combined to proceed to protein extraction and digestion, off-line peptide fractionation by high-pH reverse-phase high-pressure liquid chromatography (HpRP-HPLC) and mass-spectrometry analysis, following the protocol described in (Greenwood et al., 2016; Greenwood et al., 2019). Briefly, data for SILAC samples were generated using an Q Exactive Orbitrap mass spectrometer coupled to an RSLCnano3000 (Thermo Scientific). Raw MS files were processed using MaxQuant 1.3 and data were searched against a human Uniprot database (downloaded 03/06/14, 20,176 entries).

Transfection

For siRNA transfection, MCF10A, HEK293T, HeLa and HepG2 cells were plated in 6 well plates and cells were transfected with 100 nM siRNA using Lipofectamine RNAiMAX (13778150 Invitrogen) for 6 h per well. The following day, cells were re-transfected with 50 nM siRNA. When required, cells were split in the 6 or 12 well plates. For DNA transfection, MCF10A cells were seeded in 6 well plates and cells were transfected with 1 µg of DNA constructs (CTNNA1 wild type or mutants) using TransIT-2020 reagent (Mirus). HepG2 cells were cultured in 6 well plate and transfected with wild-type CTNNA1 (1 µg) by using TransIT-2020 reagent (Mirus). After 24 h, cells were re-transfected with 1 µg of cDNA in order to increase the transfection efficiency. HeLa and MCF7 cells were seeded in 6 well plates and cells were co-transfected with 1 µg of both mRFP-LC3 and mEm-CTNNA1 using TransIT-2020 reagent (Mirus). On the following day, cells were reseeded in the 6 or 12 well plates according to the experimental requirements.

Immunofluorescence microscopy

For immunofluorescence staining, cells were cultured on coverslips. After treatment of experimental requirements, cells were washed with PBS three times and then fixed with 4% paraformaldehyde (PFA, Sigma-Aldrich) for 5 min. After rinsing the cells on coverslips, cells were permeabilized with 0.1% Triton X-100 for 10 min and blocked with 3% BSA (BP1605-100, Fischer Scientific) for 1 h. Cells were incubated with primary antibodies in blocking buffer overnight at 4°C. After washing three times with PBS, cells were incubated with secondary antibodies tagged with Alexa Fluor obtained from molecular Probes for 90 min at RT. Cells on coverslips were washed with PBS and mounted in Prolong Gold Antifade reagent with DAPI (P-36931, Invitrogen).

For immunostaining of LC3B, cells were fixed and permeabilized with ice-cold methanol for 4 min. After washing three times with PBS, cells were blocked with 3% BSA for 1 h. The following steps were the same as above.

The images were performed by LSM710, LSM780 and LSM880 confocal microscopy (40x, 63x NA 1.4 Plan Aplanachromat oil immersion lens, Carl Zeiss). Further analysis was performed in Photoshop (Adobe) and ImageJ, and if required, equal adjustments were made for all the images from all control and treatment groups.

BrdU (5-Bromo-2'-deoxyuridine) staining

For cell proliferation assay, cells were seeded and grown on coverslips. Freshly prepared BrdU (5-Bromo-2'-Deoxyuridine, ab142567) was diluted to 10 µM in pre-warmed culture media and added to the cells for 2 h. The media was removed and cells were fixed in 4% PFA for 30 min and incubated with 1.5N HCl for 1 h. Then, cells were washed three times in PBS and blocked with 5% goat serum and 0.3% TritonX-100 in 1x PBS for 90 minutes. After, cells were incubated with primary anti-BrdU antibody (1:200 dilution in PBS containing 5% goat serum), overnight at 4 °C. Cells were rinsed with PBS for three times and incubated with secondary antibody (at 1:400 dilution) for 1 h at RT. After washing with PBS, the coverslips were mounted with the Prolong Gold Antifade reagent with DAPI (P-36931 Invitrogen).

Live cell imaging

MCF7 and HeLa cells were seeded at a density of approximately 1.5×10^5 cells per dish and transfected with 1 µg mEm-CTNNA1 and 0.5 µg mRFP-LC3 using Mirus Bio *TransIT*®-2020, per well of a 6-well plate. Cells were placed in EBSS with HEPES and immediately after, imaged at 37 °C on an incubated Zeiss AxioObserver Z1 microscope with a LSM780 confocal attachment using a 63× 1.4 NA Plan Aplanachromat oil-immersion lens.

Cell lysis and western blot analysis

Cells were seeded and cultured in 6 or 12 well plates. Cells were washed twice in cold phosphate buffered saline (PBS) and lysed in either RIPA buffer (150 mM NaCl, 1% NP40, 0.5% NaDoc, 0.1% SDS, 50 mM Tris/HCl pH 7.4 - all from Sigma Aldrich) containing protease and phosphatase inhibitors (from Roche Diagnostics) or directly in 1x Laemmli Sample buffer (diluted from 2x Laemmli Sample Buffer #161-0737 BioRad), on ice. The samples lysed in RIPA buffer were incubated 30 min on ice to ensure complete lysis, and then centrifuged at 16000 xg for 10 min at 4 °C, to pellet the cellular debris. The supernatant of each sample was collected in a separate E-tube and diluted with 2x Laemmli Sample Buffer (161-0737 BioRad) and boiled for 10 min at 100 °C. For western blot analysis, samples were subjected to an SDS-PAGE separation and transferred on PVDF membranes. PVDF membranes were blocked with 4% skim-milk in PBS containing 0.1% Tween for 1 h and incubated with primary antibody at 4 °C overnight. After washing with 0.1% Tween-PBS, the membranes were incubated with secondary antibody for 90 min at RT and subjected to protein visualizing using either LI-COR Odyssey scanner or the ECL enhanced chemiluminescence detection kit from GE Healthcare.

Cytoplasmic/Nuclear Fractionation

Nuclear and cytoplasmic fractionation was performed using NE-PER Nuclear and Cytoplasmic Extraction Kit (Cat# 78833 Thermofisher), according to the manufacturer's instructions.

Luciferase reporter assay

Luciferase reporter assay was performed using the Dual-Glo luciferase assay system kit (E1910 Promega), following the protocol previously described (Pavel et al., 2018a). Briefly, cells were co-transfected with 1 µg of luciferase reporter (8XGTIC) together with 0.1 µg of renilla luciferase for 24 h per well in 6 well plates. Transfected cells were lysed in 200 µl of 1x Passive lysis buffer for 15 min at RT and collected by scraping in E-tubes. After centrifugation at 16000 xg for 10 min, 20 µl of supernatant from each lysed sample were transferred in triplicate in a 96 wells microplate and mixed with 100 µl of Luciferase Assay Reagent II (LARII). The firefly luciferase activity was measured using a SPARK multimode microplate reading Luminometer (TECAN Trading AG). The renilla luciferase activity was measured immediately after adding 100 µl of Stop & Glo reagent to the reaction.

Immunoprecipitation

For immunoprecipitation of mEmerald-tagged proteins using the GFP-Trap method (gtma-100, ChromoTek), cells were lysed with lysis buffer (10 mM Tris/Cl pH 7.5; 150 mM NaCl; 0.5 mM EDTA; 0.5% NP-40) containing protease and phosphatase inhibitors from Roche Diagnostics for 30 min at 4 °C. The lysed cells were centrifuged at 13000 xg for 10 min and the supernatant transferred to a new E-tube and mixed with dilution buffer (10 mM Tris/HCl pH 7.5; 150 mM NaCl; 0.5 mM EDTA). For each sample, 50 µl of supernatant were mixed with 2x Laemmli buffer, boiled at 100 °C for 10 min and used for input loading. The samples were further incubated with pre-washed 25 µl of GFP-Trap beads for 1 h at 4 °C on a rotating surface. GFP-beads were washed three times with dilution buffer, resuspended with 2x Laemmli buffer and boiled at 100 °C for 10 min.

Immunoprecipitation of Flag-tagged proteins was performed with anti-Flag M2 Magnetic Beads (M8823, Sigma-Aldrich). Cells were lysed with NETN lysis buffer (20 mM Tris/Cl pH 7.5; 100 mM NaCl; 0.5 mM EDTA, 0.5% NP-40, supplemented with protease and phosphatase inhibitors cocktails (Roche)) for 30 min at 4 °C. The lysed cells were centrifuged at 16000 xg for 10 min and then the supernatants were collected into new E-tubes. For each sample, 50 µl of supernatant were mixed with 2x Laemmli buffer, boiled at 100 °C for 10 min and used for input loading. The samples were mixed with anti-Flag M2 Magnetic Beads and incubated at 4 °C overnight on a rotating surface. After five times washing, Flag beads were denatured with 2x Laemmli buffer and boiled at 100 °C for 10 min.

For immunoprecipitation of endogenous protein, cells were incubated with ice-cold NETN buffer for 30 min at 4 °C. After centrifugation of lysed cells at 16000 xg for 10 min, supernatants were collected into separate tubes and incubated with primary antibodies at 4 °C overnight. The following day, the immune-complexes were cleared with 20 µl of Dynabeads-Protein G (10004D, Life technologies) for 2 h at 4 °C and then, purified by boiling in 2x Laemmli buffer for 10 min.

Purification of recombinant LC3 and protein binding assay

LC3 was purified as described by Puri et al. 2020 (Puri et al., 2020). Briefly, LC3B was expressed using a pGEX-6p1 plasmid in *E. coli* for 3 h at 37 °C after induction with 1 mM IPTG. Cells were lysed in 50 mM Tris pH 7.4, 150 mM NaCl using a sonicator in the presence of proteases inhibitors and centrifuged at 180000 xg for 30 min at 4 °C. The supernatant was incubated with glutathione-Sepharose 4B beads followed by extensive washes in lysis buffer. PreScission Protease (27-0843-01, GE Healthcare) was added at 100 units/ml in a 2-bed volume of PreScission Buffer (50 mM Tris/HCl pH 7.5, 150 mM NaCl, 1 mM EDTA) freshly

prepared with 1 mM DTT and cleavage was performed overnight at 4 °C. Cleaved protein was eluted and stored at -80 °C.

Binding of LC3B (purified from *E. coli*) to CTNNA1 (TP301776, Origene) was performed by incubation of recombinant proteins at 25 °C for 1 h, followed by immunoprecipitation with rabbit anti-CTNNA1 antibody (ab51032, Abcam, 1:100) and processed for WB analysis.

Structural analysis of α -catenin

Visualization and generation of graphic illustrations of the molecular models of human CTNNA1 (pdb. 4IGG [<http://doi.org/10.2210/pdb4IGG/pdb>])(Rangarajan and Izard, 2013) were performed using the PyMOL Molecular Graphics System, Version 2.0 Schrödinger, LLC (<http://www.pymol.org>). The pdb. 4IGG [<http://doi.org/10.2210/pdb4IGG/pdb>] (Rangarajan and Izard, 2013) shows the structure of dimeric CTNNA1 (aminoacid sequences 82-878 and 82-861, respectively). As the 891-906 region is not included in the pdb. 4IGG [<http://doi.org/10.2210/pdb4IGG/pdb>] (Rangarajan and Izard, 2013), this aminoacid sequence was computed using Phyre2. The amino acids shown in blue and green were mutated for each potential LIR region, while the amino acids coloured in orange-purple corresponds to the LIR regions that were not mutated (those amino acids are facing the interior of the CTNNA1 molecule and therefore they are unlikely to interact with LC3).

Bioinformatic analysis of putative LIR regions

Many Atg8/LC3/GABARAP-interacting proteins, contain a basic hydrophobic LIR motif with the core consensus sequence (WFY) xx (ILV). The residues marked in bold (positions 3 and 6) correspond to the most crucial residues for the interaction with Atg8-family proteins(Alemu et al., 2012). The iLIR database (<https://ilir.warwick.ac.uk>), a freely available web resource(Jacomin et al., 2016), was used to identify the potential 6 LIR regions in the CTNNA1/2/3 aminoacids sequences. For CTNNA1, the putative LIR regions correspond to: 146 DVYKLL 151, 175 IQYKAL 180, 243 LIYKQL 248, 417 KEYAQV 422, 509 DDFLAV 514, 617 LVIYDGI 622. The LIR region (895 QALSEF 900) was determined experimentally, as expression of the construct GFP-alpha-E-Catenin 3xFP4 (895) (no. 67936, Addgene) (Leerberg et al., 2014), which lacks the last 11 amino acids of the full length Ctnna1 (896 ALSEFKAMDSI 906), did not show accumulation within mRFP-LC3 vesicles by live cell imaging.

Statistical analysis

Densitometry of western-blot bands was performed using either ImageJ (when using ECL-protein revealing) or Image Studio (for LI-COR protein revealing). The graphs show the mean of independent experiments. One sample t- test (when the control was initially set up to 100 %), two-tailed Student's t-test, two way ANOVA, chi-squared test and multinomial logistic regression were used to quantify p-values in Origin v8.1 or SPSS Statistics v25.0. The statistical details of all experiments (including *n* numbers, error bars, *P*-value statistical significance and the statistical test performed) are reported in the figure legends. The colocalization Mander's and Pearson's coefficients were analysed using both ImageJ and Volocity softwares.

1.2.1.4. Results

YAP/TAZ activity is inhibited by autophagy compromise in MCF10A cells

We previously reported that the transcriptional regulators YAP/TAZ induce autophagy by altering the expression of actin cytoskeleton genes in various cell lines: MCF10A, HeLa, HaCaT cells, primary mammary epithelial cells (pMECs) and primary mouse embryonic fibroblasts (pMEFs) (Pavel et al., 2018a). Here, we examined if an initial perturbation in the

autophagy pathway would impact YAP/TAZ activity. Depletion of key genes governing autophagosome biogenesis by single ATG16L1 or double ATG7/ATG10 knockdowns in MCF10A cells shifted YAP/TAZ localisation from the nucleus (where they are transcriptionally active) to the cytoplasm (where they are inactive) (Fig. 1A,B), and decreased TEAD luciferase activity (a reporter for YAP/TAZ activities, since YAP/TAZ activate TEAD transcription factors) (Fig. 1C). We confirmed these data in HEK293T cells, which are widely used to study Hippo signalling. Importantly, reduced YAP/TAZ nuclear activities were also seen in primary mammary epithelial cells isolated from mice with a hypomorphic mutation in *Atg16L1*, which results in only modest impairment of autophagy (Cadwell et al., 2008; Wu et al., 2016) (Fig. 1D-F).

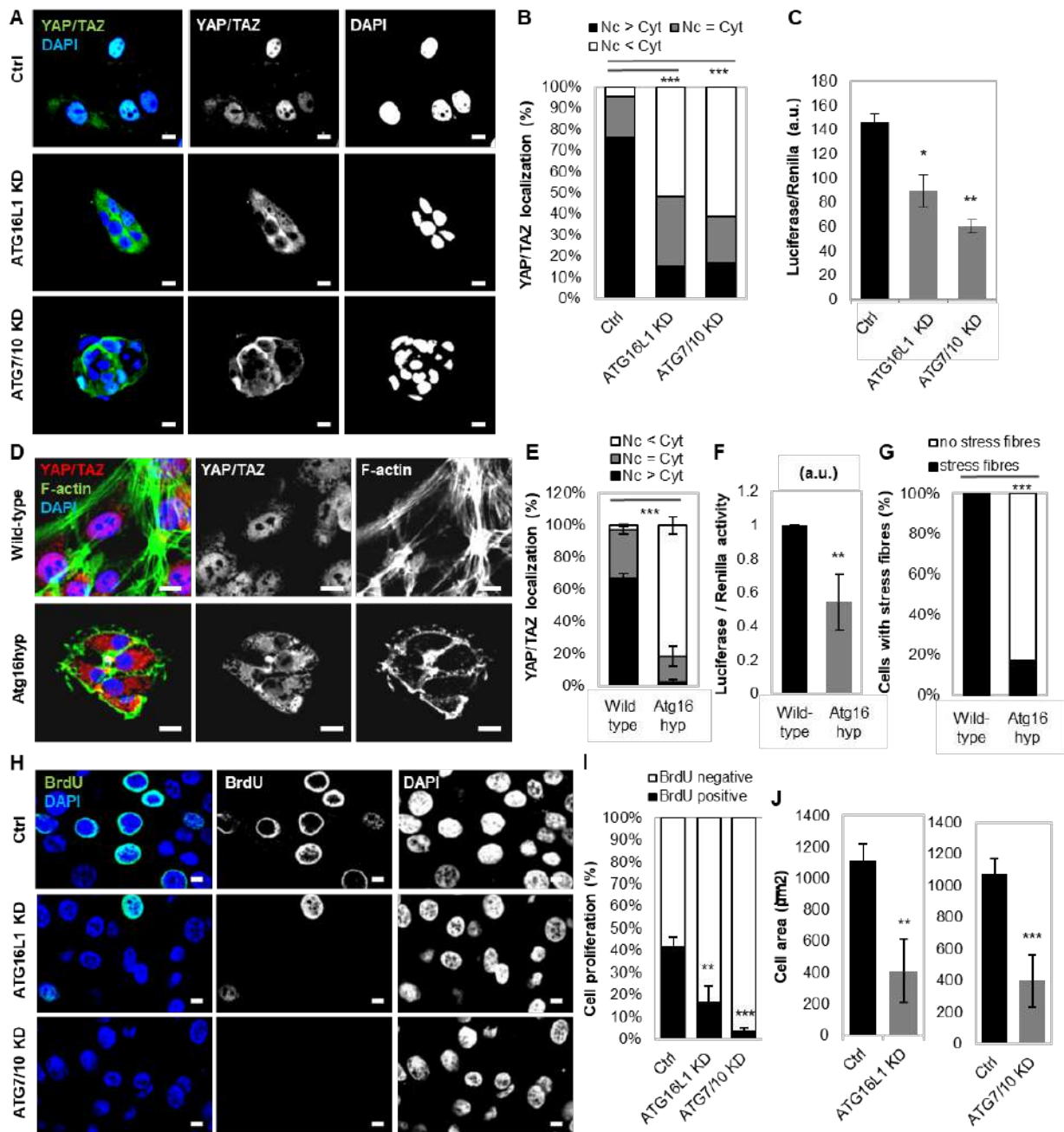


Figure 1. YAP/TAZ activity is inhibited in autophagy-deficient mammary epithelial cells. (A) Representative confocal images of YAP/TAZ endogenous immunostaining in MCF10A cells exposed to control, ATG16L1 or ATG7/10 siRNAs. DAPI=nucleus. Scale bars are 10 µm. The experiment was repeated twice with similar results. (B) YAP/TAZ localisation (nuclear—Nc or

cytoplasmic—Cyt) in MCF10A cells exposed to control, ATG16L1 or ATG7/10 siRNAs ($n = 126$ (Ctrl), 170 (ATG16L1 KD), 166(ATG7/10 KD) cells; **** $P < 0.0001$; chi-squared test). The experiment was repeated twice with similar results. (C) Luciferase assay for YAP/TAZ activity in MCF10A cells exposed to control, ATG16L1 or ATG7/10 siRNAs. Bars represent the mean \pm s.d. ($n = 3$ independent experiments; ** $P < 0.01$, * $P < 0.05$; two-tailed one sample t -test). (D) Representative confocal images of endogenous YAP/TAZ and F-actin (Phalloidin) in primary mammary epithelial cells (pMECs) isolated from wild-type and Atg16L1 hypomorph (Atg16hyp) mice. Scale bars are 10 μ m. The experiment was repeated twice with similar results. (E) YAP/TAZ localisation in wild-type ($n = 3$ mice) and Atg16hyp ($n = 4$ mice) pMECs. Bars represent the mean \pm s.d. (**** $P < 0.0001$; two-way ANOVA). (F) Luciferase assay for YAP/TAZ activity in wild-type and Atg16hyp pMECs. Bars represent the mean \pm s.d. ($n = 3$ mice; ** $P < 0.01$; two-tailed one sample t -test). (G) Percentage of cells with F-actin stress fibres in wild-type and Atg16hyp pMECs ($n = 98$ (wild-type) and 292 (Atg16hyp) cells; **** $P < 0.0001$; chi-squared test). The experiment was repeated twice with similar results. (H) Representative images of BrdU immunostaining in MCF10A cells exposed to control, ATG16L1 or ATG7/10 siRNAs. Scale bars are 10 μ m. The experiment was repeated twice with similar results. (I) The graphs show the percentages of BrdU-positive MCF10A cells, after exposure to control, ATG16L1 or ATG7/10 siRNAs: mean \pm s.d. ($n = 3$ independent experiments; **** $P < 0.0001$, ** $P < 0.01$; two-tailed t -test). (J) Size of autophagy inhibited cells: MCF10A cells exposed to control, ATG16L1 ($n = 3$ independent experiments) or ATG7/10 ($n = 5$ independent experiments) siRNAs. Confocal images of each cell type were analysed to measure cell area using ZEN software. Bars represent the mean \pm s.d. (**** $P < 0.0001$, ** $P < 0.01$; two-tailed t -test). Exact P values for asterisks: C (from left to right) 0.0132, 0.0010; F 0.0033; I 0.0058; and J 0.0061.

Consistent with the impaired actin stress-fibre formation known to result from YAP/TAZ inhibition (Pavel et al., 2018a), we observed reduced stress-fibre formation and myosin-II levels in autophagy-compromised cells (Fig. 1D,G). Additionally, cell proliferation (Johnson and Halder, 2014; Moroishi et al., 2015; Totaro et al., 2018; Yu et al., 2015) (as assessed by BrdU positivity) and cell area (Perez Gonzalez et al., 2018; Tumaneng et al., 2012), which are positively regulated by YAP/TAZ, were significantly reduced in autophagy-depleted MCF10A cells (Fig. 1H-J).

Similar phenomena were observed for primary mammary epithelial cells (pMECs), HEK293T and HeLa cells (Fig. 2A,B). In 3D cell culture systems, one of the hallmarks of reduced YAP/TAZ activity is the formation of spherical cellular structures (acini) (Aragona et al., 2013a; Panciera et al., 2017; Totaro et al., 2019). Indeed, in soft matrix conditions (characterised by inactive, cytoplasmic YAP/TAZ (Dupont et al., 2011a; Pavel et al., 2018a)), control MCF10A cells form spherical acini structures, while, when grown in stiff extracellular collagen matrix, the cells start to lose their intimate contacts and spread to form arborescent, disorganised cellular branches. Interestingly, upon autophagy inhibition this stiff-matrix phenotype was reversed to soft-like cellular compact structures (Fig. 2C,D). Moreover, the diameter of the acini was diminished upon downregulation of autophagy genes (Fig. 2E-G).

We next investigated the effect of decreased Atg16L1 levels on the development of mammary acini. Mammary glands isolated from Atg16hyp (hypomorph) female mice at E16.5 gestation had reduced YAP/TAZ immunostaining intensity and smaller acini structures (area and interior perimeter), compared to their wild-type counterparts, confirming the previous data achieved while culturing pMECs isolated from those tissues (Fig. 1D-G, Fig. 2A,B,D-G). Similar 3D culture phenotypes associated with impaired YAP/TAZ activity were achieved upon either lysosome inhibition with bafilomycin A1 (BafA1), which blocks autophagosome degradation, or with chemical suppression of autophagosome biogenesis using a VPS34 selective inhibitor, VPS34-IN1. Thus, autophagy inhibition impairs YAP/TAZ nuclear localisation and activities, leading to cellular phenotypes consistent with suppression of these transcriptional regulators.

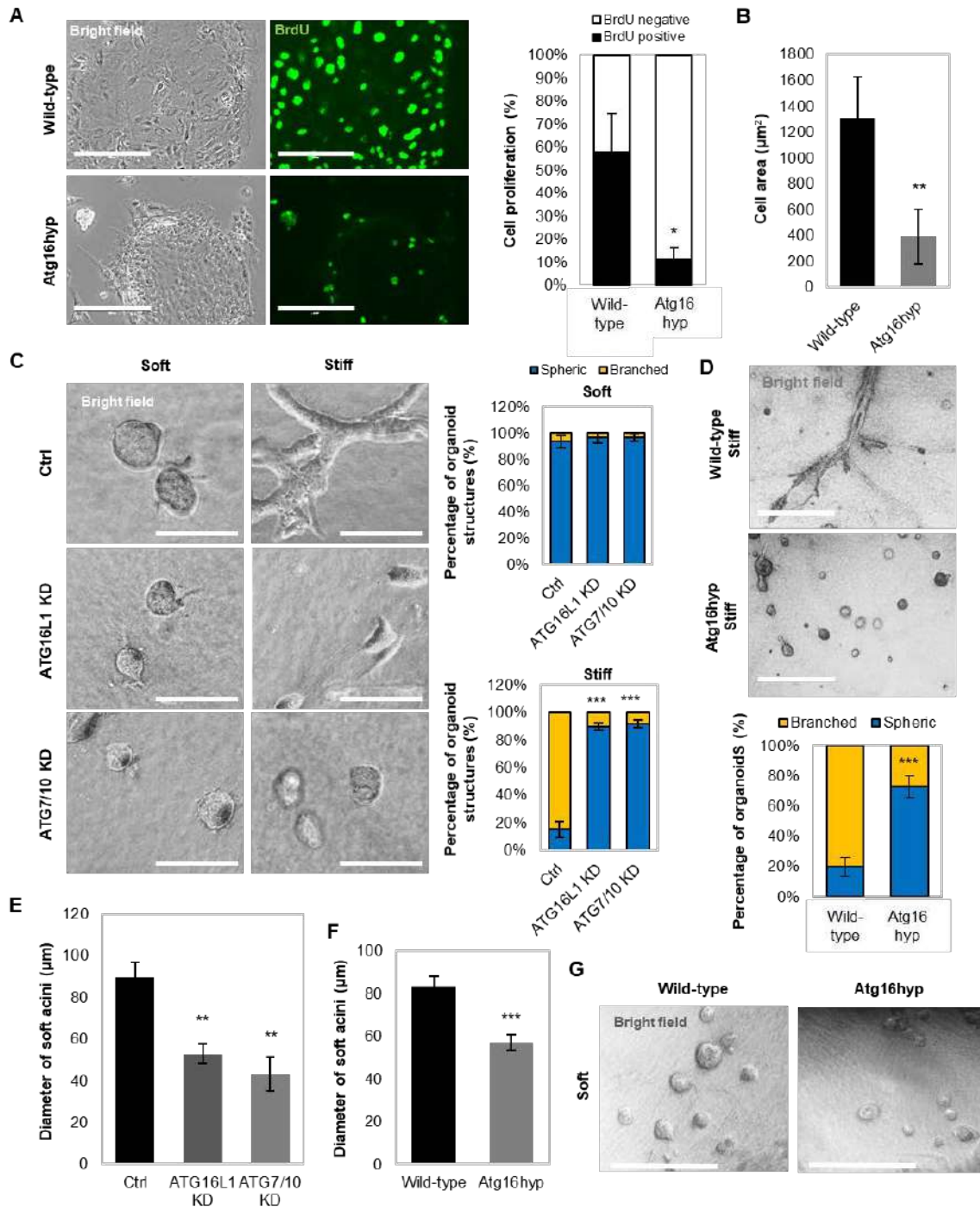


Figure 2. Formation of acini structures is perturbed in autophagy-deficient primary mammary epithelial cells. (A) (left) Representative bright-field images and BrdU immunostaining in primary mammary epithelial cells (pMECs) isolated from wild-type and Atg16L1 hypomorph (Atg16hyp) mice. Scale bars are 200 μm . (right) Percentage of BrdU-positive pMECs isolated from wild-type ($n = 2$) and Atg16hyp ($n = 3$) mice. Bars represent the mean \pm s.d. ($*P < 0.5$; two-way ANOVA). (B) Size of pMECs isolated from wild-type ($n = 3$) and Atg16hyp ($n = 4$) mice. Bars represent the mean \pm s.d. ($**P < 0.01$; two-tailed t -test). (C) Representative confocal images of MCF10A cells plated on either soft or stiff ECM. MCF10A cells were previously exposed to control, ATG16L1 or ATG7/10 siRNAs. Scale bars are 200 μm . The bars represent the percentage of organoid/ spherical structures in soft ($n = 3$ independent experiments) or stiff ($n = 5$ independent experiments) ECM: mean \pm s.d. ($****P < 0.0001$; two-tailed t -test). (D) Representative images of wild-type ($n = 3$ independent experiments) and Atg16hyp ($n = 5$ independent experiments) pMECs plated on stiff ECM. Scale bars are 400 μm . The

bars represent the percentage of branched structures: mean \pm s.d. (**** $P < 0.0001$; two-tailed t -test). (E) Diameter of soft acini in MCF10A cells exposed to control, ATG16L1 or ATG7/10 siRNAs. Bars represent the mean \pm s.d. ($n = 3$ independent experiments; ** $P < 0.01$; two-tailed t -test). (F) Diameter of soft acini in wild-type or Atg16hyp pMECs. Bars represent the mean \pm s.e.m. ($n = 33$ (wild-type), $n = 27$ (Atg16hyp) soft acini; *** $P < 0.001$; two-tailed t -test). The experiment was repeated with similar results. (G) Representative images of wild-type and Atg16hyp pMECs plated on soft ECM. Scale bars are 400 μm . The experiment was repeated twice with similar results. Exact P values for asterisks: A 0.0163; B 0.0050; E (from left to right) 0.0017, 0.0018; and F 0.0001.

YAP/TAZ activity is up-regulated by autophagy activation in MCF10A cells

To examine the consequences on YAP/TAZ when autophagy is upregulated, we either cultured confluent MCF10A cells in EBSS (to mimic starvation-induced autophagy) or exposed them to well characterised autophagy activators: Tat-Beclin1, Trehalose or SMER28. All these conditions induced nuclear translocation of YAP/TAZ, the formation of stress fibres and increased the cell area in 2D cultures (Fig. 3A-I, Fig. 4A-F). Confluent MCF10A cells, with lower initial YAP/TAZ nuclear fractions (Pavel et al., 2018a), were used in these experiments in order to emphasize the YAP/TAZ activation mediated by autophagy induction. In 3D soft-matrix conditions, these autophagy enhancers promoted the formation of branched disorganised structures rather than spherical organoids (Fig. 4G-J).

Direction of the YAP/TAZ response to autophagy perturbation is inverted in HepG2 cells

Intriguingly, our data outlined above contrast with previous published literature claiming that autophagy inhibition activates YAP/TAZ and promotes their nuclear localisation. This was attributed to YAP being a direct autophagy substrate (Lee et al., 2018; Wang et al., 2019). Accordingly, we investigated the effect of autophagy inhibition in HepG2 cells, as one of these two studies focused on liver systems (Lee et al., 2018). Consistent with the published data, downregulation of key autophagy genes in HepG2 cells promoted YAP/TAZ activity and nuclear localisation. Therefore, we hypothesised that the cells we studied (MCF10A, HEK293, HeLa cells and pMECs) have means to counter autophagic degradation of YAP (Lee et al., 2018; Wang et al., 2019), in order to increase YAP/TAZ activity in parallel with autophagic induction.

Autophagy inhibition causes accumulation of α -catenins

In order to identify plausible autophagy substrates responsible for YAP/TAZ inhibition, we performed SILAC experiments and identified the most abundant proteins that accumulated under prolonged BafA1 treatment (24 hours). Among well-known autophagy substrates (NCOA4, TAX1BP1, NBR1, SQSTM/p62) we also identified CTNNA3, one of the three α -catenins (Fig. 5A). α -catenin is known to sequester and inhibit YAP/TAZ in the cytosol (Schlegelmilch et al., 2011) and this may explain the why YAP/TAZ are inhibited in the cell lines we initially studied after autophagy inhibition. We confirmed the SILAC data by showing that endogenous α -catenins (CTNNA3 and CTNNA1) accumulated after double ATG7/ATG10 knockdowns (Fig. 5B,C), BafA1 treatment, or single ATG16L1 knockdown in MCF10A cells.

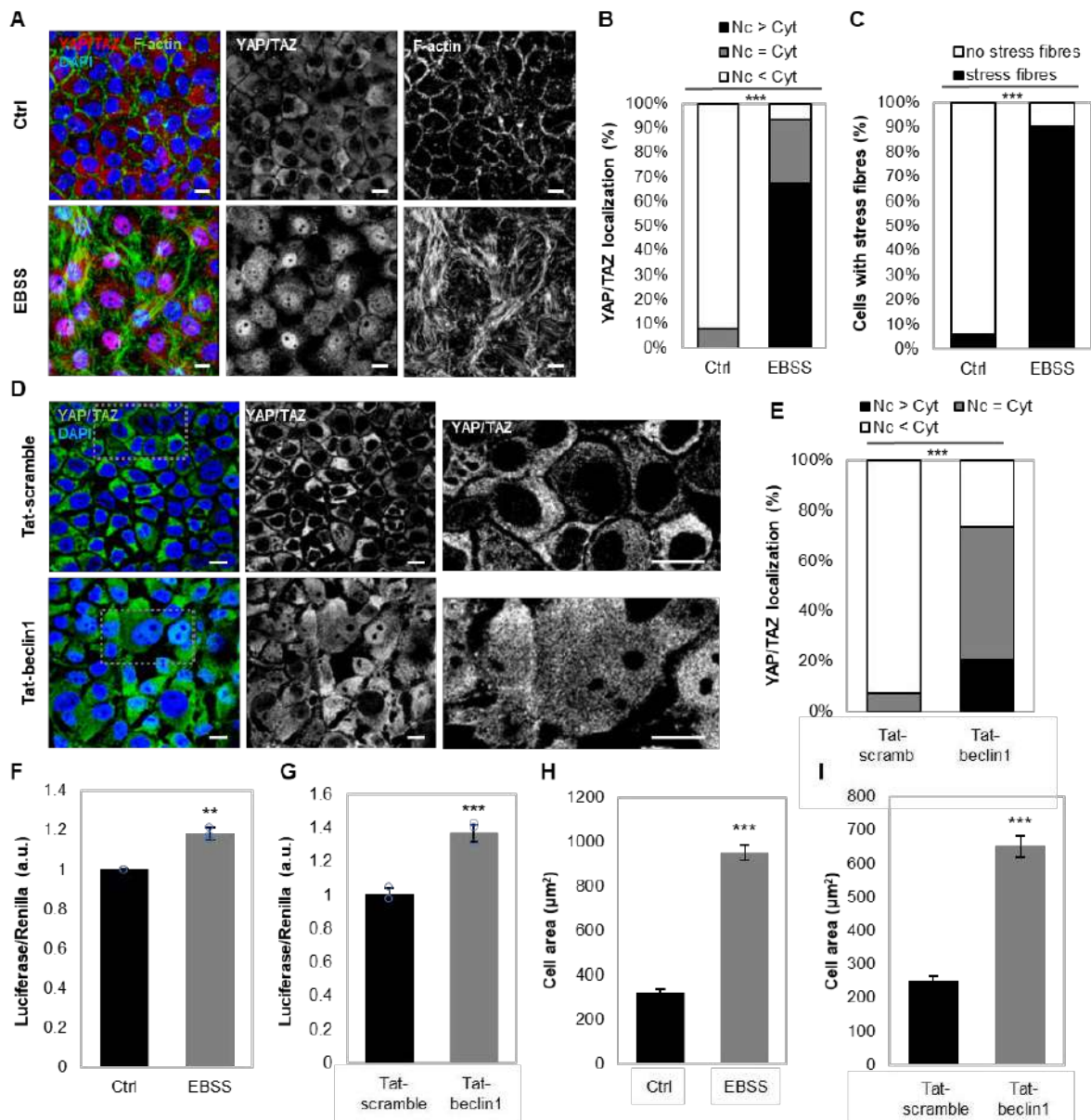


Figure 3. YAP/TAZ is activated upon autophagy induction (EBSS, Tat-beclin1) in MCF10A cells. (A) Representative confocal images of YAP/TAZ and F-actin (phalloidin) immunostaining in MCF10A cells cultured at high confluency in EBSS for 6 h. Scale bars are 10 μm . The experiment was repeated twice with similar results. (B) YAP/TAZ localisation in MCF10A cells exposed to EBSS for 6 h ($n = 143$ cells (Ctrl), $n = 146$ cells (EBSS); $****P < 0.0001$; chi-squared test). The experiment was repeated twice with similar results. (C) Percentage of MCF10A cells with stress fibres upon starvation (EBSS, 6 h) ($n = 143$ cells (Ctrl), $n = 146$ cells (EBSS); $****P < 0.0001$; chi-squared test). The experiment was repeated twice with similar results. (D) Representative confocal images of YAP/TAZ immunostaining in MCF10A cells cultured at high confluency and exposed to either Tat-scramble (control) or Tat-beclin1 peptide (20 μM , 48 h). Scale bars are 10 μm . The experiment was repeated twice with similar results. (E) YAP/TAZ localisation in MCF10A cells exposed to either Tat-scramble (control) or Tat-beclin1 peptide (20 μM , 48 h) ($****P < 0.0001$; chi-squared test). The experiment was repeated with similar results. (F) TEAD luciferase activity in MCF10A cells starved with EBSS for 6 h. Bars represent the mean \pm s.d. ($n = 3$ independent experiments; $**P < 0.01$; two-tailed one sample t -test). (G) TEAD luciferase activity in MCF10A cells treated with Tat-beclin1 peptide (20 μM , 48 h). Bars represent the mean \pm s.d. of a representative experiment performed in triplicates ($***P < 0.001$; two-tailed t -test). (H) Size of MCF10A cells starved in EBSS. Bars represent the mean \pm s.e.m. ($n = 42$ cells, $****P < 0.0001$; two-tailed t -test). (I) Size of MCF10A cells treated with Tat-beclin1 peptide

(20 μ M, 48 h). Bars represent the mean \pm s.e.m. ($n = 45$ cells; **** $P < 0.0001$; two-tailed t -test). Exact P values for asterisks: **F** 0.0096; and **G** 0.0006.

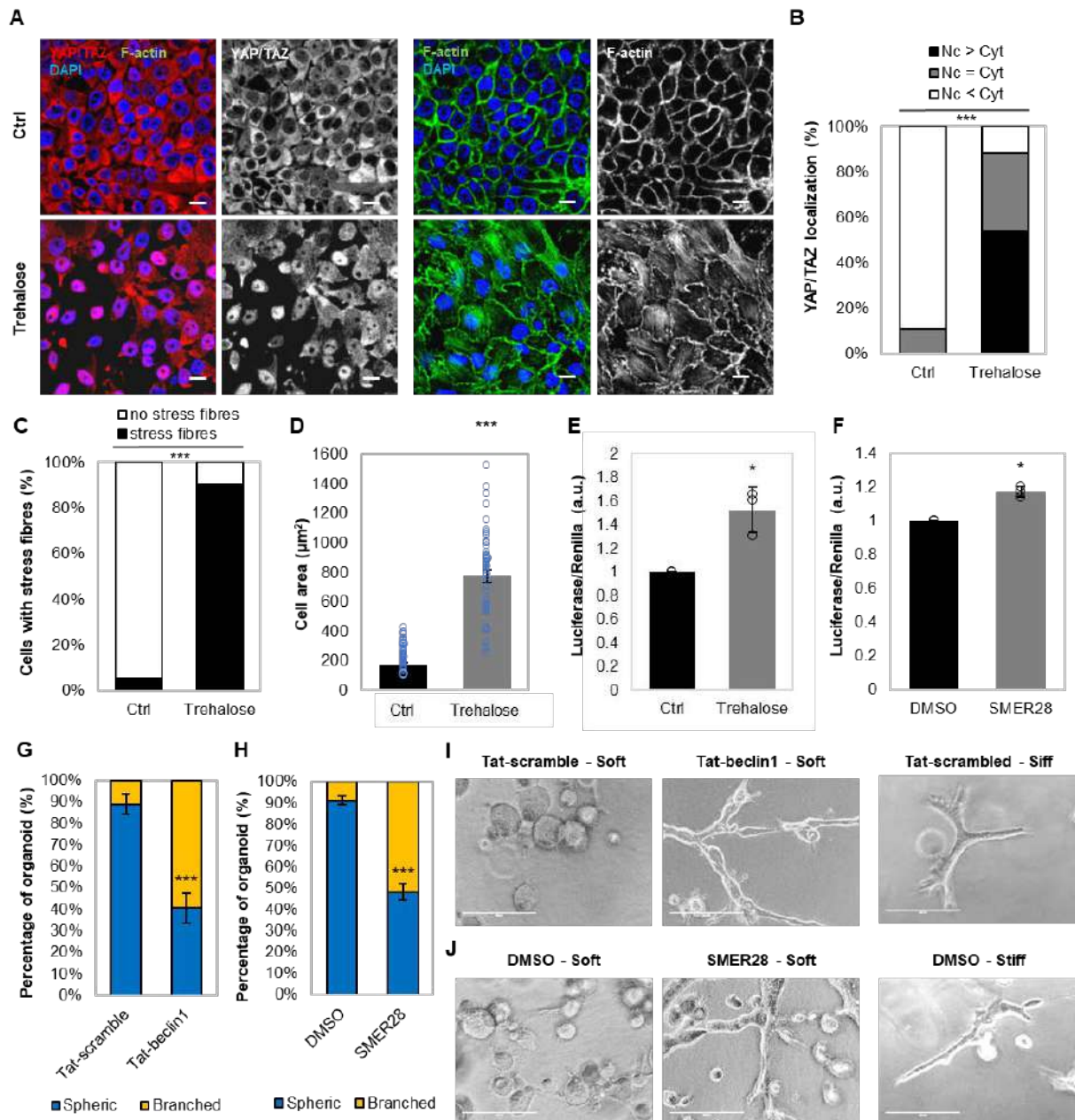


Figure 4. YAP/TAZ is activated upon autophagy induction (Trehalose, SMER28) in MCF10A cells. (A) Representative confocal images of YAP/TAZ and F-actin (phalloidin) immunostaining in MCF10A cells cultured at high confluency and exposed to trehalose (100 mM for 24 h). Scale bars are 10 μ m. The experiment was repeated at least once with similar results. (B) YAP/TAZ localisation in MCF10A cells exposed to trehalose (100 mM for 24 h) with at least 100 cells analysed per condition (**** $P < 0.0001$; chi-squared test). The experiment was repeated with similar results. (C) Percentage of MCF10A cells with stress fibres exposed to trehalose (100 mM for 24 h) ($n = 100$ cells; **** $P < 0.0001$; chi-squared test). The experiment was repeated with similar results. (D) Cell area of MCF10A cells exposed to trehalose (100 mM for 24 h). Bars represent the mean \pm s.e.m. ($n = 50$ cells; **** $P < 0.0001$; two-tailed t -test). (E) TEAD luciferase activity of MCF10A cells treated with trehalose (100 mM for 24 h). Bars represent the mean \pm s.d. ($n = 3$ independent experiments; * $P < 0.05$; two-tailed one sample t -test). (F) TEAD luciferase activity of MCF10A cells treated with SMER28 (50 μ M, 6 h). Bars represent the mean \pm s.d. ($n = 3$ independent experiments; * $P < 0.05$; two-tailed one sample t -test). (G) Quantification of branched and spherical cellular structures of MCF10A cells

exposed to either Tat-scrambled (control) or Tat-beclin1 peptide (20 μ M, 48 h). Bars represent the mean \pm s.e.m. ($n = 3$ independent experiments; *** $P < 0.001$; two-tailed t -test). **(H)** Quantification of branched and spherical cellular structures of MCF10A cells exposed to either DMSO (control) or SMER28 (50 μ M). Bars represent the mean \pm s.e.m. ($n = 3$ independent experiments; **** $P < 0.0001$; two-tailed t -test). **(I)** Representative bright-field images of MCF10A cells exposed to Tat-beclin1 peptide (20 μ M, 48 h) and cultured in soft 3D extracellular matrix. Tat-scrambled was used to treat the control cells. Scale bars are 200 μ m. The experiment was repeated twice with similar results. **(J)** Representative bright-field images of MCF10A cells exposed to SMER28 (50 μ M) and cultured in soft 3D extracellular matrix. DMSO was used to treat the control cells. Scale bars are 200 μ m. The experiment was repeated twice with similar results. Exact P values for asterisks: **E** 0.0421; **F** 0.0113; and **G** 0.0006.

Indeed, primary neurons (Fig. 5D) and primary mammary epithelial cells isolated from Atg16hyp mice had higher levels of endogenous α -catenins, compared to their wild-type littermates. Autophagy inducers (EBSS, Tat-Beclin1) had the opposite effect of reducing endogenous levels of α -catenins (Fig. 5E-G). BafA1 enhanced the levels of transiently expressed mEm-CTNNA1 (Fig. 5H), while SMER28 and EBSS reduced the levels of mEm-CTNNA1 or Flag-CTNNA1 in dose- and time-dependent manners (Fig. 5I).

α -catenins colocalise and directly interact with LC3

We were struck that endogenous CTNNA3 and overexpressed mEm-CTNNA1 colocalised with endogenous LC3 (a marker for autophagosomes) (Fig. 6A,B), and this colocalization was even more obvious after Tat-beclin1 administration (Fig. 6C). Live-cell imaging showed enrichment of mRFP-LC3 positive structures (autophagosomes and autolysosomes) with mEm-CTNNA1 in MCF7 and HeLa cells. The CTNNA1-LC3 interaction was further confirmed by *in vitro* binding assays and by co-immunoprecipitation experiments between endogenous or overexpressed α -catenins and LC3 (Fig. 6D, 7A,B). Additionally, BafA1 treatment enriched mEm-CTNNA1 accumulation in LC3-positive vesicles and increased LC3-CTNNA1 (either endogenous or exogenous) interactions. These data suggest that CTNNA1 is indeed an autophagy substrate and accumulates in autophagosomes.

α -catenins interact with LC3 via LIR domains

As we observed interactions between endogenous or overexpressed α -catenins and LC3 (Fig. 6D, 7A,B) we next searched for potential LC3 interacting regions (LIR) sequences in the structure of α -catenins and identified 7 such putative motifs. We mutated 4 of them (where the amino acids face outwards) and identified highly conserved sites, CTNNA1(Y419A-V422A) and CTNNA1(L897A-F900A), where mutations led to much less LC3 being bound, compared to wild-type CTNNA1, using both GFP- and Flag-trap methods (Fig. 7A-C). Indeed, these two CTNNA1 mutants did not colocalise with LC3, showing a preferentially perinuclear localisation (Fig. 7D,E).

As expected, the single CTNNA1(Y419A-V422A), CTNNA1(L897A-F900A) and double CTNNA1(Y419A-V422A-L897A-F900A) mutants (tagged with either mEmerald or Flag) did not accumulate upon BafA1 treatment (400 nM, 6 h) (Fig. 8A,B) and were not cleared as effectively as the wild-type by autophagy upregulation with SMER28 (20 μ M) or EBSS for 6 h (Fig. 8C-E) in MCF10A cells. These data led us to conclude that CTNNA1 is an autophagy substrate that directly interacts with LC3 via putative LIR motifs.

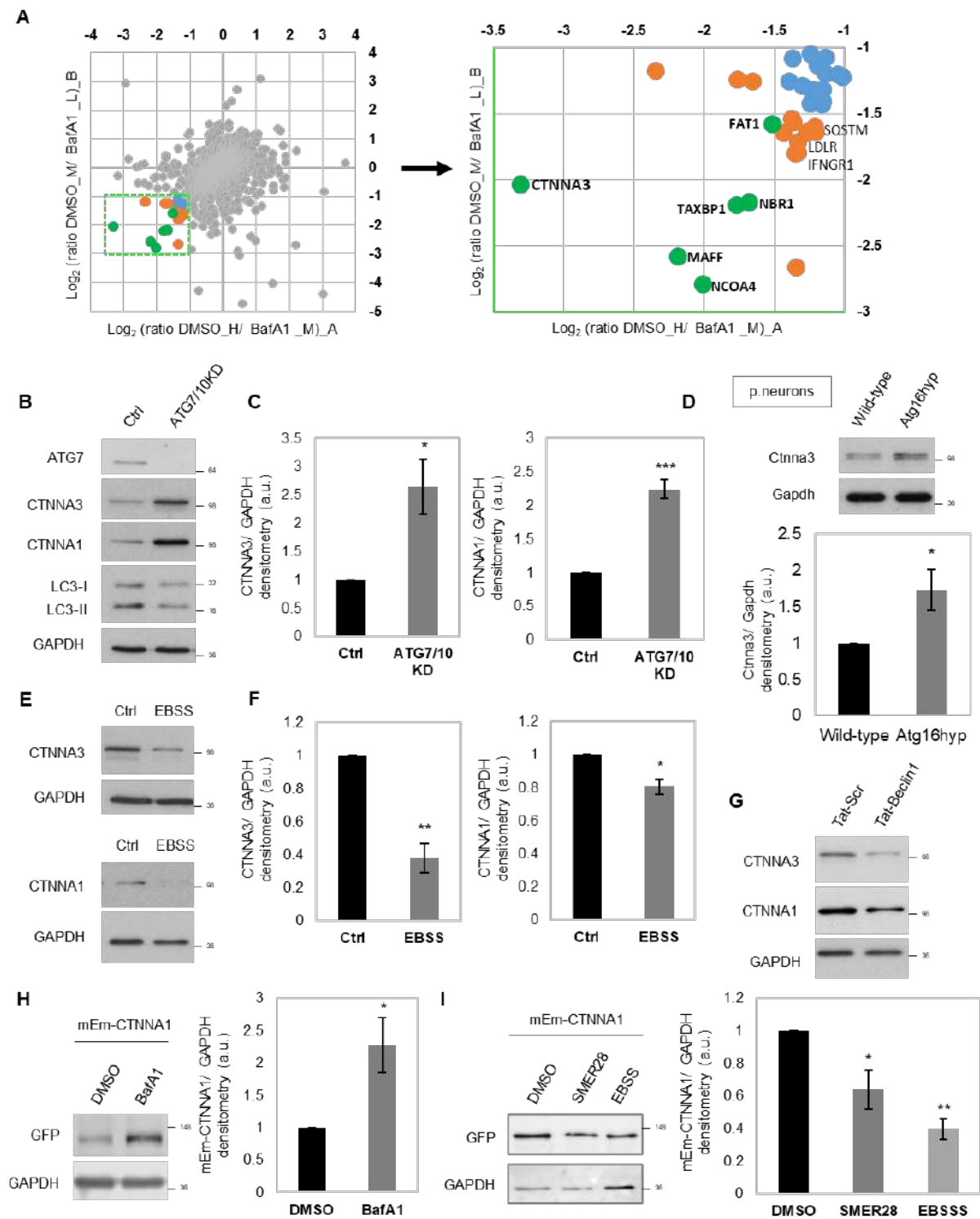


Figure 5. α -Catenins are autophagy substrates. (A) Scatterplot of all proteins uniquely identified in both SILAC experiments (L light, M medium, H heavy amino acids). Fold change (x -axis and y -axis for experiment A and B, respectively) are shown as \log_2 . Scatterplot of the proteins upregulated ≥ 2 fold under bafilomycin A1 (BafA1) treatment is shown on the right. (B) Representative α -catenins (CTNNA3 and CTNNA1) immunoblotting in double ATG7/10 knockdown MCF10A cells. The experiment was repeated at least twice with similar results. (C) CTNNA3/GAPDH (left panel) and CTNNA1/GAPDH (right panel) densitometry in MCF10A cells exposed to either control or ATG7/ATG10 siRNAs. The graphs show the mean \pm s.d. (CTNNA3/ GAPDH, $n = 3$ independent experiments) and mean \pm s.e.m. (CTNNA1/ GAPDH, $n = 5$ independent experiments; *** $P < 0.001$,

* $P < 0.05$; two-tailed one sample t -test). **(D)** Representative immunoblots of Ctnna3 levels in wild-type and Atg16L1 hypomorph (Atg16 hyp) primary cortical neurons. The graph shows the Ctnna3/Gapdh levels: mean \pm s.d. ($n = 3$ independent experiments; * $P < 0.5$; two-tailed one sample t -test). **(E)** Representative α -catenins (CTNNA3 and CTNNA1) immunoblots in MCF10A cells under starvation with EBSS (6 h). The experiment was repeated at least twice with similar results. **(F)** CTNNA3/GAPDH (left panel) and CTNNA1/GAPDH (right panel) densitometry in MCF10A cells starved in EBSS for 6 h. The graphs show the mean \pm s.d. ($n = 3$ independent experiments; ** $P < 0.01$, * $P < 0.05$; two-tailed one sample t -test). **(G)** Representative α -catenins (CTNNA3 and CTNNA1) immunoblots in MCF10A cells treated with the autophagy inducer Tat-Beclin1 peptide (20 μ M for 48 h). Tat-scrambled peptide was used as control. The experiment was repeated at least twice with similar results. **(H)** Representative immunoblot of mEm-CTNNA1 in MCF10A cells exposed to BafA1 (200 nM, 16 h). The MCF10A cells were transiently transfected with mEm-CTNNA1. The graph shows the mEm-CTNNA1/GAPDH levels: mean \pm s.d. ($n = 6$ independent experiments; * $P < 0.05$; two-tailed one sample t -test). **(I)** Representative immunoblot of mEm-CTNNA1 in MCF10A cells exposed to autophagy inducers: SMER28 (20 μ M) and EBSS for 6 h. The graph shows the mEm-CTNNA1/GAPDH levels: mean \pm s.d. ($n = 3$ independent experiments; ** $P < 0.01$, * $P < 0.05$; two-tailed one sample t -test). Exact P values for asterisks: **C** (from left to right) 0.0280, 0.0009; **D** 0.0461; **F** (from left to right) 0.0069, 0.0181; **H** 0.0301; and **I** (from left to right) 0.0340, 0.0036.

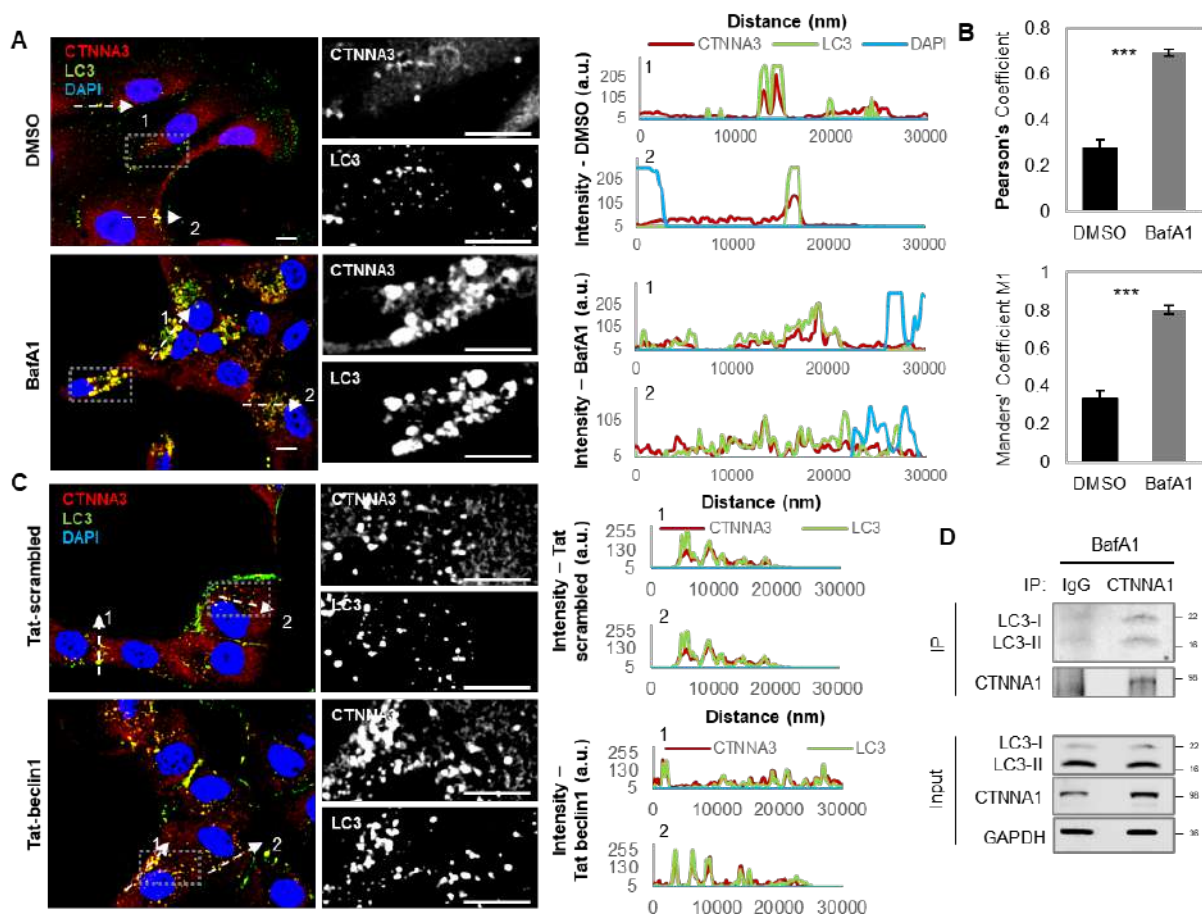


Figure 6. α -Catenins colocalise with LC3. **(A)** Representative images of endogenous CTNNA3–LC3 colocalization in MCF10A cells treated with BafA1. The control cells were treated with DMSO. Scale bars are 10 μ m. The graphs on the right show the image intensities for all channels (CTNNA3, LC3 and DAPI). Scale bars are 10 μ m. The experiment was repeated twice with similar results. **(B)** Quantification of colocalization for the experiment in **(A)**. The Pearson's and Mander's (fraction of CTNNA3 overlapping LC3) coefficients were quantified for $n = 45$ cells (DMSO)

and $n = 38$ cells (BafA1). Bars represent the mean \pm s.e.m. (**** $P < 0.0001$; two-tailed t -test). (C) Representative confocal images of endogenous CTNNA3–LC3 colocalisation in MCF10A cells exposed to either Tat-scrambled or Tat-beclin1 peptide (20 μ M, 48 h). Scale bars are 10 μ m. The graph on the right shows the fluorescent intensity for each channel (red-CTNNA3, green-LC3 and blue-DAPI) along the indicated distances. (D) Co-immunoprecipitation of endogenous LC3 with CTNNA1 in BafA1-treated MCF10A cells. The experiment was repeated three times with similar results.

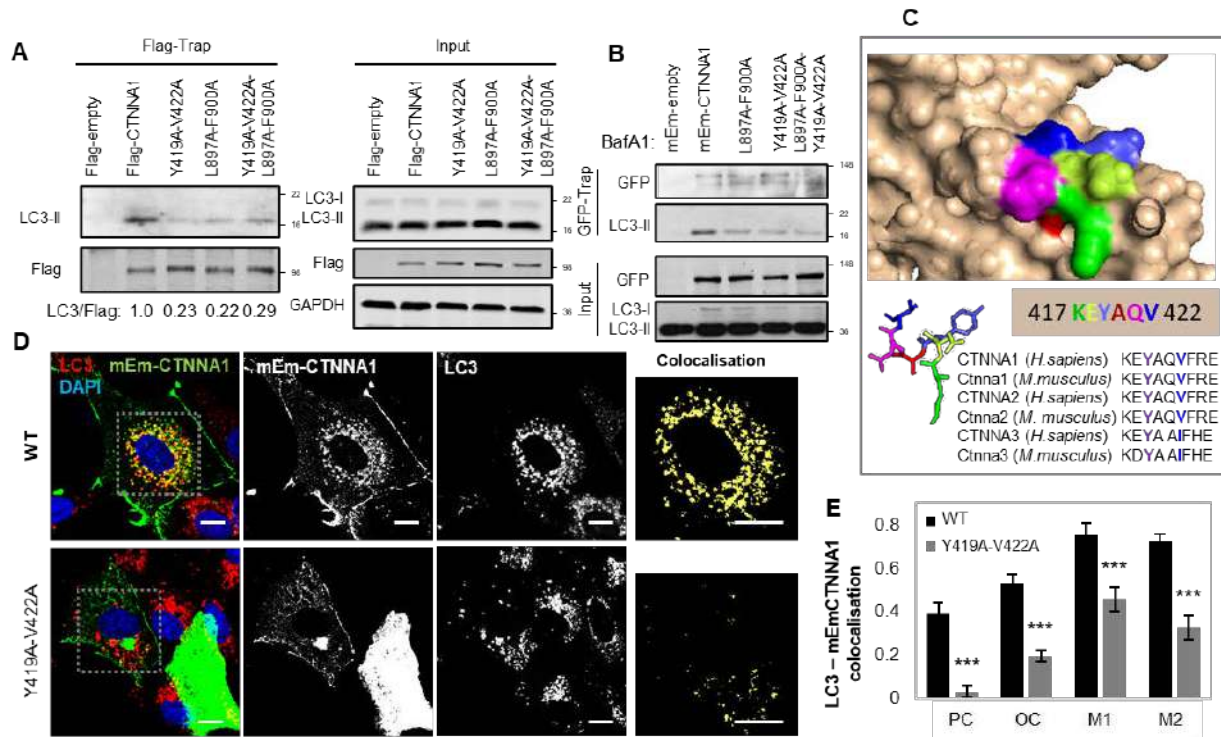


Figure 7. α -Catenins interact with LC3 via two LIR regions. (A) Co-immunoprecipitation of endogenous LC3 with wild-type and Flag-CTNNA1 mutants in BafA1-treated MCF10A cells. MCF10A cells were initially transfected with empty Flag (control vector), wild-type Flag-CTNNA1 or the indicated Flag-CTNNA1 mutants. The Flag-tagged proteins were pulled down using the Flag-Trap technology. The experiment was repeated three times with similar results. (B) Co-immunoprecipitation of endogenous LC3 with wild-type and mEm-CTNNA1 mutants. MCF10A cells were transfected with empty mEm (control vector), wild-type mEm-CTNNA1 or the indicated mEm-CTNNA1 mutants. The mEm-tagged proteins were pulled down using the GFP-Trap technology. The experiment was repeated three times with similar results. (C) 3D structure of the LIR region (417 KEYAQV 422) and its conservation among various species of α -catenins. (D) Representative images of mEm-CTNNA1—endogenous LC3 colocalization in MCF10A cells transiently transfected with either wild-type or Y419A-V422A mEm-CTNNA1. Scale bars are 10 μ m. (E) The Pearson's (PC), Overlap (OC) and Mander's (M1—fraction of LC3 overlapping mEm-CTNNA1, and M2—fraction of mEm-CTNNA1 overlapping LC3) coefficients for MCF10A cells treated as in (D). Thirty-one wild-type cells and 21 Y419A-V422A mutant cells were quantified over three independent experiments. Bars represent the mean \pm s.e.m. (**** $P < 0.0001$, *** $P < 0.001$; two-tailed t -test). Exact P values for asterisks: E 0.0009.

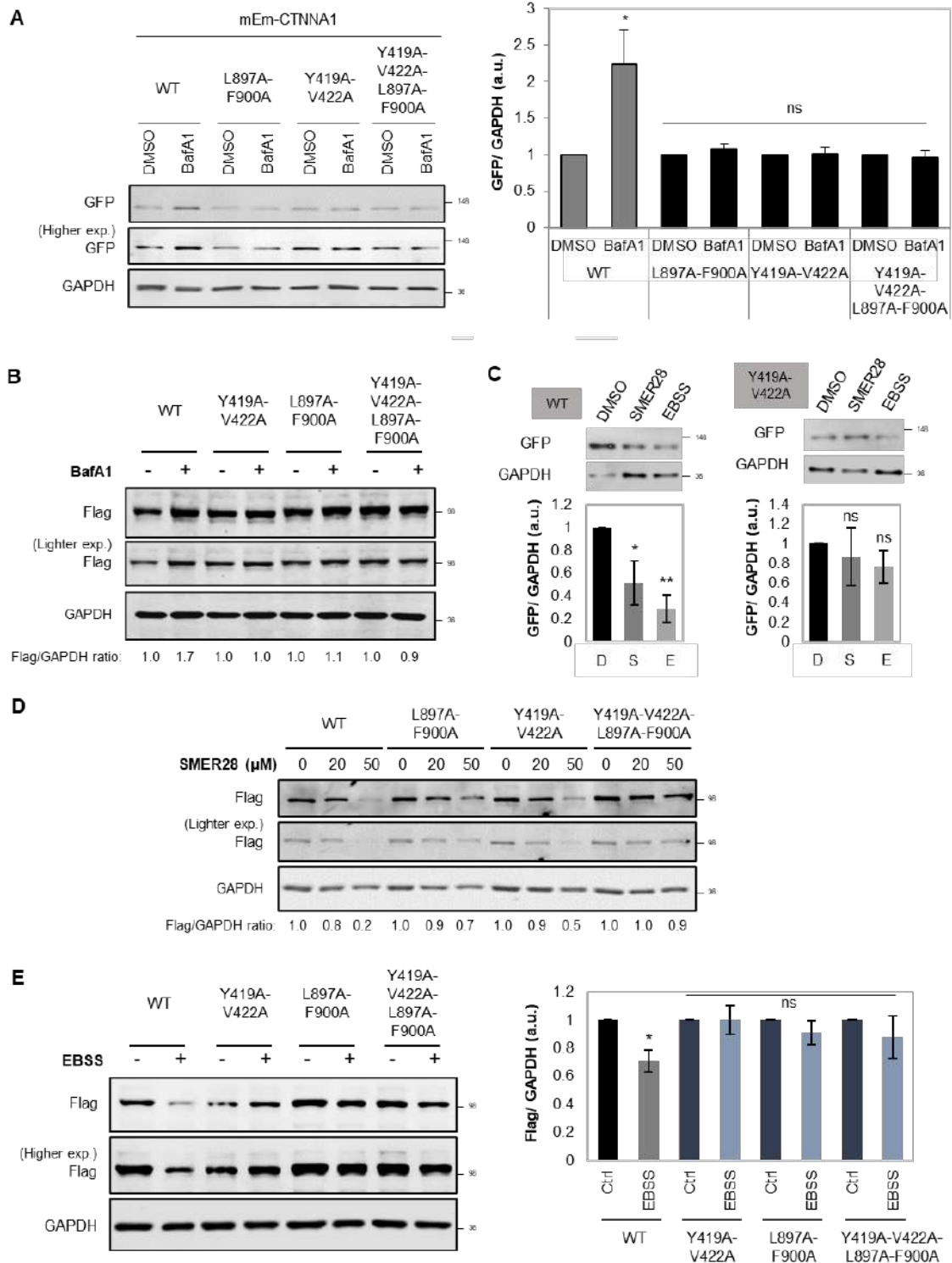


Figure 8. LIR-defective CTNNA1 mutants are not autophagy substrates.

(A) Representative immunoblots of MCF10A cells transiently expressing wild type, L897A-F900A, Y419A-V422A or Y419A-V422A-L897A-F900A mEm-CTNNA1 constructs and exposed to BafA1 treatment (400 nM, 6 h). GFP/GAPDH densitometry is shown on the right: mean \pm s.d. ($n = 5$ independent experiments; $*P < 0.05$, ns not significant; two-tailed one sample t -test). (B) Representative immunoblot of MCF10A cells expressing Flag-wild-type and the indicated CTNNA1 mutants upon BafA1 treatment (400 nM, 6 h). (C) Representative immunoblots of MCF10A cells transiently expressing wild-type or Y419A-V422A mEm-CTNNA1 and exposed to autophagy inducers: SMER28 (20 μ M) and EBSS for 6 h. The graphs show the GFP/GAPDH densitometry of one representative experiment: mean \pm s.d. ($n = 3$ independent experiments; $**P < 0.01$, $*P < 0.05$, ns not

significant; two-tailed one sample *t*-test). The experiment was repeated with similar results. **(D)** Representative immunoblot of MCF10A cells expressing Flag-wild-type and the indicated CTNNA1 mutants upon exposure to different concentrations of SMER28 (20 and 50 μ M) for 24 h. **(E)** Representative immunoblot of MCF10A cells expressing Flag-wild-type and the indicated CTNNA1 mutants upon exposure to EBSS for 4 h. Bars represent the mean \pm s.e.m. ($n = 4$ independent experiments; * $P < 0.05$, ns not significant; two-tailed one sample *t*-test). Exact *P* values for asterisks: **A** (from left to right) 0.0317, 0.1743, 0.4750, 0.3386; **C** (from left to right) 0.0496, 0.0096, 0.5166, 0.1364; **E** (from left to right) 0.0336, 0.9923, 0.3824, 0.4799.

Wild-type α -catenins, and not LIR-defective mutants, are autophagy substrates

As CTNNA1 interacts with YAP/TAZ, we considered if the CTNNA1-LC3 interaction could account for the decrease in YAP/TAZ activity after autophagy inhibition in the cells we studied. Overexpression of CTNNA1(Y419A-V422A), CTNNA1(L897A-F900A) and CTNNA1(Y419A-V422A-L897A-F900AA) mEmerald-tagged mutants reduced the nuclear localization of YAP/TAZ, increasing its cytosolic fraction (Fig. 9A,B) to levels similar to those achieved upon BafA1 treatment (Fig. 9C). These mutants, which have compromised LC3 binding and autophagic clearance, had more marked effects of reducing the YAP nuclear fraction than wild-type CTNNA1, suggesting that YAP/TAZ cytosolic retention in our autophagy-compromised cells may be due to reduced autophagic degradation of α -catenins. The LIR-defective CTNNA1 mutants also reduced the nuclear YAP/TAZ localisation more markedly than wild-type CTNNA1 when expressed in CTNNA1-depleted cells and CTNNA1 knockdown increased the YAP/TAZ nuclear localisation which was reduced upon CTNNA1 (wild-type) re-expression (Fig. 9D). TEAD luciferase activity (Fig. 9E), cell proliferation (Fig. 9F,G), and cell area (Fig. 9H), additional correlates of YAP/TAZ activities, were all decreased in MCF10A cells expressing the LIR defective CTNNA1 mutants to a greater extent than the wild-type protein. To further confirm the role of α -catenins (CTNNA1, CTNNA3) as effectors for the YAP/TAZ phenotype caused by autophagy perturbation, MCF10A cells were initially exposed to ATG7/10 siRNAs for 48 hours in order to reach an autophagy-deficient status, and only after knockdowns, α -catenins were depleted using CTNNA1/3 siRNAs for other 48 hours. While ATG7/10-knockdown caused accumulation of α -catenins and subsequent YAP cytosolic sequestration (Fig. 10A-B) with consequent changes in the actin cytoskeleton morphology (Fig. 10C) and cell area (Fig. 10D) in MCF10A cells, the subsequent knockdown of α -catenins in the autophagy-compromised cells was, indeed, able to partially rescue those previously-perturbed YAP/TAZ-related phenotypes (Fig. 10A-D). Thus, in cells like MCF10A, autophagy positively regulates YAP/TAZ activity by enhancing degradation of α -catenins, which otherwise sequester YAP/TAZ in the cytoplasm.

α -catenins levels determine differential autophagy effects on YAP/TAZ activity

The inhibition of YAP/TAZ upon autophagy suppression was only seen in certain cell types: MCF10A, HEK293T, HeLa and pMECs (Figs. 1-4). The opposite YAP/TAZ response is seen in other cells, including HepG2, THLE2, and A549 cells (Lee et al., 2018; Wang et al., 2019). As we described previously that YAP/TAZ positively regulate autophagosome biogenesis (Pavel et al., 2018a) and our current data suggest that α -catenins (known inhibitors of YAP/TAZ) are autophagy substrates, we considered whether a YAP/TAZ-autophagy-YAP/TAZ feedback loop operates in cells, with starting the levels of α -catenins explaining the output differences among various cellular systems. As autophagy is a dynamic process and we are postulating a feedback loop, we have considered the possibility that one might see different effects on YAP/TAZ activity at various times after initiating the autophagy perturbation. To explore this possibility, we created a numerical mathematical model based on 3 differential

equations to measure the dynamics of autophagy levels, YAP/TAZ activity and levels of α -catenins, when autophagy is primarily impaired.

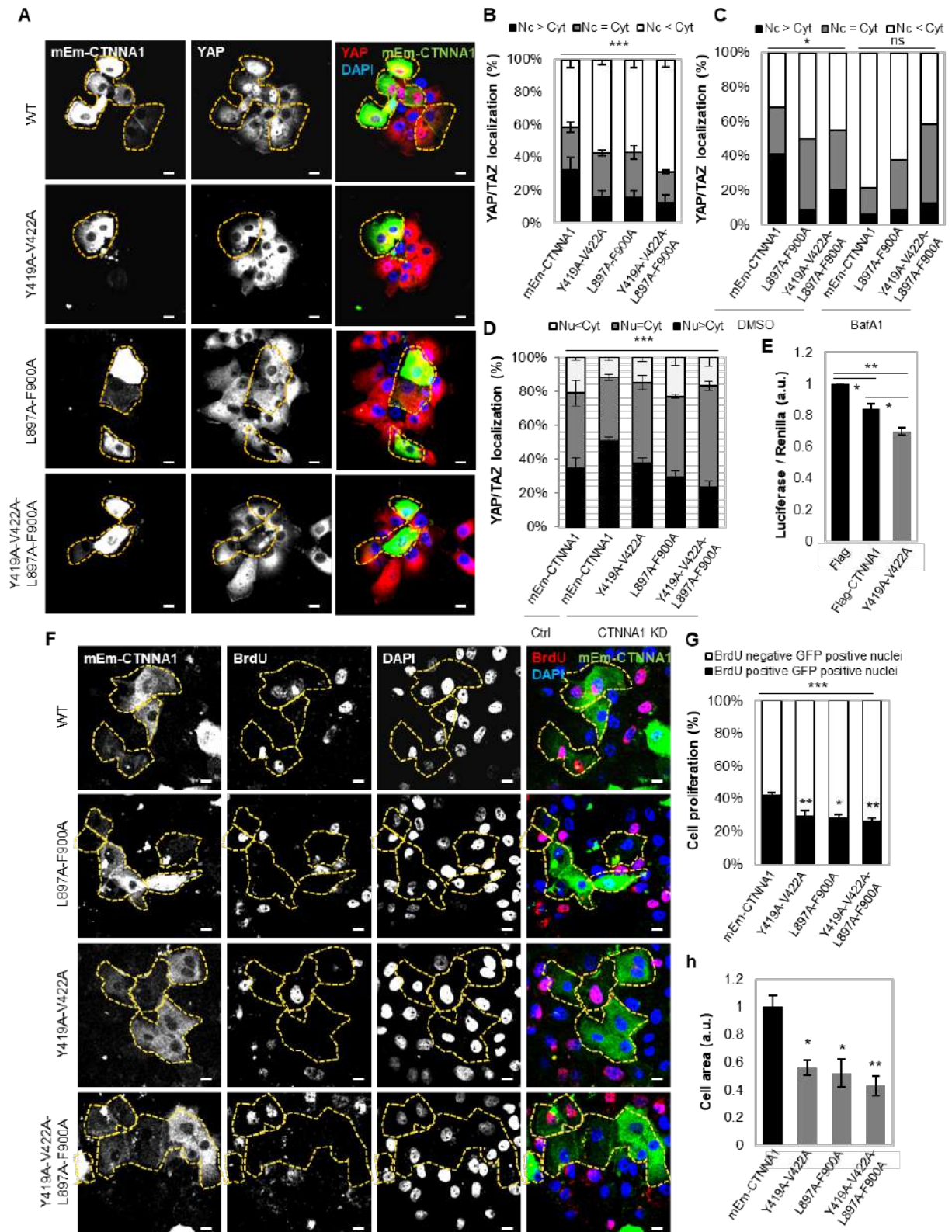


Figure 9. Expression of LIR-defective CTNNA1 mutants inhibits YAP/TAZ activity. (A) Representative confocal images of YAP/TAZ endogenous immunostaining in MCF10A cells expressing either wild-type or mutant (Y419A-V422A, L897A-F900A or Y419A-V422A-L897A-

F900A) mEm-CTNNA1. Scale bars are 10 μm . The experiment was repeated three times with similar results. **(B)** YAP/TAZ localisation in MCF10A cells transfected with wild-type or mEm-CTNNA1 mutants. Bars represent the mean \pm s.e.m. ($n=4$ independent experiments; $***P < 0.001$; two-way ANOVA). **(C)** YAP/TAZ localisation in MCF10A cells transfected with wild-type or mutants of mEm-CTNNA1 upon BafA1 exposure (200 nM, 16 h). Around 100 cells were analysed per condition — $*P < 0.05$, ns not significant; chi-squared test. **(D)** YAP/TAZ localisation in MCF10A cells transfected with wild-type or mutant forms of mEm-CTNNA1 upon α -catenin knockdown. Bars represent the mean \pm s.d. ($n=3$ independent experiments; $****P < 0.0001$; two-way ANOVA). **(E)** TEAD luciferase activity in MCF10A cells expressing either wild-type or mutant (Y419A-V422A) Flag-CTNNA1. Bars represent the mean \pm s.d. ($n=3$ independent experiments; $**P < 0.01$, $*P < 0.05$; two-tailed one sample t -test). **(F)** Representative confocal images of BrdU-positive MCF10A cells transfected with wild-type or mutant forms of mEm-CTNNA1. Scale bars are 10 μm . The experiment was repeated three times with similar results. **(G)** Percentages of BrdU-positive cells in MCF10A cells transfected with wild-type or mutant forms of mEm-CTNNA1. Bars represent the mean \pm s.e.m. ($n=4$ independent experiments; $***P < 0.001$, $**P < 0.01$, $*P < 0.05$; two-way ANOVA). **(H)** Size of MCF10A cells expressing either wild-type or the indicated mEm-CTNNA1 mutants. $n=25$ cells per condition were analysed for measuring cell area using ZEN software. Bars represent the mean \pm s.e.m. ($**P < 0.01$, $*P < 0.05$; two-tailed t -test). Exact P values for asterisks: **B** 0.0003; **E** (from left to right) 0.0146, 0.0022, 0.0049; **G** (from left to right) 0.0043, 0.0207, 0.0019; **H** (from left to right) 0.0153, 0.0102, 0.0010.

This model also took into account the effect of the previously described positive regulation of autophagy by YAP/TAZ (YAP/TAZ inhibition lowers autophagy levels, at both autophagosome biogenesis (Pavel et al., 2018a) and autophagosome-lysosome fusion (Totaro et al., 2019) steps) and the direct effect of autophagy on degrading YAP (Lee et al., 2018). Among the parameters we varied, the initial values of intracellular α -catenins (α -cat) and the strength of the feedback loop (the variable which controls the YAP/TAZ influence over autophagy, v_Y) had the highest impact on the behaviour of the autophagy-YAP/TAZ loop (Fig. 10E). However, the initial intracellular values of α -catenins had the strongest influence over the YAP/TAZ activity upon autophagy depletion in our mathematical model: higher initial α -cat values (>0.5 in Fig. 10E, corresponding to cells with basal α -catenins levels of at least 50 % of those found in MCF10A cells) promoted a reduction in YAP/TAZ activity, while small initial α -cat values (<0.3 in Fig. 10E, corresponding to cell lines with lower initial CTNNA1 levels compared to MCF10A cells by at least 70 %) promoted the opposite effect (of increased YAP/TAZ activity) when autophagy was primarily compromised.

To support these numerical findings, we next assessed the CTNNA1 protein levels in various cell lines. Indeed, cell lines like HEK293T, HeLa, pMECs, which behave similarly to MCF10A cells in relation to the autophagy-YAP/TAZ loop (cells where autophagy compromise inhibits YAP/TAZ activity and autophagy induction promotes YAP/TAZ activity) have higher CTNNA1 levels (the relative ratio of CTNNA1 basal levels > 0.5 , in Fig. 10F,G). On the other hand, cell lines that show decreased YAP/TAZ signalling after autophagy induction (HepG2, THLE2, A549) (Lee et al., 2018; Wang et al., 2019) have lower CTNNA1 levels (the relative ratio of CTNNA1 basal levels being around 0.3 or less – Fig. 10F,G). Our modelling also predicts that cell lines characterised by lower α -cat will accumulate less α -catenins upon autophagy inhibition. To corroborate this effect, ATG7 and ATG10 were depleted in various cell lines. Indeed, HepG2 characterised by low α -cat values, showed small CTNNA1 increases of only 12% and 15%, respectively, when compared to MCF10A (125% increase) or HEK293T (85% increase) cells (Fig. 11A).

Our data posits that starting levels of α -catenins determine the direction of the YAP/YAZ signalling response to autophagy perturbation (Fig. 10G), and can explain the divergent effects of autophagy perturbation on YAP/TAZ signalling in MCF10A cells (high starting levels of α -catenins) versus HepG2 cells (low starting levels of α -catenins).

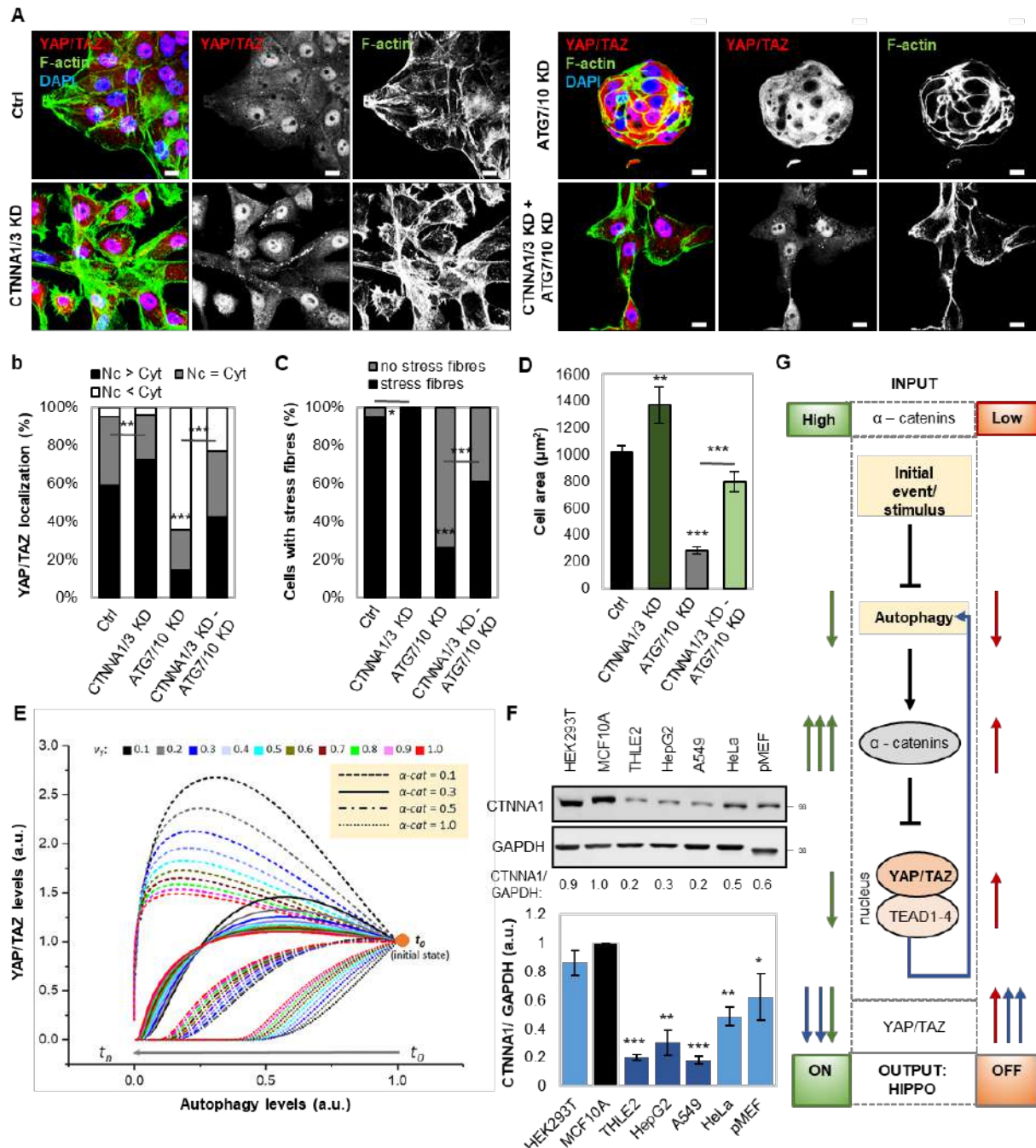


Figure 9. Autophagy regulates YAP/TAZ activity via α -catenins. (A) Representative confocal images of endogenous YAP/TAZ and F-actin immunostaining in MCF10A cells. MCF10A cells were initially exposed to ATG7/10 siRNAs for 48 h, and only after, followed by α -catenin depletion using CTNNA1/CTNNA3 siRNAs (together with ATG7/10 siRNAs) for other 48 h. Scale bars are 10 μ m. The experiment was repeated with similar results. (B) YAP/TAZ localisation in MCF10A cells treated as in (A). CTNNA1/3 KD partially rescues the YAP/TAZ localisation phenotype in ATG7/10 KD cells. The experiment was repeated with similar results (n (from left to right) = 280/304/299/333 cells; $**P < 0.01$, $****P < 0.0001$; chi-square test). (C) Quantification of percentages of MCF10A cells with F-actin stress fibres. MCF10A cells were initially exposed to ATG7/10 siRNAs for 48 h, followed by α -catenin depletion using CTNNA1/CTNNA3 siRNAs for other 48 h. The experiment was repeated with similar results (n (from left to right) = 202/ 200/ 206/ 233 cells; $*P < 0.05$, $****P < 0.0001$; chi-square test). (D) Size of MCF10A cells initially exposed to ATG7/10 siRNAs for 48 h, followed by α -catenin depletion using CTNNA1/CTNNA3 siRNAs for other 48 h. Confocal images of 25 cells per condition were analysed for measuring cell area using ZEN software. Bars represent the mean \pm s.e.m

(**** $P < 0.0001$, ** $P < 0.01$; two-tailed t -test). **(E)** Mathematical modelling of YAP/TAZ activity when reducing autophagy levels. The graph shows the dependency of YAP/TAZ activity on the initial levels of α -catenins and the strength of the feedback loop involving YAP/TAZ control of autophagy v_Y . **(F)** Representative immunoblot of α -catenin in various cell lines. Bars represent the mean \pm s.d. ($n = 3$ independent experiments; **** $P < 0.0001$, ** $P < 0.01$, * $P < 0.05$; two-tailed one sample t -test). **(G)** Model for the autophagy-dependent YAP/TAZ activity in two initial conditions: low and high α -catenin levels. Autophagy inhibition in cells with high initial α -catenin levels promotes α -catenin accumulation which sequester YAP/TAZ into the cytosol (Hippo signalling is ON). However, autophagy inhibition in cells with low initial α -catenin levels causes only a small increase in these proteins, increase unable to sequester YAP/TAZ into the cytosol (as their levels also increase, being also autophagy substrates)—Hippo signalling is OFF.

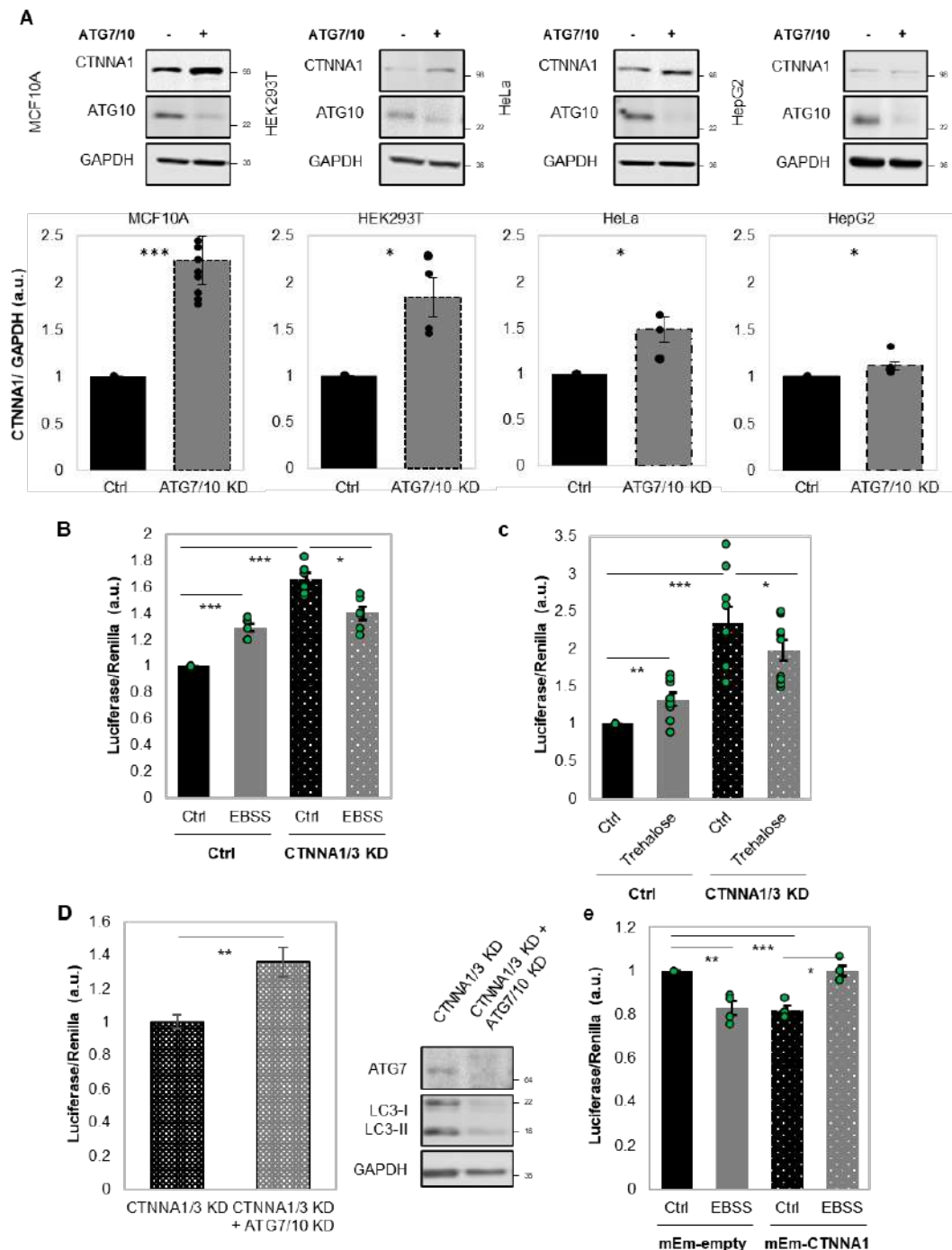


Figure 11. α -Catenin intracellular protein levels direct the YAP/TAZ response to autophagy perturbations. (A) Representative immunoblots of CTNNA1 in multiple cell lines: MCF10A,

HEK293T, HeLa, HepG2 after exposure to ATG7/10 siRNAs. Bars represent the mean \pm s.e.m. (n (from left to right) = 10/4/4/6 independent experiments; *** P < 0.001, * P < 0.05; two-tailed one sample t -test). **(B)** TEAD luciferase activity in MCF10A cells exposed to CTNNA1/3 siRNAs, followed by treatment with EBSS (6 h), as indicated. Bars represent the mean \pm s.e.m. (n = 6 independent experiments; *** P < 0.001, * P < 0.05; two-tailed one sample t -test). **(C)** TEAD luciferase activity in MCF10A cells exposed to CTNNA1/3 siRNAs, followed by treatment with Trehalose (100 mM, 24 h), as indicated. Bars represent the mean \pm s.e.m. (n = 9 independent experiments; *** P < 0.001, ** P < 0.01, * P < 0.05; two-tailed one sample t -test). **(D)** TEAD luciferase activity in MCF10A cells initially exposed to CTNNA1/3 siRNAs for 48 h followed by double ATG7/10 KD for other 48 h, as indicated. Bars represent the mean \pm s.e.m. (n = 6 independent experiments; ** P < 0.01; two-tailed one sample t -test). **(E)** TEAD luciferase activity in HepG2 cells transfected with mEm-empty or wild-type mEm-CTNNA1, and after, exposed to EBSS for 6 h. Bars represent the mean \pm s.e.m. (n = 4 independent experiments; ** P < 0.01, * P < 0.05, ns not significant; two-tailed one sample t -test). Exact P values for asterisks: **A** (from left to right) 0.0017, 0.0281, 0.0459, 0.0405; **B** 0.0001, <0.0001, 0.0160; **C** 0.0056, 0.0012, 0.0332; **D** 0.0046; **E** (from left to right) 0.0065, 0.0012, 0.0112.

To further test the central role of α -catenin levels in this model, we have engineered MCF10A cells to have low levels of α -catenins (using siRNA knockdowns) and HepG2 cells to have high levels of α -catenins by overexpression (Fig 11). In MCF10A cells previously depleted of α -catenins by siRNA knockdowns for 48 hours, untreated cells had higher YAP/TAZ activity than those exposed to autophagy stimuli with EBSS for 6 h (the experimental YAP/TAZ activity data is shown in Fig. 11B) or Trehalose 100 mM for 24 h (the experimental YAP/TAZ activity data is shown in Fig. 11C). Conversely, a short-time exposure to ATG7/10 siRNAs (2 days) in MCF10A cells previously depleted of α -catenins for 48 hours, increased TEAD-YAP luciferase activity (the experimental YAP/TAZ activity data is shown in Fig. 11D) similar to cells characterised by initial low levels of α -catenins, such as HepG2.

Consistent with our model, in HepG2 cells overexpressing the mEm-CTNNA1 construct, EBSS treatment for 6 h enhanced the YAP/TAZ activity in the HepG2 cells (the experimental YAP/TAZ activity data is shown in Fig. 11E). Thus, the HepG2 cells overexpressing wild-type CTNNA1 phenocopied what we had seen in MCF10A cells (Fig. 3F). Overall, these experimental results suggest that initial levels of α -catenins determine the dynamics of YAP/TAZ response to various autophagy perturbations.

1.2.1.5. Discussions

Here, we identified the surprising finding that autophagy inhibition causes divergent positive and negative responses in YAP/TAZ activity in different cell types as a result of different starting levels of a common key signalling effector, which acts also as an autophagy substrate: α -catenin. Importantly, this mechanism is further completed by the dynamic mutual regulation of YAP/TAZ by autophagy and of autophagy by YAP/TAZ. Thus, we are showing that when α -catenins levels are low, autophagy inhibits YAP/TAZ activity, and when α -catenins levels are high, autophagy up-regulates YAP/TAZ activity.

Collectively, our data suggest, focusing on the YAP/TAZ signalling output, that autophagy may impact on cell identity, causing completely opposite effects in cells with different starting points (different α -catenin levels). This is physiologically relevant, as the principles underlying the described mechanism in this study may extend to other signalling pathways, which may respond to autophagy perturbations with contrasting reactions in distinct cells, tissues, organs or even individuals. This type of biology may explain many apparent discrepancies in the literature in signalling responses to different stimuli. This data further reveal how feedback loops enable the post-transcriptional determination of cell identity. Our results raise important points that need to be carefully considered for biological replication

purposes: output differences in signalling pathways, here described for YAP/TAZ, are tightly conditioned by the initial experimental set-up, the order and time-span of cellular perturbations.

Final remarks

These findings are directly relevant in explaining human pathology and may help define therapeutic strategies based on autophagy modulation – for example, autophagy inhibition may differentially affect oncogenic pathways in different directions in different cells types. Indeed, our data suggest that autophagy inhibition impairs YAP/TAZ activity and proliferation of primary mammalian epithelial cells, while autophagy compromise in hepatocytes induces YAP activity and increases liver size, cell proliferation and carcinogenesis (Lee et al., 2018; Wen and Klionsky, 2019).

In conclusion, the general mechanism of considering multiple feedback-forward loops when characterizing the complexity of autophagy-YAP/TAZ axis may be extended to other signaling intracellular pathways known to control tumorigenesis and/or apoptosis. This hypothesis was the rationale behind the following studies presented next.

1.2.2. Dynamic mathematical models explain the autophagy-YAP1 signalling crosstalk: the balance between multiple forward and feedback paths dictates the cell fate

1.2.2.1. Introduction

We have recently shown that the complex interconnection between the YAP1-WWTR1(TAZ) signalling and autophagy controls cell proliferation and survival with opposite outputs in different cell lines, but also at different time points of autophagy perturbation. More precisely, we identified α -catenin, the endogenous inhibitor of the Hippo pathway effector YAP1 (Sarpal et al., 2019; Schlegelmilch et al., 2011; Vite et al., 2018) to be a direct autophagy substrate (via two newly described LIR motifs). Consequently, autophagy positively regulates YAP1 protein levels and activity in a number of cell lines with high basal levels of α -catenins, like the non-malignant mammary epithelial (MFC10A) cells, human embryonic kidney (HEK293T) cells, human cervical epithelium (HeLa) cells, primary mouse embryonic fibroblasts (pMEFs) or primary mammary epithelial cells (pMECs) (Pavel et al., 2021a; Pavel et al., 2021b). On the other hand, previous studies have identified that Yap1 itself is an autophagy substrate (independently of p62 expression), and have further shown, using *in vivo* models (Atg7KO mice) or hepatocyte cell lines (Atg7-deficient murine AML12, or human THLE5B), that autophagy negatively impacts Yap1 activity, as Atg7-deficiency leads to the accumulation of active Yap1 that increases liver size, causing progenitor cell expansion with hepatocarcinogenesis (Lee et al., 2018). This result was also confirmed by us using various hepatocyte cell lines (THLE2, HepG2, Huh7 cells) or non-small cell lung cancer cells (A549 cells), as all these cells have a low basal protein expression of α -catenins (Pavel et al., 2021a; Pavel et al., 2021b). In other words, one may conclude that cells that have the capacity to bind a significant portion of the YAP1 pool by α -catenins will respond to autophagy inhibition by reducing cell proliferation, size and migration capacities, while cells that have transcriptional changes or PTMs that overcome or lower this interaction will behave in completely opposite way, as the direct ability of autophagy to degrade YAP1 will be dominant: autophagy inhibition would activate YAP1 (Fig. 12A).

The autophagy-YAP1 picture is further entangled by a feedback path, since YAP1 regulates autophagy. We previously also showed that YAP1/TAZ positively modulates autophagy by upregulating the transcriptional expression of myosin-II genes in a series of cell lines, like MFC10A, HeLa cells, human keratinocyte (HaCaT) cells, primary mouse embryonic fibroblasts (pMEFs) or primary mammary epithelial cells (pMECs) (Pavel et al., 2018a).

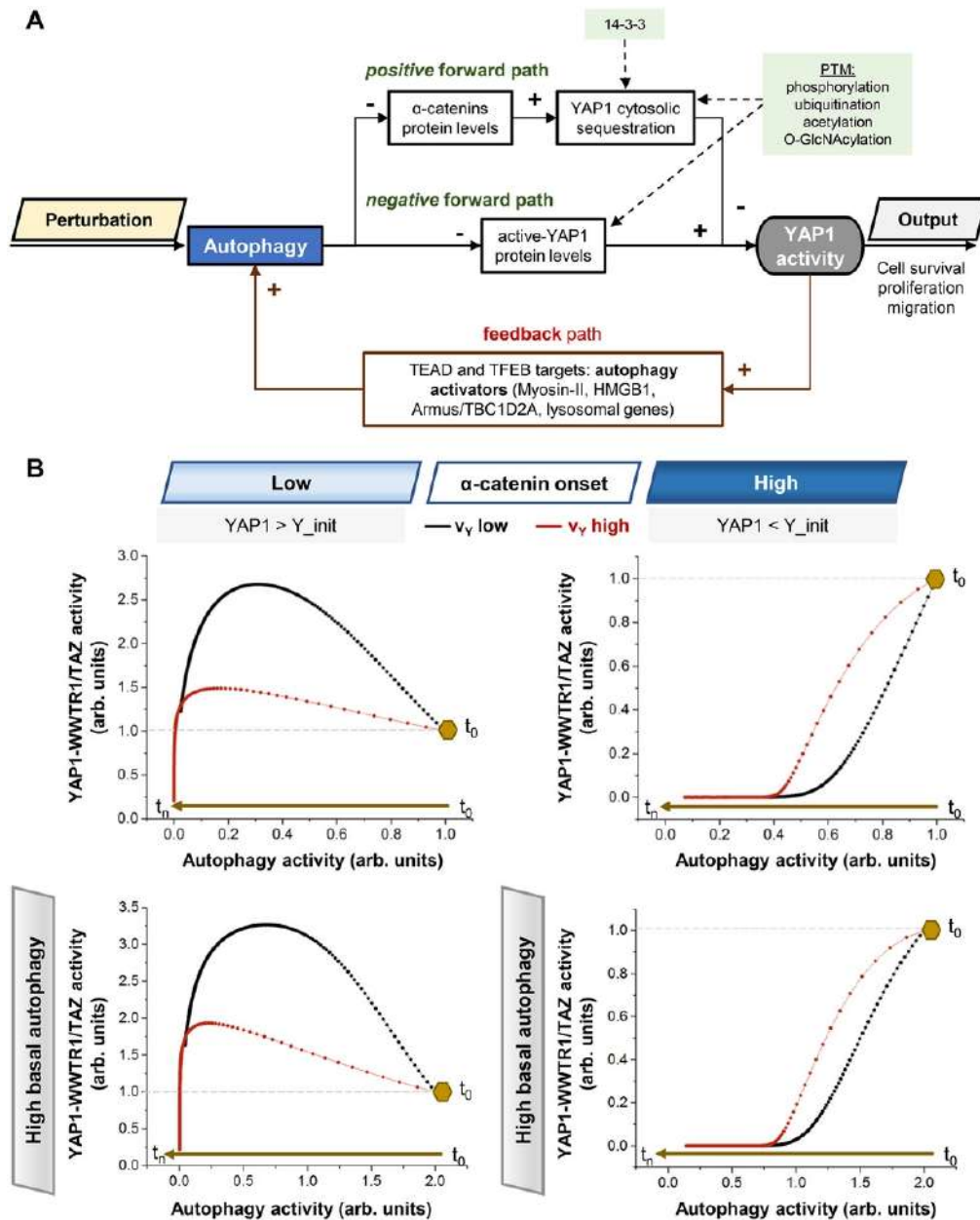


Figure 12. Schematic representation of the autophagy-YAP1 signalling control system.

(A) The two contrasting effects of autophagy on cell survival and proliferation resulting from degrading either α -catenin (YAP1 inhibitor) or YAP1 are named as positive and negative forward paths, respectively. Various posttranslational modifications (PTMs) impact differently on the strengths of the two forward paths. The positive feedback path is represented by the transcriptional control exerted by YAP1 (in conjunction with TFEB or TEAD) on key autophagy genes. (B) Schematic diagram of the effect caused by the feedback path/loop in cells with either low or high basal levels of α -catenins, and normal or high initial autophagy flux/activity. The strength of the feedback loop is denoted by the parameter v_Y . Y_{init} indicates the initial YAP1 activity. YAP1 activity increases in low basal α -catenin

conditions ($YAP > Y_{init}$), and decreases in high basal α -catenin cells ($YAP1 < Y_{init}$) upon autophagy inhibition.

Other studies have confirmed this general observation that YAP1 is required for proper autophagy, but suggest various distinct mechanisms. YAP1 transcriptional targets include Armus, a protein of the RAB-GAP family, which is required for the proper fusion of autophagosomal vesicles with lysosomes (Totaro et al., 2019) and HMGB1, the well-known activator of Beclin-1 (which displaces the inhibitor protein Bcl-2 from its interaction with Beclin-1) (Sun and Tang, 2014; Tang et al., 2010) in human glioma (U251 and U87) (Zhao et al., 2021) cell lines. Autophagy flux is further increased by the interaction of YAP1 with the master transcription factor EB (TFEB) (Ikeda et al., 2021) or TEAD (Song et al., 2015) and co-transcriptional regulation of autophagy and lysosomal genes in neonatal rat cardiomyocytes and human breast cancer cells (MCF7 or MDA-MB-231). This feedback loop (of YAP1 controlling autophagy) is important, as the strength of the effect exerted by YAP1 on autophagy controls the magnitude of the YAP activity outcome after autophagy perturbations (Fig. 12B). For instance, in cells with low basal α -catenin protein levels, events that enhance the control of YAP over the autophagy pathway will lead to a lesser increase in YAP activity than the cases with negligible feedback effects upon autophagy inhibition. In cells with high basal α -catenin expression, a high feedback effect (of YAP1 controlling autophagy) will cause a lesser reduction in the YAP activity output upon autophagy compromise, but only at earlier time points (Pavel et al., 2021a; Pavel et al., 2021b). For cancer cells (Xu et al., 2013), the typically heightened autophagy flux is expected to cause an increase in the magnitude of the observed effect only for the low α -catenin cases. A second general observation could be made at this point: the feedback paths control the magnitude of the investigated effects in a time-dependent manner.

1.2.2.2. Aim

In this study we aimed to answer the following question: how these apparently contradicting observations (positive and negative controls) can be integrated to define a general model for a particular pathway (e.g. autophagy-YAP/TAZ) to enable a better understanding of the outputs empirically observed after various perturbations, and to allow prediction of the cellular behaviour in new situations?

1.2.2.3. Methods

Mathematical-numerical model

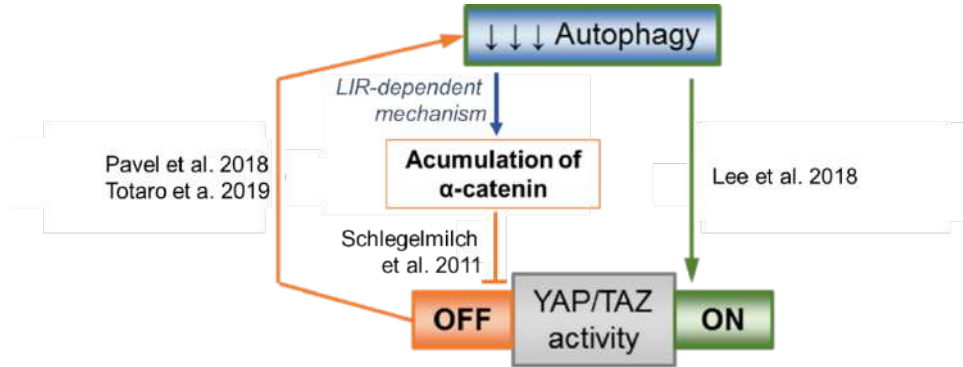
Our mathematical model is based on a set of three non-linear ordinary differential equations (ODEs), represented by autophagy levels (A), YAP/TAZ activity (Y) and α -catenin protein levels (C). Each term in the system of ODEs represents one single action.

The following basic assumptions were considered (see the scheme bellow):

- (i) Reduction in YAP/TAZ activity leads to autophagy decrease via previously described mechanisms (Pavel et al., 2018a; Totaro et al., 2019). When initial YAP levels are high, the extent of autophagy inhibition is also high, and when initial YAP levels are low, there is still a loss of autophagy, but the effects are small.
- (ii) YAP/TAZ activity results from the balance between two opposite mechanisms: I) *reduction in YAP/TAZ activity* as a consequence of YAP/TAZ being sequestered into the cytosol by α -catenin (the LIR-dependent mechanism experimentally described herein), and II) *increase in YAP/TAZ activity* as a consequence of perturbed autophagy (the mechanism experimentally described by Lee et al. 2018) – when initial autophagy is high, the increase in YAP resulting from autophagy

inhibition is large, and when initial autophagy is low, there is still an increase in YAP, but marginal.

- (iii) α -catenin protein levels accumulate upon autophagy perturbation (the mechanism experimentally described herein) – the rate of α -catenin accumulation is high when initial autophagy is high, and is low when autophagy is low.



The ODEs of our model are stated below:

$$(1) \frac{dA}{dt} = -cA - v_Y(1 - e^{-\delta_A Y})A$$

$$(2) \frac{dY}{dt} = -r_1 YC + r_2(1 - e^{-\delta_Y A})\left(1 - \frac{Y}{Y_{\max}}\right)Y$$

$$(3) \frac{dC}{dt} = r_3 v_C v_Y(1 - e^{-\delta_C A})\left(1 - \frac{C}{C_{\max}}\right)C,$$

where $v_C = kC(0)$, $C_{\max} = k_C C(0)$ and $Y_{\max} = k_Y Y(0)$.

Equation (1) determines the autophagy levels as a consequence of the cumulative effects of the primarily depletion rate (genetic or chemical inhibition) (first term) and the decrease in autophagosome formation rate caused by reduction in YAP/TAZ activity (second term). The effectiveness of the feedback effect caused by YAP/TAZ on autophagy levels is bounded, as we have previously seen (Pavel et al., 2018a). More precisely, only strong YAP/TAZ depletion (corresponding to the case of high initial YAP and low output/final YAP) causes a major inhibition of autophagy, while a small reduction in YAP/TAZ levels (corresponding to the case of low initial YAP) barely impacts autophagy, similar to a plateau effect (Pavel et al., 2018a). We therefore used a saturation term $(1 - e^{-\delta_A Y})$, adapted from (de Pillis et al., 2009; Wang et al., 2012b), to represent this described effect. The strength of the feedback loop, which may vary between different cell types, was represented by the variable v_Y .

Equation (2) determines the YAP activity levels as the difference between the accumulation YAP/TAZ rate (second term) and the sequestration YAP/TAZ rate by α -catenin (first term) upon autophagy depletion. YAP activity follows a saturation curve of a maximum value of Y_{\max} .

Equation (3) determines the α -catenin levels which accumulate upon autophagy inhibition (α -catenin is an LC3-interacting protein and a direct substrate of autophagy). The accumulation of α -catenin depends on the initial α -catenin levels (as we noticed a higher CTNNA1 protein levels after autophagy depletion in cell lines with high initial values– see Fig. 10a). α -catenin protein levels follow a saturation curve of a maximum value of C_{\max} . To simplify the model, the protein synthesis rates were neglected.

These three ODEs were numerically solved using MAPLE software. Specifically, the following values were used to define the constants included in this mathematical model $c = 0.1$, $r_1 = 1.0$, $r_2 = 1.2$, $r_3 = 3.0$, $k = 1.0$, $k_C = 3.0$, $k_Y = 4.0$ and $\delta_A = \delta_C = \delta_Y = 1.0$. At $t = 0$ (initial state, t_0), $A = 1.0$ and $Y = 1.0$, labeled as A_{init} and Y_{init} in the MAPLE code, respectively. The variables v_Y (which define the strength of the feedback loop – how YAP/TAZ

impacts on autophagy levels) and v_C (which equals the α -catenin protein levels at time t_0 , α -cat) were varied from 0.1 to 1.0 (number of steps: 10). The parameters A_{init} and Y_{init} were further swept from 0.1 to 2.0. The MAPLE code is included as `Script.mw`, together with step-by-step instructions (the files named `README.md` and `Maple_Installation_guide.txt`) and a typical output example (`Data_Output.zip`) in the GitHub repository <https://github.com/rтуаic/Pavel-Nature-Communications-2021>.

1.2.2.4. Results

Description of the mathematical model used for depicting the autophagy-YAP1 signalling crosstalk

We first developed a mathematical model of three interconnected differential equations that describe the dynamics of the three key players (autophagy, YAP1 activity, and α -catenin levels) in a time-dependent manner, starting from the three main constituent processes (Fig 13): i) autophagy positively modulates YAP1 activity by degrading its inhibitor, α -catenin (so-called *positive forward path*; the α -catenin that accumulates upon autophagy inhibition interacts with YAP1 and sequesters it into the cytoplasm) (Schlegelmilch et al., 2011); ii) autophagy negatively modulates YAP1 activity by facilitating its direct degradation (so-called *negative forward path*; active-YAP1 accumulates upon autophagy inhibition) (Lee et al., 2018); iii) the feedback path of YAP1 positively controlling autophagy (by monitoring autophagosome formation, maturation, and fusion with lysosomes) (Ikeda et al., 2021; Pavel et al., 2018a). Thus, during autophagy inhibition, the rate of autophagy decrease is controlled by both the decay rate due to the applied perturbation (parameter c) (Han et al., 2014; Pavel et al., 2021a), and the strength of the feedback path (parameter v_Y).

The rate of YAP1 variation relies on the balance between the strengths of the two, *positive* (controlled by parameter r_1 , which defines the strength of the cytosolic-sequestration rate of YAP1 by α -catenins) and *negative* (controlled by parameter r_2 , which defines the strength of active-YAP1 accumulation rate upon autophagy inhibition) *forward paths*, while the rate of α -catenin accumulation depends on its degradation rate by autophagy (controlled by parameter r_3). It is also important to understand that the intracellular compartmentalisation of various key players may vary based on the cell type and nutrient environmental conditions, and thus influencing the values of r_1 , r_2 and r_3 parameters. For example, the nutrient rich conditions activate mTOR on peripheral lysosomes, which inhibits autophagy and promotes the YAP1 activation (increased r_2 value) (Liang et al., 2014; Rabanal-Ruiz and Korolchuk, 2018) or α -catenin accumulation (increased r_3 value).

For an initial (basic) simulation model, we only varied the starting levels of our interconnected key players (autophagy, YAP1 activity, and α -catenin levels) and the strength of the feedback loop (parameter v_Y), while the other parameters (c , r_1 , r_2 , and r_3) were assumed as constants for the numerical simulations, their values being extrapolated from experimental observations.

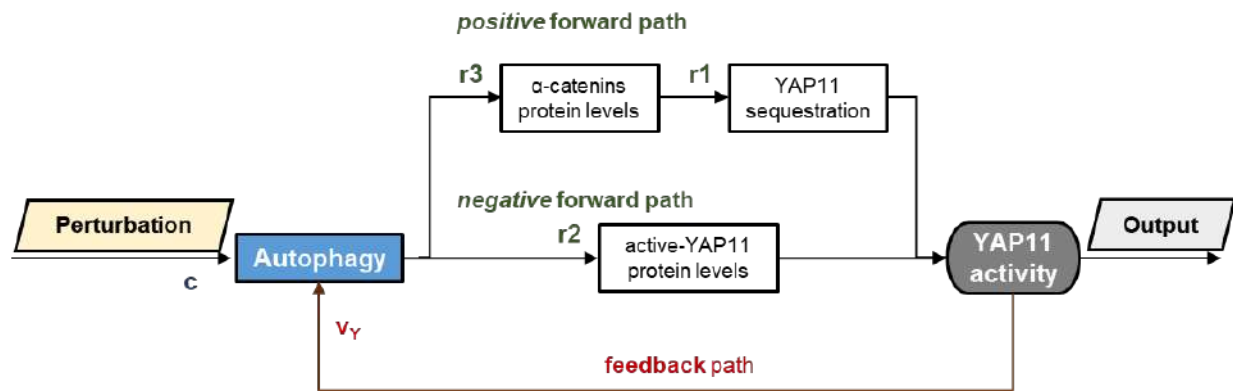


Figure 13. The mathematical model proposed for the crosstalk between autophagy and YAP/TAZ signalling.

Using this mathematical model, we were able to reconcile the controversial observations present in the field of YAP1 and autophagy research, and identify the basal α -catenin levels (by appropriate experimental validation) as the main driver for the direction of YAP1 output (activation/ inhibition) upon autophagy perturbation with considerable input in the magnitude of the effect offered by the strength of the feedback path, v_Y .

The model may also predict a time-dependent effect on YAP/TAZ activity when the initial YAP activity (Figs. 14-15) or autophagy (Figs. 16-17) levels are varied. Specifically, higher initial YAP values ($Y_{init} > 1$) are predicted to cause slightly smaller relative increases in YAP activity (YAP/Y_{init} – bottom graph in Fig. 14) when compared to lower initial YAP conditions ($Y_{init} < 1$) at initial time points, but only in the cells with low initial α -cat values (< 0.3 , Figs. 14-15). For the cases characterised by high basal α -cat values (> 0.5), the initial levels of YAP activity are not predicted to have major influences on the system outputs (Figs. 14-15). When initial autophagy levels are varied (with $Y_{init}=1$), the numerical model estimates that YAP/TAZ activity changes faster upon autophagy inhibition in systems characterised by basal lower autophagy ($A_{init} < 1$), compared to higher initial autophagy conditions ($A_{init} > 1$), and this effect is amplified when initial α -cat values are increased (Figs. 16-17). Thus, we may conclude from our numerical simulations, that the initial levels of YAP activity appear to predominantly impact the magnitude of the output (YAP/TAZ activity), rather than influencing its direction (of increasing or decreasing) or its time period, while the initial autophagy levels mainly impact on the time-span of the output-effect.

It is interesting to note that our modelling predicts that in low initial α -catenin conditions, YAP/TAZ activity will increase, as autophagy is inhibited at early time points (YAP increases while autophagy decreases –Fig. 18, R correlation coefficient < -0.5). This effect is driven by the ability of autophagy to degrade YAP/TAZ (Lee et al., 2018; Wang et al., 2019) dominating the negative effect of impact of α -catenin accumulation on YAP/TAZ when α -catenin levels are low. However, when autophagy is inhibited then α -catenin also starts to increase and after a certain period of time α -catenin levels will reach a threshold when α -catenin sequestration of YAP/TAZ dominates the autophagy-mediated degradation of YAP/TAZ. From this timepoint onwards, YAP decreases as autophagy inhibition continues –Fig. 18, $R > 0.5$). In high initial α -catenin conditions, YAP/TAZ activity is predicted to positively correlate with autophagy levels at any relevant experimental time of the applied perturbation (Figs. 14,16).

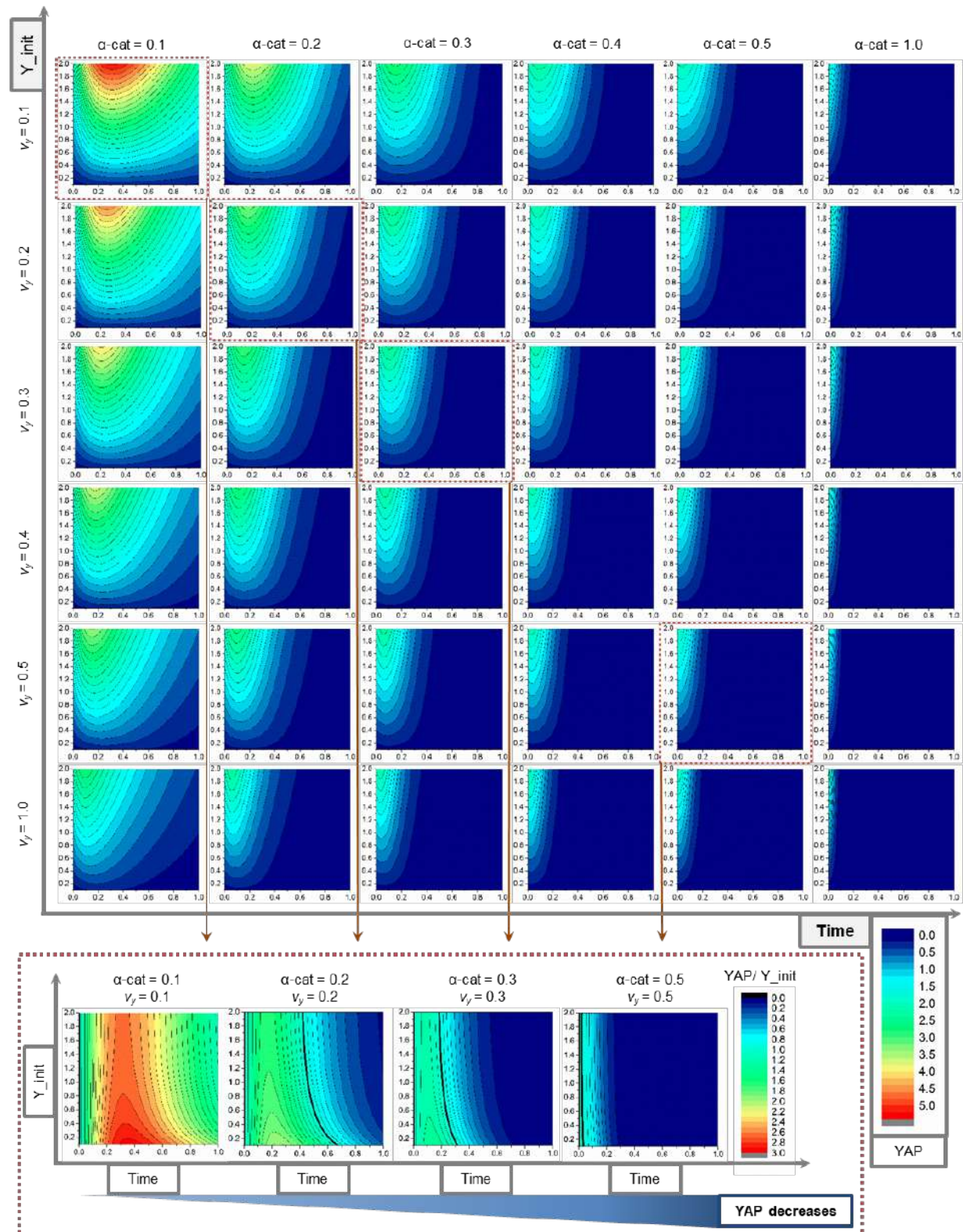


Figure 14. Time variation of YAP/TAZ activity when different initial YAP, α -cat and v_Y values are considered upon autophagy downregulation. Predicted time variation of absolute YAP/TAZ activity when various initial YAP (Y_{init}), α -cat and v_Y values are considered ($A_{init}=1.0$). Time parameter is shown on the horizontal axis, while the Y_{init} is varied on the vertical axis. Initial α -cat levels have the strongest influence on final YAP/TAZ activity upon autophagy inhibition at lower time points. The colour code on the bottom right indicates the estimated absolute values of YAP/TAZ activity. Predicted relative YAP/TAZ activity (to initial values) in the indicated conditions are shown

on the graph on the bottom. In low initial α -cat and v_Y conditions, YAP/TAZ increases upon autophagy inhibition at any time, while increasing initial α -cat and v_Y conditions YAP/TAZ is reduced by autophagy inhibition at increasing time points.

Note: Y_{init} represents the initial value for YAP activity (before applying the autophagy perturbation); A_{init} represents the initial autophagy level (before applying the autophagy perturbation); α -cat represents the initial α -catenin level (before applying the autophagy perturbation); v_Y represents the strength of the feedback loop / the strength of YAP influence on autophagy levels (Pavel et al. 2018); YAP represents the YAP activity level at the indicated time point of autophagy inhibition (after applying the autophagy perturbation).

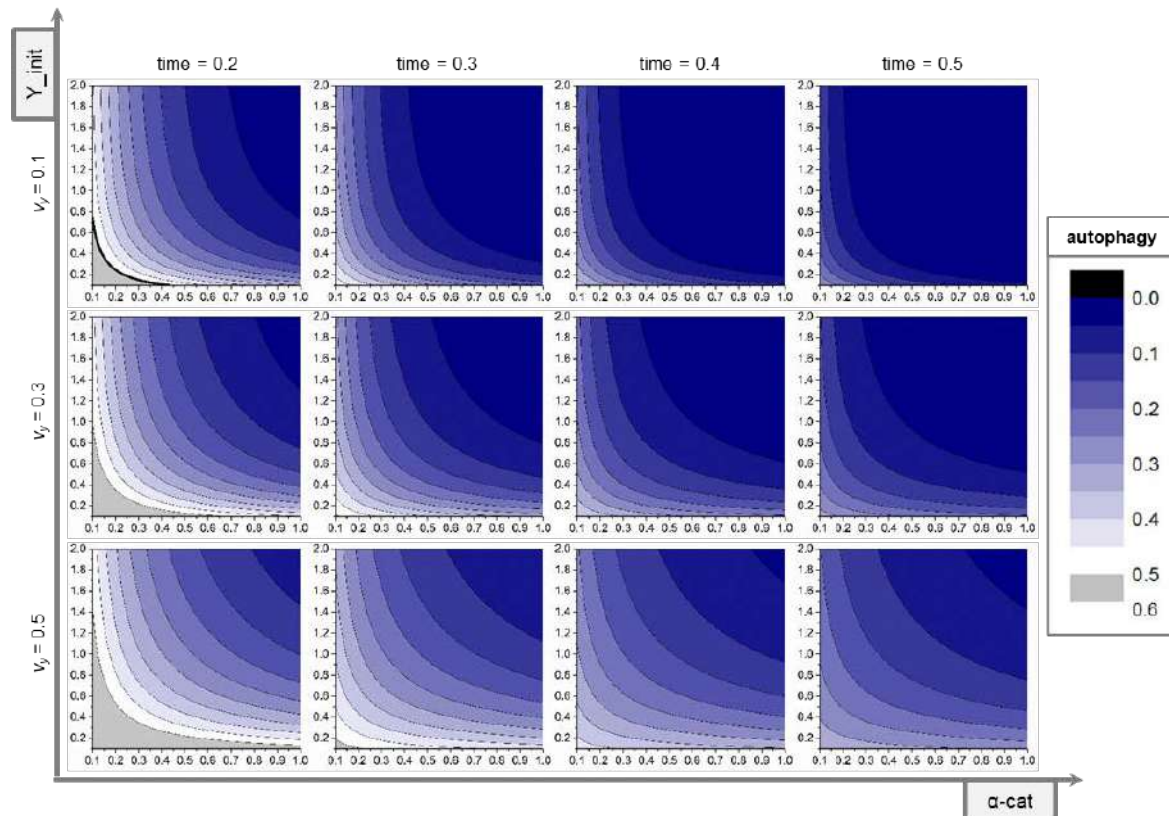


Figure 15. YAP/TAZ activity at different time points of autophagy inhibition when initial YAP, α -cat and v_Y values are varied. Predicted absolute YAP/TAZ activity when various initial YAP, α -cat and v_Y values are considered at different time points of autophagy inhibition ($A_{init}=1.0$). α -cat parameter is shown on the horizontal axis, while the Y_{init} is varied on the vertical axis. Initial v_Y levels have the strongest influence on final YAP/TAZ activity upon autophagy inhibition at higher time points. The colour code on the right indicates the estimated relative autophagy values.

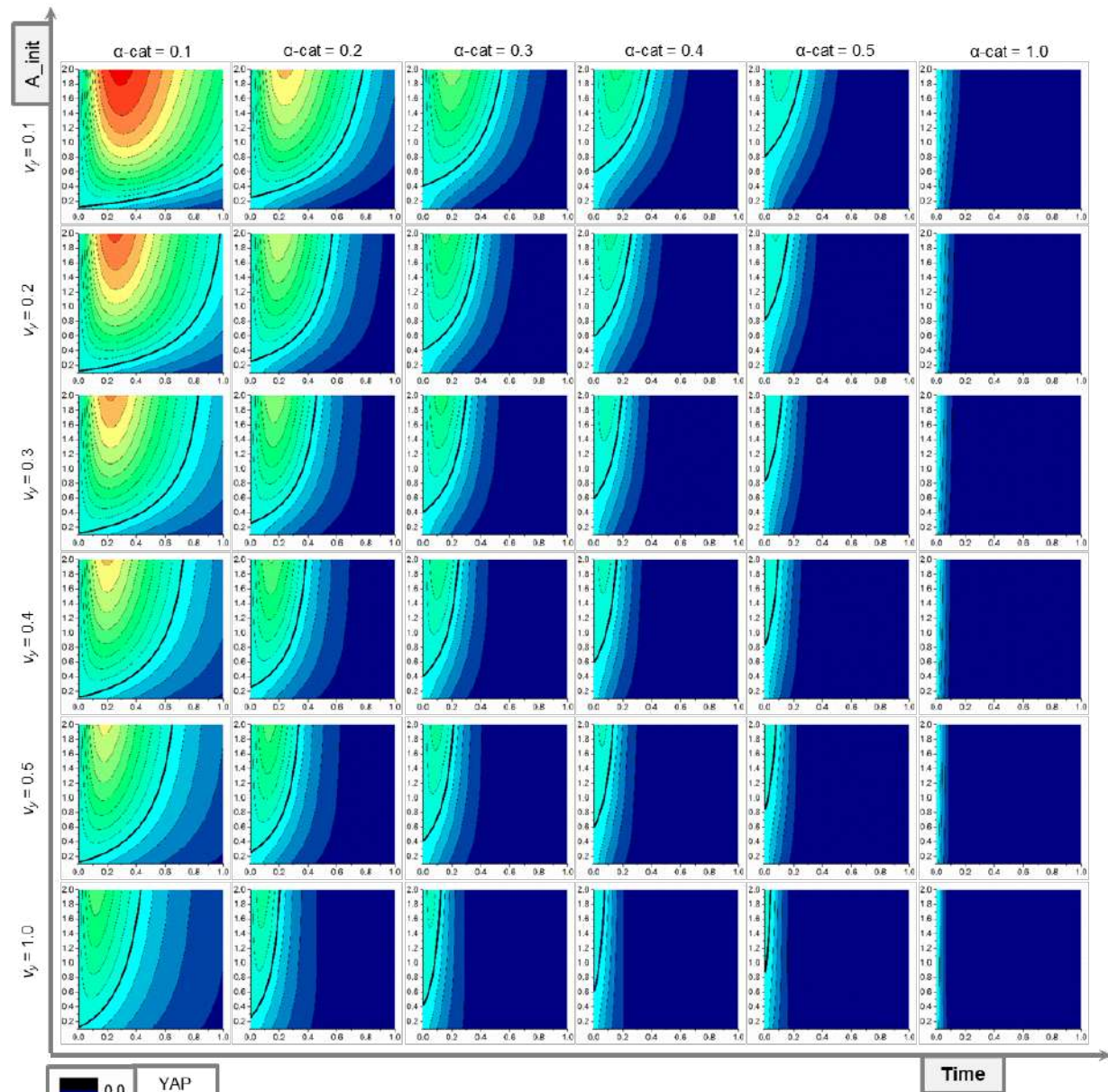


Figure 16. Time variation of YAP/TAZ activity when different initial autophagy, α -cat and v_γ values are considered upon autophagy down-regulation. Predicted time variation of absolute autophagy activity when various initial autophagy, α -cat and v_γ values (the strength of YAP influence on autophagy levels (Pavel et al. 2018)) are considered ($Y_{init}=1.0$, initial YAP activity level). Time parameter is shown on the horizontal axis, while the A_{init} (initial autophagy level) is varied on the vertical axis. Initial α -cat levels have the strongest influence on final YAP/TAZ activity upon autophagy inhibition at lower time points. The colour code on the bottom right indicates the estimated absolute values of YAP/TAZ activity.

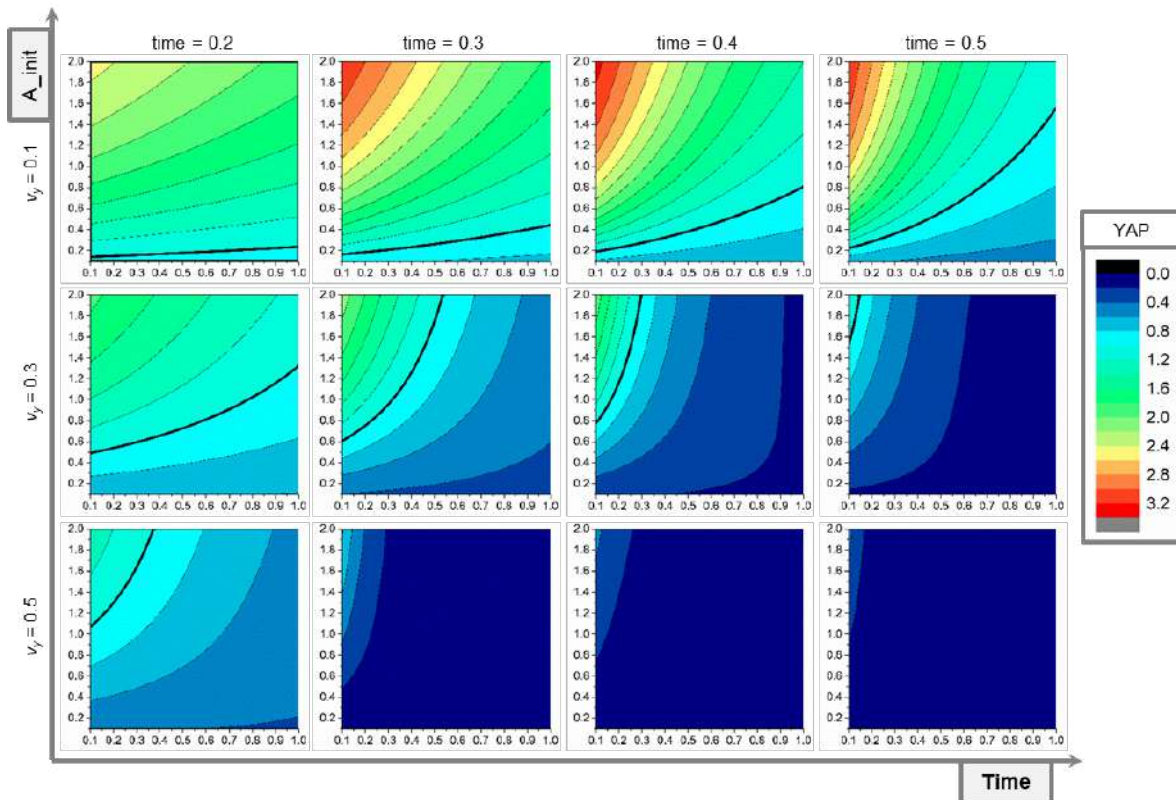


Figure 17. YAP/TAZ activity at different time points of autophagy inhibition when initial autophagy, α -cat and v_Y values are varied. Predicted relative YAP/TAZ activity (to initial values) for the indicated conditions activity when various initial autophagy, α -cat and v_Y values are considered at different time points of autophagy inhibition ($Y_{init}=1.0$). Time parameter is shown on the horizontal axis, while the A_{init} is varied on the vertical axis. The colour code on the right indicates the estimated relative values of YAP/TAZ activity. The black line corresponds to relative YAP=1.0. The conditions with YAP values above the line are those that increase YAP upon autophagy inhibition.

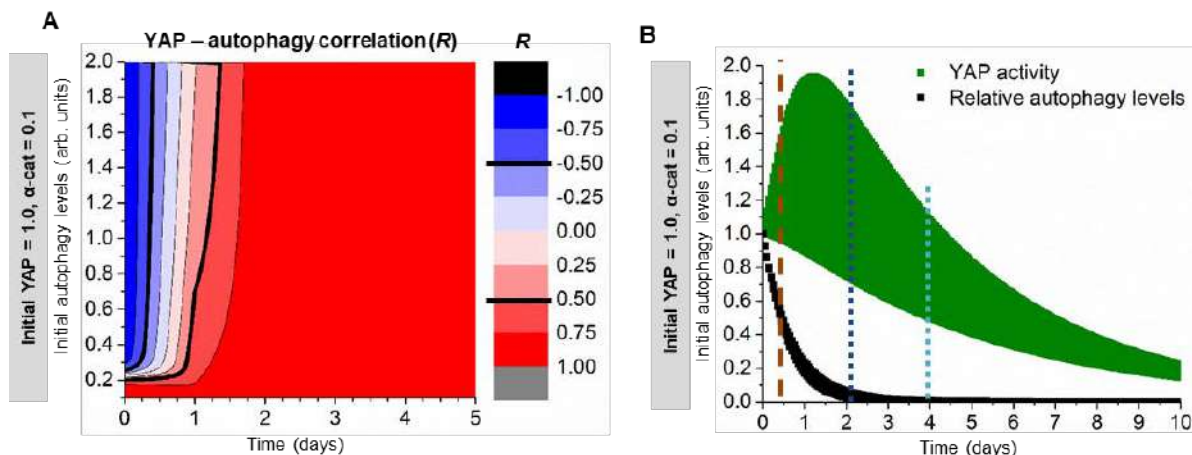


Figure 18. Time variation of YAP/TAZ activity in cells with low α -cat levels in low and high initial autophagy conditions upon autophagy down-regulation. (A) Time-dependent correlation (R - Pearson correlation coefficient) between YAP activity and autophagy levels in cells with low initial α -cat (0.1). At early time points: YAP inversely correlates with autophagy (YAP increases upon autophagy reduction); at later time points: YAP positively correlates with autophagy (YAP decreases upon autophagy reduction). (B) Time-dependency of YAP-activity and autophagy values in cells with low initial α -cat (0.1).

However, if one wants to extend the model to a broader range of cell types and systems, the variations in the other parameters (c , r_1 , r_2 , and r_3) should be carefully evaluated. Thus, we considered possible scenarios that would lead to such variations, in order to understand, at least theoretically, their potential impact over the outputs.

The autophagy decay rate, modelled by parameter c , dictates the YAP1 output in low basal α -catenin cells and/or low feedback strength conditions

The autophagy decay rate (parameter c) may vary, as it depends on the nature of the perturbation stimulus: if there is a chemical (inhibitors/activators that may require minutes-hours to impact autophagy) or genetic manipulation (siRNA knockdown experiments with visible effects in hours-days, or knockout cell lines – days-weeks). As most of our experiments were siRNA knockdown experiments and had prolonged treatments in our previous study, the autophagy decay rate was relatively slow.

Interestingly, increasing the value of parameter c (as would occur in biological systems exposed to a rapid perturbation decay rate) can change the outcome of the output effect (e.g. YAP1 activity) in cells characterized by low basal α -catenin and/or little feedback effect (low v_Y): switching from YAP1 activation (what we observed in our recent publications) (Pavel et al., 2021a; Pavel et al., 2021b) to YAP1 inhibition – Fig. 19. Conversely, the effect exerted by the autophagy decay rate in biological systems characterized by both high α -catenin levels and a strong feedback effect (high v_Y), is almost neglectable – Fig. 19 and Fig. 20. The initial levels of autophagy and YAP1 activity only impact on the magnitude/extent of the final outcome (e.g. reducing the basal autophagy levels or initial YAP1 activity will produce the same effect - of either activation or inhibition, but to a lower extent) – Fig. 20.

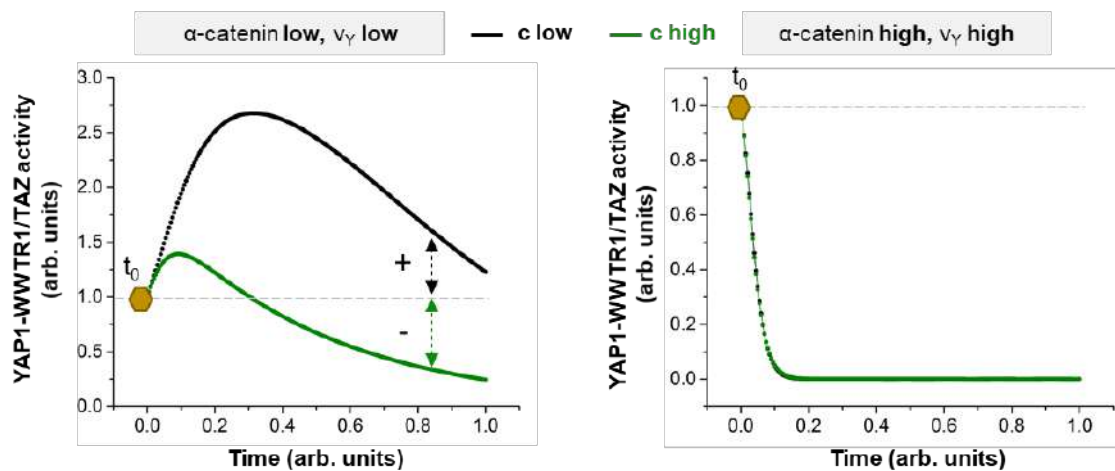


Figure 19. Schematic representation of the effects exerted by the variation of c parameter upon autophagy inhibition. Variation of parameter c (the *autophagy decay rate* caused by external perturbation): increase in c value should cause YAP1 inhibition, and not activation at later time points in cells with low basal α -catenin protein levels.

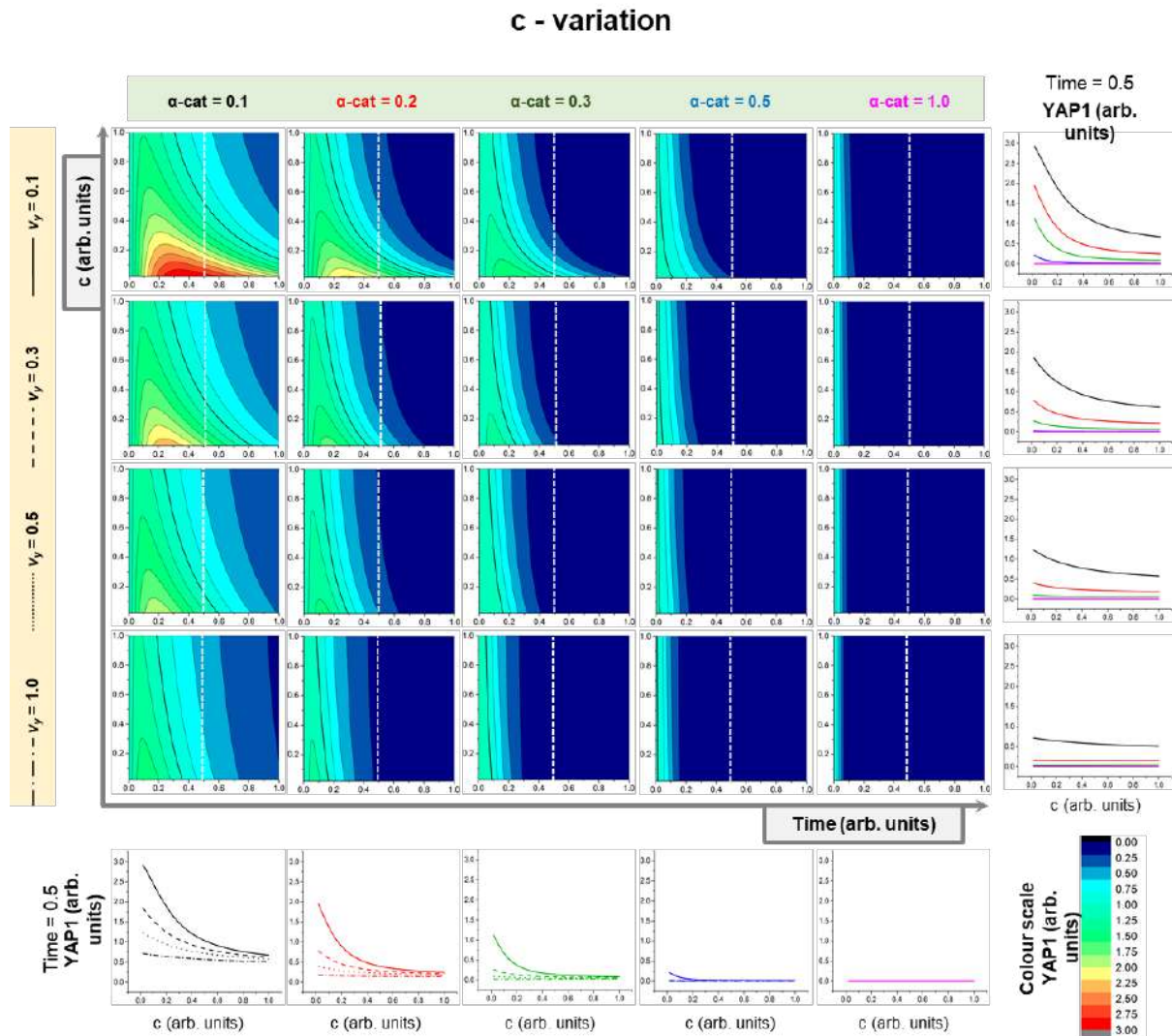


Figure 20. The effect of parameter c on the dynamics of YAP1 activity when different initial α -cat and v_Y values are considered upon autophagy down-regulation. Predicted time variation of absolute YAP1 activity (arbitrary units) when various initial α -cat and v_Y values (the strength of YAP1 influence on autophagy levels (Pavel et al. 2018)) are considered. Time parameter is shown on the horizontal axis, while the parameter c is extended on the vertical axis. The colour scale on the bottom right indicates the estimated arbitrary values of YAP1 activity for the contour plots. The black highlighted contour line corresponds to YAP1=1.0 (values below 1.0 denote reduction in YAP1 activity, while values above 1.0 denote increase in YAP1 activity). The profiles indicated by vertical white dotted lines (corresponding to the time step=0.5) are pictured in the line graphs plotted on the bottom (v_Y is varied; X axis – c variation, Y axis – YAP1 activity) or on the right (initial α -cat is varied; X axis – c variation, Y axis – YAP1 activity). For all plots: $A_{init}=1.0$, $Y_{init}=1.0$.

The strength of the positive forward path, modelled by parameter $r1$, dictates the YAP1 output in low basal α -catenin cells

Regarding the cases where the strength of the cytosolic interaction between YAP1 and α -catenin varies, which influences the strength of the *positive* forward path, it is worth considering the possibilities of PTMs that facilitate (e.g. phosphorylation of YAP1) or disrupt this protein-protein interaction. The disruption may be caused by PTMs like ubiquitination, that amplifies the proteasomal-mediated degradation of YAP1 and/or α -catenins and/or 14-3-3 proteins (which are the molecules that intermediate the interaction between YAP1 and α -

catenin), or acetylation of 14-3-3 proteins that shut-off their functions as intermediary binding partners (Choudhary et al., 2009; Mortenson et al., 2015). The strength of the *positive* forward path is controlled by the value of parameter $r1$. For instance, a relatively moderate increase in parameter $r1$ (e.g. doubling its value) would cause a decrease in the YAP1 activity in low basal α -catenin cells, even reversing the final output effect at later time points of autophagy perturbation (switching from the previously expected YAP1 activation to YAP1 inhibition) – Fig. 21. The YAP1 activity in cells with high basal α -catenins is not sensitive to moderate changes (up to two folds increase) of this parameter – Figs. 21-22.

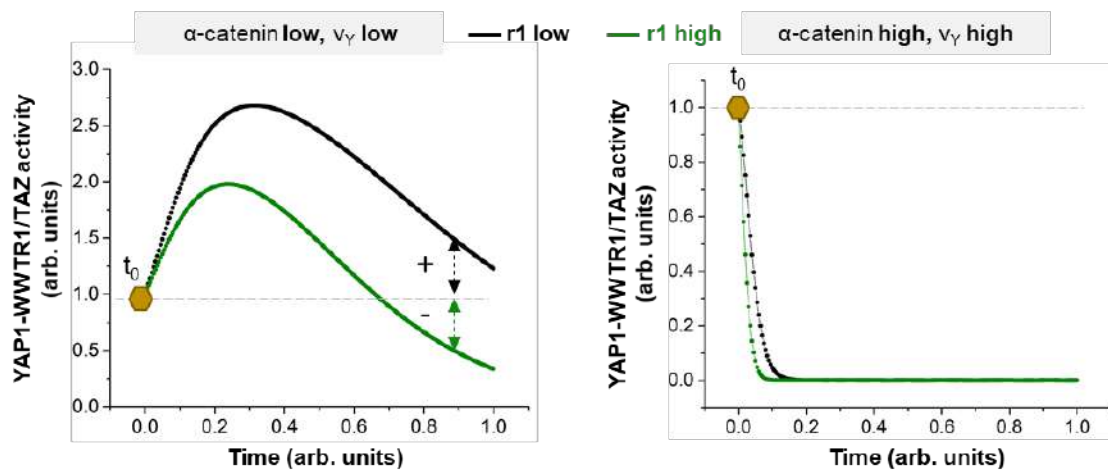


Figure 21. Schematic representation of the effects exerted by the variation of $r1$ parameter upon autophagy inhibition. Variation of parameter $r1$ (controls the *strength of the positive forward effect on YAP1 activity*): increasing $r1$ lowers the YAP1 activity, even causing YAP1 inhibition at later time points of autophagy inhibition in cells with low basal α -catenin protein levels.

The strength of the negative forward path, modelled by parameter $r2$, dictates the YAP1 output in low basal α -catenin cells

When considering the effect caused by the strength of active-YAP1 accumulation rate upon autophagy inhibition (controlled by parameter $r2$ – Fig. 13), over final YAP1 activity, it is important to understand the dynamics of the process. For instance, a system characterized by an increased cytosolic YAP1 delivery rate into autophagosomes (and followed by an accelerated autophagosome-lysosome fusion rate) would actually show *a reduction in the active-YAP1 accumulation rate* at earlier time points of autophagy inhibition using siRNA experiments targeting key ATGs: while the number of newly forming autophagosomes decreases (as this is not an instant process, rather a prolonged one that takes hours-days), the remaining autophagosomes are trying to maximize the cytosolic YAP1 degradation, being still able to deliver it into lysosomes, at the extent of active-YAP1 accumulation rate. While the YAP1 delivery rate into autophagosomes depends rather on the cytoplasmic pool of YAP1 and its autophagy adaptors, the YAP1 clearance is rather linked to the autolysosome formation and degradation capacity.

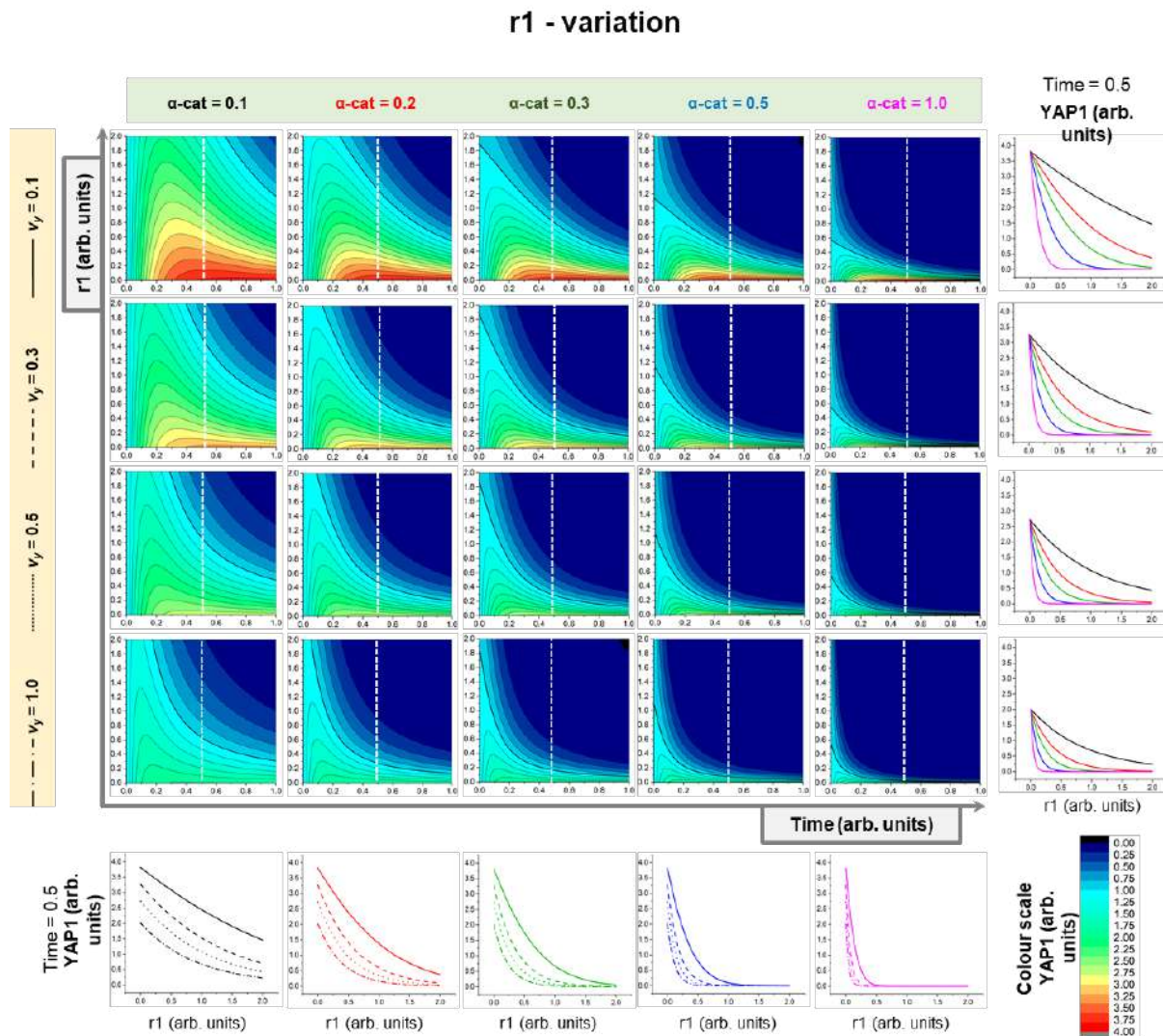


Figure 22. The effect of parameter $r1$ on the dynamics of YAP1 activity when different initial α -cat and v_Y values are considered upon autophagy down-regulation. Predicted time variation of absolute YAP1 activity (arbitrary units) when various initial α -cat and v_Y values (the strength of YAP1 influence on autophagy levels (Pavel et al. 2018)) are considered. Time parameter is shown on the horizontal axis, while the parameter $r1$ is extended on the vertical axis. The colour scale on the bottom right indicates the estimated arbitrary values of YAP1 activity for the contour plots. The black highlighted contour line corresponds to $YAP1=1.0$ (values below 1.0 denote reduction in YAP1 activity, while values above 1.0 denote increase in YAP1 activity). The profiles indicated by vertical white dotted lines (corresponding to the time step=0.5) are pictured in the line graphs plotted on the bottom (v_Y is varied; X axis – $r1$ variation, Y axis – YAP1 activity) or on the right (initial α -cat is varied; X axis – $r1$ variation, Y axis – YAP1 activity). For all plots: $A_{init}=1.0$, $Y_{init}=1.0$.

In situations characterised by a decreased accumulation rate of active-YAP1 (which is defined by a decreased value of parameter $r2$) it is worth mentioning the types of PTMs that facilitate the proper cytosolic YAP1 delivery into autophagosomes by promoting its interaction with various cytosolic autophagy adaptor proteins like p62, NBR1, co-chaperone BAG3 (phosphorylation of YAP1 and various components of the autophagy machinery – LC3, GABARAP, GABARAPL1, ATG9, ATG31-ATG29 complex; YAP1 ubiquitination linked to K63 or K27 (Wani et al., 2015), or decreased YAP1 O-GlcNAcylation – that causes YAP1 instability and promotes its degradation) (Zhang et al., 2017), or increased autophagosome-lysosome fusion and recycling (eg. dephosphorylation of TFEB) (Settembre et al., 2011).

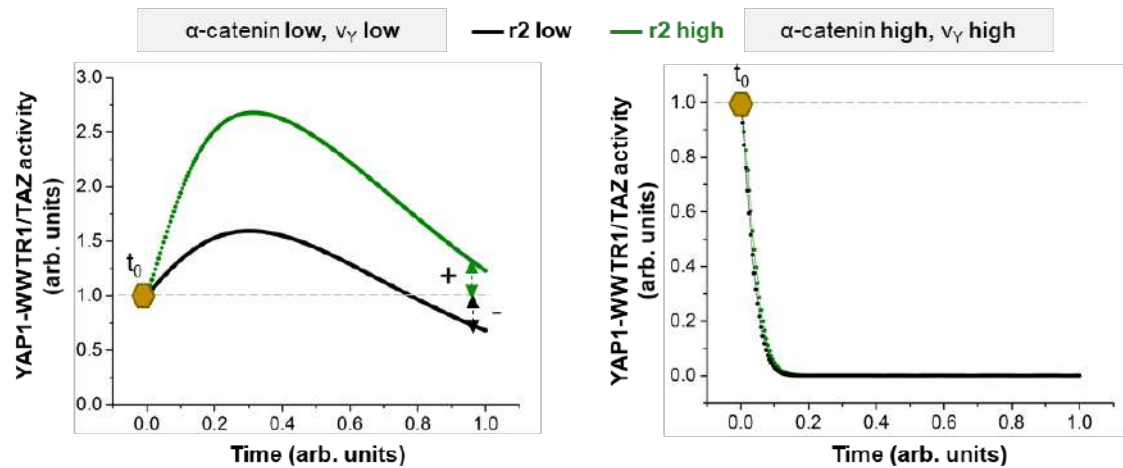


Figure 23. Schematic representation of the effects exerted by the variation of $r2$ parameter upon autophagy inhibition. Variation of parameter $r2$ (controls the *strength of the negative forward effect on YAP1 activity*): reducing $r2$ lowers the YAP1 activity, even causing YAP1 inhibition at later time points of autophagy inhibition in cells with low basal α -catenin protein levels.

The $r2$ decrease displays a similar trend as $r1$ increase over the outcome. For instance, a relatively moderate reduction in parameter $r2$ (e.g. decrease by half) would lessen the YAP1 activity, even reversing the expected output phenotype in low basal α -catenin cells at later time points of autophagy perturbation (switching from the previously expected YAP1 activation to YAP1 inhibition) – Figs. 23-24. Changes in the initial levels of autophagy, YAP1 or the strength of the feedback path only impact the magnitude of the output measures – Fig. 25. Interestingly, if there is a high discrepancy between the strengths of the two *positive* (defined by parameter $r1$) and *negative* (defined by parameter $r2$) forward paths, the effect caused by distinct basal α -catenin levels is only minor. For instance, if the strength of the direct YAP1 autophagic accumulation rate (*negative forward path*) is 5 times higher than the strength of the YAP1 cytosolic sequestration rate by α -catenins (*positive forward path*) (ratio of $r2/r1$ – Fig. 26), one may observe that the cells with high basal α -catenin expression start to behave similarly to those with initially low α -catenins levels at early-time points: they increase the YAP1 activity output – Figs. 26, 27.

The effect of variations in parameter $r3$ (the rate of α -catenin accumulation) over the final YAP1 activity levels is only minor if compared to the $r1$ and $r2$ parameters – Fig. 28. Importantly, the autophagic flux is additionally regulated, at least in yeast, by the number and size of the forming autophagosomes which directly correlates with the cellular pool of Atg8, the ortholog of the mammalian LC3 protein (Backues et al., 2014; Delorme-Axford et al., 2015; Jin and Klionsky, 2014; Loos et al., 2014).

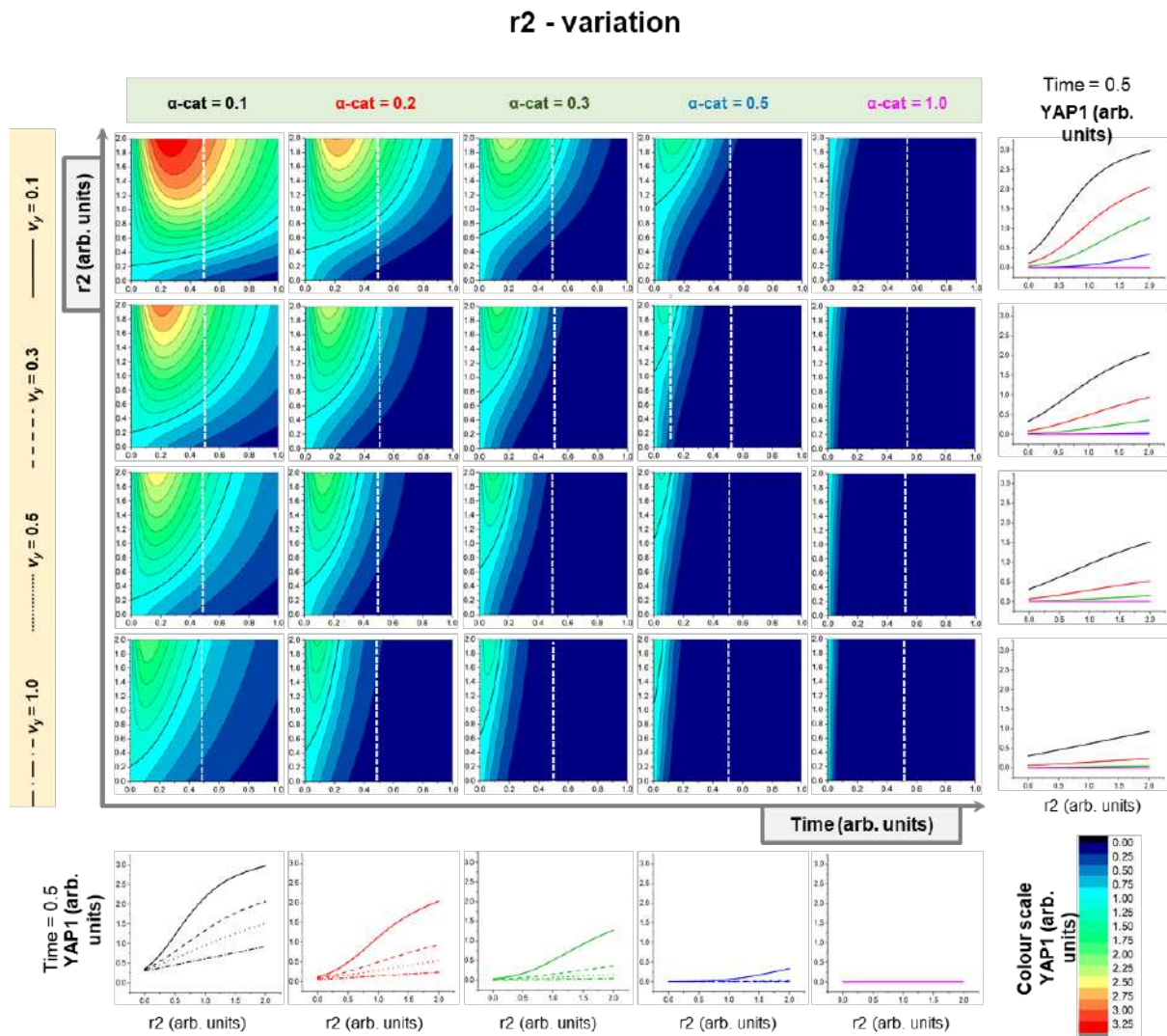


Figure 24. The effect of variable r_2 on the dynamics of YAP1 activity when different initial $\alpha\text{-cat}$ and v_Y values are considered upon autophagy down-regulation. Predicted time variation of absolute YAP1 activity (arbitrary units) when various initial $\alpha\text{-cat}$ and v_Y values (the strength of YAP1 influence on autophagy levels (Pavel et al. 2018)) are considered. Time parameter is shown on the horizontal axis, while the parameter r_2 is extended on the vertical axis. The colour scale on the bottom right indicates the estimated arbitrary values of YAP1 activity for the contour plots. The black highlighted contour line corresponds to $\text{YAP1}=1.0$ (values below 1.0 denote reduction in YAP1 activity, while values above 1.0 denote increase in YAP1 activity). The profiles indicated by vertical white dotted lines (corresponding to the time step=0.5) are pictured in the line graphs plotted on the bottom (v_Y is varied; X axis – r_2 variation, Y axis – YAP1 activity) or on the right (initial $\alpha\text{-cat}$ is varied; X axis – r_2 variation, Y axis – YAP1 activity). For all plots: $A_{\text{init}}=1.0$, $Y_{\text{init}}=1.0$.

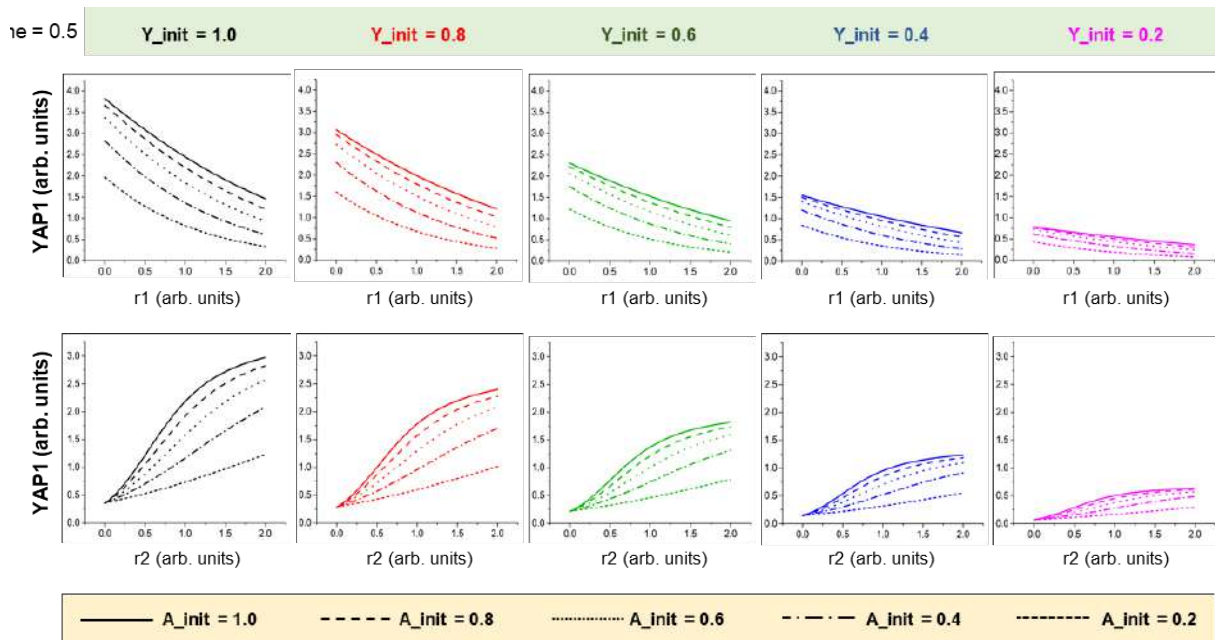


Figure 25. The effect of variables $r1$ and $r2$ on the dynamics of YAP1 activity when different initial autophagy (A_{init}) and YAP1 (Y_{init}) values are considered upon autophagy down-regulation. Predicted dynamics of YAP1 activity (arbitrary units) when various initial autophagy (A_{init}) and YAP1 activity (Y_{init}) values are considered at a fixed time after initiation of autophagy downregulation (time=0.5), and $\alpha\text{-cat}=0.1$, $v_Y=0.1$. The profiles at the indicated time point are pictured as line graphs: Y-axis – YAP1 activity; X-axis – $r1$ (on top) and $r2$ (on bottom). The colour legend for initial YAP1 variation is shown on the top of the graph, while the initial autophagy values are listed on the bottom (different line styles).

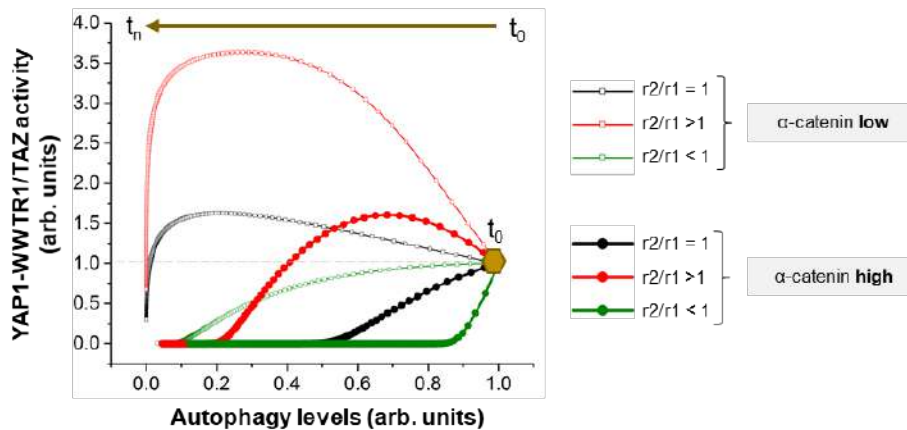


Figure 26. Schematic representation of YAP1 activity upon autophagy inhibition when one arm of the forward path is dominant. When the two arms (*positive* or *negative*) of the forward path are not balanced, the dominating arm dictates the YAP output irrespective of the initial α -catenin levels. For instance, large increase in negative arm (controlled by $r2$ parameter; over 5 times) or large decrease in the positive arm (controlled by parameter $r1$) would increase the YAP1 activity upon autophagy inhibition at early time points irrespective of the initial α -catenin levels. Conversely, large reduction in the negative arm would cause the opposite effect: decreased YAP1 activity upon autophagy inhibition irrespective of the initial α -catenin levels.

accumulation of α -catenins. For cells with low basal levels of α -catenins, the YAP1-WWTR1 activity will initially increase (as the direct effect exerted by autophagy dominates the indirect one), but as α -catenins accumulate, the strength of the indirect effect rises, up to a time-point when it actually dominates the system, and therefore, YAP1 activity start to decrease from this step onwards.

This study, focusing on the YAP1-WWTR1 activity as output, reveals how autophagy modulates cell behavior in a time-dependent manner, causing completely opposite effects in cells with different starting levels of an intermediary protein (α -catenin). It will be interesting to apply the principles underlying the mathematical model used to explain these cellular controversies in other signaling pathways, where autophagy perturbations appear to cause contrasting reactions in distinct tissues, organs or individuals. Our new perspective also highlights the important issue that cellular responses to perturbations often change over time, and that better understanding of such dynamic effects may be important for our appreciation of the roles of autophagy and related processes in health and disease.

Final remarks

To summarize what we generally learnt from our proposed model:

- i) distinct basal expression of one single protein (e.g. α -catenins) is sufficient to define the cell fate upon external/internal perturbations;
- ii) distinct time periods of applied perturbations may cause contradictory outcomes in the same cellular system;
- iii) the strength of the feedback path (e.g. YAP1 controlling autophagy) impacts on the magnitude of the outcome, but has only minor effects on the cell fate (i.e. directionality of outcome);
- iv) internal/external perturbations (e.g. responsible for controlling the strength of the positive and negative forward paths exerted by autophagy over YAP1 activity) may influence the cell fate in cells with low expression of inhibitors;
- v) if one of the contrasting effects is predominant, it may override the outcome irrespective of any other basal conditions.

These new perspectives also highlight the important issue that cellular responses to perturbations often change over time, and that better understanding of such dynamic effects may be important for our appreciation of the roles of autophagy and related processes in health and disease. Thus, future systematic experimental work is required for properly appreciating and predicting the outcome of a certain stimulus on distinct signalling pathways.

1.2.3. Crosstalk between autophagy and other intracellular transduction pathways perturbed in cancers: forward and feedback paths

1.2.3.1. Introduction

The physiological relevance of autophagy is related to the normal turnover of the cellular components and the clearance of misfolded long-lived proteins or damaged organelles (Ashkenazi et al., 2017b; Menzies et al., 2017a; Pavel and Rubinsztein, 2013). Under stress conditions, such as starvation or oxidative stress, autophagy is upregulated to degrade dispensable macromolecules and restore nutrient balance (Singh and Cuervo, 2011).

A series of autophagy-related (ATG) proteins participate in the main steps of the autophagy pathway: formation of autophagosomal membranes, maturation and final fusion with lysosomes (Behrends et al., 2010; Menzies et al., 2017a; Pavel and Rubinsztein, 2017). Briefly, downstream of mTORC1 complex inhibition and other signalling cascades, several protein complexes (ULK1/ATG1 complex; class III phosphatidylinositol 3-kinase/VPS34 complex containing Beclin1/BECN1-p150-ATG14; ATG12-ATG5-ATG16L1 complex) are formed, and initiate the assembly of the autophagosomal membranes delivered by ATG 9 (Menzies et al., 2017a; Pavel and Rubinsztein, 2017). The microtubule-associated protein 1 light chain 3 (MAP1-LC3 or simply LC3) family of proteins is conjugated to phosphatidylethanolamine in the nascent autophagosome membranes in a defining step in autophagosome biogenesis (Klionsky et al., 2021). Fully formed autophagosomes finally fuse with lysosomes through a process mediated by SNAREs and other proteins (Bento et al., 2016c; Djajadikerta et al., 2020).

The destinations, functions, and activities of ATGs or autophagic cargoes are mainly regulated by posttranslational modifications (PTMs) - such as phosphorylation, acetylation, O-GlcNAcylation, ubiquitination, lipidation, glycosylation, and proteolysis (Wani et al., 2015). Monitoring the effects that these distinct PTMs have on the overall rate of autophagic degradation helps defining the general autophagy pathway control. For instance, phosphorylation of serine and threonine residues regulates the interaction between various ATG proteins to form complexes (e.g. ATG12-ATG5-ATG16L1, ULK1 or VPS34 complexes), modulates the catalytic activities of various kinases (e.g. AMPK, mTOR, ULK1, VPS34), or defines the cellular localisation (nuclear *vs.* cytoplasm) of the transcription factors involved in the positive (TFEB (Settembre et al., 2011), YAP1-TEAD (Pavel et al., 2018a)) or negative (ZKSCAN3 (Chauhan et al., 2013)) transcriptional control of autophagy. However, phosphorylation may cause opposite outcomes on the autophagy pathway depending on the target: either induction (when AMPK, ULK1/ATG1, ATG9, or p62 are phosphorylated) (Matsumoto et al., 2011; Papinski et al., 2014; Xie et al., 2015) or repression of autophagy (p-BECN1) (Wang et al., 2012a). In addition to being modified by phosphorylation, serine and threonine residues of autophagy proteins can also be modified by the O-GlcNAcylation (O-linked attachment of β -N-acetyl-glucosamine) with similar contrasting effects: autophagy activation, when AMPK is O-GlcNAcyated (Bullen et al., 2014) or inhibition, when BECN1 is posttranslationally modified in this way (Marsh et al., 2013). Additionally, K63 polyubiquitination of aggregate-prone proteins is believed to dictate their degradation via the autophagic-lysosomal route, while the K48 or K11 polyubiquitinated proteins are rather delivered to the ubiquitin-proteasome system (UPS) (Xie et al., 2015). Adaptor molecules (such as p62/SQSTM1, NBR1, NDP52, optineurin, VCP) through their ability to bind both LC3/GABARAP (they have a LC3 Interacting Region - LIR domain) and K63 polyubiquitinated proteins (often via an Ub-binding - UBA domain), manage to selectively target the cargo to the autophagy pathway (Kirkin et al., 2009b; Lippai and Low, 2014). Ultimately, the autophagy receptors are degraded together with their cargos in autolysosomes (Itakura and Mizushima, 2011; Kirkin et al., 2009a).

PTMs impact differently on the autophagy route with regard to its forming intermediates (autophagosomes and autolysosomes) causing either changes in their pool size of directly affecting the autophagosome synthesis rate, fusion rate or cargo degradation rate. These autophagy perturbations further signal to control the transcription of genes, cell growth and proliferation or the balance between cell survival and apoptosis *via* various transduction pathways. The tight interconnections between autophagy and various signalling routes ultimately dictate cell fate and often serve as the main control systems that defines cell identity (Pavel et al., 2021a; Pavel and Rubinsztein, 2017).

We have previously identified that various posttranslational and transcriptional interconnections between YAP1/TAZ (Hippo signalling) and autophagy cause opposite outputs in different cell lines, at distinct time-points of autophagy perturbation, and proposed a mathematical model for predicting the cellular behavior under such variations. The previous mathematical-numerical model used for explaining the autophagy-YAP1 link might serve as an example that could be extended to autophagy and its cross-talk with other transduction pathways (Wnt/ β -catenin signalling, TGF- β /Smads signalling, NF- κ B or XIAP/cIAP-mediated cell survival) where similar major axes have been identified: a) a *positive* forward path, when autophagy indirectly up-regulates that particular signalling pathway (e.g. autophagy degrades the pathway's inhibitors); b) a *negative* forward path, when autophagy directly inhibits the signalling (e.g. autophagy directly degrades the pathway's components); c) a feedback regulatory path exerted by the transduction pathway over autophagy.

1.2.3.2. Aim

Further insights that may connect the contrasting, but extremely valuable observations from the literature in the field of autophagy and intracellular signalling is indeed required. In the following sections, we aimed to outline some possibilities that may inform future efforts aiming to reconcile apparent contradictions in the literature.

1.2.3.3. Results

Autophagy and Wnt/ β -catenin signalling

Autophagy was shown to positively regulate the activation of Wnt/ β -catenin signalling in hepatocellular carcinoma cells, causing increased cancer cell glycolysis (Fan et al., 2018). On the other hand, it has been reported that autophagy induction was able to repress the Wnt/ β -catenin signalling pathway by stimulating the autolysosomal degradation of key pathway-components, like β -catenin (Petherick et al., 2013) and Dishevelled (Dvl) (Gao et al., 2010) – Fig. 28. If the β -catenin is directly delivered to the forming autophagosomal membranes (a LIR-mediated process) in a series of cell lines (HT29 and RKO carcinoma-derived cell lines, HEK293T cells, HCT116 cells, intestinal epithelial mouse cells), Dvl2 first requires PTMs (ubiquitylation mediated by the von Hippel-Lindau/VHL protein) that would favour its aggregation and binding to p62, which further mediates the delivery of Dvl2 to the autophagy-lysosomal system in cell lines like HeLa, HEK293T, SW480, and immortalized mouse embryonic fibroblasts (MEFs) or biopsy pieces from human colon carcinoma tissues (Gao et al., 2010). The feedback loop caused by Wnt/ β -catenin controlling autophagy complicates the picture, as Wnt/ β -catenin signalling (activated through the Wnt3 ligand) positively regulated autophagy in squamous cell carcinoma of the head and neck, promoting the cancer cell radioresistance (Jing et al., 2019). Conversely, other studies have shown that the Wnt/ β -catenin pathway negatively modulates autophagy: activation of this signalling route attenuated Beclin-1-dependent autophagy in human osteosarcoma cells, while inhibition led to increased expression of key autophagy genes (eg. *LC3B*, *BECN1*, *P62*), and downregulation of autophagy inhibitory proteins (e.g. Bcl-2) in multiple myeloma cells (Su et al., 2016), glioblastoma cells (Nager et al., 2018) or mammary epithelial cells (Cicchini et al., 2014).

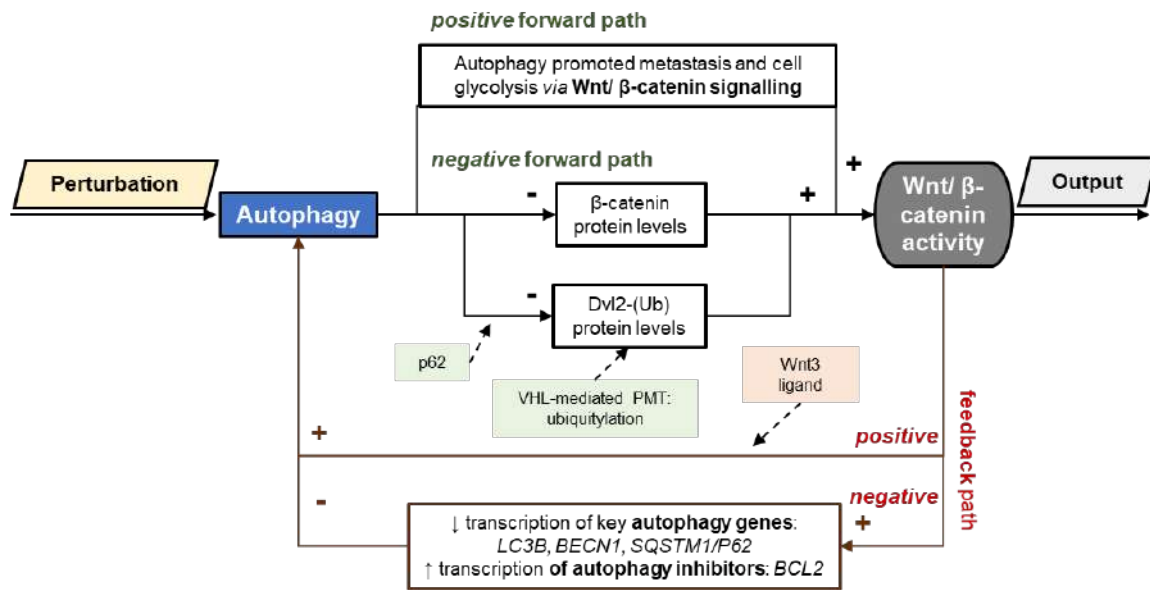


Figure 28. Schematic representation of the autophagy-Wnt/ β -catenin signalling control system. Both forward and feedback paths present two arms: *positive* and *negative*.

Autophagy and TGF β /Smads signalling

For the TGF β signalling and autophagy link, two distinct studies, one from Javad Alizadeh and co-workers studying TGF β 1, and another one by Yan Sun et al focusing on TGF β 2, have shown that autophagy positively modulates the TGF β -Smads signalling-induced epithelial to mesenchymal transition (EMT), cellular migration and contraction in non-small cell lung cancer cells (NSCLC – A549, H1975 cell lines) (Alizadeh et al., 2018) and primary rabbit lens epithelial cells by controlling the phosphorylation status of Smad2/3 proteins (Sun et al., 2021). A recent study further reinforces these observations, supporting the role of autophagy in mediating the TGF β /Smads-induced fibrosis in human trabecular meshwork cells (specialised ocular tissue which maintains intraocular pressure) by controlling the transcription of the TGF β antagonist, BMP and activin membrane bound inhibitor (BAMBI) (Nettesheim et al., 2019). With relevance to the innate immune antiviral response, autophagy also triggers the activation of TGF β production and Smad2/3 signalling in Human respiratory syncytial virus (RSV)-infected primary mouse macrophages and -RAW 264.7 (mouse macrophage cell line) cells to induce the production of optimal IFN β (Pokharel et al., 2016) – Fig. 29.

This biology appears to include a negative regulation loop, as it has been reported that autophagy degrades TGF β , reducing the protein levels without alterations in the mRNA levels, in primary mouse renal tubular epithelial cells (RTEC) and human HK-2 (human proximal RTEC) cells (Ding et al., 2014). For the feedback loop (how the TGF β signalling controls autophagy), multiple studies have shown that TGF β signals by upregulating the expression of key autophagy genes (*LC3B*, *BECN1*, *ATG5*, *ATG7*), and thus induces autophagy, which, in turn, facilitates the phosphorylation status of Smad2/3 to control fibrosis in primary human atrial myofibroblasts (Ghavami et al., 2015) or cell growth in HuH7 (human hepatocellular carcinoma) cells, MDA-MB-231 (mammary carcinoma) cells (Kiyono et al., 2009), or normal bovine mammary epithelial BME-UV1 cells (Gajewska et al., 2005). Interestingly, a recent study described that TGF β signals through Smad proteins to induce TFEB expression and facilitate the TFEB-driven autophagy in a panel of pancreatic cancer cell lines (eg. MIA PaCa-2, PANC-1, Panc03.27 lines) and patients' tissues (He et al., 2019).

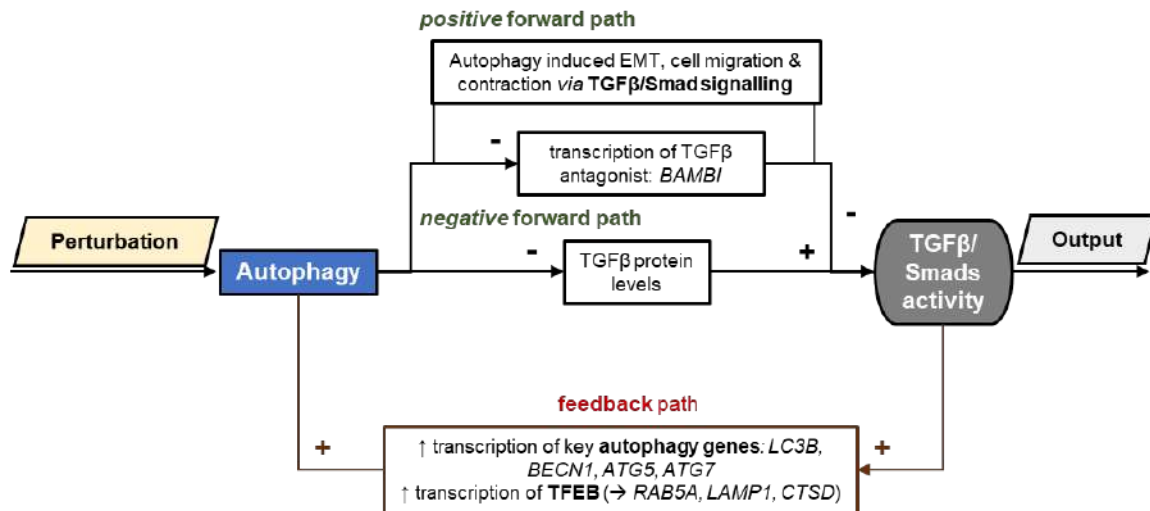


Figure 29. Schematic representation of the autophagy-TGFβ/Smads signalling control system. The forward path presents two arms: *positive* and *negative*, while the feedback is only *positive*.

Autophagy and NF-κB signalling

NF-κB transcription factors are key regulators of cell survival and aberrant NF-κB signalling has been involved in the pathogenesis of most human malignancies. The cross-talk between NF-κB signalling and autophagy is also complex. For instance, autophagy positively regulates NF-κB signalling by promoting the degradation of its well-known inhibitor IκBα in a set of intestinal epithelial cell lines (HT29, HCT116, HCT15, HCA7, SW48, RKO, and HCT8) and MEFs (Colleran et al., 2011). Interestingly, autophagy also negatively impacts NF-κB signalling by promoting the degradation of key activators (IKK alpha, beta, gamma, and NIK – the activator of IKK) by several mechanisms – Fig. 30. One mechanism implies that the autophagic degradation of IKK is accelerated in the absence of its binding-partner Hsp90 and independently of its ubiquitination status in HEK293, Jurkat cells, Human B-cell line Ramos RG69, mouse fibroblasts ts20, and MEFs (Qing et al., 2006). Kelch-like ECH-associated protein 1 (KEAP1), an E3 ubiquitin ligase, further promoted the delivery of IKKbeta to the autolysosomal system for degradation by competing with HSP90 for the direct binding to IKKbeta. KEAP1, in addition to diminishing the expression of IKKbeta, also causes inactivation of IKKbeta by reducing its phosphorylation status in HEK293 and HeLa cells (Kim et al., 2010). Another E3 ubiquitin ligase, Ro52, facilitates the monoubiquitination of the phosphorylated active form of IKKbeta induced by the Tax oncoprotein of HTLV-1, a PTM involved in the subcellular translocation of the active IKKbeta to autophagosomes with subsequent lysosomal degradation, leading to the inactivation of NF-κB pathway in HEK293 and HeLa cells (Niida et al., 2010). The active IKKbeta may also be delivered to autophagosomes via an adaptor protein, an F-box protein, S-phase kinase associated protein 2 (SKP2), that bridges IKKbeta and the autophagic cargo receptor p62, thus promoting p62-mediated selective autophagic degradation of IKKbeta followed by NF-κB inhibition in HEK293 and HeLa cells (Liu et al., 2018). With relevance to the innate immune anti-bacterial response, Atg7 was found as a binding partner for the phosphorylated IκBα. Thus, the loss of Atg7 (independently of autophagy) led to the p-IκBα release from the interaction promoting its ubiquitination and UPS-mediated degradation, and ultimately triggering the NF-κB activation in murine macrophages (Ye et al., 2015). ATG5 deficiency also augmented NF-κB-mediated inflammation in proximal tubular epithelial cells (Peng et al., 2019).

This pathway may also involve a feedback loop (how NF- κ B impacts on autophagy pathway?), as several studies have confirmed that NF- κ B/IKK signals to stimulate autophagy by up-regulating the expression of several genes involved in the formation and maturation of the autophagic machinery (eg. *BECN1*, *ATG5*, *LC3*, *LAMP1*, *RAB7*) in a set of cell lines including MEFs (Comb et al., 2011), HeLa, and MCF10A cells (Lin et al., 2015). However, NF- κ B also suppresses autophagy, by upregulating the expression of several well-known autophagy repressors (A20, Bcl-2 family members, phosphatase and tensin homolog/mammalian target of rapamycin (PTEN/mTOR) and nitric oxide (NO)), and/or by suppressing some autophagy inducers (Bcl-2 interacting protein 3 (BNIP3), JNK1, p53 and ROS) in distinct cell lines and time points after perturbation/signalling (rat primary cortical neurons, MEFs, HeLa, immature B cell lymphoma WEHI 231 cells, and sarcoma cells) (Catz and Johnson, 2001; Djavaheri-Mergny et al., 2006; Sarkar et al., 2011; Verzella et al., 2020).

NF- κ B signalling has been associated to the upregulation of several inhibitors of apoptosis (IAPs) family members, including cellular inhibitor of apoptosis 1 (cIAP1) and 2 (cIAP2), X chromosome-linked inhibitor of apoptosis (XIAP) (Baldwin, 2012; Bavi et al., 2011; Karin and Lin, 2002; Luo et al., 2005; Wang et al., 1998).

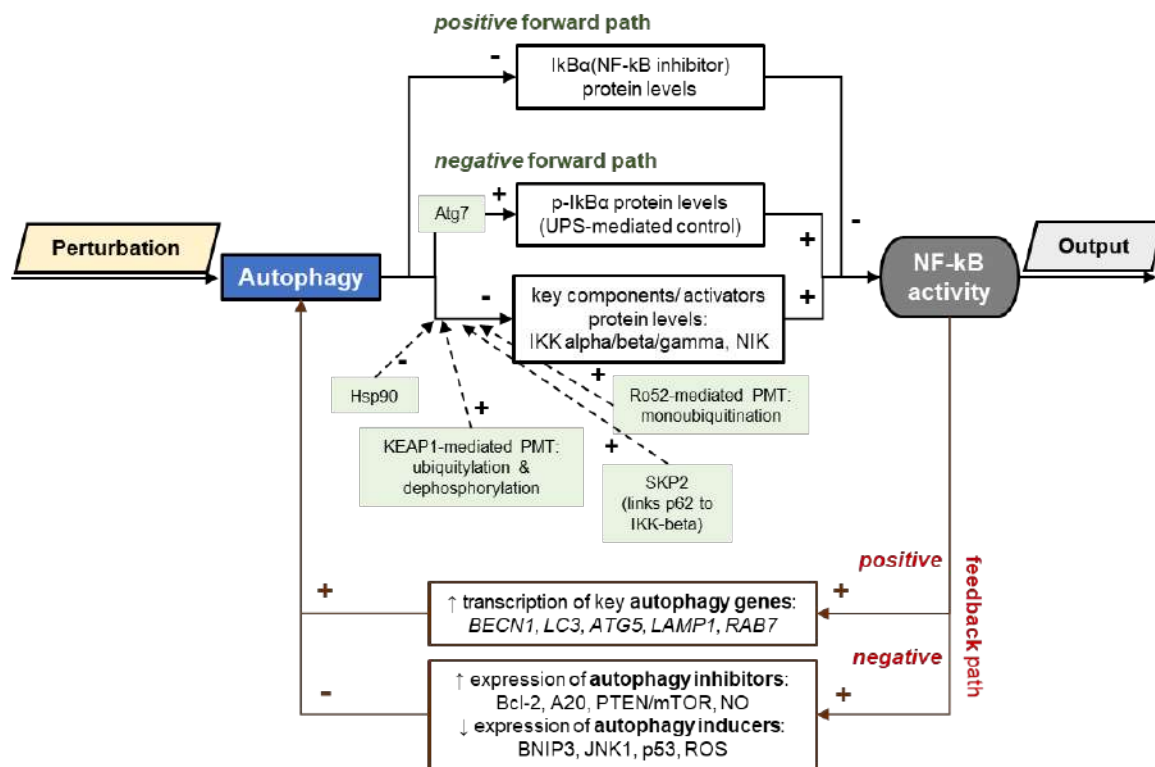


Figure 30. Schematic representation of the autophagy-NF- κ B signalling control system. Both forward and feedback paths present two arms: *positive* and *negative*.

Autophagy and XIAP/cIAP-mediated cell survival

Controversial literature also exists for the role of autophagy in controlling the balance between cell survival and apoptosis. If one searches for the links between the E3 ubiquitin ligases, XIAP/cIAPs, and autophagy, one may observe that short periods of autophagy activation promote cell survival via the NF- κ B mediated upregulation of anti-apoptotic genes (Bcl-2 (Kapuy et al., 2013), Bcl-XL, XIAP, cIAP1, cIAP2...) in various cancer cell types: human glioma cell lines (A172, U87, U251 cell lines) (Tsuboi et al., 2009), fibrosarcoma cell lines, or human diffuse large B cell lymphoma cell lines (DLBCL - RIVA, OCI-LY3, SUDHL-

2, HBL-1 and SUDHL-5) (Chen et al., 2016; Dutta et al., 2006; Karin, 2006; Wang et al., 1998). However, induction of autophagy by Timosaponin AIII caused the lysosomal degradation of ubiquitinated XIAP and induced apoptosis in hepatocarcinoma cells (Wang et al., 2013). The critical role of ubiquitination as a PTM in facilitating the autophagy-dependent proteolysis of XIAP was also confirmed using E1 enzyme inhibitors (Wang et al., 2013). In support of these last findings, prolonged autophagy induction with rottlerin caused apoptosis by downregulating the expression levels of XIAP, cIAP-1, Bcl-2 and Bcl-XL protein levels in pancreatic cancer stem cells (Singh et al., 2012) – Fig. 31.

When considering the feedback loop (how XIAP/cIAP1/2 proteins impact on autophagy?), it is important to highlight that XIAP and cIAP1, through their E3 ubiquitin ligase activities, positively regulate autophagy: either by increasing the NF- κ B capacity to promote the transcription of *BECN1* in HeLa, MEFs, MCF10A and DLBCL cell lines (SUDHL-5, SUDHL-8 and SUDHL-10) (Lin et al., 2015), or by assisting the efficient fusion of lysosomes with autophagosomes in HeLa, MEFs and dermal fibroblasts (Gradzka et al., 2018). Distinct studies have shown the opposite effect of XIAP on autophagy by a distinct mechanism: phosphorylated active XIAP acts as an E3 ligase that mediates the rapid proteasomal degradation of Mdm2 (the major ubiquitin E3 ligase and inhibitor of p53), thus upregulating the cytosolic p53 levels which ultimately suppress autophagy (Huang et al., 2013). This last effect was shown in a set of cell lines also used in the previous studies (MEFs and MCF10A cells) and additional ones (HCT116, HepG2, HEK293T, A549, MCF7 cells), but using different time points of exposure and concentrations of the XIAP inhibitor, embelin: short periods (1-4 hours) and very low concentrations (50-200 nM) (Huang et al., 2013) vs longer time periods (16 hours) at higher concentrations of 10-20 μ M in another study (Lin et al., 2015). Additional studies have found that XIAP acts as an E3 ubiquitin ligase for p62 promoting its UPS-mediated degradation, thus suppressing the p62-selective autophagy in HCT116, HepG2, HEK293T, A549, and MDA-MB-cells (Huang et al., 2019).

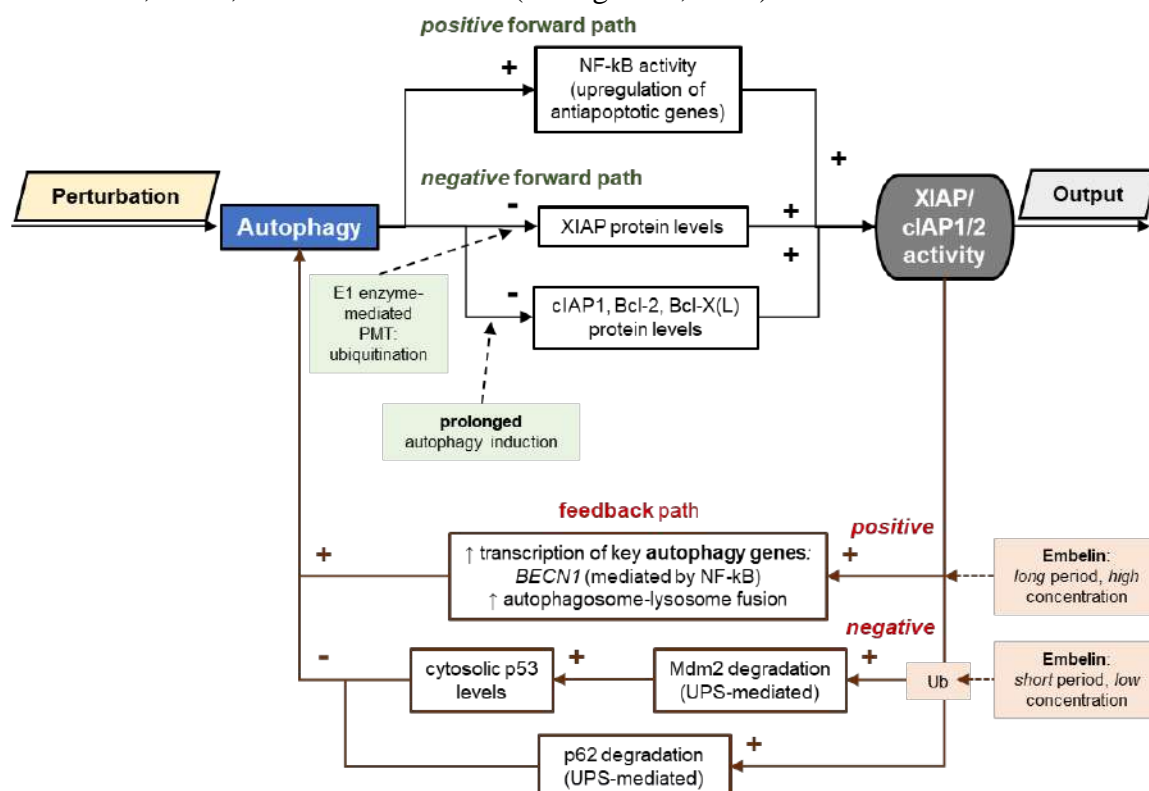


Figure 31. Schematic representation of the autophagy-XIAP/cIAP signalling control system. Both forward and feedback paths present two arms: *positive* and *negative*, each of them with multiple mechanisms.

These different interactions between autophagy and diverse signalling pathways suggest that distinct initial conditions (intracellular networks and PTMs) may explain why various studies have obtained contrasting results when using different biological systems, or even the same systems but unrelated time points (or concentrations) of perturbations/ treatments.

1.2.3.4. Concluding remarks and open questions

We believe that multiple points of influence determined by PTMs (phosphorylation, ubiquitylation, acetylation, O-GlcNAcylation...), apart from the basal protein expression, modify the final outcomes in biological systems and define cell fate, acting as a switch on/off button. For example, both abnormal acetylation and deacetylation are known to translate towards pathological conditions, particularly neurodegenerative diseases and cancer (Son et al., 2021; Son et al., 2019; Son et al., 2020). Our observations point out that a heterogeneous biological system (same cell type, but with slightly different basal conditions or altered posttranslational processes) leads to different outcomes at the individual cell level and at different time points after perturbation. This supposition may explain how tumorigenic changes might start in only one or few cells in a dynamic process of alternating on-off steps, as the parameters involved might vary over time and space (e.g. transcriptional or PTMs caused by various environmental perturbations).

Our proposed models used for understanding the crosstalk between a signalling pathway and autophagy, might provide insight into therapeutic opportunities in a variety of cancers (hepatocarcinoma, pancreatic adenocarcinoma, breast cancers, cancers of the head and neck etc.). Nevertheless, multiple parameters bring complexity to the system being considered, but, at the same time shed light on the importance of understanding tissue heterogeneity. This highlights the requirement for single cell analysis to assess transcriptional and post-translational modification levels in order to achieve the proper understanding of the biological processes that characterize the patient's cancer cells, by integrating the single-cell fluorescence analysis of autophagy (Loos et al., 2014), with data acquired from high-throughput omics platforms and machine-learning algorithms (Loos et al., 2020; Toit et al., 2020). This may allow for the identification of intracellular changes that need to be repaired for reversing the cellular status to a benign state. Importantly, any biological process should be followed kinetically, as the same perturbation applied for different time periods might end up with contrasting outcomes.

Final remarks

Perturbing a metabolic process, either autophagy or any other catabolic/anabolic route, will inevitably impact on multiple transduction pathways. For instance, when common cancer hallmarks (increased cell proliferation, cell glycolysis) are investigated as readouts, one should be careful in designing the experiments and interpreting the data: the initial perturbation of one cellular process (e.g. autophagy) will disturb multiple signalling cascades with contrasting effects. For example, cell proliferation, differentiation and/or survival are promoted by YAP1, Wnt, and NF- κ B signalling, but inhibited by TGF β . Nevertheless, these signalling routes may react distinctively at various time points as different axes are switched on/off at early *vs.* late responses, or short *vs.* long perturbations: short periods of autophagy induction promote resistance to cell death via NF- κ B, while longer activation may induce autophagy-dependent cell death (Denton and Kumar, 2019; Kriel and Loos, 2019; Tavassoly et al., 2015). The system biology is further complicated and controlled, apart from the feedback loops, by the vast regulatory links (many still unknown) existing between the different axes affected by the initial perturbation (e.g. autophagy), and all systems-level properties of the control networks should be integrated into relevant mathematical models (Kapuy et al., 2021; Kapuy et al., 2013; Pavel

et al., 2021a; Pavel et al., 2021b; Tavassoly et al., 2015). Thus, the cellular biological complexity requires further in-depth study.

In conclusion, the highest priority for further research should be given to gathering and merging the existing research information to define the integrated relevant cellular networks using specialised bioinformatics platforms to facilitate the understanding and prediction of cell responses to external/internal stimuli with relevance to designing successful precision therapies.

1.3. Autophagy and neurodegeneration interlink

One area of particular interest is the relevance of autophagy to neurodegenerative diseases. Many neurodegenerative diseases, including Alzheimer's disease, Parkinson's disease, and Huntington's disease, arise from the accumulation of oligomers and aggregates of misfolded proteins. As these proteins exert toxic effects on cells, lowering the levels of these proteins can be therapeutically favourable (Menzies et al., 2017a). Autophagy degrades many of the toxic aggregate-prone proteins responsible for disease, including mutant huntingtin (mHTT), alpha-synuclein (α -syn), tau and other aggregate-prone proteins (Ravikumar et al., 2004a). Many of these proteins also cause disruptions in autophagy (Ashkenazi et al., 2017a; Winslow and Rubinsztein, 2011), raising the possibility that their ability to hinder autophagy contributes to their toxicity. In further support of a relationship between autophagy and neurodegenerative disease, some risk genes linked to neurodegenerative diseases play a role in the autophagy pathway (Menzies et al., 2017a). This considerable body of evidence linking autophagy and neurodegeneration gives rise to the possibility that autophagy upregulation may be a viable therapeutic strategy in some neurodegenerative diseases.

Understanding the interplay between autophagy and neurodegeneration requires a knowledge of the multiple steps involved in the autophagy pathway (Fig 32).

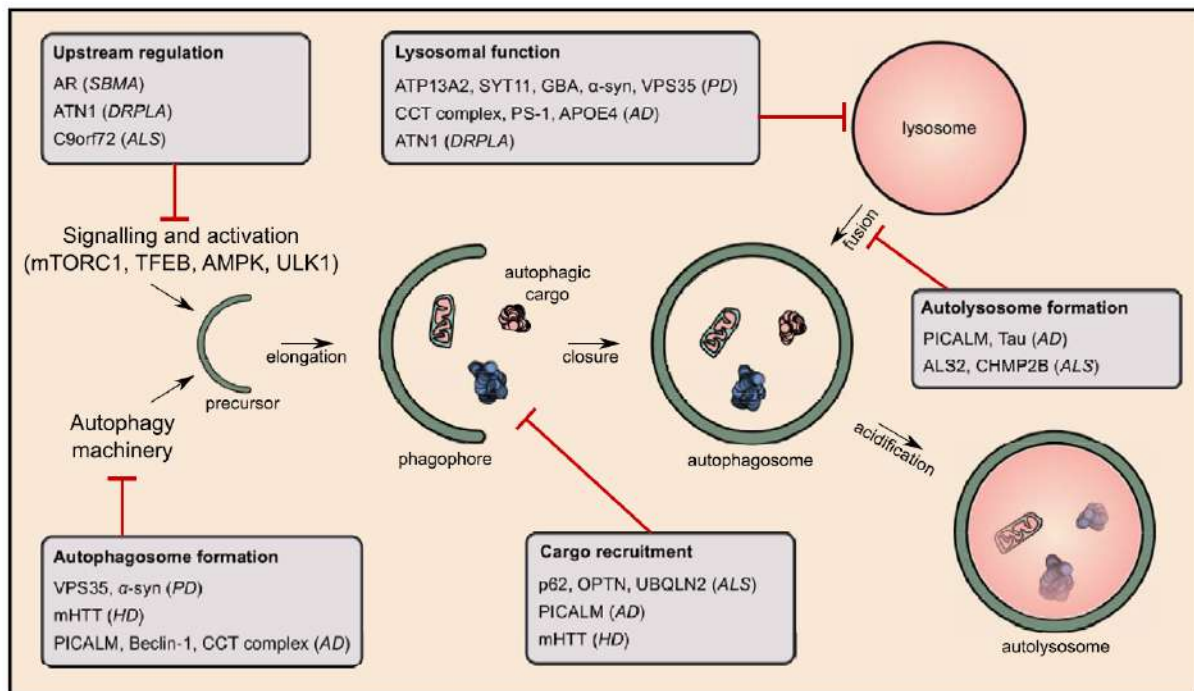


Fig. 32. Defective autophagy and neurodegenerative disease. A number of risk genes linked to neurodegenerative diseases play a role in the autophagy pathway. These genes intersect with the autophagy pathway at many different stages, as indicated here. Disruptions to autophagy caused by pathogenic changes to the relevant genes may contribute to disease pathogenesis.

The process of autophagy involves a series of regulated mechanical steps, including autophagosome formation, maturation and closure (Bento et al., 2016b; Rubinsztein, 2012). The initial stages of autophagy are marked by cup-shaped, double-membraned phagophores, the formation of which requires PI(3)P generation by the Beclin-1-VPS34 complex. The edges of these phagophores subsequently extend and fuse to form autophagosomes. These are trafficked towards the proximity of lysosomes via the dynein machinery on microtubules, which allows fusion with lysosomes and degradation of autophagosomal contents. Each of these steps is subject to regulation by various upstream signalling pathways, notably via mTORC1, a major regulator of cell metabolism, (Hosokawa et al., 2009a) and TFEB (Settembre et al., 2011), a key transcriptional regulator of autophagy and lysosomal biogenesis. Autophagic flux thus depends on multiple steps and requires coordination between autophagosome biogenesis and lysosomal degradation. Interventions aimed at inducing autophagy have been targeted towards various stages in this process, potentially leading to different effects on disease progression.

1.3.1. Polyglutamine tracts regulate beclin 1-dependent autophagy in neurodegenerative diseases

1.3.1.1. Introduction

Nine neurodegenerative diseases are caused by expanded polyglutamine (polyQ) tracts in different proteins, like huntingtin in Huntington's disease (HD) and ataxin-3 in spinocerebellar ataxia type 3 (SCA3) (DiFiglia et al., 1997; Riess et al., 2008). Age-at-onset decreases with increasing polyglutamine length in these proteins and the normal length is also polymorphic (Imarisio et al., 2008). Importantly, the wild-type counterparts of these disease proteins have shorter polyglutamine tracts that are conserved in many species, suggesting that they have biological functions. One possibility is that this domain contributes to protein-protein interactions but the functional understanding of the roles of these domains is limited. The presence of the same expansion mutation in different proteins suggests a common pathogenic mechanism. One process shared across these diseases is the propensity of the mutant proteins to aggregate (Rubinsztein, 2006). While this process has been implicated in pathogenesis, soluble forms of these proteins have also been shown to be toxic (Arrasate et al., 2004). However, toxic molecular mechanisms of such soluble expanded polyQ-containing species have been elusive.

When these mutant proteins reside in the cytoplasm, they have a high dependence on autophagy for their clearance. This is likely because the aggregated-oligomeric species are inaccessible to the proteasome and chaperone-mediated autophagy. Induction of autophagy enhances clearance of polyQ-expanded mutant proteins, like mutant HTT (huntingtin) and ATXN3, thereby attenuating their toxicity in cell and mouse models of Huntington disease and spinocerebellar ataxia, respectively (Menzies et al., 2010; Ravikumar et al., 2004b).

1.3.1.2. Aim

For this study we aimed to understand the interplay between polyQ disease proteins and autophagy, and thus, we investigated how wild-type ataxin-3, a deubiquitinating enzyme (Burnett et al., 2003; Chai et al., 2004) with polyQ domain and widely expressed in the brain (Paulson et al., 1997; Trottier et al., 1998), affects this degradation intracellular process and its role in neurodegenerative disease pathogenesis.

1.3.1.3. Materials and methods

Reagents and cell lines

The primary antibodies used in the study include rabbit anti-actin (A2066), mouse anti-Flag M2 (F3165) and mouse anti-tubulin (T9026) from Sigma; rabbit anti-LC3 (NB 100-2220) and rabbit anti-atrophia-1 (NB100-2336) from Novus Biologicals; mouse anti-HA.11 (MMS-101P) from Covance; mouse anti-p62 (610833) from BD Bioscience; rabbit anti-beclin 1 (3738), rabbit anti-VPS34 (4263), rabbit anti-K48 polyUb (8081) and rabbit anti-K63 polyUb (5621) from Cell Signalling; rabbit anti-GFP (ab6556) from Abcam; mouse anti-ataxin 3 (MAB5360) and mouse anti-polyglutamine (MAB1574) from Millipore; mouse anti-GFP (632375) from Clontech; mouse anti-androgen receptor (sc-7305) from Santa Cruz; anti-mouse (NA931V) and anti-rabbit (NA934V) horseradish peroxidase (HRP)-conjugated secondary antibodies from GE Healthcare; goat anti-rabbit 800CW secondary antibodies (926-32211) from LI-COR; and Alexa Fluor 555- (A21428) conjugated goat anti-rabbit secondary antibodies from Invitrogen/Life Technologies.

Human cervical carcinoma (HeLa) cells and striatal neuronal cell lines derived from wild-type HTT Q7/Q7 and heterozygous HTT Q7/Q111 knock-in mice (Coriell Institute CH00097 and CH00096, respectively) were grown at 37 °C (for HeLa) and at 33 °C (for striatal cells) in DMEM (Sigma) supplemented with 10% FBS, 100 U ml⁻¹ penicillin/streptomycin, 2 mM L-glutamine and 1 mM sodium pyruvate (basal medium) in 5% CO₂. HeLa cells stably expressing GFP-LC3 and HeLa cells stably expressing the mTagRFP-mWasabi-LC3 reporter were cultured in basal medium supplemented with 500 µg ml⁻¹ G418 (Sigma).

Food deprivation in Huntington's disease model mice

We used HD-N171-82Q mice (B6C3F1/J-Tg(HD82Gln)81 Dbo/J, Jackson Laboratory). These mice carry an N-terminal fragment expressing the first 171 amino acids of human huntingtin with 82 glutamine repeats under the mouse prion promoter. The Huntington's disease transgenic mice and non-transgenic littermates were males and females at the age of 6 weeks in the study. The mice fasted and were deprived of food for a total period of 48 h with free access to water throughout the procedure. After 22.5 h starvation, mice were given free access to food for 1.5 h followed by a second round of starvation for another 22.5 h. At the end of this period, the mice were killed by a schedule 1 method. The brain was collected and frozen for western blot analysis. The mice were weighed at every stage of this experiment in order to monitor weight loss. Half brain samples from starved and fed mice were dissected, homogenized and resuspended in tissue lysis buffer on ice (50 mM Tris pH 7.4, 0.5% Triton X-100 and protease inhibitor cocktail) and the supernatant was centrifuged twice. Proteins were resolved by SDS-PAGE for further analysis.

Immunohistochemistry

Thirty-micrometre sections of brains derived from Huntington's disease transgenic young and adult mice (6 and 12 weeks old, respectively) were analysed for neuronal aggregates. Primary fibroblasts from 9 controls and 13 patients with mutant polyQ diseases were grown at 37 °C in DMEM supplemented with 10% FBS, 100 U ml⁻¹ penicillin/streptomycin, GlutaMAX 1:100 (35050061, ThermoFisher) and 1 mM sodium pyruvate (basal medium) under 5% CO₂. In some experiments, cells were starved in HBSS medium for 4 h or treated for 4 h with 400 nM BafA1. The following patient fibroblasts were obtained from Coriell Biorepository, Coriell Institute for Medical Research: Huntington's disease (HD) (GM04285, GM04287, GM04476, GM04867), DRPLA (GM13716, GM13717), SCA3 (GM06151, GM06153) and SCA7 (GM03561). The following patient fibroblasts were provided by F.Sq. A program to collect biological specimens at the Mendel Institute of Human Genetics for research purposes, including skin biopsies to derive fibroblast cell lines, was

approved by the Ethical Committee from Casa Sollievo della Sofferenza Foundation, section of Istituto Tumori Giovanni Paolo II in Bari. Informed consent was obtained from healthy control subjects and from patients with DRPLA (AT2140102) or Huntington's disease (HD 940-01, HD960-01) and from the legal representative of another patient with Huntington's disease (HD305-01).

Isolation and culture of primary cortical neurons

Primary cortical neurons were isolated from C57BL/6 mouse (Jackson Laboratories) embryos at embryonic day (E)16.5 as previously described (Jimenez-Sanchez et al., 2015).

Western blot analysis

Cells were lysed in lysis buffer (20 mM Tris-HCl, pH 6.8, 137 mM NaCl, 1 mM EGTA, 1% Triton X-100, 10% glycerol and protease inhibitors cocktail) and protein samples were boiled in Laemmli buffer for 5–7 min at 100 °C, separated by SDS–PAGE, transferred onto PVDF membranes, subjected to western blot analysis, and visualized using an ECL enhanced chemiluminescence detection kit (GE Healthcare), or with direct infrared fluorescence detection on an Odyssey Infrared Imaging System.

Immunoprecipitation and ubiquitination assays

Cells were lysed with IP buffer (20 mM Tris-HCl, pH 7.2, 150 mM NaCl, 2 mM MgCl₂, 0.5% NP-40 and protease inhibitors cocktail). For ubiquitination experiments, cells were treated with a proteasome inhibitor MG132 (10 μM) in the last 6 h before lysis with the IP buffer supplemented with 1 mM PMSF and 10 mM iodoacetamide. Whole-cell lysates obtained by centrifugation were incubated with 2–5 μg of antibody overnight at 4 °C followed by 2 h incubation with protein A sepharose beads (GE Healthcare). The immunocomplexes were then washed with IP buffer for three times and separated by SDS–PAGE for further western blotting assay.

Structural analysis of polyQ binding to beclin 1

Glide software (Schrödinger, LLC) was used for studying potential ligand (polyQ7 stretch)–receptor (human beclin 1 ECD; pdb 4DDP, ref. 39) interactions. Protein and ligand preparation were performed first, followed by generation of possible ligand binding sites using site-map. A receptor grid was then generated for each of the putative binding sites and standard precision peptide (SP-peptide) docking was performed. Although several potential binding sites were found, docking scores for two of the sites were substantially higher than for the others. It should be noted that that binding sites surrounding the N-terminal helix of beclin 1 ECD (pdb 4DDP) were not considered, as the yeast Vps30-BARA domain structure (pdb 5DFZ, ref. 40) shows that this helix is likely to be out of place, being part of the coiled-coil domain (CCD) of beclin 1. Docking poses from the best sites were used to generate figures. Visualization and generation of graphic illustrations of the molecular models were performed using PyMOL (<http://www.pymol.org>).

Statistics

Statistical analysis was done using Microsoft Excel and GraphPad Prism v5. For ANOVA analysis involving multiple sample comparisons, post testing was performed to discriminate significance relationships. For *t*-test analysis, one-tailed test were performed for independent samples, as indicated in the figure legends. Error bars shown in the figures are standard deviation (s.d.) or standard error (s.e.m.), as stated. Sample sizes were chosen on the basis of extensive experience with the assays we have performed. The experiments were appropriately randomized.

1.3.1.4. Results

Conjugation of the autophagy protein (Atg) Atg8/LC3-I to phosphatidylethanolamine on autophagosomal membranes forms LC3-II. Hence, LC3-II levels (relative to loading controls like actin) correlate with autophagosome load (Kabeya et al., 2000; Weidberg et al., 2011; Xie and Klionsky, 2007). Ataxin-3 knockdown in primary neurons (Fig. 33A) lowered LC3-II levels in the presence of bafilomycin A1 (BafA1). As BafA1 inhibits LC3-II degradation, this suggests that ataxin-3 knockdown impaired autophagosome synthesis. Decreased LC3-II levels (but not LC3-I) were also observed in ataxin-3-depleted, BafA1-treated, neurons in starvation media (Fig. 33B). Moreover, ataxin-3 knockdown in HeLa cells lowered LC3-II levels and increased the levels of the autophagy substrate, p62. Ataxin-3 knockdown decreased the number of autophagosomes and autolysosomes scored with mTagRFP-mWasabi-LC3, consistent with impaired autophagosome formation.

The decreased autophagosome biogenesis following ataxin-3 knockdown was associated with lower beclin 1 levels (Fig. 33C). The phosphatidylinositol 3-phosphate (PI3P) formed by the beclin 1/VPS34 complex is particularly important for autophagy induction (LC3-II formation in BafA1) after nutrient depletion and such defects are seen in cells with monoallelic *beclin 1* deletion (He et al., 2015; Liang et al., 1999; Tassa et al., 2003). Decreased PI3P-positive structures in starvation, characteristic of beclin 1-depletion (He et al., 2015) were seen in ataxin-3-depleted cells. In both fed and starved conditions, loading back exogenous PI3P to ataxin-3-depleted cells increased LC3 vesicle numbers to levels comparable to control cells. Ataxin-3 overexpression increased the numbers of puncta positive for the PI3P-binding autophagy effector, WIPI2, which binds to PI3P at autophagy initiation membranes (Dooley et al., 2014; Vicinanza et al., 2015). This effect was reversed when ataxin-3 overexpressing cells were treated with the PI3 kinase inhibitor, wortmannin. After fasting mice, livers depleted of ataxin-3 failed to upregulate beclin 1 and LC3-II levels (Fig. 33D,E) and had increased p62 levels, compared to wild-types. Therefore, ataxin-3 knockdown decreases beclin 1 level, which can explain reduced PI3P levels and consequent impaired autophagosome biogenesis.

As ataxin-3 interacted with beclin 1 (Fig. 34A), we tested if ataxin-3 deubiquitinase activity protected beclin 1 from proteasomal degradation. Beclin 1 levels declined more in ataxin-3-depleted cells, compared to controls, after inhibition of protein synthesis, suggesting accelerated beclin 1 turnover. Beclin 1 levels were restored in ataxin-3 knockdown cells treated with a proteasome inhibitor and when ataxin-3-depleted cells were transfected with wild-type ataxin-3 but not with ubiquitin protease dead mutant (C14A).

Under proteasome inhibition, endogenous beclin 1 ubiquitination was increased when ataxin-3 was knocked down (Extended Data Fig. 3d), and recombinant ataxin-3 but not the protease dead mutant (C14A) deubiquitinated beclin 1 *in vitro* (Fig. 34B). The percentage of cells with mutant huntingtin exon 1 aggregates correlates with levels of this protein and decreases when autophagy is induced (Ravikumar et al., 2004b). Consistent with autophagy induction, overexpression of wild-type (but not C14A) ataxin-3 decreased the percentage of such mutant huntingtin-expressing cells with aggregates.

Our mass spectrometry analysis and others (Kim et al., 2011b) suggested beclin 1 lysine 402 was modified with a lysine 48 (K48) ubiquitin chain, a signal for proteasomal degradation (Fig. 34C). Lysine 402 in the evolutionary conserved domain (ECD) is conserved in fish, mouse and humans (Fig. 34C). K48-linked beclin 1 polyubiquitination was increased by ataxin-3 depletion and mutation of lysine 402 to arginine (K402R) decreased K48-linked beclin 1 polyubiquitination, confirming K402 as a site for K48 ubiquitination (Fig. 34D). Consequently, the levels of K402R beclin 1 were already more abundant than wild-type beclin 1 in cells and did not further increase after treatment with proteasome inhibitors. Ataxin-3 expression in HeLa cells increased wild-type beclin 1 levels and did not increase levels of beclin 1 K402R.

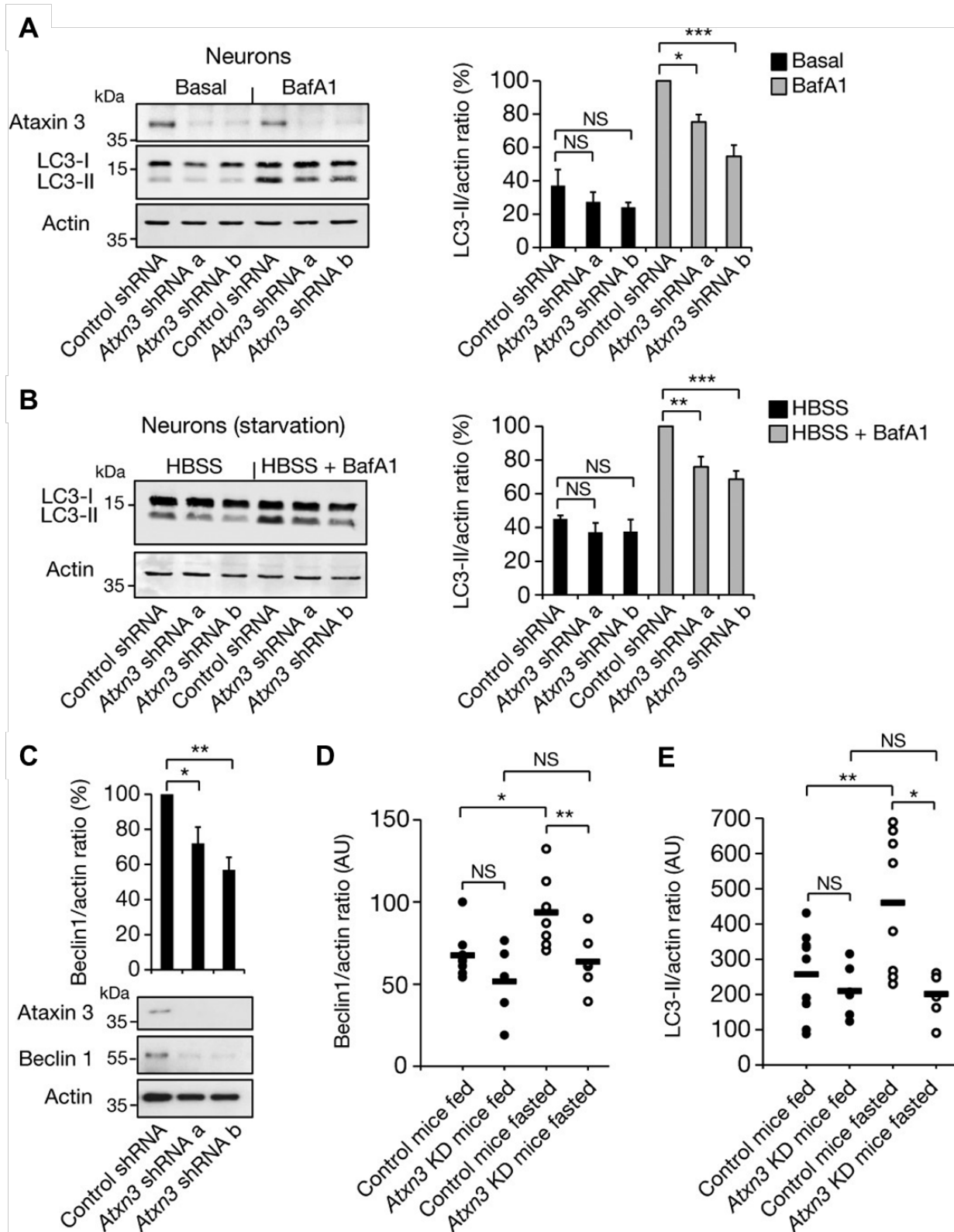


Figure 33. Ataxin 3 contributes to autophagosome formation by regulating the levels of beclin 1. (A-C) Mouse cortical neurons were transduced with control or *Atxn3*-targeting lentiviral shRNAs and analysed for LC3-II levels with or without BafA1 (A); LC3-II levels in starvation medium (HBSS) with or without BafA1 (B); and beclin 1 levels in the starved cells (C). Results are mean \pm s.e.m; $n = 5$ replicates from two independent cultures. (D, E) Control mice and mice depleted of liver ataxin 3 (*Atxn3* KD) were fed or starved for 24 h. Liver samples were analysed for beclin 1 (D) and LC3-II (E). Control fed $n = 9$, *Atxn3* knockdown fed $n = 6$, control fasted $n = 8$, *Atxn3* knockdown fasted $n = 6$. AU,

arbitrary units. Two-way ANOVA with Bonferroni's post-test (**A**, **B**, **D**, **E**). One-way ANOVA with post hoc Tukey's test (**c**). * $P < 0.05$, ** $P < 0.01$, *** $P < 0.001$; NS, not significant.

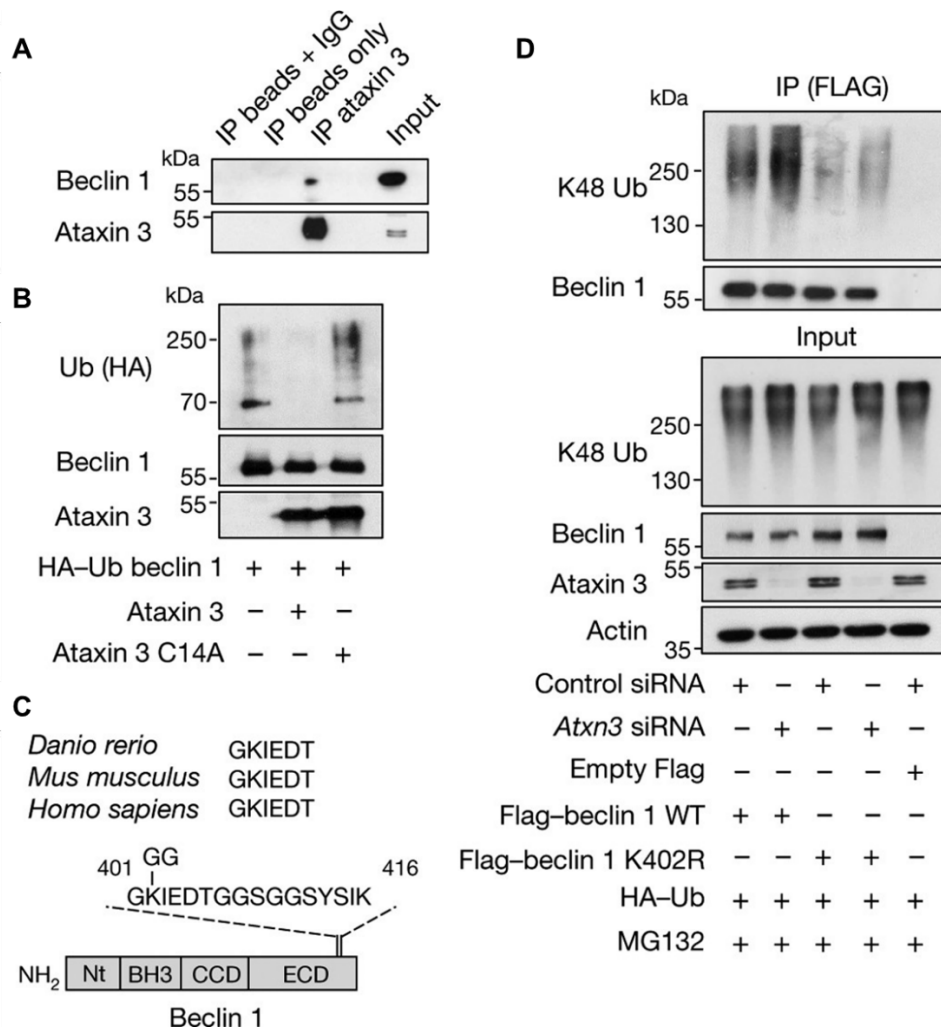


Figure 34. Deubiquitination of beclin 1 by ataxin 3. (A) Endogenous ataxin 3 was immunoprecipitated (IP) from HeLa cell lysates and blots probed for endogenous beclin 1 and ataxin 3. (B) Ubiquitinated (Ub) beclin 1 was incubated *in vitro* with recombinant ataxin 3 or ataxin 3 C14A for 2 h and analysed for beclin 1 ubiquitination using anti-haemagglutinin (HA) antibodies. (C) Evolutionary conservation of region around beclin 1 K402. (D) Control and ataxin-3-depleted (*Atxn3* small inhibitory RNA (siRNA)) HeLa cells were transfected as indicated for 24 h and incubated for the last 6 h with the proteasome inhibitor MG132 (10 μ M). Wild-type (WT) Flag-tagged beclin 1 and mutant Flag-tagged beclin 1 K402R were immunoprecipitated with anti-Flag antibodies for ubiquitination analysis.

Deletion of the polyQ domain from ataxin-3 dramatically reduced its binding to beclin 1 (Fig. 35A) and an isolated polyQ stretch was sufficient to bind beclin 1 (Fig. 35B). Thus, the polyQ domain is important for the ataxin-3-beclin 1 interaction, but is not the only binding domain. The beclin 1 ECD interacted with ataxin-3 (Fig. 35C) and also bound the polyQ tract alone, suggesting that beclin 1 ECD contained polyQ-binding domains, consistent with structural docking models revealing two highly scored polyQ-binding pockets in the beclin 1 ECD (Fig. 35D). As some binding was observed with beclin 1 lacking the ECD, other domains of beclin 1 may also interact with ataxin-3.

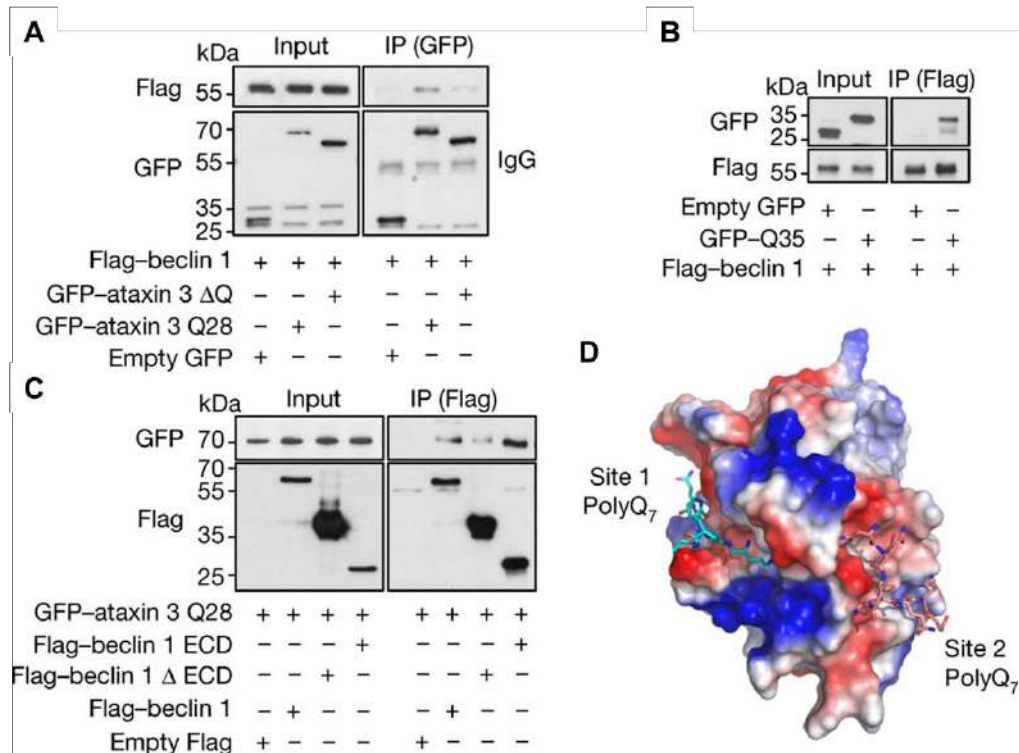


Figure 35: The ataxin 3 polyQ domain contributes to the interaction between ataxin 3 and beclin 1. (A-C) Constructs were transfected into HeLa cells for 24 h. **a**, Cell lysates were immunoprecipitated with anti-GFP antibodies and immunocomplexes analysed with anti-Flag antibodies. (B-C) Cell lysates were immunoprecipitated with anti-Flag antibodies and immunocomplexes analysed with anti-GFP antibodies. (D) Structural docking modelling reveals two interaction sites between beclin 1 ECD and polyQ₇. Surface charge illustration of human beclin 1 ECD showing high-scored docking pose of polyQ₇ stretch (docking scores for site 1 and site 2 are -10.394 and -10.721, respectively).

GFP-tagged isolated polyQ tracts could bind to beclin 1, while longer stretches (Q81) bound beclin 1 more strongly than shorter tracts (Q35) (Fig. 36A). Remarkably, beclin 1 K48-polyubiquitination was increased in cells overexpressing GFP Q35 versus empty GFP, and was increased even further with GFP Q81 overexpression (Fig. 36A), consistent with a model where these constructs compete with the ataxin-3 polyQ stretch for binding and deubiquitination of beclin 1. Indeed, overexpression of GFP-polyQ constructs decreased ataxin-3-beclin 1 binding (Fig. 36B). GFP Q35 (which does not aggregate in our conditions) decreased beclin 1 levels, impaired starvation-induced autophagy and increased p62 levels in starved cells. No change in the number of LC3-II vesicles was observed when the Q35 tract was expressed in beclin 1-depleted cells and the inhibitory effect of Q35 on beclin 1 levels and autophagy in beclin 1-expressing cells was rescued by ataxin-3 overexpression, compatible with the model that the Q35 acts by impairing ataxin-3 control of beclin 1 levels.

A wild-type (Q17) huntingtin fragment (N-terminal 350 residues) bound to beclin 1 and this interaction was largely lost when the polyQ stretch was deleted. Furthermore, mutant polyQ-expanded, full-length huntingtin competed with wild-type ataxin-3 for beclin 1 binding. To test the general principle on autophagy, we used an N-terminal exon 1 fragment to exclude any confounding effects of the huntingtin C-terminus on autophagy (Rui et al., 2015). In stable-inducible HEK293 cells expressing wild-type (Q23) and mutant (Q74) huntingtin exon 1 at similar levels (where there is no overt toxicity or aggregation (<1%) during the experiment), we observed lower beclin 1 levels and impaired starvation-induced autophagy, after switching on the huntingtin transgene. These effects were more pronounced in mutant

cells. As these phenomena occur in both wild-type Q23-huntingtin cells and Q35-expressing cells, they cannot simply be explained by beclin 1 sequestration into aggregates (Shibata et al., 2006).

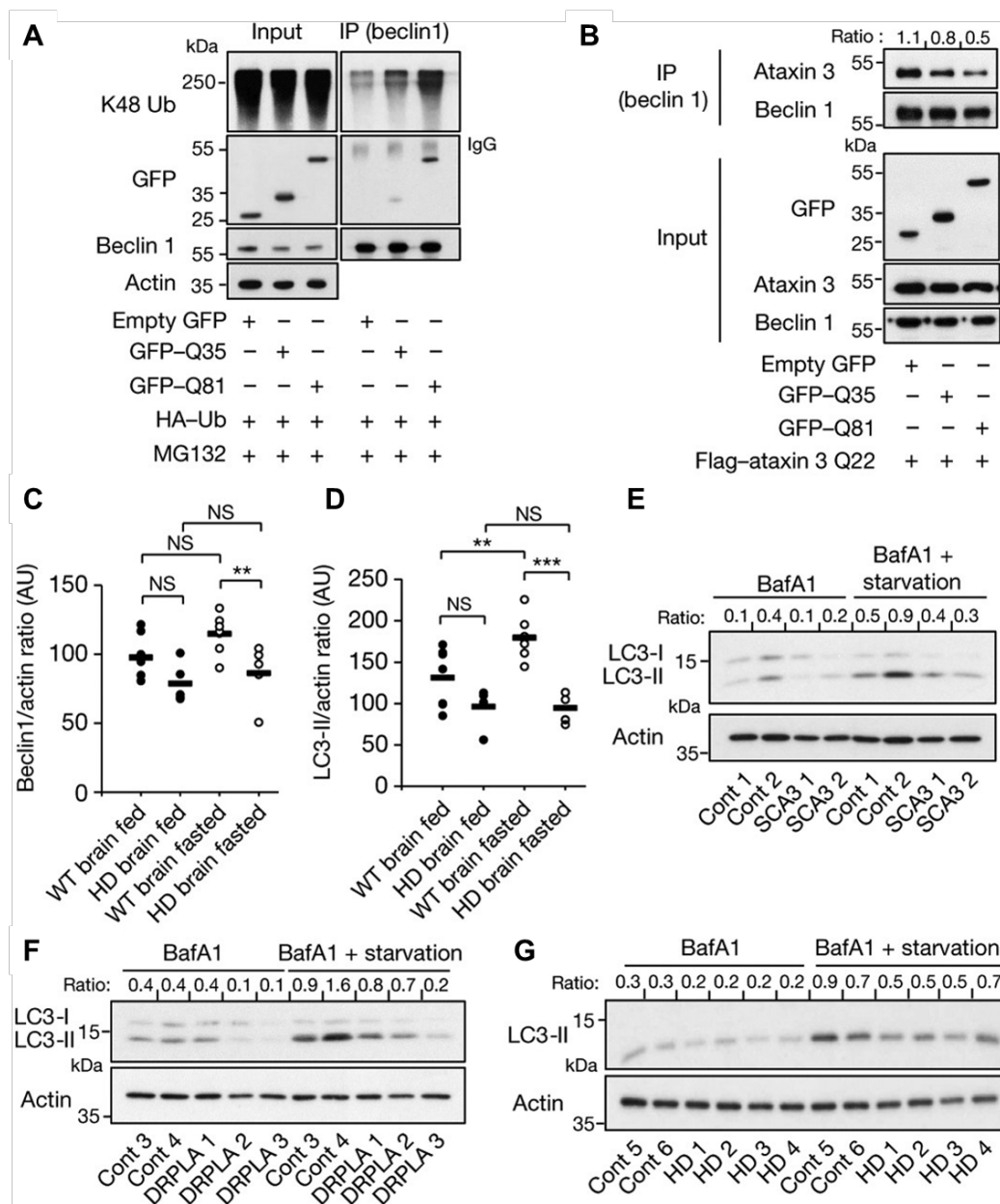


Figure 36: Expanded polyQ tracts inhibit ataxin 3–beclin 1 interaction, decrease beclin 1 levels and impair starvation-induced autophagy. (A,B) HeLa cells were transfected with indicated constructs for 24 h and immunoprecipitated for endogenous beclin 1. (A) Cells treated for the last 6 h with proteasome inhibitor (MG132, 10 μ M) were analysed for beclin 1 ubiquitination and for beclin 1-bound polyQ using anti-GFP antibodies. (B) Immunocomplexes were analysed for beclin 1-bound ataxin 3 using anti-Flag antibodies. The bound ataxin 3/beclin 1 ratio is shown at the top. (C,D) Brain samples from wild-type (WT) mice and Huntington’s disease (HD) model transgenic mice were analysed for beclin 1 (C) and LC3-II (D). WT fed $n = 7$, HD fed $n = 5$, WT fasted $n = 7$, HD fasted $n = 6$; AU, arbitrary units. Two-way ANOVA with Bonferroni’s post-test. ** $P < 0.01$, *** $P < 0.001$; NS, not significant. (E-G) Primary fibroblasts from healthy controls (Cont) or patients with different polyQ diseases (SCA3, DRPLA or HD (Huntington’s disease)) treated with BafA1, in full or starvation medium analysed for LC3-II/actin ratio.

Next, we studied cell lines derived from the striatum, the brain region most sensitive to the HD mutation, from heterozygous mutant huntingtin (Q7/Q111) and matched wild-type huntingtin knock-in mice (Q7/Q7) both humanised for huntingtin exon 1 (Trettel et al., 2000). Mutant huntingtin striatal-derived cells (Q7/Q111) had lower beclin 1 levels and defects in starvation-induction of WIPI2 dots and LC3-II levels, compared to wild-type cells (Q7/Q7). Likewise, brains from young mutant huntingtin exon 1 transgenic mice, when there is minimal overt aggregation, had decreased beclin 1 levels in fasting conditions, failed to upregulate LC3-II with fasting, and had increased p62 levels, compared to wild-type littermate brains (Fig. 36C,D).

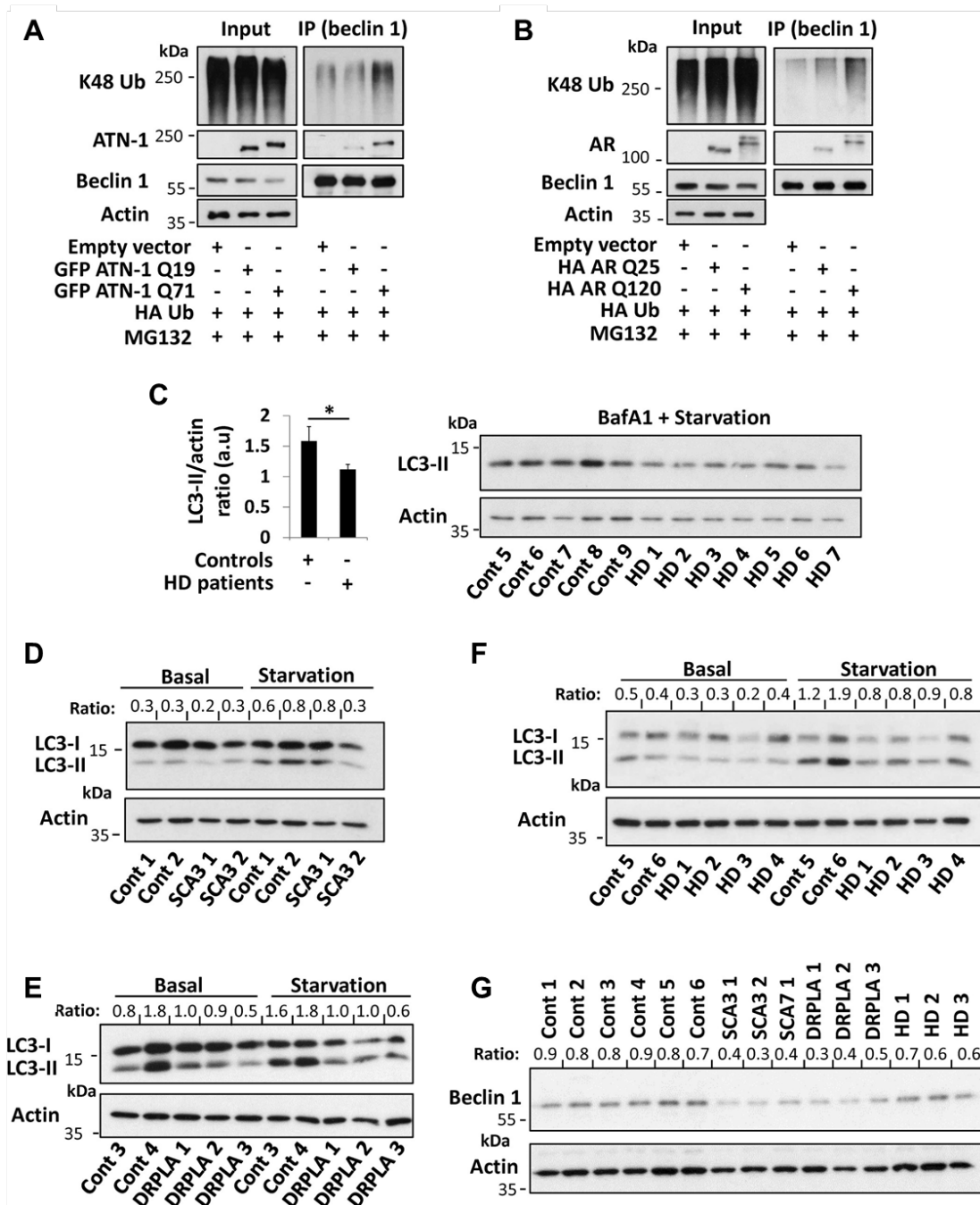


Figure 37. Effect of different human disease proteins with polyQ expansion on beclin 1 ubiquitination, beclin 1 levels and starvation-induced autophagy. (A) HeLa cells were transfected with empty vector, GFP–atrophin 1 (ATN-1) Q19, or GFP–ATN-1 Q71 along with HA–Ub for 24 h

and treated for the last 6 h with MG132 (10 μ M). Endogenous beclin 1 was immunoprecipitated from the lysates for ubiquitination analysis and for detection of bound ATN-1 using anti-ATN-1 antibody. **b**, HeLa cells were transfected with empty vector, HA-androgen receptor (AR) Q25, or HA-AR Q120 along with HA-Ub for 24 h and treated for the last 6 h with MG132 (10 μ M). Endogenous beclin 1 was immunoprecipitated from the lysates for ubiquitination analysis and for detection of bound AR using anti-AR antibody. **(C)** Primary fibroblasts derived from healthy controls (Cont) (n=5) and from patients with Huntington's disease (HD) (n=7) were starved with HBSS together with BafA1 (400 nM) for 4 h and analysed for LC3-II levels. Results are mean \pm s.e.m. *P < 0.05, one-tailed Mann-Whitney test. **(D-F)** Primary fibroblasts derived from healthy controls and from patients with different polyQ diseases (d, SCA3; e, DRPLA; f, Huntington's disease) were kept in full medium or starved with HBSS for 4 h and analysed for LC3-II levels (LC3-II/actin ratio is presented). The BafA1 experiments for these sets of patients are presented in Fig. 36. **(G)** Beclin 1 levels (beclin 1/actin ratio is presented) in the starved control cells compared to cells from patients with SCA3, SCA7, DRPLA or Huntington's disease.

We then tested if this mechanism applied to mutant ataxin-3, as decreased beclin 1 levels are seen in SCA3 rodent models (Nascimento-Ferreira et al., 2011). Expansion of the polyQ domain in ataxin-3 decreased its deubiquitinase activity towards beclin 1. Transfecting expanded ataxin-3 Q84 into ataxin-3 knockdown cells partially rescued LC3 dot numbers but was not as effective as wild-type ataxin-3 Q28, consistent with decreased deubiquitinase activity of the mutant protein. However, the Δ polyQ ataxin-3 did not rescue the number of LC3 dots. When overexpressed in cells, mutant ataxin-3 had a stronger interaction with beclin 1, associated with increased beclin 1 K48 polyubiquitination, while no obvious change was observed in beclin 1 K63 polyubiquitination. Thus, the longer polyQ stretches in mutant ataxin-3 bind beclin 1 more strongly than wild-type ataxin-3 but the mutant protein also has decreased deubiquitinase activity. This likely results in a partial dominant-negative effect of mutant ataxin-3 towards beclin 1 levels, with similar consequences on this autophagy pathway as observed with mutant huntingtin fragments.

Apart from mutant huntingtin and ataxin-3, beclin 1 also interacted with atrophin-1 and the androgen receptor that are mutated in the polyQ diseases dentatorubral-pallidolusian atrophy (DRPLA) and spinal and bulbar muscular atrophy, respectively. PolyQ-expanded atrophin-1 and androgen receptor showed increased interactions with beclin 1 that elevated beclin 1 K48-polyubiquitination. Finally, we observed decreased beclin 1 levels and impaired starvation-induced autophagy in fibroblasts derived from DRPLA, SCA3 and HD patients, compared to controls (Figs. 36E-G, 37).

1.3.1.5. Discussions

Our data reveal novel roles for polyQ tracts in health and disease. The wild-type ataxin-3 polyQ stretch is required for binding to beclin 1 that enables deubiquitination of this key autophagy inducer (Levine et al., 2015) and protects it from proteasome-mediated degradation. Importantly, this wild-type polyQ-mediated interaction was competed for by diverse disease proteins with polyQ expansion mutations. The observed defect in starvation-induced autophagy caused by mutant polyQ proteins may reflect a less obvious impairment of basal autophagy, which is magnified under starvation conditions. More precisely, our data suggest that isolated polyQ tracts are able to bind BECN1, whereas the longer expansions, which cause polyQ diseases, bind BECN1 to a greater extent than the shorter forms (Fig. 38). Indeed, overexpression of disease proteins with polyQs (other than ATXN3) increases BECN1 ubiquitination and its degradation. This BECN1 degradation leads to impaired starvation-induced autophagy, a phenotype characteristic of BECN1 depletion. For example, we provided evidence, at least by overexpression studies, that the HTT exon 1 has these deleterious effects on autophagy. N-terminal fragments of HTT containing expanded polyQ domains are found in

brains of Huntington disease patients and cause toxicity in cells and in Huntington disease mouse models. Furthermore, full-length mutant HTT binds BECN1 and competes for BECN1 binding with ATXN3, and fibroblasts from Huntington disease patients have impaired starvation-induced autophagy.

Importantly, our data suggest that the described competition effects can be mediated by soluble forms of proteins with polyQ stretches, thereby revealing a possible toxic function of nonaggregated mutant proteins with polyQ expansions.

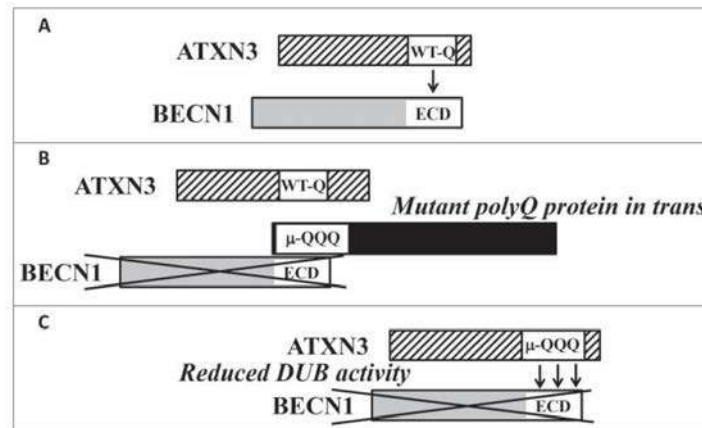


Figure 38. A proposed model describing ATXN3 activity in autophagy and its downregulation by mutant polyQ disease proteins. (A) The polyQ domain in wild-type ATXN3 (WT-Q) interacts with the evolutionarily conserved domain (ECD) of BECN1. This interaction allows the deubiquitinase activity of ATXN3 to protect BECN1 from degradation by the proteasome and thus enables autophagy. **(B)** Some expanded polyQ proteins (m-QQQ) can compete in trans with the shorter polyQ stretch in wild-type ATXN3 for BECN1 binding. This competition destabilizes BECN1. **(C)** Expansion of the polyQ domain in ATXN3 decreases the deubiquitinase (DUB) activity toward BECN1 and enhances the interaction of mutant ATXN3 with BECN1. This would outcompete wild-type ATXN3 binding to BECN1 and destabilizes BECN1.

Final remarks

The phenomena we have described are likely to be one of many mechanisms contributing to toxicity by mutant polyQ proteins. Indeed, there may be features of these proteins that affect autophagy via distinct mechanisms, as has been reported for mutant HTT. Furthermore, our proposed mechanisms will probably be nuanced due to the vast heterogeneity of the genetic landscapes associated with these diseases. First, the length of the polyQ tract in wild-type ATXN3 is polymorphic in humans, and it would be interesting to understand the extent to which this affects binding and activity. Furthermore, the disease alleles in all these conditions are also polymorphic in polyQ length, with longer expansions causing earlier disease onset. Further work will be required to test if shorter polyQ disease alleles have similar effects to longer disease alleles. An additional variable that is likely to have an impact on disease is the relative expression levels of ATXN3, the polyQ disease protein (e.g., mutant HTT) and BECN1 in different neuronal populations. This may contribute to the differential vulnerabilities of different brain regions in these diseases. Finally, it would be interesting to test if polyQ-containing cleavage products of some of the disease proteins are more toxic in this paradigm, compared with their uncleaved full-length counterparts.

These data raise the question of whether and to what extent polymorphisms in the wild-type and expanded polyQ stretches may contribute to the variabilities in clinical onset, presentation and progression of these devastating diseases. This scientific hypothesis should be investigated thoroughly in further research, together with the search for compounds that stabilize the wild-type ataxin3 activity.

The impact of this Nature study is reflected not only by the high number of ISI citations (over 200), but mainly by the fact that it formed the ground for other projects. For instance, the ATP-ase VCP/97 (the vasolin-containing protein which is mutated in inclusion body myopathy, Paget's disease of the bone, and frontotemporal dementia) was identified to promote the deubiquitinase activity of ataxin-3 towards Beclin-1, thus stabilizing the Beclin-1 level and promoting autophagy biogenesis and clearance of toxic aggregates (Hill et al., 2021).

1.4. Autophagy and ageing

While the accumulation of protein aggregates is traditionally associated with neurodegenerative diseases, studies of post-mortem brains of aged individuals, who were not diagnosed with neurological conditions, shows the presence of amyloid plaques, neurofibrillary tangles, Lewy bodies, synaptic dystrophy and neuronal loss, consistent with the notion that the integrities of degradative pathways are challenged with age (Simonsen et al., 2008). Indeed, there is increasing evidence suggesting that autophagy declines during ageing in many organisms and that this reduction plays a role in the functional deterioration of biological functions with age (Lipinski et al., 2010b).

In multiple studies, autophagy gene transcripts decrease with age in the brain and muscle of *Drosophila* (Demontis and Perrimon, 2010; Sarkis et al., 1988; Simonsen et al., 2008a). Transcriptional downregulation of *ATG5*, *ATG7* and *BECN1* with age was found in post-mortem human brains (Del Roso et al., 2003; Wilhelm et al., 2017). This correlates with the age-related decrease in autophagy proteins in the mouse hypothalamus and human muscle, as well as lysosomal proteins in rat livers (Donati et al., 2001). In a spatiotemporal analysis of autophagy in *C. elegans*, an age-dependent decrease in the numbers of autolysosomes and autophagosomes was observed in the intestines, muscles and neurons, corresponding with another study showing decreased autophagic activity in whole-body extracts of aged *C. elegans* (Melendez et al., 2003; Terman, 1995). Electron microscopy analyses have shown an accumulation of autophagic vacuoles and decreased ability to clear autophagic vesicles in mouse and rat livers with age (Cavallini et al., 2001; Juhasz et al., 2007; Ma et al., 2011).

Additionally, studies have shown a correlation between autophagy and lifespan. In *C. elegans*, decreased expression of orthologues of the mammalian *ATG1*, *ATG7*, *ATG12*, *BECN1* and *ATG18* lead to shortened lifespan (Donati et al., 2008). Deletion of core autophagy genes, such as *Atg7* in flies, reduce life-span and cause accumulation of aggregated proteins in degenerating neurons (Bai et al., 2013), which was supported by findings revealing reduced lifespan in mutant flies with reduced *Atg1* and *Atg8* expression (Simonsen et al., 2008). A study in senescence-accelerated mouse-prone 8 (SAMP8) mice, a rodent model with accelerated ageing, showed an accumulation of autophagic vesicles in hippocampal neurons along with deficits in learning and memory with increasing age (Lapierre et al., 2013). The age-dependent decline in autophagic function and lysosomal degradation was prevented with dietary restriction (Fernandez et al., 2018; Sun et al., 2016).

Overexpression of specific autophagy genes extends lifespan in flies and mice (Green et al., 2011; Rana et al., 2017). Additionally, overexpression of the TFEB orthologue, helix-loop-helix transcription factor *hlh-30* in *C. elegans* extended lifespan in an autophagy-dependent manner (Schiavi et al., 2015). Disruption of the interaction of Beclin-1 with its negative regulator Bcl-2 achieved by introducing a point mutation in *BECN1(F121A)* in mice led to increased lifespan and decreased age-related renal and cardiac pathological changes and spontaneous tumorigenesis (Ryu et al., 2016).

In addition to bulk autophagy, a decline in selective forms of autophagy, such as the autophagic degradation of mitochondria has been observed in aged worms, flies, mice and humans (Matecic et al., 2010), possibly accounting for the increased presence of inefficient and toxic mitochondria that have been implicated in neurodegenerative and inflammatory pathologies (Alvers et al., 2009). In accordance with this notion, upregulation of mitophagy, as well as pharmacological induction of mitophagy was found to improve longevity in worms (Harrison et al., 2009; Hars et al., 2007).

It is evident that the progressive loss of the degradative capacity can lead to an accumulation of toxic proteins, as autophagy gradually decreases with age. As mentioned earlier, autophagic decline is especially relevant to neurons, as post-mitotic cells are unable to segregate dysfunctional proteins and organelles from daughter cells using mitosis, resulting in an increased reliance on autophagy. This can have a detrimental impact on neuronal health and may play a role in manifestation of neurodegenerative diseases.

1.4.1. Therapeutic potential of autophagy in ageing

In addition to therapeutic potential in neurodegenerative conditions, autophagy upregulation is also suggested to ameliorate phenotypes associated with normal ageing and extend healthy lifespan. Caloric restriction drives autophagy-dependent lifespan extension in both *S. cerevisiae* (budding yeast) and *C. elegans* (Bjedov et al., 2010). Similar results are reported using *daf-2* mutant *C. elegans*, which exhibit lifespan extension due to defective insulin-like signalling dependant on autophagy (Hars et al., 2007; Melendez et al., 2003). Transgenic mice moderately overexpressing the core autophagy protein ATG5 in all tissues live 17% longer than wildtype controls and also exhibit ‘anti-ageing’ phenotypes, such as enhanced insulin sensitivity (Pyo et al., 2013). Whether these phenotypes result directly from increased autophagy is not addressed in this study. More recently, however, mice expressing a constitutively active Beclin-1 have been found to exhibit lifespan extension, as well as milder age-related heart and kidney phenotypes, dependent on increased flux through the autophagy pathway (Fernandez et al., 2018). Pharmacological upregulation of autophagy has also been suggested to extend lifespan. For example, a multicentre trial has demonstrated that feeding aged mice (600 days old) rapamycin significantly increases age at 90% mortality (Harrison et al., 2009). This result has also been seen in *Drosophila* with rapamycin-induced lifespan extension dependent on expression of the core autophagy protein ATG5 (Bjedov et al., 2010).

Although we can currently only speculate that autophagy induction would ameliorate age-related phenotypes in the brain and nervous system, neurodegeneration undeniably occurs predominantly against the backdrop of normal ageing. Accordingly, there is growing appreciation that research into normal ageing and age-related neurodegenerative diseases should be drawn closer together (Moldovan et al., 2016). This includes incorporating ageing into models of neurodegenerative disease, which should increase model fidelity, leading to more efficient discovery of translatable disease-modifying therapies. Other considerations relevant to autophagy modulation as therapy in age-related neurodegenerative diseases include the mechanism through which autophagy is upregulated. The mTOR pathway for example, regulates numerous autophagy-independent processes such as cell growth and immunity (Laplante and Sabatini, 2012). Hence, autophagy inducers that function by inhibiting mTOR may have deleterious side effects. Variations between the pathology and primary disease-causing mechanism(s) exhibited by different individuals with the same neurodegenerative disease is another important consideration, as is variation between the pathological stage in different cells in the same individual at different stages of a neurodegenerative disease. Furthermore, an autophagy inducer might be beneficial in slowing the onset of a neurodegenerative condition, but not improve (or even worsen) end-stage symptoms. This heterogeneity may stem in part from individuals with different variants of the same

neurodegenerative disease exhibiting defects at different locations in the autophagy pathway. It is also possible for autophagy defects to be of differential importance as a neurodegenerative disease progress. A nuanced approach that takes into consideration the complex relationship between autophagy, ageing and neurodegeneration is therefore required if the therapeutic potential of autophagy modulation is to be realised and produce new disease-modifying treatments for age-related neurodegenerative diseases.

1.4.2. The role of vinexin-YAP/TAZ axis in promoting the autophagic brain decline

1.4.2.1. Introduction

Increasing experimental evidence suggests autophagic decline is a ‘hallmark of ageing’; manifesting during normal ageing, with amelioration extending healthy lifespan and exacerbation accelerating age-related changes (López-Otín et al., 2013). Autophagy was first linked to lifespan extension in the invertebrate *C. elegans*, with normal lifespan restored in long-lived *daf-2* mutants when core autophagy genes are silenced (Melendez et al., 2003). More recently, lifespan extension has been observed in mice with increased autophagosome biogenesis driven either by overexpression of the core autophagy gene *Atg5* (Pyo et al., 2013) or an activating knockin mutation in the autophagy regulator *Becn1* (Fernández Á et al., 2018). Mice with increased autophagy show amelioration of age-induced phenotypes, including improved glucose sensitivity and motor function (Pyo et al., 2013), together with reduced fibrosis and nuclear damage in the heart and kidney (Fernández Á et al., 2018).

Reduced autophagosome formation and clearance is reported in liver tissue from mice aged to 20 months (Terman, 1995) and subsequently this finding has been replicated in aged mouse kidney and heart tissue (Fernández Á et al., 2018). However, neither reduced autophagosome biogenesis nor impaired flux through the autophagy pathway have previously been demonstrated in aged mammalian brain tissue. Autophagic decline is especially relevant to neurons, as post-mitotic cells are not able to segregate dysfunctional proteins and organelles from daughter cells using mitosis (Wong et al., 2020), which results in an increased reliance on autophagy to persevere cytoplasmic homeostasis. Consistent with this observation, dysfunction autophagy is implicated in common, age-related neurodegenerative conditions such as Alzheimer’s disease and Parkinson’s disease (Menziés et al., 2017b). Autophagy upregulation is therefore considered a potential therapeutic strategy in these conditions.

1.4.2.2. Aim

As autophagy is known to be critical protective pathway in neurons and ageing is the primary risk factor for common neurodegenerative diseases, we aimed to investigate the changes in autophagosome biogenesis with age in mouse brains and identify the molecular factors that control those changes.

1.4.2.3. Materials and methods

Antibodies

The following primary antibodies were used for western blot and immunofluorescence: rabbit polyclonal vinexin (alpha and beta isoforms) (ab126971, WB 1:500 dilution), rabbit monoclonal AMOTL1 (ab171977, WB 1:1000), mouse monoclonal GAPDH (ab8245, WB 1:3000), rabbit polyclonal Lamin B (ab16048, Abcam, 1:1000 dilution), mouse monoclonal CD63 (ab8219, IF 1:100) from Abcam, Goat polyclonal CTGF (sc-14939, WB 1:200), mouse

monoclonal YAP/TAZ (sc-101199, WB 1:200, IF 1:50) from Santa Cruz. Rabbit polyclonal ERK1/2 (9102, WB 1:1000), rabbit polyclonal p70S6K (9202, WB 1:1,000) rabbit polyclonal P-p70S6K (T389) (9205, WB 1:1,000), rabbit polyclonal ULK1 (4773, WB 1:1000), rabbit polyclonal P-ULK1 (S556) (5869, WB 1:1,000), rabbit polyclonal P-ULK1 (S758) (14202, WB 1:1000), rabbit monoclonal P-YAP (S127) (13008, WB 1:1000), rabbit monoclonal ATG16L1 (8089, IF 1:100) from Cell signaling. Rabbit polyclonal actin (A2066, Sigma-Aldrich, WB 1:2000), mouse monoclonal Flag (A2220, Sigma-Aldrich, 1:1000), rabbit polyclonal HA (H6908, Sigma-Aldrich, WB 1:1000, IF 1:100), mouse monoclonal tubulin (T9026, Sigma-Aldrich, 1:10000), rabbit polyclonal GFP (632592, Clontech, 1:10000), rabbit polyclonal LC3 (NB100-2220, Novus Biologicals, WB 1:10000), mouse monoclonal paxillin (610619, BD Biosciences, WB 1:1000, IF 1:100), mouse monoclonal vinculin (MAB3574, Millipore, IF 1:100).

Bafilomycin A1 (BAF; Sigma-Aldrich 19-148) was resuspended in DMSO from Sigma-Aldrich and used at 400 nM for 4 hours to block flux through the autophagy pathway. Latrunculin A (Santa Cruz, sc-202691) was resuspended in DMSO. In order to inhibit actin polymerisation, cells were treated with latrunculin A at 0.5 μ M (diluted in complete media) for 6 hours. In experiments using BAF and latrunculin A an equivalent volume of DMSO was used as the vehicle control.

Cell culture

HeLa (human cervical adenocarcinoma) cells (validated by STR profiling and purchased from ATCC (American Type Culture Collection)), SH-SY5Y (human neuroblastoma; ATCC), RPE (human retinal pigment epithelium; ATCC) cells and HEK (human embryonic kidney) 293 cells (purchased from European Collection of Authenticated Cell Cultures) were maintained in high glucose (4500 mg/L) DMEM (Dulbecco's Modified Eagle Medium; Sigma-Aldrich D6546) completed with 10% fetal bovine serum (Sigma-Aldrich F7524), 100 units/mL penicillin-streptomycin (Sigma-Aldrich P0781) and 2 mM L-glutamine (Sigma-Aldrich G7513) at 37 °C, 5% carbon dioxide. HeLa cells stably expressing GFP-LC3 and GFP-mRFP-LC3 have been described previously (Kimura et al., 2007). All cell lines were incubated at 37 °C and 5% CO₂, humidified atmosphere and were regularly tested for mycoplasma contamination every two weeks.

mRFP-GFP-LC3 (tfLC3) transgenic mice

The mRFP-GFP-LC3 reporter mouse line was generated in our lab as previously described (Pavel et al., 2016). All studies and procedures were performed with the jurisdiction of appropriate UK Home Office Project and Personal animal licenses and with the approval of the University of Cambridge Animal Welfare and Ethical Review Body for animal study.

siRNA and DNA transfection

For siRNA transfection, HeLa, RPE and HEK293 cells were seeded in 6 well plates and cells were transfected with 80 nM of siRNA using Lipofectamine 2000 (ThermoFisher 11668019) and cells were post-transfected with 80 nM of siRNA using Lipofectamine 2000.

shRNA lentivirus production and infection

shRNA lentiviral particles were produced and transduced following the RNAi Consortium (TRC) protocols. Briefly, HEK-293T packaging cells in 100mm dishes were transfected at 50–60% of confluence with a mix of 2.5 μ g psPAX2 vector (packaging vector), 270 ng pMD2.G vector (envelope vector) and 2.7 μ g hairpin-pLKO.1 vector using TransIT-LT1 (Mirus) transfection reagent according to the manufacturer's instructions. Transfected cells were cultured in high-serum medium. After 40 hours, cell culture medium was harvested and replaced by high-serum medium at three times repeatedly for 24 hours intervals. Viral preps were then concentrated by centrifugation at 160,100g for 90 min.

For infection in primary neurons, viral titres were added to the cells in the presence of 6 µg/ml polybrene (Sigma Aldrich) and incubated overnight. On a following day, medium was replaced by full medium and cells were further incubated for an additional 3-4 days before testing the knockdown effects.

Luciferase reporter assay

Luciferase reporter assay was examined by Dual-Glo luciferase assay kit (Promega E1910). Cells cultured in 6-well plates were transfected with 0.4 µg pGL3b-8xGTIIc-luciferase and 40 ng pRL-CMV (renilla luciferase). After 24 hours post-transfection, cells were lysed in 300 µL 'Passive Lysis Buffer' per well for 20 minutes at room temperature. Lysates were centrifuged at 15,000 rpm for 5 minutes at 4 °C. The pellets were discarded and 10 µL of each supernatant combined with 50 µl 'Luciferase Assay Buffer II' (LARII) in white 96-well plates. Firefly luminescence was measured using a GloMax 96 Microplate Luminometer (Promega). 50 µl 'Stop & Glo Buffer' (again prepared following the manufacturer's instructions) was subsequently added to all wells. After 5 minutes, Renilla luminescence was measured using the GloMax 96 Microplate Luminometer. Firefly luciferase activity relative to Renilla luciferase activity was calculated as a ratio for each well.

mRFP-GFP-LC3 mouse ageing study

mRFP-GFP-LC3 mice and Wild Type littermates were aged to 2, 12, 18 and 24 months. Following anaesthetisation using standard procedures, mice were perfused with 10 ml PBS followed by 40 ml 4% PFA. Perfusion was performed at a rate of 4 ml/min. At this point the mouse tails were collected for genotyping. Following successful fixation, brains were removed and placed in 10 ml tubes with 4% PFA. After 3 - 4 hours, the PFA was removed and 30% sucrose in deionized H₂O was added. The brains in sucrose were placed in 4°C until the brains sank to the bottom of the tube. The two hemispheres were separated and each hemisphere was placed on OCT embedding medium (ThermoScientific), frozen on dry ice and stored at -80°C. At this point Wild Type brain tissue (identified by tail genotyping) remained in storage, while the mRFP-GFP-LC3 brain tissue was prepared for imaging. The fixed mRFP-GFP-LC3 brains were sectioned sagittally into 8 µm thick sections on a cryostat (Leica CM3050S). Sections were collected on Superfrost slides (ThermoScientific) and either air-dried for 1h for staining or stored at -80°C until further use. To reduce autofluorescence, the brains were subjected to Sudan Black B (SBB) staining. The brain sections were first air-dried for 1h before being dipped into containers with 0.05% SBB in 70% methanol for 7 min. The sections were air-dried for 10 min before being mounted with the nuclear counterstain DAPI (1 µg/ml; ThermoFisher) in antifadent mountant solution (Citifluor). The brain sections were imaged with a 63x objective with the LSM710 confocal microscope. For each mouse, 5 images were taken of the motor cortex and autophagosomes (mRFP/GFP-double positive vesicles) and autolysosomes (mRFP-single positive vesicles) were counted manually.

Wild-type mouse ageing study

Wild-type mice were aged to 2, 12, 18 and 24 months of age. The animals were perfused and brains fixed as described above. Coronal sections of the left brain hemispheres were cut using a brain matrix (WPI) for precision. The brain area of interest was identified using a mouse brain atlas. The rills in the matrix enabled cutting a selected 2 mm section of each brain using a razorblade. This area chosen contains motor cortex, somatosensory cortex and striatum. The tissue was transferred to a glass homogenizer and homogenized with 500 µl Trizol (Ambion) in a fume hood on ice. The lysate was passed through a 27G syringe 10 times and transferred to a 1.5 ml tube. The lysate was centrifuged at 13200 rpm for 3 min at 4°C and RNA was extracted using the RNA extraction kit (Qiagen, RNeasy Mini Kit) as per manufacturer's protocol. Following elution of RNA, the concentration and purity were determined using a NanoDrop 2000c spectrophotometer. The spectrophotometer analysed the A₂₆₀/A₂₈₀ and

A260/230 ratios, which must be above 1.8 for quality RNA. The RNA was stored at -80°C until 1 μg in 60 μl buffer was shipped to deCODE, NeurOmics (Iceland) for RNA sequencing (RNA-Seq).

RNA sequencing data analysis

The RNA samples from mouse brain tissue were sequenced by deCODE, NeurOmics. Quality control assessment was performed on the RNA-Seq data and the reads were aligned to a mouse reference genome. Data frames for rpkM (Reads Per Kilobase of transcript per Million) values for the genes of interest were generated in R (Team, 2020). Scatter plots with linear regression lines were then generated in R for a selection of genes (*Sorbs3*, *Camk4*, *Eda2r* and *Tuba1a*). Overall significance of the regression analysis was established by F-test performed in R, with the adjusted coefficient of determination (adjusted R²) also calculated.

RNA sequencing data from 'neuropathological normal' human frontal cerebral cortex and hippocampal tissue was obtained from the Genotype-Tissue Expression (GTEx) Consortium, Release 6 (GTExConsortium, 2013). Donors labelled as follows in the subject metadata file were excluded: amyotrophic lateral sclerosis, Alzheimer's disease OR dementia, Alzheimer's disease, dementia with unknown cause, major depression (unipolar depression, major depressive disorder), active encephalitis, Creutzfeldt Jakob relatives, active meningitis, multiple sclerosis, Parkinson's disease, Reyes syndrome, schizophrenia, syphilis infection, unexplained weakness. Donors were also excluded when cause of death was annotated with the following ICD10 codes: C70 to C72 (malignant neoplasms of brain and other parts of central nervous system), F00 to F99 (mental and behavioural disorders), G00 to G99 (diseases of the nervous system) and I60 to I69 (cerebrovascular disease). RpkM values for the genes of interest in both tissues were provided by the GTEx Consortium, Release 6 (GTExConsortium, 2013). Data frames for rpkM values and sample metadata were generated in R (Team, 2020) for both tissues, with the rpkM data filtered to exclude mitochondrial and Y chromosome genes. Scatter plots with linear regression lines were then generated in R for a selection of genes (*SORBS3*, *CAMK4*, *EDA2R* and *TUBA1A*). Overall significance of the regression analysis was established by F-test performed in R, with the adjusted coefficient of determination (adjusted R²) also calculated.

Statistical analysis

Initial calculations were performed in Excel (Microsoft), before statistical testing and graph construction using PRISM software (version 5.01, GraphPad). As appropriate, PRISM was used to perform: paired t-tests (equivalent to one-sample t-tests for normalised western blotting data; see below), student's t-tests, one-way ANOVAs followed by Tukey's multiple comparison test and odds ratios followed by 2-tailed Fisher's exact test. Error bars indicate the standard deviation (SD), standard error of the mean (SEM) or 95% confidence interval, as appropriate to the data presented (see figure legends). Unless otherwise stated, #=ns (p value), *=p < 0.05, **=p < 0.01, ***=p < 0.001.

1.4.2.4. Results

Vinexin negatively regulates autophagy in multiple cell lines, including human neuroblastoma cells and mouse primary neurons.

During ongoing screening for autophagy modulators, we investigated vinexin using siRNA against *SORBS3* (si*SORBS3*) in HeLa (cervical cancer), SH-SY5Y (human neuroblastoma), RPE (retinal pigment epithelium) and HEK 293 (embryonic kidney) cells. In all cell lines, vinexin beta (~37 kDa) was the only vinexin isoform expressed at the protein level and si*SORBS3* treatment caused a robust reduction in expression (Fig. 39A). We assayed autophagy by western blotting for the autophagic vesicle marker LC3-II in the presence and

absence of bafilomycin A1 (BAF), which prevents autophagosome-lysosome fusion/LC3-II degradation (Yamamoto et al., 1998). *siSORBS3* increased LC3-II (lower band of LC3 doublet) under basal conditions (DMSO vehicle control) and in cells treated with BAF at a saturating concentration (Fig. 39A,B), which is consistent with increased autophagosome formation in vinexin beta-depleted cells (Klionsky et al., 2012). In addition, increased GFP-LC3 puncta (autophagosomes) were identified in vinexin beta-depleted HeLa cells stably expressing GFP-LC3 (Fig. 39C). We discriminated non-acidified autophagosomes from acidified autolysosomes using mRFP and GFP tandemly tagged to LC3 (mRFP-GFP-LC3), as the GFP signal is quenched by acidic pH relative to the mRFP (Kimura et al., 2007). *siSORBS3* increased both autophagosome (mRFP/GFP-double positive puncta) and autolysosome (mRFP-single positive puncta) numbers in HeLa cells stably expressing mRFP-GFP-LC3 (Sup. Fig. 39C,D). Similarly, autolysosome numbers (mRFP-single positive puncta) and LC3-II levels were increased in vinexin beta-depleted mouse primary neurons (Fig. 39D-F).

We next addressed whether increased vinexin expression downregulated autophagy. Overexpressing mEmerald-tagged vinexin alpha, which comprises vinexin beta plus an additional N-terminal SoHo domain (Kioka et al., 1999), decreased LC3-II in both DMSO and BAF-treated SH-SY5Y cells (Fig. 39G,H).

Finally, we investigated whether vinexin beta depletion impacts clearance of disease-relevant autophagy substrates. The first such substrate we examined was the aggregate-prone model autophagy substrate GFP-Htt(Q74) (GFP-tagged huntingtin exon 1 fragment containing 74 glutamine repeats) (Ravikumar et al., 2002). *siSORBS3* treatment reduced the percentage of GFP-positive cells containing GFP-Htt(Q74) aggregates (which corresponds to autophagy substrate levels (Ravikumar et al., 2002)) in autophagy-competent (Cas9 Cntrl) HeLa cells, but not autophagy-deficient HeLa cells lacking *ATG16L1* (*ATG16L1* CRISPR; Fig. 39I). We next utilised A53T mutant alpha-synuclein that causes Parkinson's disease (Polymeropoulos et al., 1997) and is also an autophagy substrate (Webb et al., 2003). *siSORBS3* treatment promoted GFP-tagged alpha-synuclein A53T clearance in Cas9 Cntrl HeLa cells, but not autophagy-deficient *ATG16L1* CRISPR HeLa cells (Fig. 39J,K). Taken together, these data suggest vinexin negatively regulates autophagy and autophagic substrate levels in multiple experimental set-ups, including mouse primary cortical neurons.

Vinexin beta depletion upregulates autophagy through YAP/TAZ.

We and others have linked the transcriptional coactivators YAP and TAZ to both autophagosome formation (Pavel et al., 2018b) and autophagic flux (Song et al., 2015; Totaro et al., 2019). We therefore addressed whether altered vinexin expression impacted YAP/TAZ. Vinexin beta depletion using *siSORBS3* increased nuclear YAP/TAZ in HeLa cells (Wild Type; Fig. 40A,B), which correlates with to increased YAP/TAZ transcriptional activity (Zhao et al., 2007a). In order to address the growing body of literature implicating autophagy (both directly and indirectly) in YAP/TAZ regulation (Chen et al., 2019a; Lee et al., 2018; Liang et al., 2014; Wang et al., 2019; Yuan et al., 2020), this result was confirmed in autophagy-deficient HeLa cells (*ATG16L1* CRISPR; Fig. 40A,B). This finding suggests vinexin beta depletion promotes YAP/TAZ transcriptional activity independent to upregulating autophagy.

As expected, *siSORBS3* treatment also increased nuclear YAP/TAZ and decreased cytosolic YAP/TAZ levels in HeLa cells when examined biochemically using nuclear/cytosolic fractionation (Fig. 40D,E). This corresponded to increased YAP/TAZ transcriptional activity mediated through TEAD transcription factors, measured using a YAP/TAZ-responsive synthetic TEAD promoter driving luciferase expression. Luminescence was significantly higher in *siSORBS3* treated wild-type HeLa cells, together with *ATG16L1* CRISPR HeLa cells and autophagy-competent controls (Cas9 Cntrl; Fig. 40F). Expression of the YAP/TAZ/TEAD direct target gene *CTGF* also increased at the protein level in vinexin beta-depleted cells (Fig.

40G,H). These data support *SORBS3* knockdown promoting YAP/TAZ transcriptional activity independent to increasing autophagy.

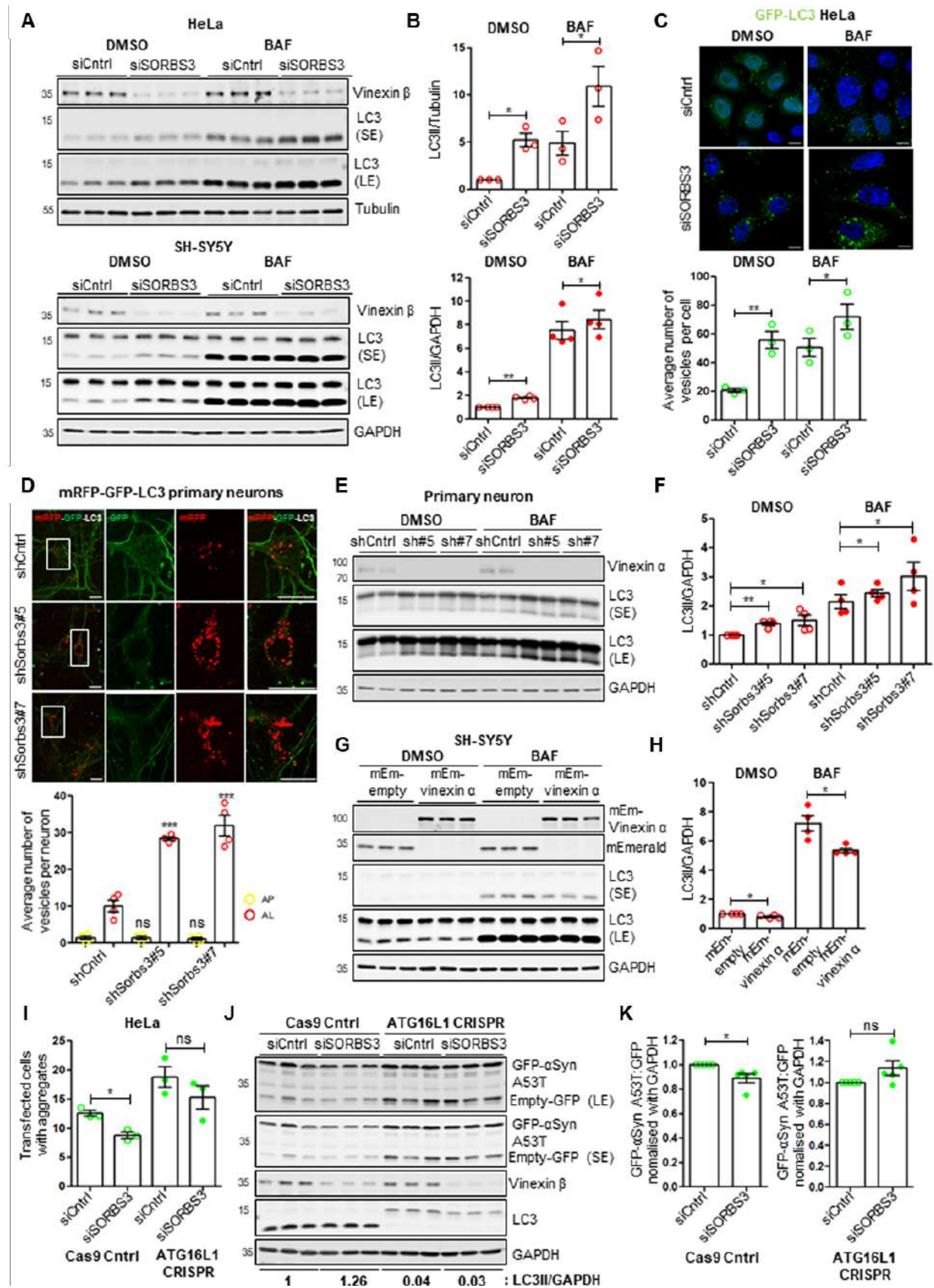


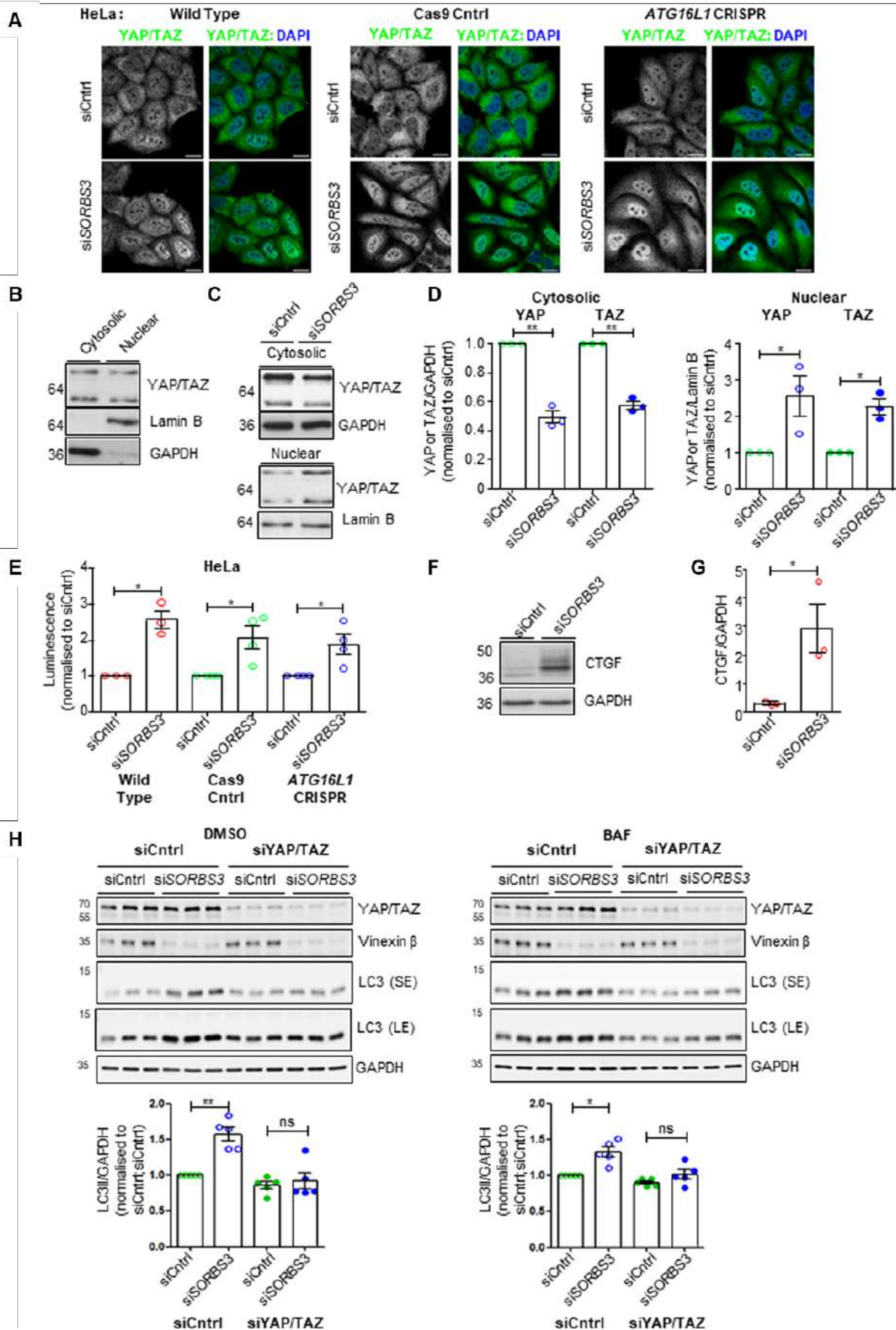
Figure 39. Vinexin negatively regulates autophagy. (A) HeLa and SH-SY5Y cells were depleted of

vinexin beta using an individual siRNA oligonucleotide against SORBS3. Cells were incubated with bafilomycin A1 (BAF; 400 nM) or DMSO vehicle control for 4 h. Endogenous tubulin, GAPDH, LC3 and vinexin beta protein levels were examined by western blotting. Representative blots from three or four independent experiments per cell line are shown. SE = short exposure; LE = long exposure; molecular weights shown in kDa. **(B)** Quantification of 3 (HeLa) or 4 (SH-SY5Y) independent experiments per cell line. LC3-II (lower band of LC3 doublet) levels are expressed relative to loading control (tubulin or GAPDH) and normalised to LC3-II/tubulin or LC3-II/GAPDH in control siRNA (siCntrl) treated cells. $*=p < 0.05$; $**=p < 0.01$ by two-tailed paired *t*-test. Error bars indicate SEM. **(C)** HeLa cells stably expressing GFP-LC3 were depleted of vinexin beta as in **a**. Cells were treated with BAF (400 nM) or DMSO vehicle control for 4 h. GFP-LC3 was examined by confocal microscopy. Representative images from 3 independent experiments are shown. Scale bars indicate 10 μ m. (bottom). Quantification of three independent experiments is shown. $*=p < 0.05$; $**=p < 0.01$ by two-tailed paired *t* test. **(D)** (top) Mouse primary cortical neurons from mRFP-GFP-LC3 (tfLC3) transgenic mice were infected with either control shRNA (shCntrl) or shRNA against Sorbs3 lentiviral vector. Scale bars indicate 20 μ m. Representative images from four independent experiments are shown. (bottom) In total, 25–35 cells analysed per condition per experiment in four independent experiments. $ns=p > 0.05$; $***=p < 0.001$ by two-tailed Student's *t* test. **e** Mouse primary cortical neurons from wild-type mice were infected with either control or Sorbs3 shRNA lentiviral vector. Infected cells were incubated with either DMSO or bafilomycin A1 (BAF; 400 nM) for 4 h. **(F)** Quantification of four independent experiments. LC3-II levels are expressed relative to GAPDH loading control and normalised to LC3-II/GAPDH in control shRNA (shCntrl) infected cells. $*=p < 0.05$; $**=p < 0.01$ by two-tailed paired *t*-test. Error bars indicate SEM. **(G)** SH-SY5Y cells were transfected with either mEmerald-empty (mEm-empty) or mEmerald-vinexin alpha (mEm-vinexin α). **(H)** Quantification of four independent experiments. **(I)** Autophagy-competent (Cas9 Cntrl) and autophagy-deficient (ATG16L1 CRISPR) HeLa cells were depleted of vinexin beta using an individual siRNA oligonucleotide against SORBS3 (siSORBS3; oligo 7). Cells were transfected with an aggregate-prone GFP-tagged huntingtin exon 1 fragment containing 74 glutamine repeats [GFP-Htt (Q74)] for 48 h. Quantification of three independent experiments is shown. $ns=p > 0.05$; $*=p < 0.05$ by two-tailed paired *t*-test. Error bars indicate SEM. **(J)** Cas9 Cntrl and ATG16L1 CRISPR HeLa cells were depleted of vinexin beta as in **A**, then transfected with both EGFP-tagged mutant alpha-synuclein (pEGFP-A53T α -syn) and pEGFP-empty vector (Empty-GFP). Representative blot from five independent experiments per cell line is shown. **(K)** Quantification of 5 independent GFP-A53T α -syn degradation assays represented in **J**. The ratio of GFP-A53T α -syn to GFP level (normalised to GAPDH) is shown for Cas9 Cntrl (left panel) and ATG16L1 CRISPR (right panel) HeLa cells. $ns=p > 0.05$; $*=p < 0.05$ by two-tailed paired *t*-test. Error bars indicate SEM.

To address whether vinexin regulates autophagy dependent on YAP/TAZ, HeLa cells were treated with siSORBS3 in the presence and absence of siRNA against YAP and TAZ. YAP/TAZ knockdown ameliorated the increase in LC3-II observed in vinexin beta-depleted cells (Fig. 40I,J). This finding suggests YAP/TAZ upregulation not only occurs upstream to autophagy in our system, but is necessary for increased autophagosome formation in vinexin beta-depleted cells.

Increased YAP/TAZ transcriptional activity and autophagosome formation upon SORBS3 knockdown are F-actin dependent.

As the Hippo pathway is the principal YAP/TAZ regulatory mechanism (Varelas, 2014), we examined Hippo pathway kinase activity in our system. To our surprise, siSORBS3 treatment did not significantly alter YAP phosphorylation at the Hippo pathway kinase LATS1/2 target residue serine 127 (P-YAP; Fig. 41A,B).



siRNA oligonucleotide against *SORBS3*. Endogenous YAP/TAZ were examined by immunofluorescence and confocal microscopy. Representative images from three independent experiments per cell line are shown. Scale bars indicate 20 μm . **(B)** Wild type HeLa cell lysate was subject to nuclear/cytosolic fractionation. Representative blot from the two independent experiments is shown. Molecular weights shown in kDa. **(C)** HeLa cells were depleted of vinexin beta using si*SORBS3* and lysates subject to nuclear/cytosolic fractionation and western blotting, as described in **b**. Representative blots from the two independent experiments in technical triplicate are shown. Molecular weights shown in kDa. **(D)** Quantification of the representative nuclear/cytosolic fractionation experiment in technical triplicate. YAP (upper band of YAP/TAZ doublet) and TAZ (lower band of YAP/TAZ doublet) are expressed relative to GAPDH (cytosolic fraction) or lamin B (nuclear fraction) loading control. **(E)** Cells were co-transfected with synthetic TEAD (YAP/TAZ-responsive) promoter driving luciferase expression (pGL3b-8xGTIC-luciferase) and Renilla luciferase control reporter for 24 h. Luminescence (firefly luciferase activity relative to Renilla luciferase activity) was measured by dual-luciferase reporter assay and normalised to control siRNA (siCntrl) treated cells. **(F)** Levels of CTGF protein (YAP/TAZ/TEAD direct target) and GAPDH (loading control) were examined by western blotting. Representative blot from the one experiment in biological triplicate is shown. **(G)** Quantification of 3 independent experiments as shown in **F**. $^* = p < 0.05$ by two-tailed Student's *t*-test. Error bars indicated SD. **(H)** (top) HeLa cells were depleted of vinexin and YAP/TAZ were incubated with bafilomycin A1 (BAF; 400 nM) or DMSO vehicle control for 4 h. (bottom) Quantification of five independent experiments described in **H**. LC3-II levels are expressed relative to GAPDH loading control and normalised to LC3-II/GAPDH in siCntrl treated cells. $ns = p > 0.05$, $^* = p < 0.05$; $^{**} = p < 0.01$ by two-tailed paired *t*-test. Error bars indicate SEM.

Independent of the Hippo pathway, YAP/TAZ transcriptional activity increases with extracellular matrix stiffness, consequent to changes in actin cytoskeleton dynamics and independent of Hippo signalling (Aragona et al., 2013b; Dupont et al., 2011a). Using fluorophore-labelled phalloidin to visualise F-actin, we observed that vinexin beta depletion increased the numbers of F-actin structures per cell and decreased average F-actin structure size (Fig. 41C,D). The actin cytoskeleton modulator latrunculin A was used to address how this observation relates to increased YAP/TAZ transcriptional activity in cells treated with si*SORBS3*. Latrunculin A inhibits actin polymerisation through G-actin (monomeric actin) sequestration (Coue et al., 1987) and was used under conditions previously shown to downregulate YAP/TAZ (0.5 μM for 6 hours) (Dupont et al., 2011a). Latrunculin A treatment destroyed cytoskeletal F-actin in both vinexin beta-depleted cells and controls (Fig. 41E), which ameliorated the increase in YAP/TAZ nuclear localisation caused by si*SORBS3* (Fig. 41E,F). Similarly, latrunculin A treatment ameliorated the increase in LC3-II caused by vinexin beta depletion in HeLa cells (Fig. 41G,H). These data suggest that autophagy upregulation following si*SORBS3* treatment results from increased YAP/TAZ transcriptional activity, which is dependent on increased F-actin structures.

Increased F-actin structures in vinexin beta-depleted cells upregulate autophagy by inhibiting YAP/TAZ cytosolic sequestration by angiomotins.

The angiomotin family of proteins (AMOTs) bind YAP/TAZ in the cytosol, thereby inhibiting YAP/TAZ nuclear translocation, independent of Hippo signalling (Chan et al., 2011; Wang et al., 2011; Zhao et al., 2011). This interaction utilises AMOT L/PPxY motifs, which closely flank the AMOT F-actin binding region (Mana-Capelli et al., 2014). Thus, F-actin and YAP/TAZ compete for AMOT binding. We examined YAP/TAZ/AMOT binding by endogenous immunoprecipitation and found much less AMOTL1 (angiomotin-like protein 1) was pulled down with YAP/TAZ from HeLa cells following si*SORBS3* treatment (Fig. 42A).

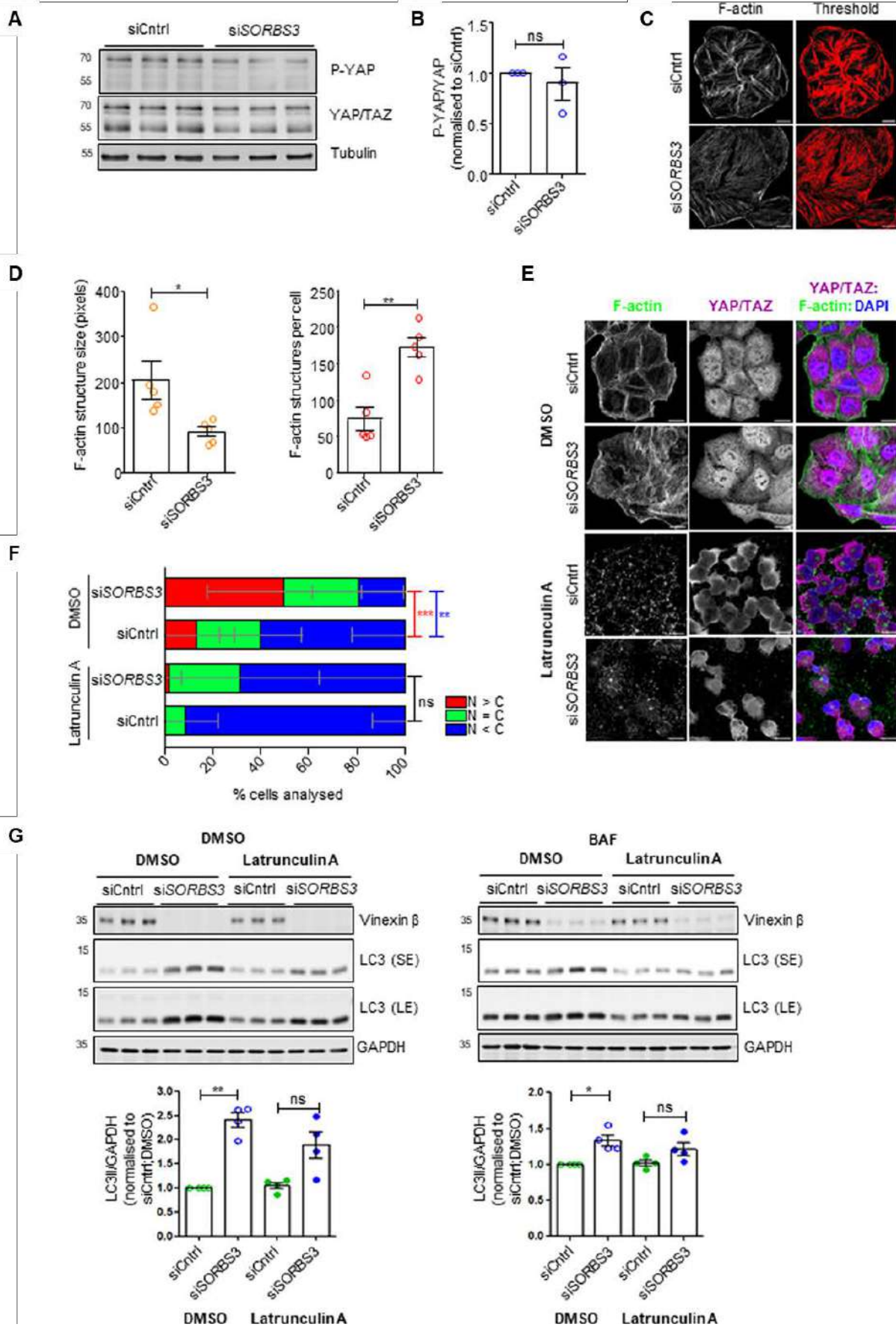


Figure 41. Vinexin depletion upregulates YAP/TAZ through a Hippo pathway-independent, filamentous actin-dependent mechanism. (A) HeLa cells were depleted of vinexin beta using an

individual siRNA oligonucleotide against *SORBS3*. Representative blot from three independent experiments is shown. **(B)** Quantification of three independent experiments. P-YAP and YAP (upper band of YAP/TAZ doublet) are expressed relative to tubulin loading control, the ratio of P-YAP/tubulin: YAP/tubulin taken and then normalised to P-YAP/YAP in siCntrl treated cells. **(C)** Cells were depleted of vinexin beta as in **A**. Endogenous filamentous actin (F-actin) was visualised using Alexa Fluor 488-conjugated phalloidin and confocal microscopy. Scale bars indicate 20 μm . **(D)** Quantification of F-actin structures per cell and F-actin structure size (pixels) from five independent experiments described in **C**. **(E)** HeLa cells were depleted of vinexin and treated with latrunculin A (0.5 μM) or DMSO vehicle control for 6 h. Endogenous F-actin was visualised using Alexa Fluor 488-conjugated phalloidin and YAP/TAZ was examined by immunofluorescence. Scale bars indicate 20 μm . **(F)** Quantification of the representative experiment shown in **A**. **(G)** (top) HeLa cells were depleted of vinexin and treated with latrunculin A (0.5 μM) or DMSO vehicle control for 2 h and then incubated with BAF (400 nM) or DMSO vehicle control for 4 h (total of 6 h treatment with latrunculin A or DMSO in the presence or absence of BAF). (bottom) Quantification of four independent experiments. $*=p < 0.05$; $**=p < 0.01$; $***=p < 0.001$; two-tailed paired t-test. Error bars indicate SEM.

In order to confirm the role of F-actin, HeLa cells were co-transfected with Flag-tagged YAP (Flag-YAP) and haemagglutinin-tagged full-length AMOT p130 (HA-AMOT(p130)), then treated with latrunculin A or DMSO vehicle control. Significantly more HA-AMOT(p130) pulled down with Flag-YAP from latrunculin A treated cells (Fig. 42B,C). These data suggest increased F-actin structures in vinexin beta-depleted cells reduce YAP/TAZ/AMOT binding, thereby increasing YAP/TAZ nuclear translocation. Using endogenous YAP/TAZ localisation as a proxy measure for YAP/TAZ transcriptional activity, we found that overexpression of AMOT p130 ameliorated the increased nuclear localisation of YAP/TAZ in si*SORBS3*-treated HeLa cells (Fig. 42D,E). This indicates that AMOT p130 overexpression saturates AMOT/F-actin binding (even in si*SORBS3*-treated cells with increased F-actin structures), leaving excess AMOTs free to retain YAP/TAZ in the cytosol. AMOT p130 overexpression significantly decreased LC3-II in HeLa cells treated with BAF (Fig. 42F,G), consistent with decreased autophagosome formation (Klionsky et al., 2012). Furthermore, AMOT p130 overexpression countered the increase in GFP-LC3 puncta resulting from si*SORBS3* treatment in HeLa cells stably expressing GFP-LC3 (Fig. 42H,I). Taken together, these data support a molecular mechanism (summarised in Fig. 42J) in which vinexin beta depletion increases F-actin structures that compete with YAP/TAZ for AMOT binding in the cytosol. This facilitates YAP/TAZ transcriptional activity in the nucleus, leading to autophagy upregulation.

Autophagy declines in aged mouse cerebral cortex, corresponding to increased *SORBS3* mRNA expression in mouse and human brain tissue.

Although impaired autophagy has previously been described in aged mouse liver, kidney and heart tissue (Fernández Á et al., 2018; Terman, 1995), to our knowledge autophagic vesicles and flux through the autophagy pathway have never been directly visualised in aged mammalian brain tissue. We therefore examined cortical sections from transgenic mice expressing mRFP-GFP-LC3 (Pavel et al., 2016) aged to 2, 12, 18 and 24 months. Autophagic vesicles decreased with age in the mouse motor cortex, with significant reductions in autophagosomes (GFP/mRFP-double positive vesicles) and autolysosomes (mRFP-single positive vesicles) in mice aged to 18 months and a further significant reduction in autolysosomes in mice aged to 24 months (Fig. 43A,B). These data indicate autophagic decline in normal mouse brain ageing.

We explored whether this finding corresponded to increased *SORBS3* expression. Regression analysis was used to examine the relationship between chronological age and vinexin expression measured by RNA-Seq. *Sorbs3* mRNA expression in wild-type mouse brain

tissue (combined motor cortex, somatosensory cortex and striatum) positively correlated with age (Fig. 43C).

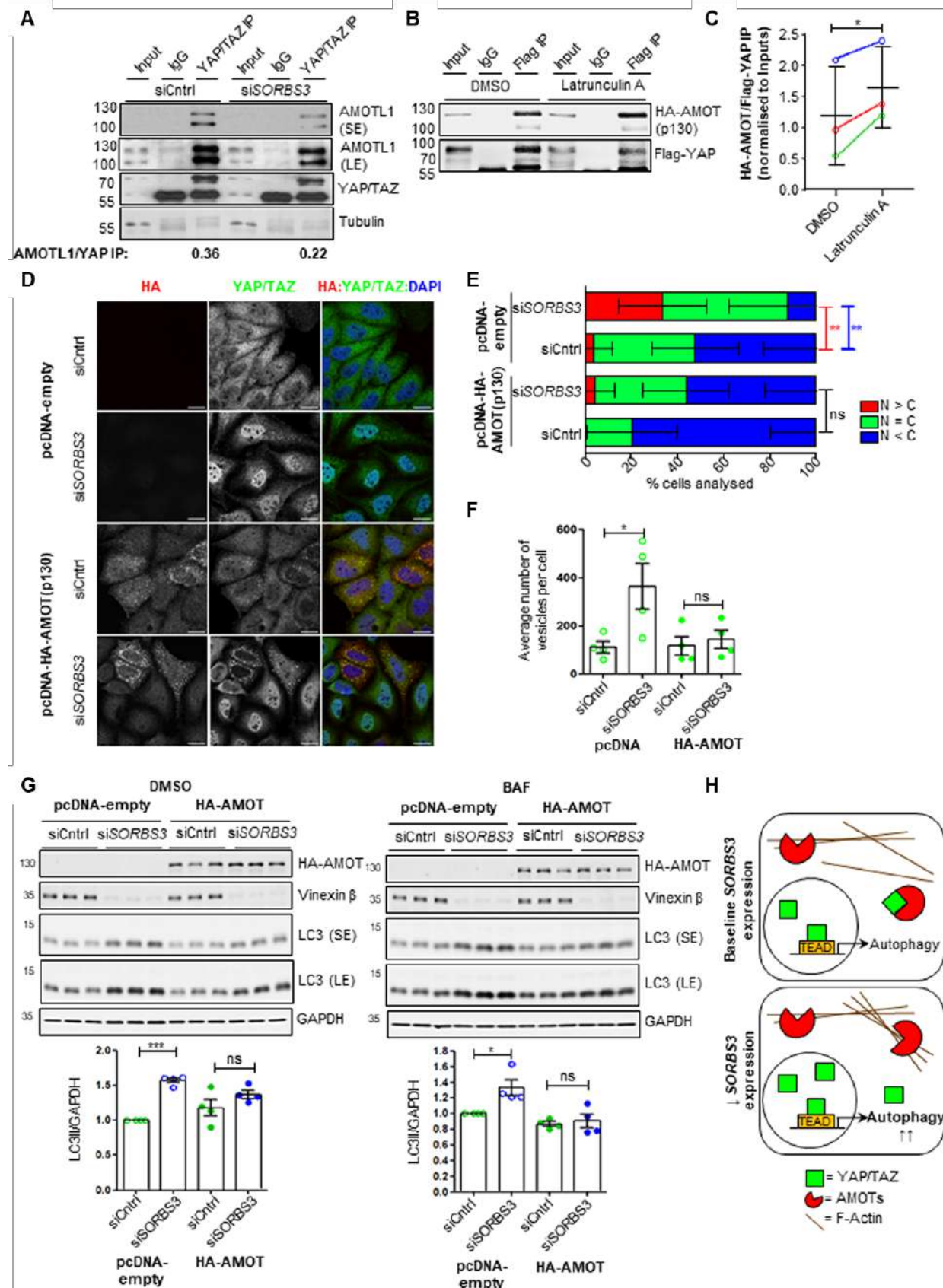


Figure 42. Vinexin depletion upregulates YAP/TAZ by countering YAP/TAZ cytosolic sequestration by angiominins. (A) HeLa cells were depleted of vinexin beta using an individual

siRNA oligonucleotide against *SORBS3* Endogenous angiomin-like protein 1 (*AMOTL1*), YAP/TAZ and tubulin were examined by western blotting. **(B)** HeLa cells were co-transfected with Flag-YAP and HA-AMOT(p130) for 48 h. Cells were treated with latrunculin A (0.5 μ M) or DMSO vehicle control for 6 h. Exogenous Flag-YAP was immunoprecipitated using a mouse antibody against Flag (Flag IP). Representative blot from three independent experiments is shown. **(C)** Quantification of three independent experiments described in **B**. **(D)** HeLa cells were depleted of vinexin beta as in **a**. siCntrl and si*SORBS3* treated cells were transfected with pcDNA-HA-AMOT(p130) or empty vector control (pcDNA-empty) for 24 h. Haemagglutinin (HA) and endogenous YAP/TAZ were examined by immunofluorescence. **(E)** Quantification of the representative experiment shown in **D**. **(F)** HeLa cells stably expressing GFP-LC3 were depleted of vinexin beta. siCntrl and si*SORBS3* treated cells were transfected with pcDNA-HA-AMOT(p130) or empty vector control (pcDNA-empty) for 24 h. Quantification of 4 independent experiments is shown. **g** (top) HeLa cells were transfected with either siCntrl or si*SORBS3* and then transfected with pcDNA-HA-AMOT(p130) or empty vector control (pcDNA-empty) for 24 h. Representative blots from four independent experiments are shown. (bottom) Quantification of the four independent experiments is shown below. ns= $p > 0.05$; *= $p < 0.05$; ***= $p < 0.001$ by two-tailed paired t-test. Error bars indicate SEM. **h** Schematic of proposed mechanism.

We successfully validated our approach using appropriate positive (*Camk4* and *Eda2r*) and negative (*Tuba1a*) controls (Fig. 43C). The same approach was applied to RNA-Seq data from 'neuropathologically normal' human donors sourced through the GTEx consortium (GTEx Consortium, 2013). *SORBS3* mRNA expression positively correlated with age in human frontal cortex (Fig. 43D) and hippocampus (Fig. 43E), with the positive (*CAMK4* and *EDA2R*) and negative (*TUBA1A*) controls correlating as expected (Fig. 43D,E). These findings are consistent with previously published microarray analysis, which found increased *SORBS3* mRNA expression in older (≥ 70 -year-old) human cerebral cortex, compared with younger (≤ 40 -year-old) cortex from an independent brain tissue set (Lipinski et al., 2010b; Loerch et al., 2008).

Finally, we investigated how increased *SORBS3* mRNA expression impacted YAP/TAZ transcriptional activity in older mouse and human brain tissue. In keeping with our molecular mechanism (summarised in Fig. 44), while *YAP1* and *TAZ* mRNA expression correlated positively with *SORBS3* expression, expression of the known YAP/TAZ-TEAD target genes *MLC2*, *MYH10*, *BIRC2*, *ERBB4*, *RUNX2*, *CCND1* and *DAB2* often negatively correlated with age in wild-type mouse brain tissue, human frontal cerebral cortex and human hippocampus, particularly *MYH10*, *BIRC2*, and *ERBB4* (Fig. 44A). Notably, our lab has previously identified myosin light chain 2 (encoded by *MLC2*), myosin heavy chain 10 (encoded by *MYH10*) and several other actin-related genes (*MYH9*, *MYH14*, *ACTN1* and *ACTB*) as downstream targets of YAP/TAZ that function in autophagosome biogenesis.

To confirm the relationship between vinexin-regulated autophagy and actin-related YAP/TAZ target genes, we examined *MLC2*, *MYH10*, *MYH9*, *MYH14*, *ACTN1* and *ACTB* mRNA expression by RT-qPCR in si*SORBS3* treated HeLa cells. mRNA expression of these genes, known to function downstream to YAP/TAZ in autophagosome biogenesis, was significantly increased in HeLa cells treated with si*SORBS3* (Fig. 44B). Our data indicate *SORBS3* mRNA expression increases with age across human brain regions (frontal cortex and hippocampus) and across species (human and mouse). Given this occurs alongside reduced autophagy (measured in mouse motor cortex), as well as reduced YAP/TAZ-TEAD target gene expression in mouse and human brain tissue, vinexin is a likely contributor to autophagic decline in normal brain ageing via decreased YAP/TAZ transcriptional activity.

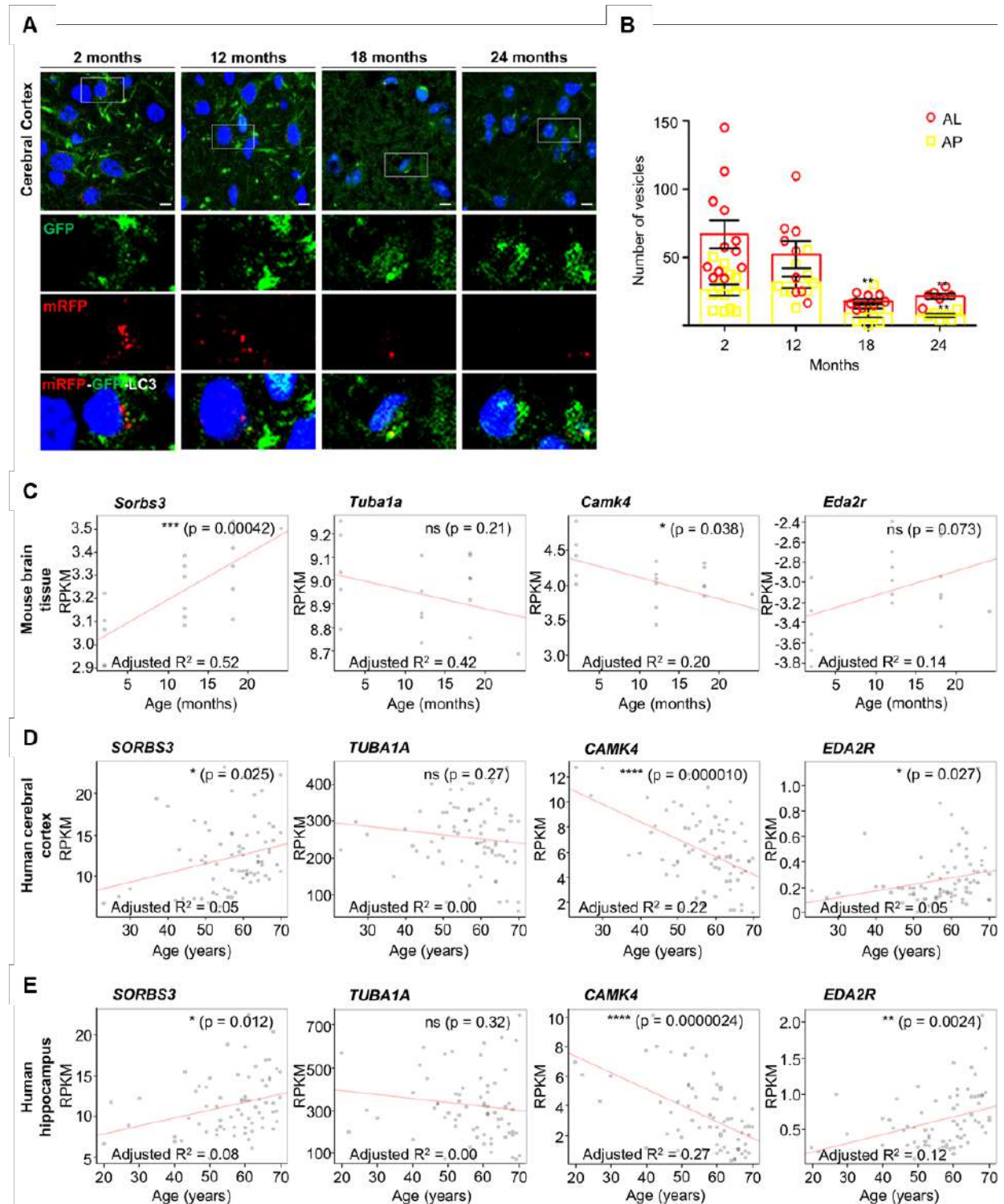


Figure 43. Autophagy declines with age in mouse motor cortex, corresponding to increased SORBS3 mRNA expression in mouse and human brain tissue. (A) Representative confocal images of sections of mouse motor cortex obtained from GFP-mRFP-LC3 mice aged to 2, 12, 18 and 24 months. **(B)** Manual quantification of autolysosomes (AL) and autophagosomes (AP) in the motor cortex of 2 ($n=12$), 12 ($n=9$), 18 ($n=8$) and 20–24 ($n=3$) months old GFP-mRFP-LC3 mice. **(C)** Sorbs3 mRNA expression, Camk4 mRNA expression (positive control), Eda2r mRNA expression (positive control) and Tuba1a mRNA expression (negative control) determined by RNA sequencing of samples from wild-type mouse brain tissue (combined motor cerebral cortex, somatosensory cerebral cortex and striatum) plotted against chronological age of the animals in months. **(D-E)** SORBS3 mRNA expression, CAMK4 mRNA expression (positive control), EDA2R mRNA expression (positive

control) and TUBA1A mRNA expression (negative control) determined by RNA sequencing of samples from ‘neuropathological normal’ human (D) frontal cerebral cortex and (E) hippocampus plotted against chronological age of the donors in years.

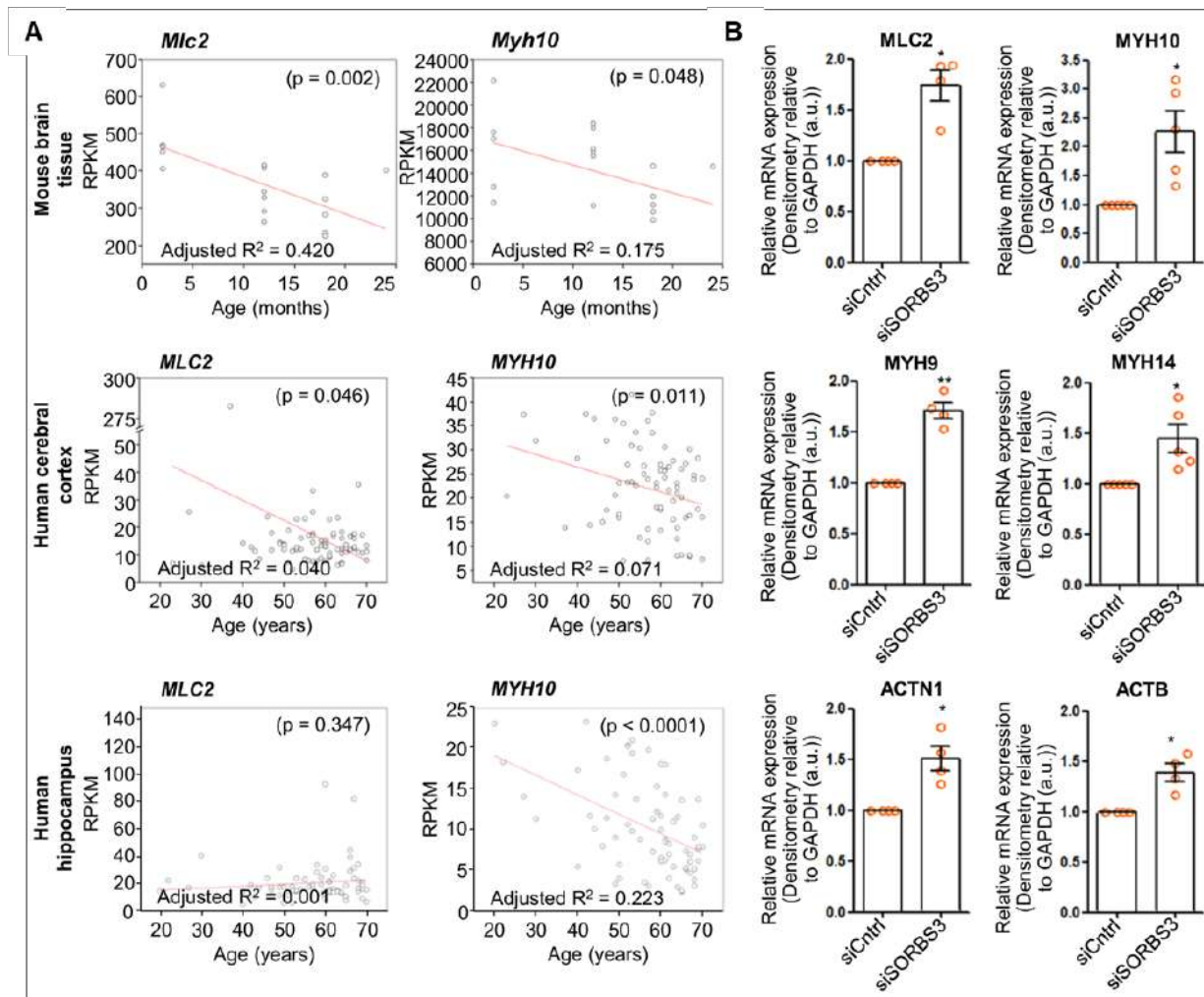


Figure 44. Expression of actin-related YAP/TAZ target genes negatively regulated by vinexin decreases with ageing mouse and human brain tissue. (A) mRNA expression determined by RNA sequencing of actin-related YAP/TAZ target genes (*MLC2* and *MYH10*) in samples from wild-type mouse brain tissue (combined motor cerebral cortex, somatosensory cerebral cortex and striatum), ‘neuropathological normal’ human frontal cerebral cortex and ‘neuropathological normal’ human hippocampus plotted against chronological age in months (mice) or years (human). **(B)** mRNA expression determined by RT-qPCR of actin-related genes (*MLC2*, *MYH10*, *MYH9*, *MYH14*, *ACTN1* and *ACTB*) in HeLa cells treated with either control siRNA (siCntrl) or *SORBS3* siRNA (si*SORBS3*). Quantification of 4 (*MLC2*, *MYH9*, *ACTN1* and *ACTB*) or 5 (*MYH10*, *MYH14*) independent experiments. *= $p < 0.05$, **= $p < 0.01$ by two-tailed paired t-test. Error bars indicate SEM.

1.4.2.5. Discussions

Vinexin was previously identified as a candidate autophagy regulator from a genome-wide image-based siRNA screen that suggested si*SORBS3* treatment increased autophagosome numbers due to decreased lysosomal processing, implying compromised autophagic flux (Lipinski et al., 2010a). While the previous data were not followed-up, our data in multiple cell lines, including mouse primary neurons, indicate that vinexin depletion using multiple reagents

increases autophagic flux and substrate clearance by promoting autophagosome biogenesis. We have defined a pathway whereby *SORBS3* knockdown increases F-actin structures, which compete with YAP/TAZ for binding to AMOTs in the cytosol. This promotes YAP/TAZ translocation into the nucleus, thereby increasing YAP/TAZ transcriptional activity and autophagy (Fig. 45).

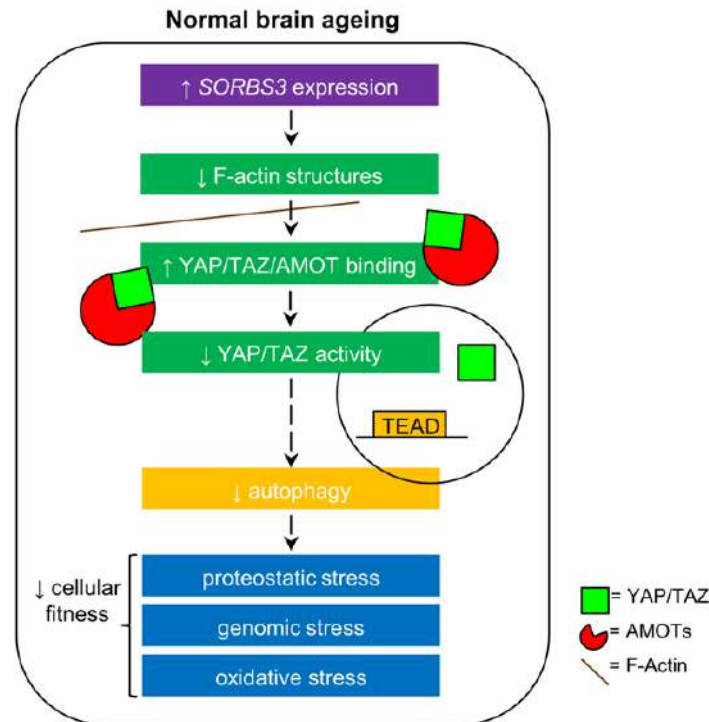


Figure 45. Schematic mechanism. Increased *SORBS3* expression, as observed in normal brain ageing, decreases F-actin bundles. This enables angiominins (AMOTs) to retain YAP/TAZ in the cytosol, which downregulates autophagy. Possible deleterious consequences, contributing to the age-related decline in ‘cellular fitness’ include impaired proteostasis, genomic instability stemming from crosstalk between autophagy and DNA repair mechanisms and reduced mitophagy causing oxidative stress.

We identify fewer autophagosomes and autolysosomes in motor cortex from mice aged to 18 and 24 months. This sits alongside increased *SORBS3* mRNA expression in brain tissue (combined motor cortex, somatosensory cortex and striatum) from aged mice, as well as frontal cortex and hippocampus from older human donors. We therefore hypothesise that increased vinexin expression contributes to autophagic decline in normal brain ageing. It is likely that vinexin is not the only contributor to decreased mammalian brain autophagy with age, as lower levels of core autophagy gene (*ATG5*, *ATG7* and *BECN1*) expression have been observed in cerebral cortex from older human donors (Lipinski et al., 2010b; Shibata et al., 2006).

Impaired autophagy in normal brain ageing is thought to contribute to an age-related decline in ‘cellular fitness’. Mechanisms attributable, at least in part, to reduced autophagy include impaired proteostasis causing toxic protein species to accumulate in the cytoplasm, genomic instability stemming from crosstalk between autophagy and DNA repair mechanisms and reduced abnormal mitochondria clearance by autophagy (mitophagy) leading to increased oxidative stress (Cheon et al., 2019; Vilchez et al., 2014; Wong et al., 2020). In all cases, neurons (as post-mitotic cells) are especially vulnerable, being unable to divide to relieve proteostatic, genomic or oxidative stress (Wong et al., 2020). Impaired autophagy is implicated in common neurodegenerative conditions such as Alzheimer’s disease and Parkinson’s disease (Menzies et al., 2017b), while aging is the primary risk factor for these conditions.

Our findings are also interesting to consider from an evolutionary standpoint. If increased vinexin expression does contribute to a deleterious reduction in autophagy in aging brain tissue, why does this persist across species (mouse and human) and over evolutionary time? The simplest explanation is that the strength of natural selection declines dramatically with respect to genes influencing outcomes subsequent to an organism's reproductive years. Another intriguing possibility is that *SORBS3* exhibits antagonistic pleiotropy and causes a 'fitness trade-off' (Elena and Sanjuán, 2003). Specifically, *SORBS3* has been identified a tumour suppressor in hepatocellular carcinoma (Ploeger et al., 2016; Roessler et al., 2012), while our findings indicate increased *SORBS3* expression could promote an age-related decline in cellular (and especially neuronal) fitness.

Final remarks

Here we identified reduced autophagosome biogenesis in aged mouse brains that may be explained, at least in part, by increased expression of the adaptor protein vinexin. We characterise vinexin (encoded by *SORBS3*) as a negative regulator of autophagy and define the molecular mechanism. Vinexin depletion increases filamentous actin (F-actin) bundles, which compete with the transcriptional coactivators YAP and TAZ for binding to cytosolic angiostatins (AMOTs). This releases YAP/TAZ to enter the nucleus and increase transcriptional activity, thereby upregulating autophagy. We show that *SORBS3* mRNA expression increases with age in mouse and human brain tissue. This corresponds to fewer autophagic vesicles in cerebral cortex samples from aged mice.

Altogether, our data suggest that increased *SORBS3* expression is an important contributor to autophagic decline in mammalian brain ageing. Further research is required for identifying other potential internal age-related inhibitors of autophagy using a similar strategy by combining bioinformatics analysis with experimental validation, which could lead to the identification of molecules that can be targeted by various already approved FDA compounds (or even new generated ones).

Chapter 2: The molecular mechanisms of immune system regulation in health and disease

2.1. The landscape of immune cells in haematological malignancies

2.1.1. State of art

Acute myeloid leukemia (AML) is a rapidly proliferating hematologic malignancy, in which relapsed/refractory patients face a dismal prognosis (Papaemmanuil et al., 2016). Since the relapse rates following conventional chemotherapy is high, the general interest in searching for novel therapies, including immunotherapy, is increasing. However, the development of immunotherapy in AML has been hindered so far by its remarkable genetic, antigenic and clonal heterogeneity (Cancer Genome Atlas Research et al., 2013; Talati and Sweet, 2018) and the risk of significant off-target hematologic toxicity, but also by the lack of biomarkers defining patient populations more likely to benefit from it (Davidson-Moncada et al., 2018).

The immune biology of AML is strikingly different from that of solid tumours: 1) it originates in the immune privileged, Treg enriched milieu of the bone marrow (BM); 2) it has a low neoantigenic fitness, resulting in relatively few leukemia-specific antigens that can elicit immune responses; 3) it expresses nonetheless both major histocompatibility complex (MHC)-II and B7 checkpoint molecules (Curran et al., 2017). Further studies have thus demonstrated that AML blasts can not only function as APCs, but can also fine tune the activity of CD4+ and CD8+ T-cells by upregulating their expression of checkpoint-ligands as the Programmed-Death Ligand 1 (PD-L1), PD-L2, and B7.2 (Antohe et al., 2020) under the influence of interferon-gamma (IFN- γ) (Berthon et al., 2010; Kondo et al., 2010; Kronig et al., 2014). Moreover, the expression levels of the MHC-II antigen-presenting machinery and B7 immune checkpoint-ligands holds prognostic relevance in AML. It is worth mentioning that in 2018, the research field of immune checkpoint blockade was awarded with the Nobel Prize for Physiology and Medicine, shared by James P Allison and Tasuku Honjo. Thus, given the AML origin within an immune-privileged, Treg abundant BM niche (Chamuleau et al., 2004), its low mutational load (Talati and Sweet, 2018), deficient antigen presentation (van Luijn et al., 2010a; van Luijn et al., 2010b), aggressive growth and bloodstream dissemination (Dudenhoffer-Pfeifer and Bryder, 2018; Zhang et al., 2013), this hematological malignancy was regarded as a poorly immunogenic tumour, with a rather leukemia microenvironment (LME) “immune-desert” phenotype (Davidson-Moncada et al., 2018), in which immunoediting is either absent or a rather late event (Loke and Allison, 2004).

Noteworthy, the LME of some AML cases displays evidence of a prior anti-leukemic immune response, restrained by immune escape mechanisms such as CTLA-4 (Cytotoxic T lymphocyte associated protein-4)/ B7.1/2 and PD-1 (Programmed death-1)/ PD-L1 signaling, indolamine-deoxygenase-1 expression or regulatory T cell (Treg) expansion (Davidson-Moncada et al., 2018). B7 molecules are key structures of the immune checkpoints that regulate T cell activation (Kondo et al., 2010). Previous research has shown that up-regulation of B7 ligands such as PD-L1, PD-L2, B7.2 on AML blasts is inducible by exposure to interferon γ (IFN- γ) (Greaves and Gribben, 2013; Kronig et al., 2014) which indicates a “T-cell inflamed” immune profile. Hijacking of these immune checkpoint molecules is used by leukemia cells to evade immune surveillance (Uckun et al., 2021).

Additional mechanisms appear to also contribute to tumour escape from the immune surveillance in AML (Stabile et al., 2017). For instance, the natural killer (NK) cells are known to play an important role in clearing leukemic cells to control disease progression, thus being involved in the therapy response and disease prognosis (Costello et al., 2002; Fauriat et al.,

2007). They achieve this goal with the help of a highly diverse repertoire of germline-encoded activating and inhibitory receptors that allow NKs to recognize and target cells that lack or downregulate the expression of major histocompatibility complex (MHC) class I molecules (Geiger and Sun, 2016). Downregulation of activating receptors or upregulation of inhibitory receptors on NK cells appear to contribute to the immune escape observed in hematological malignancies, including AML and myelodysplastic syndromes (MDSs). MDSs are pre-malignant, clonal hematopoietic cell dysplasia, characterized by ineffective hematopoiesis and multilinear cytopenias which eventually progress towards AML. Multiple studies have identified various immune evasion mechanisms that allow the MDS disease-initiating hematopoietic stem precursor cells (MDS-HSPCs) to escape from the immune system surveillance and contribute to MDS installment and progression towards AML (Ades et al., 2014; Dulphy et al., 2016; Tefferi and Vardiman, 2009). It has been recently reported that NK dysfunction in AML arises from maturation impairment, which associates a low expression of cytotoxic subtypes and downregulation of activating receptors (Chretien et al., 2017; Epling-Burnette et al., 2007; Fauriat et al., 2007). Importantly, data gathered from allotransplanted patients, who were mismatched for KIR-human leukocyte antigen (HLA) compared with their respective donors, showed a lower incidence of relapse due to improved graft-*versus*-leukemia response (Hsu et al., 2005; Ruggeri et al., 2002).

In this context, characterizing the immune expression profile (MHC-II antigen presentation machinery, immune checkpoint ligands/receptors display, T cell and NK cell maturation landscapes) of the leukaemic microenvironment may provide useful biomarkers that can be used in guiding and personalizing immunotherapy as an emerging novel therapy in AML.

This research direction has been achieved by publishing the following scientific articles:

ISI ARTICLES

Ion Antohe*, **Mariana Pavel Tanasa***, Angela Dăscălescu, Cătălin Dănilă, Amalia Titieanu, Mihaela Zlei, Iuliu Ivanov, Adriana Sireteanu, Petru Cianga. *The MHC-II antigen presentation machinery and B7 checkpoint ligands display distinctive patterns correlated with acute myeloid leukaemias blast cells HLA-DR expression*, *Immunobiology* 2021; 226(1): 152049. **IF: 3.152**
<https://doi.org/10.1016/j.imbio.2020.152049> (* equal contribution)

Ion Antohe, Angela Dăscălescu, Cătălin Dănilă, Amalia Titieanu, Mihaela Zlei, Iuliu Ivanov, Adriana Sireteanu, **Mariana Pavel**, Petru Cianga. *B7-Positive and B7-Negative Acute Myeloid Leukemias Display Distinct T Cell Maturation Profiles, Immune Checkpoint Receptor Expression, and European Leukemia Net Risk Profiles*. *Frontiers in Oncology* 2020; 10: 264. **IF: 6.244**
<https://doi.org/10.3389/fonc.2020.00264>.

Vlad Andrei Cianga, Lydia Campos Catafal, Petru Cianga, **Mariana Pavel Tanasa**, Mohamad Cherry, Phillipe Collet, Emmanuelle Tavernier, Denis Guyotat, Cristina Rusu, Carmen Mariana Aanei. *Natural Killer Cell Subpopulations and Inhibitory Receptor Dynamics in Myelodysplastic Syndromes and Acute Myeloid Leukemia*, *Frontiers in Immunology* 2021; 12: 665541. **IF: 8.787**
<https://doi.org/10.3389/fimmu.2021.665541>.

Vlad Andrei Cianga, Cristina Rusu, **Mariana Pavel-Tanasa**, Angela Smaranda Dascalescu, Catalin Doru Danaila, Sebastian Harnau, Carmen Aanei and Petru Cianga. *Combined flow cytometry NK immunophenotyping and KIR/HLA-C genotyping reveal remarkable differences in AML patients, but suggest an overall impairment of the NK response*. *Frontiers in Medicine* 2023; 10: 1148748. **IF: 5.058**
<https://doi.org/10.3389/fmed.2023.1148748>.

2.1.2. Characterisation of MHC-II antigen presentation machinery and immune checkpoint ligands profile in AML

2.1.2.1. Introduction

Recent advances in understanding the cancer-immune interaction have led to spectacular progress in the field of cancer immunotherapy. In 2013, Chen and Mellman described this interaction as a continuous, stepwise process, in which immune effectors are primed and eliminate tumour cells, referred to as the cancer-immunity cycle (Chen and Mellman, 2013). Its first crucial step involves the MHC (Major Histocompatibility Complex)-mediated presentation of tumour-derived antigens and the priming of anti-tumour T-cells. The “classical” human MHC (named HLA, Human Leukocyte Antigen)-II proteins (HLA-DP, HLA-DQ, HLA-DR) are expressed on the cell surface, while the “non-classical” molecules (HLA-DN, HLA-DO, HLA-DM) mostly play intracellular regulatory roles (Horton et al., 2004; Muers, 2011). MHC-II expression is restricted to a category of cells functionally characterised as antigen-presenting cells (APC). Their physiological role of presenting MHC groove-bound peptides to CD4⁺ T-cells is of paramount importance for the maintenance of immune homeostasis (Lim and Elenitoba-Johnson, 2004; Wang, 2001).

However, tumour cells can function themselves as APCs if they express MHC-II and appropriate co-stimulatory apparatus (Barrett and Le Blanc, 2010). Two distinct, MHC-II antigen-presentation pathways are presently acknowledged. In the first one, considered as a „classical” pathway, MHC-II molecules are associated with the Invariant chain (Ii, CD74), that protects the peptide binding groove and drives the complex from the endoplasmic reticulum via trans-Golgi network into the late-endosomal MHC-II compartments (MIIC), where CD74 is being cleaved. Its MHC groove-bound fragment, namely CLIP (Class II-associated invariant chain peptide) evades degradation. The removal of CLIP and the stable binding of a high-affinity peptide are modulated by HLA-DM and its negative regulator, HLA-DO. HLA-DM is thus critical in ensuring the optimal peptide repertoire of MHC-II molecules. Thus, MHC-II ligands can be categorised as: 1) DM-sensitive, whose presentation is abolished in the presence of HLA-DM, and 2) DM-resistant, which can be presented in the presence of HLA-DM, as reviewed in (Kremer et al., 2012; Unanue et al., 2016).

The expression of CD74 on leukaemic cells was not only described, but was also associated with an increased risk of relapse of AML (van den Ancker et al., 2014), while the lack of CD74 expression on these cells favours the activation of CD4⁺ T lymphocytes targeting leukaemic cells (van Luijn et al., 2011). The surface CLIP expression, regarded as a marker of deficient antigen-presentation, has been thus linked to poor prognosis in AML, at diagnosis, as well as in remission patients displaying CLIP⁺ minimal residual disease (van Luijn et al., 2014). The variations in the expression of CLIP are linked to the presence of the peptide editors, HLA-DM and DO. Thus, a DM/DO ratio in favour of the latter promotes CLIP retention in the MHC-II groove, compromising the presentation of leukaemia-derived peptides (Chamuleau et al., 2004).

2.1.2.2. Aim

The aim of the current study was to investigate the surface expression of HLA-DR, CLIP and the intracellular expression of CD74 and HLA-DM on leukaemic blasts of newly diagnosed AML patients. These data were further correlated with the expression of B7 checkpoint-ligands on AML cells, as these molecules are of paramount importance for the anti-tumour T-cell priming.

2.1.2.3. Materials and methods

Patient selection

This study included 30 patients diagnosed between 2016 and 2019 at the Iași Regional Oncology Institute from Romania with *de novo*, non-promyelocytic AML, as well as a group of four healthy volunteers, that were all extensively characterised previously (Antohe et al., 2020). Sample collection was performed based on an informed consent. This study has been approved by the institutional ethics committee. BM samples were collected at diagnosis. The diagnosis of AML was established according to the WHO diagnostic criteria (Arber et al., 2016). The cytogenetic risk of the patients was evaluated in accordance with the 2017 European Leukaemia Net (ELN) recommendations (Dohner et al., 2017), as favourable, intermediate, or adverse.

Flow cytometry

AML blasts were analysed by multiparameter flow-cytometry (MFC) on erythrocyte-lysed fresh BM samples, as previously described (Antohe et al., 2020). We first confirmed the AML diagnosis using protocols based on the EuroFlow recommendations (Antohe et al., 2020; van Dongen et al., 2012). AML blasts gating was performed on CD45+/CD34+/CD117+ events. The HLA-DR levels were assessed based on the expression of this marker on BM monocytes. Thus, cases with reduced leukaemic blast HLA-DR expression when compared to monocytes were categorised as HLA-DR low. Subsequently, the BM leukaemic blast cells surface expression level of CLIP, ICOS-L, B7-1, B7.2, PD-L1, PD-L2, B7-H3 and the intracellular expression levels of HLA-DM and CD74 were assessed. T cell gating was performed on CD3+/CD4+ and CD3+/CD8+ events. The following T cell maturation subpopulations were defined based on their differential expression of CD28, CD27, and CD45RA: naive (N), central memory (CM), intermediate effector memory (iEM), late effector memory (late EM) (Antohe et al., 2020). Data acquisition was performed on a BD FACS ARIA III cytometer and data was interpreted using the FACS DIVA v6.1.3 software. An identical investigation protocol was applied for the CD45+/CD34+/CD117+ BM cells of all four healthy subjects.

Statistical analysis

Statistical analyses were performed using the IBM® SPSS Statistics 21.0 Software. The Chi square, Mann Whitney test and Wald test were used to analyse the associations between different variables. The Pearson correlation coefficient was calculated to investigate the relationships between numerical variables. The two-way ANOVA test was used to analyse the differences among multiple variables. A *p* value <0.05 was considered as statistically significant.

2.1.2.4. Results

Comparison of clinical characteristics of patients

Among the AML patients, but not in the healthy donors (HD) group, we have identified 7 cases (23.3%) with low HLA-DR expression of BM CD45+/CD34+/CD117+AML cells (with lower HLA-DR expression than the one identified on BM monocytes), in accord with literature data (Feller et al., 2013). Based on this observation, we have divided the AML cases in 2 distinct categories: low (*n*=7) and normal (*n*=23) HLA-DR groups. The patients included in the two HLA-DR groups were of similar age and male to female ratio. All favourable ELN risk patients had normal HLA-DR levels, summing for 34.8% of the patients (*P*=0.068), and the percentage of patients presenting an adverse ELN risk was lower in the normal HLA-DR group (21.8%) compared to HLA-DR low (42.9%). The HLA-DR MFI values of AML blasts

from the HLA-DR low group were significantly lower than those of the HLA-DR normal group ($P=0.0009$, ratio MFI HLA-DR low/ MFI HLA-DR normal=0.45)

HLA-DM expression is increased in AML cases vs. healthy donors

The percentage of CD34+/CD117+/HLA-DM+ cells was compared between the HD control group ($n=4$) and the patients with low ($n=7$) and normal HLA-DR ($n=23$) expression. While no statistical differences were seen in terms of HLA-DM intracellular expression between the two patient groups (Fig. 46A), we have noticed a remarkable 4 times higher expression when compared to the control healthy group (Fig. 46B). In terms of HLA-DM MFI values, no significant differences were seen among the three groups.

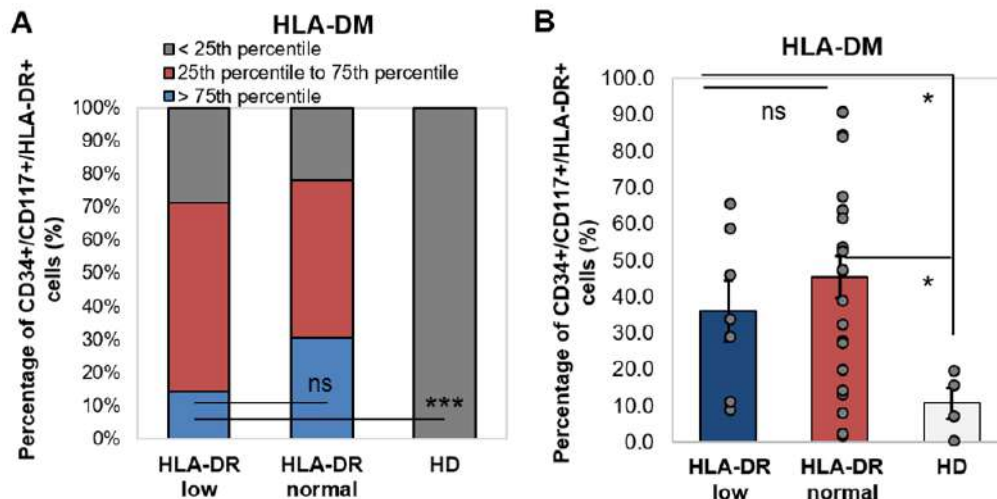


Figure 46. HLA-DM expression in AML patients and healthy donors. (A) Percentage of CD34+/CD117+/HLA-DR+ cells expressing HLA-DM in AML patients with low ($n=7$) and normal ($n=23$) HLA-DR expression and healthy donors (HD, $n=4$). The percentages of cells were categorised in three intervals based on the 25th (19.7%) and 75th (63.5%) percentile values of HLA-DM in AML patients: below 25th percentile, between 25th to 75th percentile and above 75th percentile ($***P<0.001$, ns – not significant; Wald test). Overall chi-squared test: $P=0.006$. (B) Percentage of CD34+/CD117+/HLA-DR+ cells expressing HLA-DM in AML patients with low ($n=7$) and normal ($n=23$) HLA-DR expression and healthy donors (HD, $n=4$). Individual values are represented as points. Bars represent the mean \pm SEM ($***P<0.001$, $*P<0.05$, ns – not significant; one-way ANOVA test).

CD74 levels correlate with CLIP expression in AML patients

To further characterise the HLA-DM and Ii/CLIP interconnection, we have investigated the intracellular CD74 and surface CLIP expression in the CD45+/CD34+/CD117+ BM cells. A total of 80.5% of AML patients expressed higher percentages of CD74+ cells than the HD ($P=0.001$) despite overall high CD74 expression levels (Fig. 47A). This observation suggests that among the molecules of the AML exogenous antigen-presenting system, CD74 along with HLA-DM seem to be overexpressed. Indeed, HLA-DM expression strongly correlates with CD74: $R=0.45$, $P=0.012$ (Fig. 47B).

The CD74 expression in AML cases displayed a left skewed distribution with values ranging from 3.1% to 100% and high median, 25th and 75th percentiles values of 98.4%, 97.4% and 99.8%, respectively. Among AML, all HLA-DR low cases showed medium (above the 25th percentile and less than the 75th percentile) and high (above the 75th percentile) Ii intracellular expression, while the normal HLA-DR group included 30.4% of cases with low Ii expression. All HD cases showed low percentages values for CD74+ cells (Fig. 47C). Interestingly, the HLA-DR low group expressed CD74 in 98.8% of the BM cells (with 97.5%

and 100% as minimum and maximum values, respectively), significantly higher than the normal HLA-DR (mean=90.4%, min=3.1%, max=100%; $P=0.026$) or HD (mean=87.4%, min=59.8%, max=97.2%; $P=0.049$) groups (Fig. 47D). The CD74 MFI values further confirmed these observations: reduced values by 25% and 50% in the HLA-DR normal group and HD, respectively. In two normal HLA-DR AML cases, we identified extremely low levels of CD74 expressing BM cells: 3.1% in one AML patient with *NPM1* (nucleophosmin 1) mutation and normal karyotype, and 39.9% in another AML patient with a complex karyotype comprising various chromosomal monosomies (7, 12, 20) and del(5q) (Fig. 47D).

The overall CLIP expression was very low (below 10%) in AML cases and HD, with two AML exceptions: 12% in one patient with t(1;11)-associated AML and 14.1% in a patient with *NPM1*-mutated AML with complex karyotype.

The HLA-DR low patients showed also a higher CLIP expression (Fig. 47E), which correlated with adverse or intermediate ELN risk when compared to the normal HLA-DR or HD groups. In contrast, most cases with normal HLA-DR levels and high HLA-DM intracellular expression (above 75th percentile – 63.5%) associated low CLIP levels. Interestingly, in the case of the unprocessed Ii chain, only the intermediate and low HLA-DM cases showed less CD74 expression when compared to the HLA-DR low group.

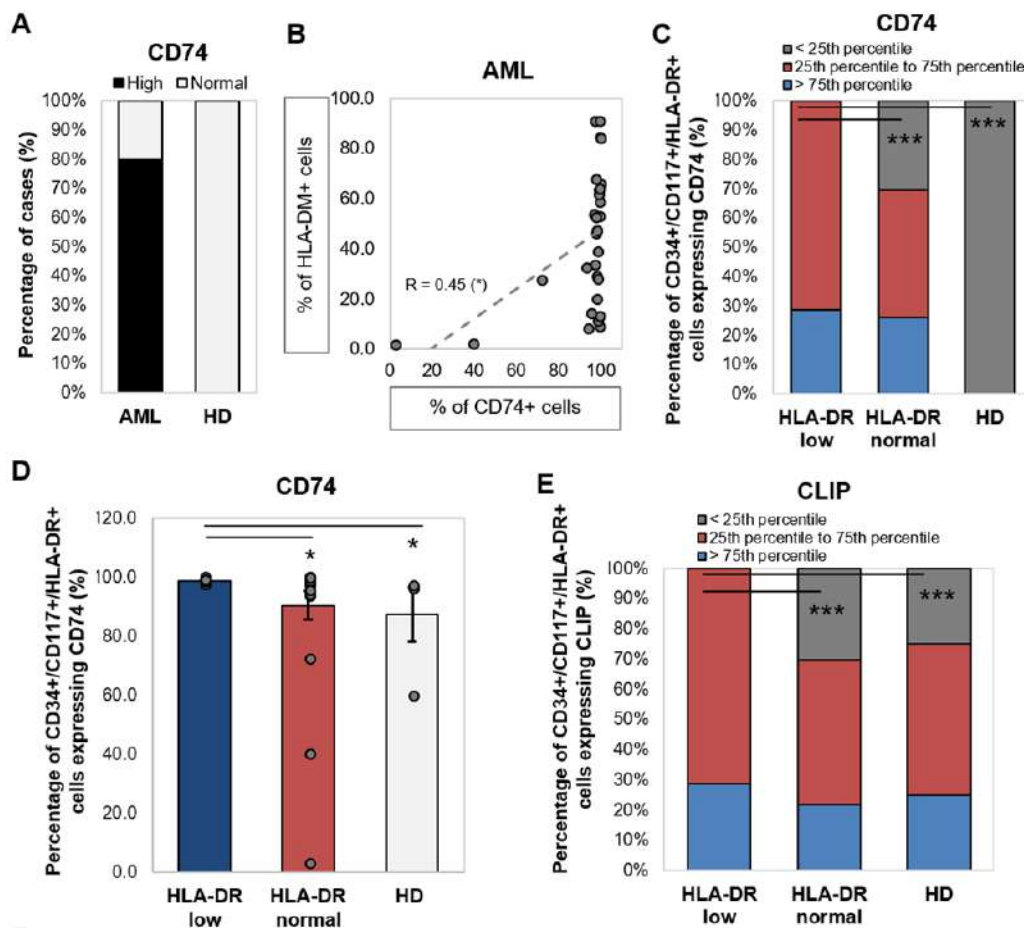


Figure 47. CD74 and CLIP expression in AML patients and healthy donors. (A) Percentage of AML cases with higher CD74 expression values than HD. Chi-squared test: $P=0.001$. (B) CD74 and HLA-DM correlation in AML patients ($*P<0.05$; ANOVA test). (C) Percentage of CD34+/CD117+/HLA-DR+ cells expressing CD74 in AML patients with low ($n=7$) and normal ($n=23$) HLA-DR expression and healthy donors (HD, $n=4$). The percentages of cells were categorised in three intervals based on the 25th (97.4%) and 75th (99.8%) percentile values of CD74 in AML patients: below 25th percentile, between 25th to 75th percentile and above 75th percentile ($***P<0.001$; Wald test). Overall chi-squared test: $P=0.003$. (D) Percentage of CD34+/CD117+/HLA-DR+ cells expressing

CD74 in AML patients with low ($n=7$) and normal ($n=23$) HLA-DR expression and healthy donors (HD, $n=4$). Individual values are represented as points. Bars represent the mean \pm SEM ($***P<0.001$, $*P<0.05$; one-way ANOVA test).

Expression of checkpoint-ligands: co-stimulatory molecules are increased in HLA-DR low AML cases, while co-inhibitory molecules are higher in HLA-DR normal AML cases

The CLIP enriched cancer cells (HLA-DR low) showed a significant increase in the expression of co-stimulatory ICOS-L (HLA-DR low vs. HD: $P=0.03$, Fig. 48A) and dual function (according to the ligand involved) B7.2 (HLA-DR low vs. HD: $P=0.014$, Fig. 48B) molecules: 10.75% vs. 2.45% and 35.93% vs. 10.1%, respectively. No statistical differences were seen between the normal HLA-DR AML cells and HD cells regarding ICOS-L and B7.2 expression. The ICOS-L and B7.2 MFI values followed similar patterns as the cellular positivity percentages (HLA-DR low vs. HD: $P=0.024$ (ICOS-L MFI) and $P=0.048$ (B7.2 MFI)).

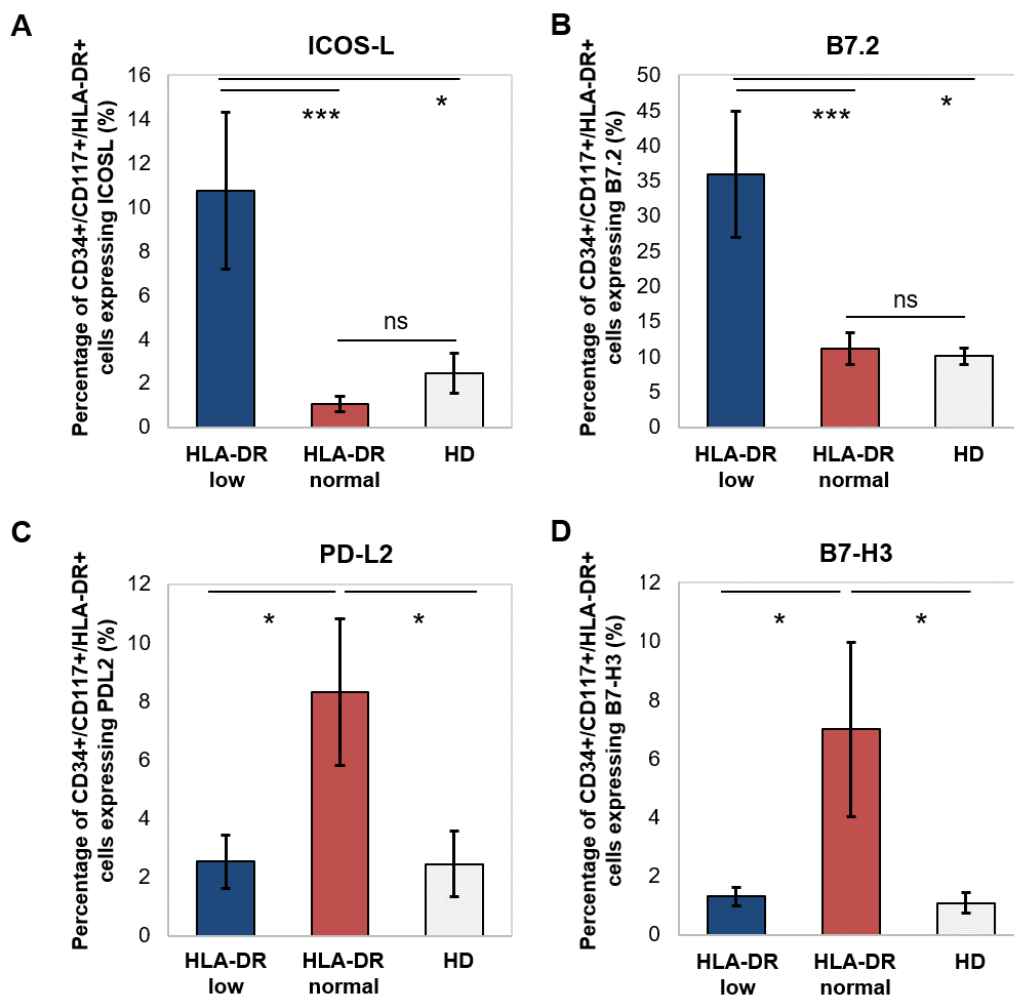


Figure 48. Expression of co-stimulatory (ICOS-L), dual function (B7.2) and co-inhibitory (PD-L2, B7-H3) B7 ligands in AML patients and healthy donors. (A) Percentage of CD34+/CD117+/HLA-DR+ cells expressing ICOS-L in AML patients with low ($n=7$) and normal ($n=23$) HLA-DR expression and healthy donors ($n=4$). (B) Percentage of CD34+/CD117+/HLA-DR+ cells expressing B7.2 in AML patients with low ($n=7$) and normal ($n=23$) HLA-DR expression and healthy donors ($n=4$). (C) Percentage of CD34+/CD117+/HLA-DR+ cells expressing PD-L2 in AML

patients with low ($n=7$) and normal ($n=23$) HLA-DR expression and healthy donors ($n=4$). **(D)** Percentage of CD34+/CD117+/HLA-DR+ cells expressing B7-H3 in AML patients with low ($n=7$) and normal ($n=23$) HLA-DR expression and healthy donors ($n=4$). Bars represent the mean \pm SEM (** $P<0.001$, * $P<0.05$, ns – not significant; one-way ANOVA test).

On the opposite side, the cases with normal HLA-DR expression had remarkably increased co-inhibitory PD-L2 (normal HLA-DR vs. HD: $P=0.021$, Fig. 48C) and B7-H3 (normal HLA-DR vs. HD: $P=0.029$, Fig. 48D) molecules: 8.3% vs. 2.45% and 7.01% vs. 1.08%. As expected, the expression of co-inhibitory PD-L2 and B7-H3 molecules was not affected in the group of HLA-DR low cases. Interestingly, the PD-L2 MFI values were reduced in the HLA-DR low, but not in the HLA-DR normal group (HLA-DR low vs. HD: $P=0.0008$). On the contrary, the B7-H3 MFI values followed a similar pattern as the above presented cellular percentages: a significant three times increase in the HLA-DR normal group compared to HD (HLA-DR normal vs. HD: $P=0.028$). Indeed HLA-DM and CD74 levels inversely correlated with the expression of B7-H3 ($R=-0.43$ and $R=-0.63$, respectively (Fig. 49A-B), while CLIP MFI values positively correlated with PD-L2 ($R=0.41$). Oppositely, the CD74 and CLIP expression (both cell percentages and MFI values) inversely correlated with the dual function B7.2 molecule in HLA-DR low cases ($R=-0.53$ for cell percentages – Fig. 49B, and $R=-0.54$ for MFI values), probably suggesting a bias of the immune system towards Th2 responses in the case of DM-sensitive peptides, most likely of endogenous tumour origin.

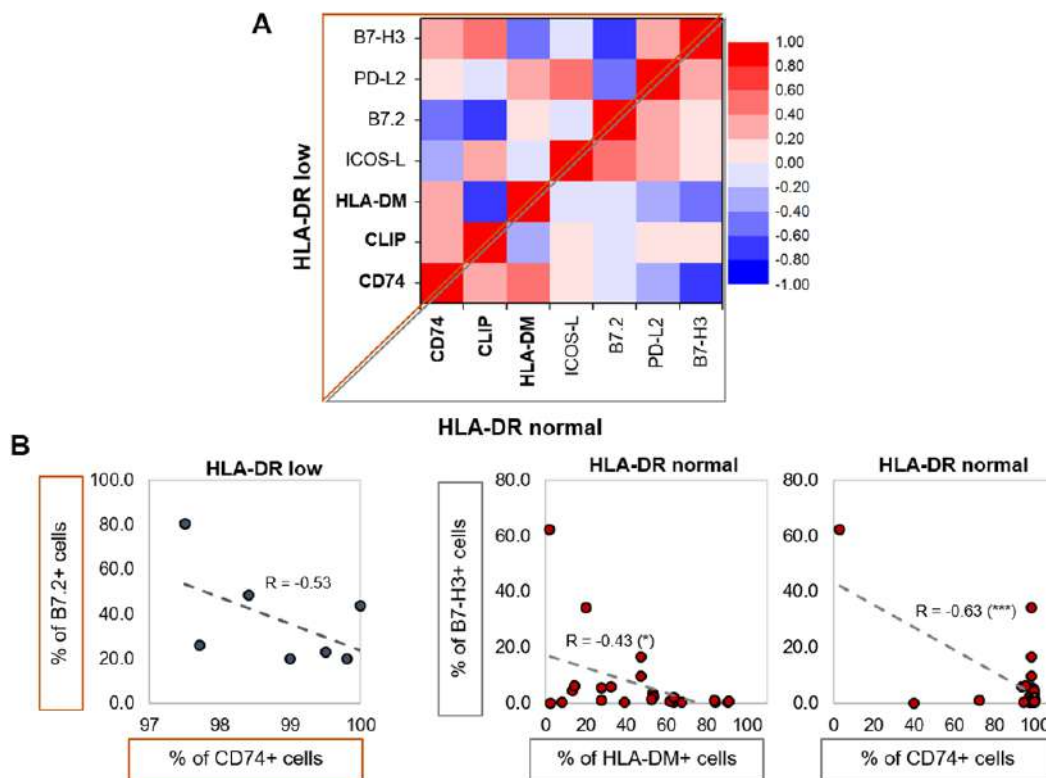


Figure 49. CD74/HLA-DM and B7 ligands co-expression in AML patients. (A) Heat map of CD74/HLA-DM and B7 ligand co-expression. **(B)** Pearson correlation coefficients (R) were computed, and ANOVA test was used to analyse the significance of the identified correlations (** $P<0.001$; * $P<0.05$).

BM CD4+ and CD8+ effector memory T cell subpopulations differ among HLA-DR low and normal AML cases

When compared to HD, HLA-DR normal patients only displayed significantly lower percentages of CD8+ T cells ($P=0.019$). Although no differences were seen regarding the percentage of naïve T cells among HLA-DR low, normal and HD cases, the effector memory T cell subpopulations showed distinct patterns: (1) the majority of the BM CD4+ and CD8+ T cells were CM cells in HLA-DR low cases, while the majority of BM CD8+ T cells were late EM in the HLA-DR normal and HD cases ($P<0.001$, chi-square test); (2) lower percentages of CD4+ lateEM (HLA-DR low vs. HLA-DR normal: $P=0.04$, HLA-DR low vs. HD: $P=0.005$) and CD8+ iEM (HLA-DR low vs. HLA-DR normal: $P=0.009$, HLA-DR low vs. HD: $P=0.04$) T cells in HLA-DR low AML patients when compared to HLA-DR normal and HD cases (Fig. 50A). Additionally, CLIP values strongly correlated with naïve T cell percentages and showed inversed correlation with effector memory T cell subsets (CD4+ iEM and late EM, C8+ lateEM) in HLA-DR low cases. These last results suggest a less efficient effector memory T cell differentiation in HLA-DR low cases.

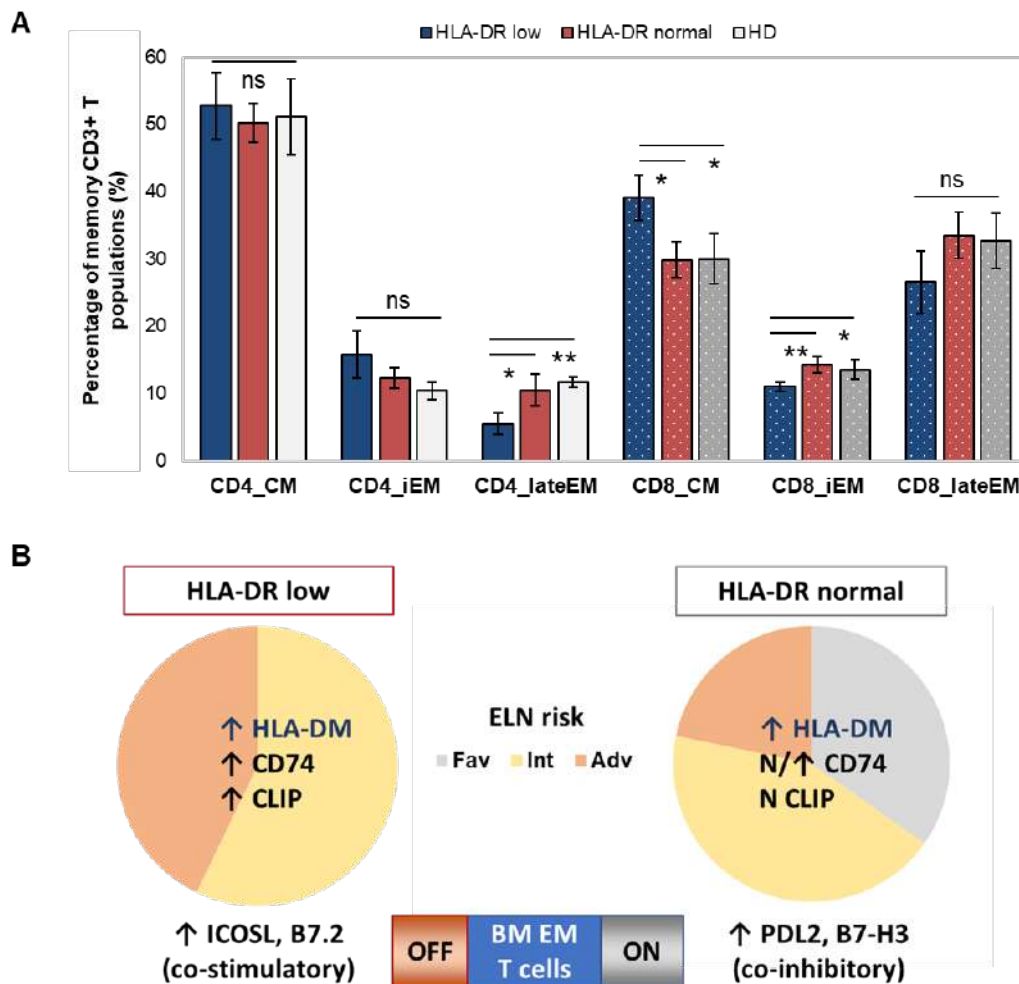


Figure 50. BM effector memory T cell subsets in AML patients. (A) Percentage of CD4+ or CD8+ T cell populations – central memory (CM), intermediate effector memory (iEM), and late effector memory (late EM) – in AML patients with low (n=7) and normal (n=23) HLA-DR expression and HD (n=4). Bars represent the mean ± SEM (**P < 0.01, *P < 0.05, ns – not significant; ANOVA test). (B) Proposed model for the interaction of HLA-II molecules and B7 ligands in AML cases (N=normal, ↑=increased, Fav=favourable, Int=intermediate, Adv=adverse).

2.1.2.5. Discussions

Immunotherapy is emerging as a promising alternative in the treatment of AML and immune gene expression profiling of the leukaemic microenvironment is establishing itself as a useful biomarker in guiding and personalizing this approach (Davidson-Moncada et al., 2018; Masarova et al., 2017). Although AML is regarded as a poorly immunogenic cancer (Curran et al., 2017), leukaemic cells are nonetheless capable of presenting a large range of leukaemia-derived immunogenic peptides, such as NPM1, PML-RARA or BCR-ABL (Biernacki and Bleakley, 2020; Greiner et al., 2017; Makita et al., 2002) to T-cells, and to elicit anti-leukaemic immune responses. Given its constitutive surface expression of MHC-II molecules, AML is a tumour type capable of presenting its own antigens (van Luijn et al., 2012). Thus, antigen-presentation is a first vital step of the cancer-immunity cycle that can be compromised by leukaemic cells in order to achieve immune evasion. Antigen-presentation is influenced by the MHC-II surface expression levels. A reduced HLA-DR expression, as we were able to show for a group of our AML patients, might be explained by three mechanisms: i) reduced transcription of MHC-II molecules ii) intra-endosomal/lysosomal sequestration iii) increased proteolysis and turnover (Roche and Furuta, 2015).

Here we analysed the interlink between the cellular expression of the MHC class II - related machinery molecules (the classical HLA-DR molecule, the non-classical HLA-DM, CLIP, CD74) and B7 ligands (ICOS-L, B7.2, PD-L1, B7-H3). Thus, we have shown that AML blasts have a significantly increased HLA-DM expression compared to the normal HD value of 10.7%. This information is extremely relevant, as the identified HLA-DM expression levels of BM cells from HD may establish a normal reference value for this marker. Further, 23.3% of AML cases displayed low HLA-DR expression on leukaemic blasts, forming a distinctive group of patients. Despite similar HLA-DM levels between the two differentially expressed HLA-DR groups (HLA-DR low vs. normal), only the HLA-DR low group had significant increased CD74 and CLIP levels. The high intracellular CD74 levels, corroborated with the increased HLA-DM levels, suggest a reinforced mechanism of the cancer cells to protect the MHC-II groove from loading endogenous derived peptides in the endoplasmic reticulum or endosomal compartments, thus preventing cross-presentation of tumour-specific DM-sensitive antigens to CD4⁺ T-cells (Kremer et al., 2014). The increased expression of surface CLIP within the HLA-DR low group might be due to an additional HLA-DO higher co-expression, as CLIP/HLA-DR ratio was shown to strongly correlate with HLA-DO/HLA-DM ratio in AML blasts (Berthon et al., 2010). This phenotype preferentially assists the presentation of a broad DM-sensitive peptide repertoire exclusively processed intracellular (Kremer et al., 2014). Since the T-cell responses against endogenous antigens rather allow the recognition of DM-sensitive antigens than the targeting of DM-resistant long-lived HLA-peptide complexes (Kremer et al., 2012; Kremer et al., 2014; van den Ancker et al., 2014), it is highly probable that the HLA-DR low AML blasts tend to present CLIP-like endogenous antigens in T-cell responses. As expected, for those cases with normal HLA-DR expression, the high HLA-DM intracellular expression (above 75th percentile – 63.4%) probably led to the removal of CLIP from the HLA-DR grooves, with the subsequent degradation of CLIP, as its surface expression did not significantly differ from the reference value corresponding to HD (3.7%). We could thus conclude that the AML blasts with an HLA-DR expression like that encountered in normal cells would promote the display of DM-resistant exogenous antigens, and these cancer cells generally tend to suppress the endogenous presentation to T-helper cells. This mechanism should be regarded as highly relevant not only for AML, but for malignant cells in general. Other classical MHC-II molecules, such as HLA-DQ, are also known to be related to HLA-DM sensitivity, and thus, further studies are required for an in-depth understanding of those phenomena.

The emerging relevance for studying the co-expression of MHC class-II machinery molecules and B7 ligands on AML blasts is directly related to the identification of strategies meant to improve leukaemia specific T-cell immunity in AML patients. There is already a vast literature pointing out that increased CLIP levels are associated with shortened disease-free survival, while its downregulation on AML blasts promotes the rate of allogeneic CD4+ T cell proliferation and CD4+ and CD8+ T cell priming (van Luijn et al., 2010b). On the other hand, lower CLIP levels direct the Th cell polarisation towards Th1 (increased IFN- γ and HLA-DR expression) and favour efficient outgrowth of effector memory CD4+ T cells (van Luijn et al., 2011). Our data indirectly support the above observation as our data show that HLA-DR low cases associate a high CLIP expression, pointing towards a potential less effective Th1 response in tumour cell removal. Furthermore, HLA-DR low cases had less BM CD4+ lateEM T cells and BM CD8+ iEM T cells as compared to the HLA-DR normal and HD cases, suggesting the deployment of a less efficient immune response in terms of effector memory differentiation.

Our study has also limitations, including the relatively small size of the AML group. Importantly, this group is exclusively made of newly diagnosed AML cases which reflect the AML heterogeneity and our observations complement our previous work (Antohe et al., 2020) and support the conclusions rising from the study of Williams et al (Williams et al., 2019) with similar number of cases. The relatively small size of the HLA-DR low ($n=7$) compared to the HLA-DR normal ($n=23$) subgroup of AML cases actually reflect the lower frequency of the first subgroup of only 23%, in accord with literature data (Feller et al., 2013). Since our study mainly aimed to investigate the potential interlink between the MHC class II machinery and B7 ligands, additional factors contributing to the leukaemia immune biology such as T helper subsets, NK cells, APC and suppressor cells were kept out from the present analysis.

Final remarks

Overall, these data show that AML patients, based on the HLA-DR expression levels on BM blasts, are categorised in two groups with distinct HLA-DM and Ii/CLIP phenotypes: i) the HLA-DR low cases, characterised by high intracellular HLA-DM, high CD74 and high surface CLIP expression and ii) the HLA-DR normal cases, characterised by high intracellular HLA-DM, normal or high CD74 and lower surface CLIP expression. Further, these two distinct groups also differ in terms of ELN risk profiles: the HLA-DR low group lacks favourable ELN risk cases, while the normal HLA-DR group has less adverse risk patients and comprises all the AML favourable cases. Interestingly, the normal HLA-DR cases had increased expression of co-inhibitory PD-L2 and B7-H3 molecules, which rather suggests an inhibition of T-cell responses, probably to compensate the increased presentation of DM-resistant peptides induced by upregulated HLA-DM. In contrast, the HLA-DR low group had significantly higher levels of expression of B7 ligands ICOS-L and B7.2 which would favour CD4+ T-cells responses. More precisely, B7.2 preferentially induces the differentiation of naïve T-helper (Th) cells towards Th2 while ICOS-L primarily sustains the humoral responses mediated by Th2 cells (Tamura et al., 2005). As Th1/CTL responses would be preferred for a better prognostic in AML, an amplified Th2 signature would divert the immune system away from a functional status. In other AML cases, a B7.2 and ICOS-L signature was shown to provoke an initial suboptimal CD4+ T-cell activation, proliferation and differentiation towards Th1 and/or Th17, marked by IFN γ , TNF α or IL-17 secretion (Dolen and Esendagli, 2013; Esendagli, 2013). In turn, the Th1 and Th17 effector cells downregulated the co-stimulatory B7.2 molecule and upregulated the co-inhibitory PD-L1 ligand on AML blasts, inducing immunosuppressive functions to AML cells by favouring a PD1-dependent Treg differentiation (Dolen and Esendagli, 2013; Esendagli, 2013). Indeed, one HLA-DR low case co-expressed high B7.2 and PD-L1 levels. However, despite the initially chosen differentiation pathway, either Th1/Th17

or Th2, the HLA-DR low AML blasts would mount an ineffective CD4+ T response. This observation might contribute in understanding the lack of association of HLA-DR low cases with favourable ELN risk.

Our findings of tumour (AML) cells with lower expression of HLA-DR to be associated with a poor prognostic, was recently confirmed by the group of Xu Junying also in the context of solid tumour: low HLA-DRA expression was associated with a poor prognosis in lung adenocarcinoma due to a less association with tumour-infiltrating immune cells (Mei et al., 2022). Next, based on the fact that autophagy is known to monitor the MHC class I and II (including HLA-DR) expressions (Munz, 2016a), the next step for my further research in collaboration with the Haematology Department would imply the use of chemical autophagy modulators (already available) in tissue cultures, and investigate, if any, the effect on antigen presentation by tumour cells on one hand, and the T cell responses on the other hand.

2.1.3. Immune checkpoint receptor expression and T cell maturation profile in AML

2.1.3.1. Introduction

The last decade has witnessed dramatic advances in the field of cancer immunotherapy. Immune checkpoint blockade (ICB) is reshaping the treatment paradigm of solid tumours (Kyi and Postow, 2016) and hematologic cancers, such as Hodgkin lymphoma (Dada, 2018). Furthermore, CD19-directed chimeric antigen receptor (CAR)-T cells and the bispecific T cell engager (BiTE[®]) blinatumomab have produced spectacular remissions in acute lymphoblastic leukemia and diffuse large B cell lymphoma (Maude et al., 2014; Roberts et al., 2018; Topp et al., 2014). Simultaneously, gene expression profiling (GEP) of tumour immune microenvironments is revolutionizing our understanding of cancer-immune interactions. Several recurrent pan-cancer immune profiles have been identified and could serve as biomarkers for predicting clinical responses to immunotherapy or for tailoring personalized treatment strategies (Chen and Mellman, 2017; Thorsson et al., 2018). Briefly, tumours with inflamed, type I and II interferon (IFN)-driven immune microenvironments (informally designated as “hot”) are ICB responsive, while “cold”, “immune-desert” tumours would rather benefit from adoptive cell transfer or tumour-peptide vaccination (Davidson-Moncada et al., 2018).

In the context of AML, recent research revealed that immune checkpoint profiles may hold prognostic and therapeutic relevance (Davidson-Moncada et al., 2018). Importantly, most of the previous research focused mainly on finding prognostic relevance of isolated B7 molecule expression in AML (Chen et al., 2008; Hu et al., 2015), and only very recently a comprehensive analysis of B7 checkpoint ligand co-expression correlated with checkpoint receptors and T cell populations was conducted (Williams et al., 2019).

2.1.3.2. Aim

The aim of this study was to simultaneously evaluate the B7 checkpoint ligand phenotype of AML blasts (B7.1, B7.2, PD-L1, PD-L2, ICOS-L, B7-H3, B7-H4) and the expression of immune checkpoint receptors (ICR) (ICOS, PD-1, CTLA-4) on helper and cytotoxic T cell maturation populations, and to correlate this data to standard prognostic factors.

2.1.3.3. Materials and methods

Patient selection

Based on informed consent, 30 patients diagnosed with *de novo*, non-promyelocytic AML between 2016 and 2019 at the Iași Regional Oncology Institute, Romania, were included in this study. This study has been approved by the institutional ethics committee. Bone marrow (BM) and peripheral blood (PB) samples were collected at diagnosis. AML diagnosis was established according to the WHO diagnostic criteria (Arber et al., 2016) and patients were risk-stratified in accordance with the 2017 European Leukemia Net (ELN) recommendations (Dohner et al., 2017). We have also analyzed the BM and PB samples of 4 healthy volunteers, after their informed consent.

Flow cytometry

AML blasts and T cells were analyzed by multiparameter flow-cytometry (MFC) on erythrocyte-lysed fresh BM and PB samples. This study comprised four phases: 1) Confirmation of AML diagnosis with EuroFlow standardized monoclonal antibody (MoAbs) panels (van Dongen et al., 2012); 2) Analysis of the expression of B7-1, B7-2, PD-L1, B7-H2, PD-L2, B7-H3, B7-H4 on AML blasts; 3) Analysis of regulatory T cells percentages and T cell maturation subsets in the BM; 4) Evaluation of Programmed Death-1 (PD-1), Inducible T cell Co-Stimulator (ICOS) and Cytotoxic T lymphocyte Antigen 4 (CTLA-4) expression on T cell maturation subsets. In line with previous research regarding B7 checkpoint ligand expression in AML but also solid cancers, B7 molecules were considered positive if present on more than 10% of the total AML cells (Hu et al., 2015; Thompson et al., 2005).

Data acquisition was performed on a BD FACS ARIA III cytometer and data was interpreted using the FACS DIVA v6.1.3 software. An identical investigation protocol was applied for all healthy subjects. AML blasts gating was performed on CD45+/CD34+/CD117+/HLA-DR+ events. Subsequently, the expression level of each B7 molecule was assessed. T cell gating was performed on CD3+/CD4+ and CD3+/CD8+ events. The following T cell maturation subsets were defined based on their differential expression of CD28, CD27 and CD45RA: naïve (N), central memory (CM), intermediate effector memory (iEM), late effector memory (late EM) (Mahnke et al., 2013; Xu et al., 2015). Treg cells were defined as CD3+/CD4+/CD25+/CD127- events (Yu et al., 2012). A T cell population was considered predominant if it outnumbered each of the other T cell subsets. Finally, the expression of ICOS, PD-1 and CTLA-4 was evaluated on BM total and maturation subsets of CD4+ and CD8+ cells. All the experiments were performed in compliance with the rules of standard biosecurity and institutional safety procedures.

Statistical analysis

Statistical analyses were performed using the IBM® SPSS Statistics 21.0 Software. Each figure contains the relevant statistical information: the *n*, total number of patients, the significance *p* value, and the statistical test used. The Chi square, Fischer's Exact Test, Mann Whitney test, and Student's t-test were used to analyze the associations between different variables. The Pearson correlation coefficient was calculated to investigate the relationships between numerical variables. The two-way ANOVA test was used to analyze the differences among multiple variables. A *p* value <0.05 was considered as statistically significant.

2.1.3.4. Results

Baseline patient characteristics

The median age at AML diagnosis was 59 years (range 27-83 years). 23.3% of patients had favorable ELN risk cytogenetics, 46.7% and 30% had intermediate and, respectively,

adverse karyotypes. Two patients harbored *FLT-3-ITD* mutations and three patients had *NPM1* mutated status. *FLT-3-ITD* and *NPM-1* mutations did not co-exist in our study group.

B7 checkpoint ligands are more frequently expressed in intermediate and adverse risk AML

Within the healthy donor (HD) group, we could evidence the isolated expression of two molecules, PD-L1 and B7.2, in two cases, while 18 patients (60%) were identified with B7 ligand expression. The B7 molecule levels differed markedly from those of HD (Fig. 51A): PDL1 (B7+ vs. B7-: $p=0.028$, B7- vs. HD: $p=0.739$), B7.2 (B7+ vs. B7-: $p=0.0003$, B7- vs. HD: $p=0.7111$) and ICOS-L (B7+ vs. B7-: $p=0.049$, B7- vs. HD: $p=0.011$). Out of the B7 positive cases, 10 expressed B7 molecule signatures and 8 had isolated B7 expression.

B7.2 was the most frequently expressed molecule (50% of cases, $n=15$), followed by PD-L1 (30%, $n=9$), PD-L2 (15%, $n=5$), ICOS-L (12%, $n=4$), B7-H3 (10%, $n=3$) and B7-H4 (10%, $n=3$). B7.1 was expressed at extremely low levels and was thus considered negative. B7.2 was equally expressed isolated or co-expressed, while all the other B7 ligands were mainly co-expressed on AML blasts as B7 signatures.

The majority of B7 positive patients (16 out of 18, 88.8%) had intermediate or adverse ELN risk AML-NOS (Not Otherwise Specified). Out of these, complex karyotype AML-NOS expressed either B7.2 isolated or co-expressed B7.2, ICOS-L and PD-L1, while normal karyotype AML-NOS also expressed PD-L2, B7-H3 and B7-H4 alongside B7.2, ICOS-L and PD-L1 (Fig. 51B). The two *FLT-3 ITD* mutated, normal karyotype AML-NOS cases displayed only an isolated B7.2 expression.

By contrast, favorable risk AML rarely expressed B7 molecules (2 out of 7 cases, 28.6%). Out of this group, *NPM1* mutated AML was the only B7 positive subtype and was correlated with B7-H3 expression ($p=0.02$) and significantly higher levels of B7-H3 when compared to the AML-NOS cases ($p=0.019$). AML with $t(8;21)(q22;q22)$ was B7 negative and expressed significantly lower percentages of B7.2 ($p=0.036$) when compared to the AML-NOS cases (Fig. 51B). Further details regarding the expression of each B7 checkpoint ligand relative to age, WHO AML type and ELN risk are provided in Table 1. We found no significant correlation between patient age, gender, hyperleukocytosis and the expression of B7 checkpoint ligands. However, B7 positivity was correlated with the presence of refractory AML ($p=0.017$, Chi Square Test) and worse overall survival ($p=0.004$, Log Rank test).

B7 positive leukemias rather express inhibitory B7 ligands

We have identified eight different B7 checkpoint ligand signatures in ten patients (Table 1): co-expression of B7.2, ICOS-L, PD-L1 (3 cases); B7.2, ICOS-L, PD-L1, B7-H4 (1 case); B7.2, PD-L1, PD-L2 (1 case); B7.2, PD-L1, B7-H3 (1 case); B7.2, PD-L2, B7-H3 (1 case); PD-L1; B7-H3 (1 case); B7.2, PD-L1, PD-L2, B7-H4+ (1 case); PD-L1, PD-L2, B7-H4+ (1 case). A mean number of three B7 ligands were co-expressed in these signatures. PD-L1 and B7.2 were regularly expressed in B7 ligand signatures (90% and 80%, respectively) and all signatures included at least one B7 molecule with clearly defined or most likely co-inhibitory role, such as B7.2 (41). Furthermore, we found statistically significant correlations between the expression levels of the following B7 ligand combinations: B7.2 - PD-L1 ($p=0.0002$), B7.2 - ICOS-L ($p=0.019$), PD-L1 - ICOS-L ($p=0.0009$), PD-L1 - B7-H4 ($p=0.0051$), PD-L2 - B7-H4 ($p < 0.0001$).

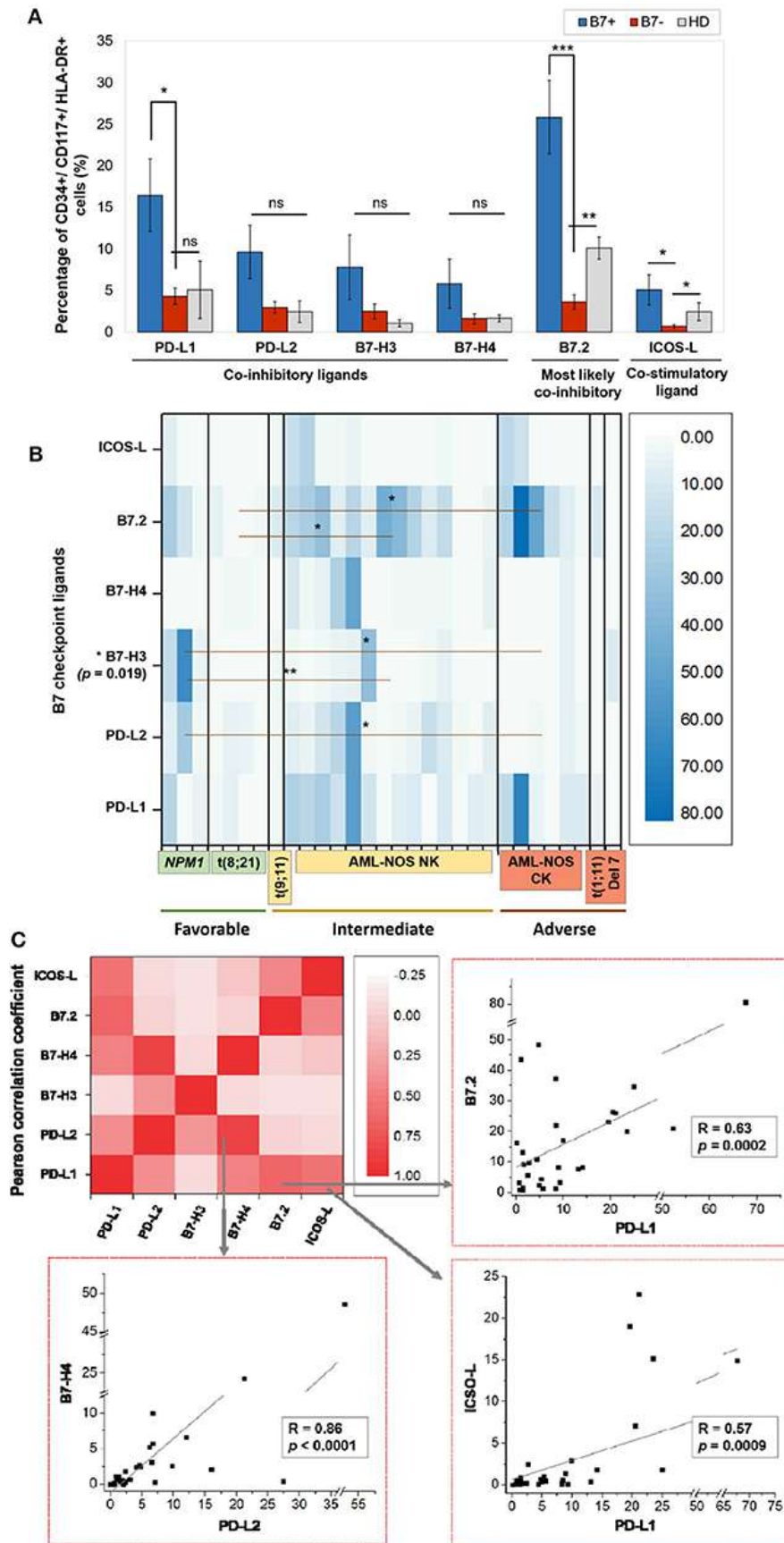


Figure 51. (A) Percentage of CD34+/CD117+/HLA-DR+ cells expressing the indicated B7 checkpoint ligands in patients, categorized as B7+ ($n=18$) or B7- ($n=12$) based on the B7 ligand expression and healthy donors (HD, $n=4$). Bars represent the mean \pm SEM (** $P < 0.01$, *** $P < 0.001$, * $P < 0.05$; ns, not significant;

two-tailed *t*-test, Mann–Whitney test). **(B)** Heat map of percentages of acute myeloid leukemia (AML) blasts expressing the indicated B7 checkpoint ligands in patients categorized based on their corresponding European Leukemia Net (ELN) risks: favorable, intermediate, and adverse (***P* < 0.01, **P* < 0.05; two-tailed *t*-test). **(C)** Heat map of B7 ligand co-expression. Pearson correlation coefficients (*R*) were computed, and ANOVA test was used to validate the significance of the identified correlations.

Table 1. Patterns of expression of B7 ligands, ICRs, T cell populations relative to WHO AML type and ELN risk.

WHO AML Type	Baseline AML characteristics				B7 Checkpoint ligands % of expression on AML blasts							CD4+ T cell subset predominance			CD4+ ICR % of expression		CD8+ T cell subset predominance			CD8+ ICR % of expression	
	Age	AML	Karyotype	ELN Risk	B7.1	B7.2	ICOSL	PD-L1	PD-L2	B7-H3	B7-H4	N	CM	Late EM	ICOS	PD-1	N	CM	Late EM	ICOS	PD-1
AML with recurrent genetic anomalies	83	<i>NPM1</i>	NK	Fav		13.2			27.4	62.4					50.1	29.9				1.9	16.7
	70	<i>NPM1</i>	NK	Fav		26.3		20.5		18.7					68.3	43.4				13.0	37.3
	34	<i>NPM1</i>	CK	Fav											62.3	13.2				40.2	35.8
	60	t(8,21)	t(8,21)	Fav											28.0	13.6				9.0	25.2
	66	t(8,21)	t(8,21)	Fav											43.4	11.6				22.1	37.4
	48	t(8,21)	t(8,21)	Fav											34.1	19.5				5.6	33.3
	44	t(8,21)	t(8,21)	Fav											32.8	12.2				16.4	25.5
27	t(9,11)	t(9,11)	Int											25.8	5.3				8.5	12.7	
AML NOS	51	NOS 5	NK	Int		20	16.9	23.5			10				69.6	21.3				11.2	24.6
	43	NOS 5	NK	Int		34.7		25	12						61.6	17.0				21.5	31.2
	38	NOS 5	NK, FLT3	Int		22									63.6	15.4				40.7	27.3
	66	NOS 5	NK	Int		43.6									54.1	23.6				32.0	45.3
	74	NOS 5	NK	Int		17									43.4	27.0				8.6	14.5
	71	NOS 4	NK	Int		20.9		52.3	52.9		48.6				91.7	11.6				58.0	6.7
	66	NOS 4	NK	Int		26.1	22.9	21.1							75.8	27.1				42.3	28.3
	41	NOS 4	NK	Int		37.2									31.4	12.6				10.9	21.4
	42	NOS 4	NK	Int											54.9	19.1				17.3	22.9
	48	NOS 1	NK	Int				14.1	21.2		24.3				69.1	37.3				42.1	35.1
	67	NOS 1	NK	Int					16						84.3	9.6				8.6	8.7
	56	NOS 1	NK	Int											83.9	12.3				71.7	35.6
	59	NOS 0	NK	Int				13.1		34.4					79.1	40.5				49.6	58.0
	71	NOS 0	NK	Int											59.3	24.0				18.1	37.4
	64	NOS 5	t(1,11)	Adv		10.9									57.0	14.1				27.6	29.9
	45	NOS 4	CK	Adv											43.6	9.4				13.7	7.0
	53	NOS 4	CK	Adv		80.5	14.9	67.6							57.1	29.9				27.1	42.2
	51	NOS 4	CK, FLT3	Adv		48.4									45.1	17.0				9.6	22.1
	69	NOS 2	CK	Adv		23.1	19	19.6							80.8	11.9				40.0	43.1
65	NOS 1	CK	Adv											65.3	22.0				29.0	16.0	
59	NOS 1	CK	Adv		16.3									52.4							
67	NOS7	Del 7	Adv											50.4	29.9				12.3	45.8	
HD1								13.9						29.9	16.5				21.3	26.7	
HD2					13.1									71.5	21.3				27.3	34.3	
HD3														64.0	2.1				16.2	24.1	
HD4														64.8	21.4				20.6	23.9	

Expression of B7 checkpoint ligand with co-stimulatory function.

Expression of B7 checkpoint ligand with co-inhibitory function.

No expression of B7 checkpoint ligand or absence of the predominance of a certain T cell population.

Predominance of a T cell subpopulation.

ICR (PD-1 or ICOS) expression >10% with the ICOS percentage surpassing PD-1 or vice versa.

ICR (PD-1 or ICOS) expression >10% without the ICOS percentage surpassing PD-1 or vice versa.

ICR expression <10%.

Adv, adverse; *AML*, acute myeloid leukemia; *CK*, complex karyotype; *ELN*, European Leukemia Net; *Fav*, favorable; *FLT3*, *FLT3-ITD* mutated; *HD*, healthy donor; *ICOS*, inducible T cell costimulator; *ICR*, immune checkpoint receptor; *Int*, intermediate; *NK*, normal karyotype; *NPM1*, *NPM1* mutated; *PD-1*, programmed death 1.

B7.2 expression was rather associated with ICOS-L and PD-L1 in the B7.2/PD-L1/ICOS-L (3 cases) and B7.2/PD-L1/ICOS-L/B7-H4 signatures (1 case). Moreover, PD-L2 was correlated to B7-H4 expression (*p* < 0.0001). However, B7.2 expression was not correlated to PD-L2, B7-H3 and B7-H4. Finally, B7-H3 and B7-H4 expression was mutually exclusive (*p*=0.027) (Fig. 51C).

Helper and cytotoxic T cells from AML patients display different maturation and ICR expression patterns

On an overall analysis, CD4+ T cells displayed predominantly a CM phenotype (80% of cases) and were rarely polarized as naïve or effector cells. CD8+ cells displayed significantly higher late EM frequencies (*p* < 0.0001) and lower naïve (*p* < 0.0001) and CM (*p* < 0.0001) cells than CD4+ cells (Fig. 52A).

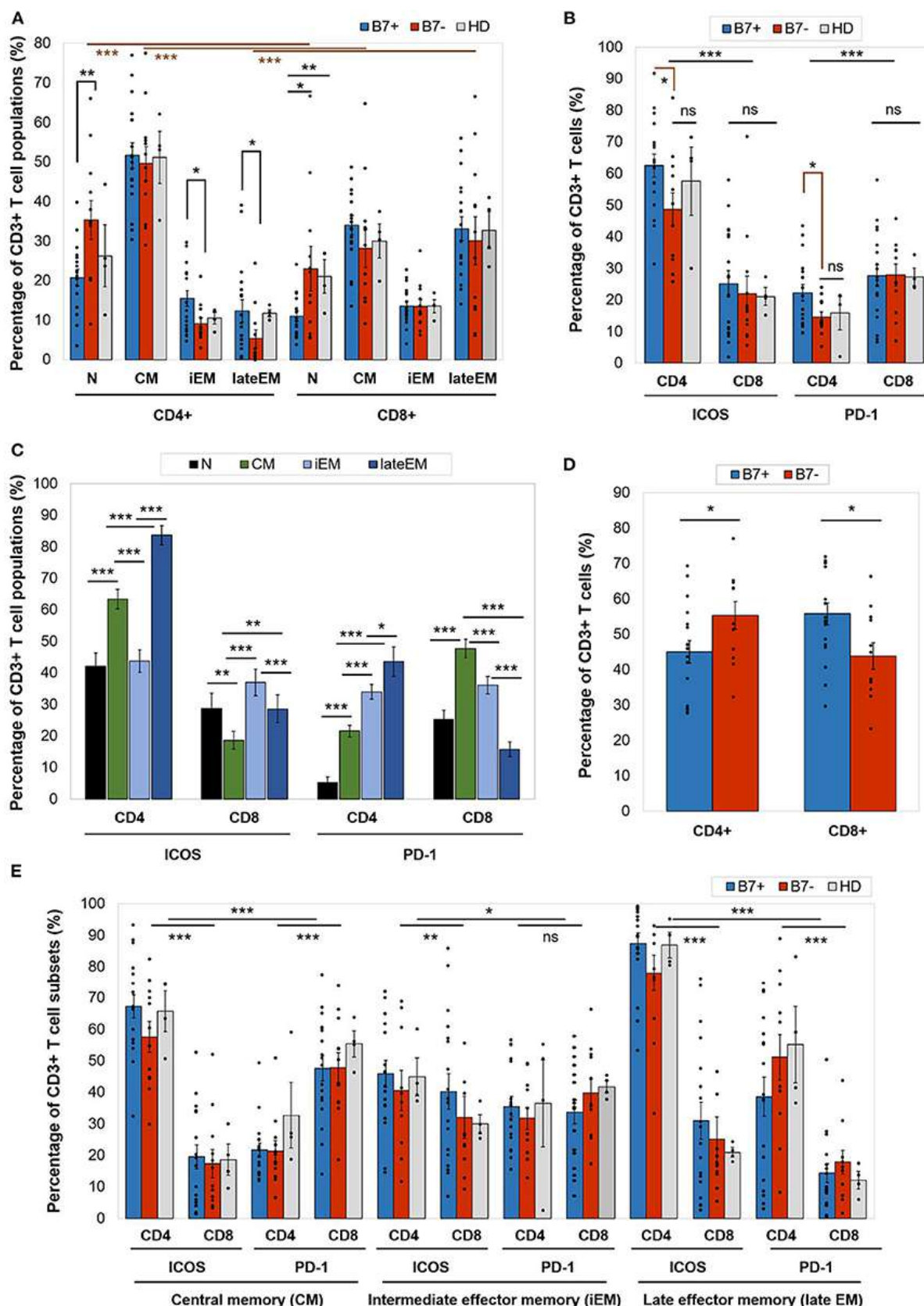


Figure 52. (A) Percentage of CD4+ or CD8+ T cell populations—naive (N), central memory (CM), intermediate effector memory (iEM), and late effector memory (late EM)—in AML patients (either B7+, $n=18$, or B7-, $n=12$) and healthy donors (HD, $n=4$). Individual values are represented as points. (B) Expression of immune checkpoint receptors [inducible T cell costimulator (ICOS) and programmed death 1 (PD-1)] on CD4+ or CD8+ T cells in AML patients (either B7+, $n=18$, or B7-, $n=12$) and

healthy donors (HD, $n=4$). Individual values are represented as points. (C) Expression of immune checkpoint receptors (ICOS and PD-1) on CD4+ or CD8+ T cells populations—N, CM, iEM, and late EM—in AML patients (D) Percentage of CD4+ or CD8+ T cells in AML patients (either B7+, $n=18$, or B7-, $n=12$). Individual values are represented as points. (E) Expression of immune checkpoint receptors (ICOS and PD-1) on CD4+ or CD8+ T cells populations—CM, iEM, and late EM—in AML patients (either B7+, $n=18$, or B7-, $n=12$) and healthy donors (HD, $n=4$). Individual values are represented as points. Bars represent the mean \pm SEM (*** $P < 0.001$, ** $P < 0.01$, * $P < 0.05$; ns, not significant; two-way ANOVA).

When comparing the CD4+ and CD8+ T cells, CD4+ T cells had significantly higher ICOS expression ($p < 0.0001$), while CD8+ expressed higher PD-1 levels ($p=0.0001$) (Fig. 52B). CTLA-4 was identified at levels below 1% on all T cell populations. Furthermore, ICOS and PD-1 expression varied across T cell maturation subsets. ICOS had the highest levels of expression on late EM CD4+ (lateEM vs. iEM: $p < 0.0001$, lateEM vs. CM: $p < 0.0001$) and iEM CD8+ (iEM vs. lateEM: $p < 0.0001$, iEM vs. CM: $p < 0.0001$) T cells (Fig. 52C).

On CD4+ cells, PD-1 expression progressively increased from the naïve towards late EM cells (N vs. CM: $p < 0.0001$, CM vs. iEM: $p < 0.0001$, iEM vs. lateEM: $p=0.027$). By contrast, on CD8+ cells the CM and iEM subpopulations expressed the highest PD-1 levels and late EM cells displayed the lowest levels (lateEM vs. CM or iEM: $p < 0.0001$) (Fig. 52C). Additionally, our analysis showed that all the PB T cell populations mirrored the BM T cell subpopulations, in both AML patients and healthy individuals.

The B7 phenotype of AML blasts is mirrored by distinct modifications in T cell maturation and ICR expression

When compared to the B7 negatives, B7 positive patients displayed significantly higher percentages of CD8+ T cells ($p=0.019$) and lower CD4+ T cells ($p=0.043$) (Fig. 52D). Although the majority of the BM CD4+ T cells were CM cells irrespectively of the B7 phenotype, two differences were noted in B7 positive cases: 1) lower percentages of naïve T cells ($p=0.008$); 2) higher percentages of iEM ($p=0.016$) and late EM ($p=0.022$) T cells. Similarly, naïve CD8+ T cells were poorly represented in B7 positive AMLs (Fig. 52A). Furthermore, B7+ patients expressed higher ICOS (CM: $p < 0.0001$, iEM: $p=0.009$, lateEM: $p < 0.0001$) and PD-1 (CM: $p < 0.0001$, iEM: $p=0.11$, lateEM: $p < 0.0001$) levels on the effector CD4+, but not CD8+ cells (Fig. 52E).

2.1.3.5. Discussions

Similarly to solid cancers (Chen and Mellman, 2017; Thorsson et al., 2018), immune profiles in AML have been broadly described as T cell “inflamed”, in which immune cells overexpress multiple B7 ligands and ICRs, and “non-inflamed”, lacking evidence of adaptive resistance-driven immune dysfunction (Davidson-Moncada et al., 2018). Briefly, an “inflamed” immune profile is characterized by efficient presentation of leukemia antigens, dendritic cell activation, IFN γ production and the priming of leukemia-specific T cells. However, the anti-leukemia immune response is gradually inhibited by immune escape axes such as PD1-PD-L1 which exhaust T cells, in parallel with tumour outgrowth. By contrast, in an “immune-desert” profile, T cell priming is reduced or absent and tolerance to leukemia is instated (Chen and Mellman, 2017). The “inflamed/”non-inflamed” AML dichotomy might explain why patients with identical AML entities and risk profiles may have different outcomes that deviate from the initial ELN prognostic prediction (Gerstung et al., 2017). Recent research has demonstrated that an “inflamed” AML immune profile can predict the resistance to cytotoxic therapy, but also the patient’s responsiveness to immunotherapies such as ICBs or

DARTs (Davidson-Moncada et al., 2018). However, future research is necessary to investigate how B7 immune profiling can complement the predictive ability of the ELN risk classification and guide immunotherapy.

In our study we have identified two groups of patients based on the B7 phenotype, that display T cell maturation profiles and ICR expression patterns that can be successfully reconciled with literature data regarding the immune pathogenesis of “inflamed” and “non-inflamed” cancer immune profiles.

The B7 positive group was predominant (60%) and was mostly characterized by the presence of molecules with known or most probably inhibitory role in cancer and AML in particular (B7.2, PD-L1, PD-L2, B7-H3, B7-H4) (28,44). B7.2 and PD-L1 were the most frequently expressed checkpoint ligands, in line with previous research (Maeda et al., 1998; Whiteway et al., 2003). B7.1 was constantly negative. B7.2, PD-L1, PD-L2 or ICOS-L were constantly expressed across B7 signatures in several combinations that showed statistical relevance (Fig. 51C), suggesting that they represent key players of AML immune evasion axes. However, statistical analysis further revealed several patterns of co-expression of the other B7 ligands that likely indicate slightly different immune evasion strategies across the various B7 positive AMLs. Thus, PD-L1 expression was correlated with B7.2 and ICOS-L positivity, but not with PD-L2, B7-H3 or B7-H4.

The B7 negative patient group was smaller (40%) and encompassed most of the AML cases with recurrent genetic anomalies, most notably with t(8;21)(q22;q22) and t(9;11)(p21;q23). The expression of B7 ligands on AML blasts has been further mirrored by polarization differences in T cell populations and ICR expression. When the B7+ and the B7- cases were analyzed separately, it turned out that the B7+ patient cases had significantly higher cytotoxic and lower T helper cell percentages, while this ratio was reversed within the B7- group. When analyzing the maturation subsets, we were able to show that most of the CD4+ T cells fall in the CM category, unlike the CD8+ T cells where the effector subsets outnumber the central memory ones. Furthermore, B7+ patients had a significantly lower number of naïve CD4+ and CD8+ T cells than the B7- patients (Fig. 2A). The similarity of the CM CD4+ and CD8+ T cells in the B7+, B7- and healthy donor groups is most probably explained by the high number of lymphocytes that do not target leukemic cells.

On an overall analysis of our AML patients, setting aside the maturation polarization, the ICOS expression was predominant on CD4+ T cells, while PD-1 was higher on CD8+ cells. When compared to B7 negatives, B7 positive patients expressed higher levels of both ICOS and PD-1 on CD4+ T cells, unlike the CD8+ cells that expressed similar levels of ICOS and PD-1 regardless of the B7 positivity or negativity. Despite the significant predominance of CD8+ T cells in B7+ AML patients, it so seems that B7 check point ligands are rather impacting the immunoediting of CD4+ BM T cells. Analyzing further the ICOS and PD-1 expression on maturation subsets, we have noted a progressive increase in PD-1 expression from the naïve towards the CD4+ effector compartment, while ICOS expression was highest on lateEM cells. By contrast, PD-1 expression on CD8+ cells was highest on CM, but not effector cells that displayed higher ICOS levels. Since CD4+ T cells promote the CD8+ T cell antitumour activity and prevent their exhaustion (Ostroumov et al., 2018), we can hypothesize that CD4 T cell PD-1 mediated exhaustion precedes CD8+ cell exhaustion in B7+ AML and, more than that, is a prerequisite for CD8+ cell exhaustion.

Finally, we have aimed to harmonize our data with the models of AML immune pathogenesis with “inflamed” and “non-inflamed” microenvironments (reviewed in (Davidson-Moncada et al., 2018)). Thus, in our study, it was the intermediate and adverse risk AML cases, which were frequently B7 positive (78.2%), as well as *NPM1* mutated AML, that displayed features holding indirect evidence of an “inflammatory” microenvironment, including the expression of mainly inhibitory B7 ligands, correlated with higher percentages

of CD4 effector cells, less CD4+ and CD8+ naïve T cells, as well as higher ICOS and PD-1 expression. *NPM1* mutated AML also presented effector differentiation of CD8+ PD-1+ T cells, which is likely a feature of immune exhaustion.

Our study has obvious limitations, including the deliberate simplification of the leukaemia immune biology, which depends on many other factors, such as functional Th polarization (Th1, Th2, Th17), NK cells, macrophages or myeloid derived suppressor cells, and a relatively small patient group made of exclusively newly diagnosed AML cases (however reflecting the heterogeneous AML patient population and confirming several conclusions emerging from the study of Williams et al. (Williams et al., 2019).

Final remarks

All in all, our results reinforce the concept that this genetically heterogeneous disease has distinct and versatile patterns of anti-tumour immune response that depend on factors beyond the intrinsic genetic traits of the tumour cells. This finding is particularly relevant since new AML drugs are being rapidly developed and immune profiles emerge as a powerful biomarker in guiding and personalizing the new immunotherapy approaches.

This study had an important *international scientific impact*, as recent studies have confirmed the importance of our findings (e.g. increased B7-H3 expression in AML cases with poor clinical outcome) and created novel monoclonal antibodies that targeted those immune checkpoint proteins that were able to successfully induce the antibody-dependent cell-mediated cytotoxicity (ADCC) mediated by NK cells using AML patient-derived xenografts (Tyagi et al., 2022).

2.1.4. NK cell maturation profile in MDS and AML

2.1.4.1. Introduction

Natural killer (NK) cells are particular and important components of the immune system, with a major role in the clearance of damaged, virally infected, and tumour cells (Deng et al., 2019; Di Vito et al., 2019). They achieve this goal with the help of a highly diverse repertoire of germline-encoded activating and inhibitory receptors that allow NKs to recognize and target cells that lack or downregulate the expression of major histocompatibility complex (MHC) class I molecules (Geiger and Sun, 2016). The major inhibitory receptors maintain NK cells in an unengaged state and are comprised of the killer immunoglobulin-like receptor (KIR) family and the CD94-NKG2A heterodimer, whereas the main activating receptors belong to the natural cytotoxicity receptor (NCR) family (NKp46, NKp30, and NKp44), alongside the NKG2D variant (Babor et al., 2013; Long et al., 2013; Martner et al., 2016). Several NK cells functional developmental stages have been described. The CD56^{bright} CD94^{hi} CD16^{-/+} NKG2A⁺ KIR⁻ subtype is primarily involved in the secretion of cytokines and soluble amplifying factors (tumour necrosis factor α , TNF α ; interferon γ , IFN γ) with pleiotropic effects, such as a high proliferative capacity, the recruitment of macrophages, the promotion of inflammation, the activation of dendritic cells, and lymphocyte priming (Carson et al., 1997; Huntington et al., 2007). The more mature CD56^{dim} CD94^{med/low} CD16⁺ NKG2A^{+/-} KIR⁺ NKs are the most numerous NK type found in peripheral blood and bone marrow and exhibit mostly cytotoxic properties, acting to clear infected, damaged, or tumour cells via the release of lytic granules and antibody-dependent cellular cytotoxicity (ADCC) (Castriconi et al., 2018; Freud et al., 2006). The expression of CD57, a marker of highly differentiated NK cells, has been correlated

with a higher cytotoxic potential and long lasting memory, a feature shared with cells that participate in adaptive immunity (Bjorkstrom et al., 2010; Lopez-Verges et al., 2010). Previously reported data show that NK cells play a paramount role in the control of the onset and progression of hematological tumours (Stabile et al., 2017).

2.1.4.2. Aim

The focus of this study was to evaluate the potential qualitative and quantitative modifications of the three major mature NK subpopulations and the expression patterns of the CD159a (NKG2A), CD158a (KIR2DL1), CD158b (KIR2DL2/DL3), and CD158e1 (KIR3DL1) inhibitory receptors under pathological conditions. Unlike most studies that have focused on evaluating circulating NK cells, we have exclusively examined bone marrow aspirates, which allowed us to better understand the immunological mechanisms that might influence the NK ontogeny.

2.1.4.3. Materials and methods

Patients and controls

Bone marrow (BM) samples were collected at the Lucien Neuwirth Institute of Cancerology (Saint-Priest-en-Jarez, France) between March 2020 and July 2020 from patients newly diagnosed with MDS (n=25) and AML (n=8), prior to starting therapy. Normal bone marrow samples (NBM; n=30) were obtained from patients investigated for various cytopenias such as isolated anemia [nontropical sprue (n=2), B-12/ folic acid deficiency anemia (n=7), anemias secondary to mechanical destruction (n=5)], isolated thrombocytopenia (drug-induced thrombocytopenia (n=9), non-hematopoietic autoimmune-mediated thrombocytopenia (n=7)], without morphological dysplastic changes in hematopoietic cells and without excess of blasts on cytological examination of bone marrow aspirates. Written informed consent was obtained from each patient and NBM control, as approved by the institutional procedures of the independent ethics committee and the Comité de Protection des Personnes - Ile de France (NCT03233074/17.07.2017). The NBM group comprised patients aged from 10 to 90 years old (median: 64 years), while the MDS and AML cases ranged from 53 to 88 (median: 74) and from 16 to 84 years (median: 79), respectively. Thus, the NBM group considered in the study included suitable controls for both MDS and AML.

The 2016 World Health Organization (WHO) criteria was used to establish the diagnosis of AML and the classification of our MDS patients (Arber et al., 2016). MDS with excess blasts (MDS-EB) type 1 (defined by 5-9% blasts in the BM and MDS-EB type 2 (defined by 10-19% in the BM) were pooled together for statistical purposes.

Flow cytometry sample preparation

Bone marrow aspirates were collected on K2-EDTA anticoagulant, and 800,000 cells, distributed in 4 tubes, were stained with the following backbone markers: mouse anti-human fluorescein isothiocyanate (FITC)-conjugated CD57 (clone HNK-1); mouse anti-human peridinin chlorophyll protein-cyanine5.5 (PerCPCy5.5)-conjugated CD3 (clone SK7); mouse anti-human allophycocyanin (APC)-conjugated CD16 (clone 3G8); mouse anti-human phycoerythrin cyanine7 (PECy7)-conjugated CD56 (clone B159); mouse anti-human PE-conjugated CD94 (clone HP-3D9), mouse anti-human APC-H7-conjugated, CD19 (clone SJ25C1), and mouse anti-human V500-conjugated CD45 (clone HI30). Thereafter, the cells were separated into 4 tubes and further stained with one of the following markers: mouse anti-human brilliant violet 421 (BV421)-conjugated CD158a (clone HP-3E4), mouse anti-human BV421-conjugated CD158b (clone DX27), mouse anti-human BV421-conjugated CD158e1 (clone DX9), and mouse anti-human BV421-conjugated CD159a (clone 131411). The

antibodies were supplied by BD Biosciences, and the optimal concentrations were set after successive titrations. Following staining, the samples were incubated for 15 minutes in the dark at room temperature (RT) and then the red blood cells were lysed with 2 ml 1× fluorescence-associated cell sorting (FACS) lysis solution (BD Biosciences, San Jose, CA, USA), followed by another 10 minutes of incubation at RT in the dark. After two successive washing steps with 2 ml phosphate-buffered saline (PBS), containing 0.2% bovine serum albumin (BSA), 0.009% sodium azide (AZ), and 0.07% ethylenediaminetetraacetic acid (EDTA) followed by centrifugation for 5 min at $400 \times g$, the samples were ready for acquisition on a FACSCanto II cytometer (BD Biosciences, San Jose, CA, USA) using BD FACSDiva v1.6 software. Details regarding sample preparation and the staining procedures were previously described (Aanei et al., 2018).

Multicolor flow cytometry (MFC) data analysis

Data were interpreted with the Infinicyt, v2.0 software. All samples were analyzed for the proportion of NK cells relative to the total number of lymphocytes and for the NK subsets relative to the total number of NK cells. The reliability of our data is confirmed by the fact that no statistical significant differences between cell counts (NK cells, T cells or total lymphocytes) were identified among the three analyzed groups of patients NBM, MDS and AML. The BM aspirates have been checked for the proportions of bright CD16 neutrophils according to previously reported data (Loken et al., 2009). Samples having $> 24\%$ bright CD16 neutrophils have been excluded from the study to avoid including samples with significant hemodilution.

After the exclusion of doublets and debris, lymphocytes were gated using the side scatter (SSC) vs CD45 dot-plots. NK cells were gated according to CD56 expression and the absence of CD3 and CD19, NK cells being defined as CD3⁻ CD19⁻ CD56⁺. We then selected NK subpopulations based on the expression patterns combination of CD94, CD16, and CD57 markers: CD56^{bright} CD94^{hi} CD16⁻ CD57⁻ cells were classified as the immature subgroup; CD56^{dim} CD94^{med} CD16⁺ CD57⁻ cells were classified as the mature subgroup; and CD56^{dim} CD94^{low} CD16⁺ CD57⁺ were classified as the hypermature subgroup (Fig. 53). The expression patterns of the investigated NK receptors (CD158a, CD158b, CD158e1, CD159a) were evaluated for each NK cell subpopulation and for each group of cases (NBM, MDS, and AML).

Statistical analysis

Statistical analysis was performed using Graph Pad Prism 5TM (Graph Pad Software, San Diego, CA, USA) and SPSS, v20TM (IBM SPSS Software, Chicago, IL, USA). Figures were created with Graph Pad Prism 5TM. Tables, bar graphs and scatter dot plots show means with standard errors (SEM). Box-and whisker plots include the median and interquartile range without outliers. The means of normally distributed variables were statistically analyzed using the unpaired t-test and one-way ANOVA with *Post-hoc* Tukey's Multiple Comparison test. The non-Gaussian distributed data were analyzed for median differences using non-parametric tests: Mann-Whitney test (the non-parametric counterpart to the two-sample t-test), and Kruskal-Wallis with Dunn's Multiple Comparison test (the non-parametric counterpart to one-way ANOVA). Paired t-test and Wilcoxon signed rank test were applied for investigating the significant differences in matched parameters. One-sample t-test and Wilcoxon signed rank test (with the hypothetical value of 1.00) were used for analyzing the individual ratios of various NK cell populations. Pearson's and Spearman's correlation coefficients were used to assess positive associations between measured variables. The P-value < 0.05 was considered significant, and $R > 0.5$ was considered a strong correlation factor.

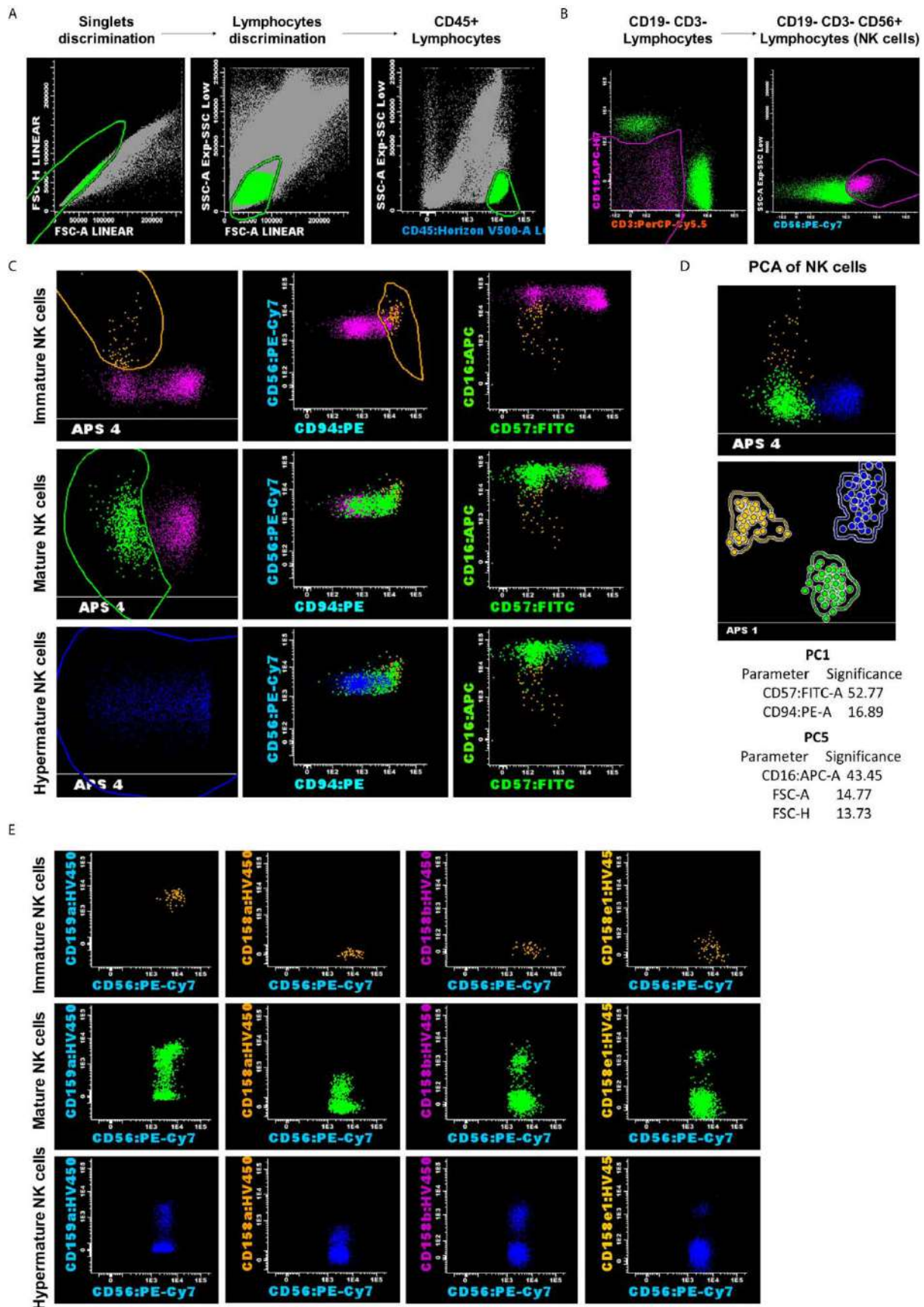


Figure 53. Representative example for NK analysis strategy and classification into three subsets: CD56^{bright} CD94^{hi} CD16⁻ CD57⁻ as the immature subset (yellow dots); CD56^{dim} CD94^{med} CD16⁺ CD57⁻ as the mature subset (green dots); and CD56^{dim} CD94^{low} CD16⁺ CD57⁺ as the hypermature subset (blue dots). (A) Lymphocytes gating on the

side scatter (SSC) vs CD45 dot-plots. **(B)** NK cells were gated according to CD56 expression and the absence of CD3 and CD19. **(C, D)** Reliable separations of NK cells into subsets were obtained using the Principal Component Analysis (PCA) for all analyzed cases, regardless of the group.

2.1.4.4. Results

Multicolor flow cytometry data gating based on principal component analysis provides the reliable separation of NK cell subsets

APS uses the PCA method as a compression instrument to condense relevant biological cell marker information into fewer (mostly two) dimensions (Folcarelli et al., 2018). The APS facilitated the classification of NK events across these three subpopulations of NK cells, particularly those belonging to the CD56^{bright} CD94^{hi} CD16⁻ CD57⁻ subset, which is the least well represented out of the three, and could easily be under- or overestimated by a biased manual analysis (Fig.53).

Similar bone marrow NK cell percentages in NBM, MDS and AML conditions

The first goal was to ascertain variations in total NK cells and NK subpopulations across the different groups of cases. The mean \pm standard error (SE) for the percentages of NK cells was 10.43% \pm 1.34% for NBM, 13.05% \pm 2.26% for MDS, and 14.23% \pm 5.99% for AML samples. Although no significant differences were observed in the NK percentages among our 3 investigated case groups, one particular FLT3-ITD mutated AML case presented the highest proportion of NK cells out of all examined populations (55% NK cells). Within the MDS group, we identified 3 patients with >30% NK cells, whereas only one healthy control presented such a high percentage of NK cells.

NK cell counts correlate with T cell counts in NBM and MDS, but not in AML

We further explored the potential correlation between the total NK cell counts and T or B lymphocyte counts in all three investigated conditions. A strong correlation emerged between NK and T cell counts in NBM ($P=0.0002$) vs a moderate correlation in MDS ($P=0.0201$), but no correlation could be noticed in AML ($P=0.9969$) (Fig. 54A-C). As for the correlation between NK and B cell counts, a strong one was revealed in NBM ($P=0.0009$) but no correlations resulted in MDS ($P=0.4397$) and AML ($P=0.5561$) (Fig. 54D-F). We also evaluated whether leukemic blasts exerted a direct or indirect influence on NK differentiation in a pathologically modified bone marrow environment. Our data revealed that no correlation could be established between the percentages of bone marrow blasts and the percentages of NK cells in MDS ($R=-0.37$, $P=0.06$) and AML samples ($R=-0.28$, $P=0.49$).

Changes in bone marrow NK subset dynamics, from the normal setting towards the MDS and AML pathological conditions

We further determined the distribution of different NK cell maturation subsets among the total NK population for each group. A significantly increased percentage of the immature CD56^{bright} CD94^{hi} CD16⁻ CD57⁻ NK cells was observed in AML samples compared with NBM samples ($P=0.0447$, Fig. 55A). A similar increasing trend was also visible in MDS cases ($P=0.0780$, Fig. 55A). Although decreased percentages of the mature CD56^{dim} CD94^{med} CD16⁺ CD57⁻ NK subpopulation were observed in the AML and MDS settings, only the MDS group was significantly different from the NBM control group ($P=0.0332$, Fig. 55B). No significant difference could be identified between the three groups when analyzing the hypermature CD56^{dim} CD94^{low} CD16⁺ CD57⁺ NK subpopulation (Fig. 55C).

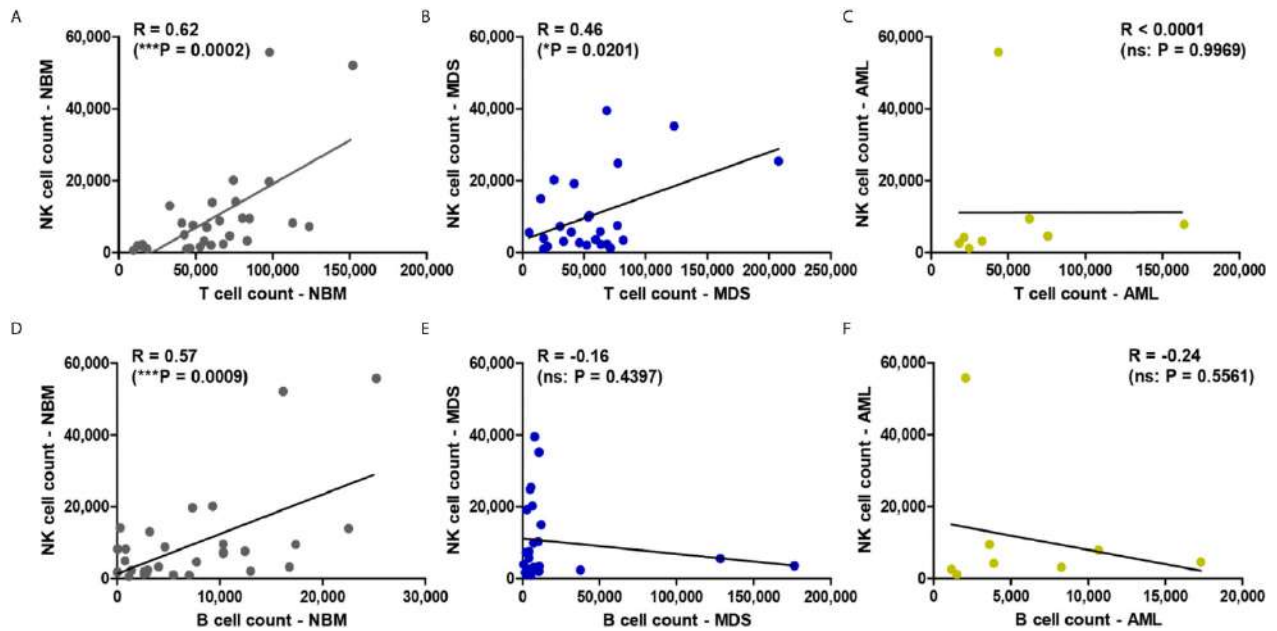


Figure 54. Regression statistics describing the relationship between bone marrow NK, T, and B cell counts for the three case groups: NBM, MDS, and AML. Correlation coefficients (R) were computed for (A) NK and T cell counts in NBM cases (n = 30). (B) NK and T cell counts in MDS (n = 25). (C) NK and T cell counts in AML (n = 8). (D) NK and B cell counts in NBM cases (n = 30). (E) NK and B cell counts in MDS (n = 25). (F) NK and B cell counts in AML (n = 8). Data are presented as scatter plots. Spearman test was used to analyze the significance of the identified correlations ($***P < 0.001$, $*P < 0.05$, ns, not significant).

Figure 55 reveals several significant differences that emerged when comparing the distributions of the NK subpopulations within the three groups. Furthermore, distinct patterns of maturation seem to characterize these subpopulations in the MDS and AML settings compared with those in the NBM. Statistical data showed that the NBM environment accommodated almost 7-fold more hypermature ($P < 0.0001$) and 10-fold more mature ($P < 0.0001$) than immature NK cells (Fig. 56A). Conversely, in MDS and AML samples, the percentages of the immature NK cells gradually increased at the expense of mature NK cells (Fig. 56B,C). Moreover, a marked heterogeneity in the ratios between hypermature and immature NK cell percentages was observed among AML cases, likely due to 3 outliers associated with the recurrent genetic mutations FLT3-ITD, IDH2, and NPM1, relative to the values for AML not otherwise specified (NOS). The AML case with the most prevalent mature NK population (69.12%) and the lowest immature NK population (1.53%) was NPM1-positive.

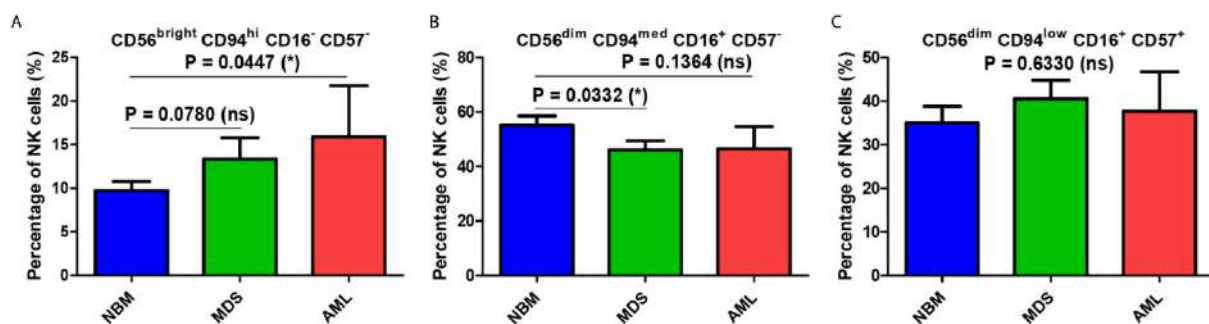


Figure 55. Comparison of cell percentages of distinct NK maturation subsets within the bone marrow microenvironment of NBM, MDS, and AML cases. (A) Percentage of bone marrow $CD56^{bright} CD94^{hi} CD16^{-} CD57^{-}$ immature NK cells in normal bone marrow (NBM, n = 30), myelodysplastic syndromes (MDS, n = 25), and acute myeloid leukemias (AML, n = 8) cases. (B)

Percentage of bone marrow CD56^{dim} CD9^{4med} CD16⁺ CD57⁻ mature NK cells in NBM (n = 30), MDS (n = 24), and AML (n = 8) cases. (C) Percentage of bone marrow CD56^{dim} CD9^{4low} CD16⁺ CD57⁺ hypermature NK cells in NBM (n = 30), MDS (n = 25), and AML (n = 8) cases. Bars represent the mean \pm SEM (ns, not significant; one-way ANOVA followed by Tukey's Multiple Comparison test).

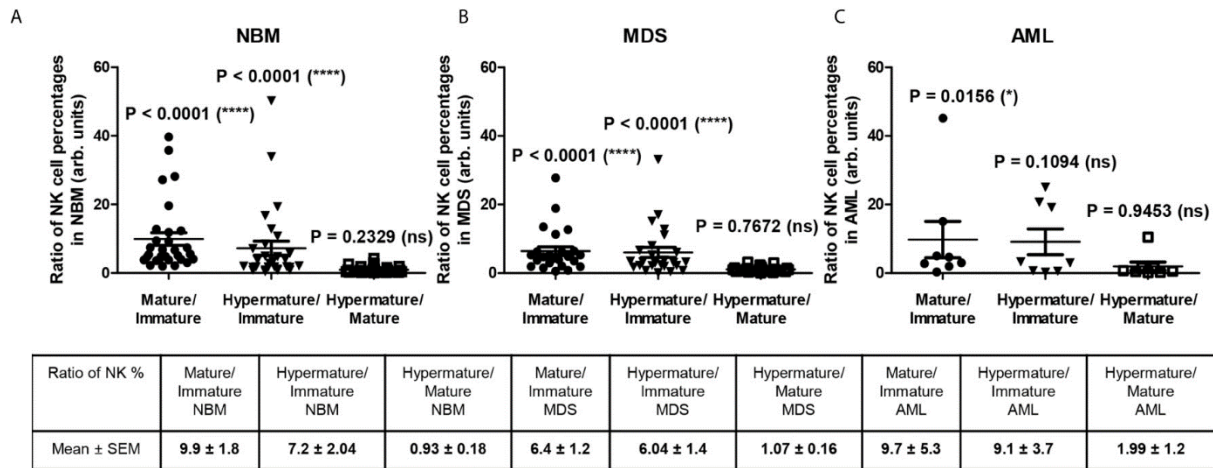


Figure 56. Ratio of cell percentages in distinct NK maturation subsets within the bone marrow microenvironment of NBM, MDS, and AML cases. (A) Ratio of cell percentages for the indicated NK maturation subsets (mature to immature, hypermature to immature, and hypermature to mature) in normal bone marrow (NBM, n = 30) cases. (B) Ratio of cell percentages for the indicated NK maturation subsets (mature to immature, hypermature to immature, and hypermature to mature) in myelodysplastic syndromes (MDS, n = 25) cases. (C) Ratio of cell percentages for the indicated NK maturation subsets (mature to immature, hypermature to immature, and hypermature to mature) in acute myeloid leukemia (AML, n = 8) cases. Data are presented as scatter dot plots, and the lines represent the mean \pm SEM (P < 0.05, **P < 0.01, ***P < 0.001, ns, not significant; Wilcoxon signed rank test).

Significant differences in NK inhibitory receptor distribution among the immature, mature, and hypermature NK cell subsets emerged in the MDS and AML settings

We further assessed the potential quantitative differences in the expression of NK receptors under MDS and AML pathological settings compared to NBM conditions. In all three investigated groups (NBM, MDS, and AML), the percentage of NK cells expressing CD159a increased from the immature (CD56^{bright}CD9^{hi}CD16⁻CD57⁻) to mature (CD56^{dim}CD9^{med}CD16⁺CD57⁻) NK state, but then dropped in the hypermature (CD56^{dim}CD9^{low}CD16⁺CD57⁺) NK stage only in the NBM (mature and hypermature: P < 0.0001) and MDS (mature and hypermature: P=0.0138) cases (Fig. 57A-C).

Under normal circumstances, the percentage of hypermature cells is lower than the mature one. However, when analyzing the individual AML cases, the percentage of hypermature CD159a⁻ positive NK cells did not significantly decrease compared to the mature population (P=0.1990), thus suggesting an actual increase in the number of hypermature NKG2A-expressing cells. In contrast, the percentages of NK cells expressing in NBM the individual KIRs (CD158a, CD158b or CD158e1) were considerably augmented in the mature and hypermature state as compared to the barely detectable levels in the immature population (Fig. 57B-D). When comparing the immature NK cell percentages measured in pathological conditions with those found in NBM, we could notice that the percentage of CD159a⁻ or KIR-positive cells increased significantly in the MDS (P=0.0175), and in some cases of AML.

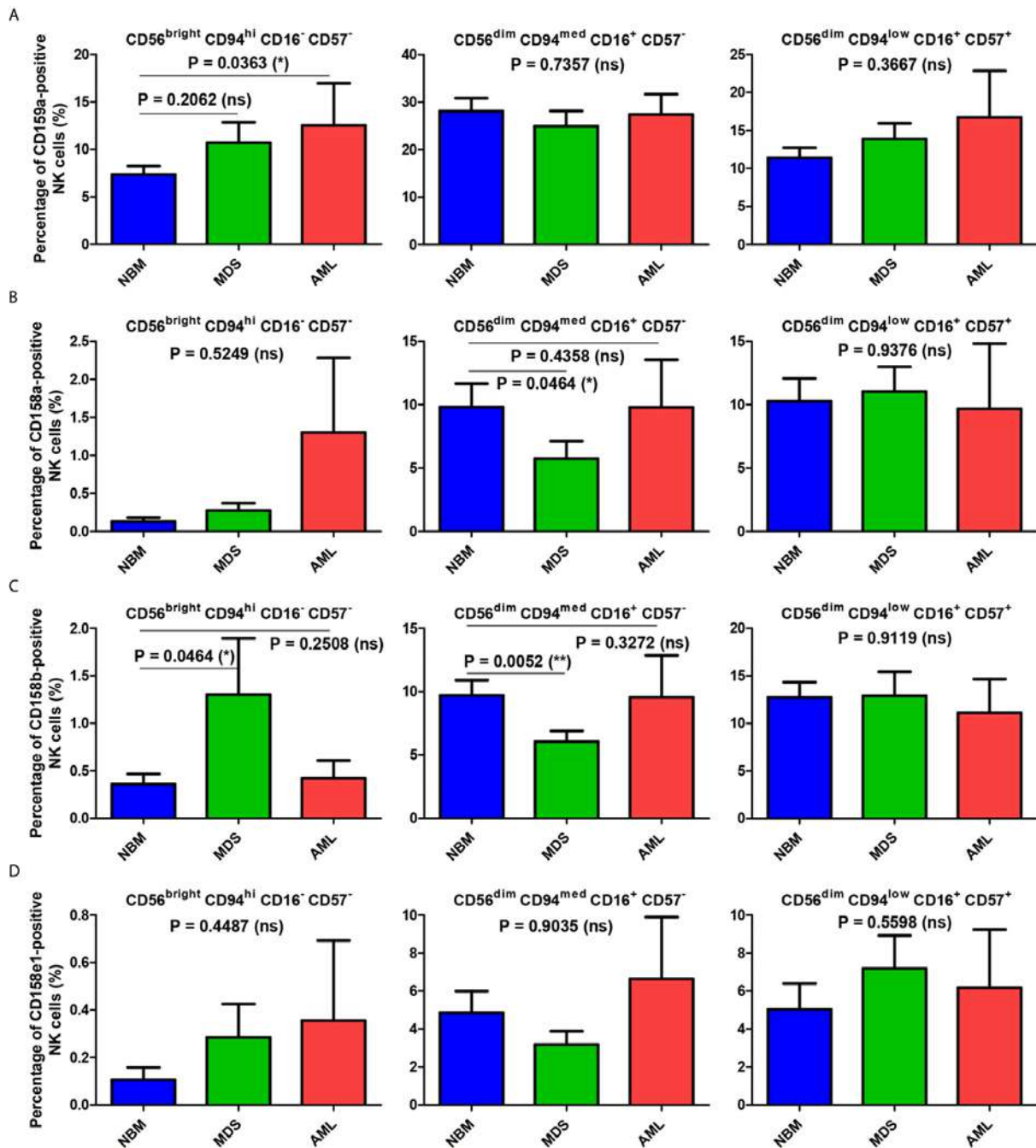


Figure 57. Comparison of the mean percentages of NK subsets expressing CD159a and KIR receptors within the bone marrow microenvironment of NBM, MDS, and AML cases. (A–D) Left panel: CD56^{bright} CD94^{hi} CD16⁻ CD57⁻ immature NK subset; middle panel: CD56^{dim} CD94^{med} CD16⁺ CD57⁻ mature NK subset; right panel: CD56^{dim} CD94^{low} CD16⁺ CD57⁺ hypermature NK subset; (A) Percentage of bone marrow CD159a-positive NK subsets in normal bone marrow (NBM, n = 30), myelodysplastic syndromes (MDS, n = 25), and acute myeloid leukemias (AML, n = 8) cases. (B) Percentage of bone marrow CD158a-positive NK subsets in NBM (n = 30), MDS (n = 24), and AML (n = 8) cases. (C) Percentage of bone marrow CD158b-positive NK subsets in NBM (n = 30), MDS (n = 25), and AML (n = 8) cases. (D) Percentage of bone marrow CD158e1-positive NK subsets in NBM (n = 30), MDS (n = 25), and AML (n = 8) cases. Bars represent the mean \pm SEM (*P < 0.05, **P < 0.01, ns, not significant; Kruskal-Wallis followed by Dunn's Multiple Comparison test).

For the mature NK subset, we noticed a homogenous behavior among all investigated inhibitory molecules in the MDS cases, showing consistent lower percentages of NK cells expressing CD159a or KIRs ($P=0.0102$), while the AML cases displayed a high heterogeneity, $P=0.8250$ (Fig. 57B-D). The data regarding this significant reduction in the population of mature NK cells expressing inhibitory receptors in MDS are further supported by the individual ratio of mature to immature NK cells also showing a significant decrease compared to the corresponding normal ratio defined by the NBM cases (Fig. 58A-B).

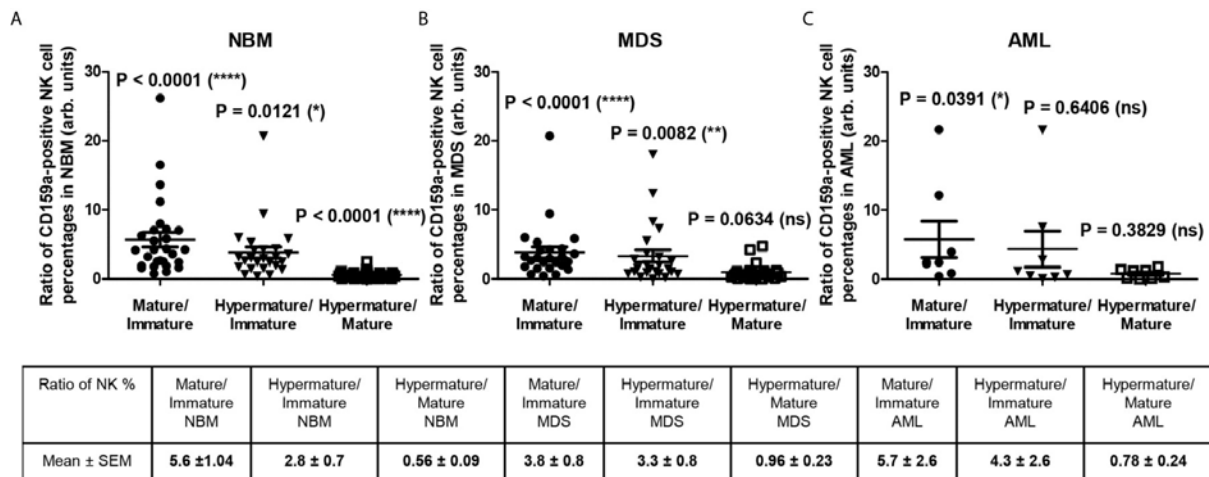


Figure 58. Ratio of cell percentages in distinct CD159a-positive NK maturation subsets within the bone marrow microenvironment of NBM, MDS, and AML cases. (A) Ratio of cell percentages for the indicated CD159a-positive NK maturation subsets (mature to immature, hyperature to immature, and hyperature to mature) in normal bone marrow (NBM, $n = 30$) cases. (B) Ratio of cell percentages for the indicated NK maturation subsets (mature to immature, hyperature to immature, and hyperature to mature) in myelodysplastic syndromes (MDS, $n = 25$) cases. (C) Ratio of cell percentages for the indicated NK maturation subsets (mature to immature, hyperature to immature, and hyperature to mature) in acute myeloid leukemia (AML, $n = 8$) cases. Data are presented as scatter dot plots, and the lines represent the mean \pm SEM (* $P < 0.05$, ** $P < 0.01$, *** $P < 0.001$, ns, not significant; Wilcoxon signed rank test).

When comparing the MFI data of pathological condition to NBM, we noticed a general significant increase of inhibitory molecules (except for CD158a), on MDS ($P=0.0192$) and AML ($P=0.0205$) immature NK cells (Fig. 60A). The higher expression phenotype was further maintained in the mature and hyperature NK populations in AML, but not MDS (Fig. 60B-C). However, among all inhibitory molecules, only CD159a consistently followed this general inhibitory behavior in AML (Fig. 59A).

In parallel, we sought to determine whether differences could be detected in terms of cellular expression intensity for these inhibitory receptors in association with different subsets of NK cells or between different groups of cases. The mean fluorescence intensity (MFI) analysis, presented in Fig. 59A revealed that the mean expression levels of CD159a gradually decreased from the immature ($CD56^{\text{bright}}$ NK cells) towards the mature and hyperature ($CD56^{\text{dim}}$) NK states, in accord to literature data (Zhong and Zhu, 2017). However, the mean expression of the investigated KIRs followed a distinct pattern if compared to CD159a (NKG2A): the MFI values increased from immature to mature NK cells, and persisted at similar levels on the hyperature cells (Fig. 59B-D). The observed MFI pattern of KIRs, but not CD159a, mirrored the cell percentages data of normal bone marrow environmental conditions.

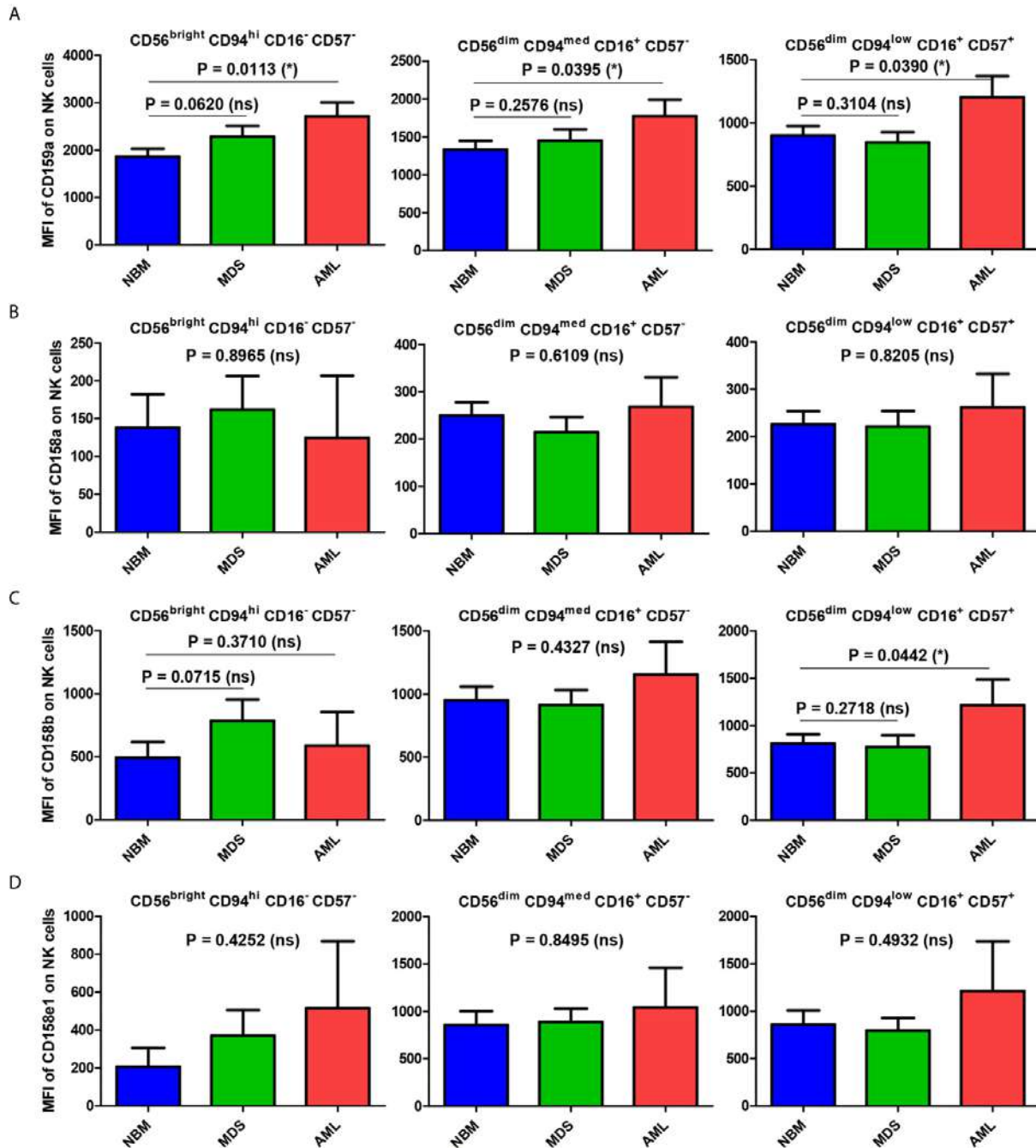


Figure 59. Comparison of CD159a and KIR receptors mean fluorescence intensities (MFI) of different NK maturation subsets within the bone marrow microenvironment of NBM, MDS, and AML cases. (A–D) Left panel: CD56^{bright} CD94^{hi} CD16⁻ CD57⁻ immature NK subset; middle panel: CD56^{dim} CD94^{med} CD16⁺ CD57⁻ mature NK subset; right panel: CD56^{dim} CD94^{low} CD16⁺ CD57⁺ hypermature NK subset; (A) CD159a MFI of different bone marrow NK maturation subsets in normal bone marrow (NBM, n = 30), myelodysplastic syndromes (MDS, n = 25), and acute myeloid leukemias (AML, n = 8) cases. Bars represent the mean \pm SEM (*P < 0.05, ns, not significant; one-tailed unpaired t-test, and Mann Whitney test only for comparing the MFI means of mature NK subsets of NBM vs. MDS: Mann Whitney test). (B) CD158a MFI, (C) CD158b MFI, (D) CD158e1 MFI of different bone marrow NK maturation subsets in NBM (n = 30), MDS (n = 24), and AML (n = 8) cases. Bars represent the mean \pm SEM (*P < 0.05, ns, not significant; one-way ANOVA followed by Tukey's Multiple Comparison test).

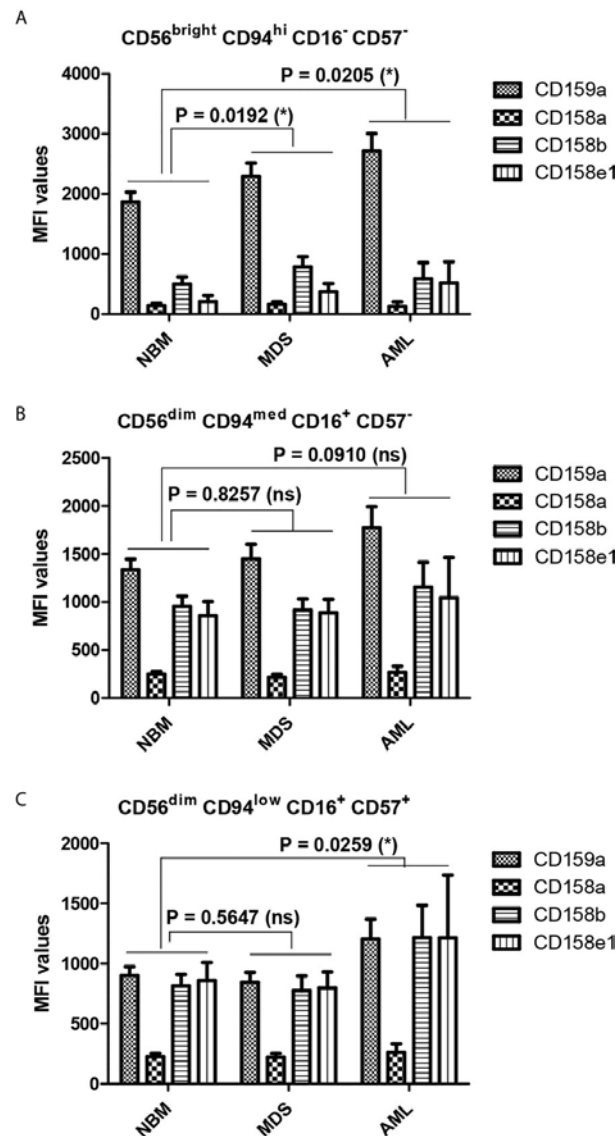


Figure 60. Differences in the repartition of CD159a and KIR receptors in distinct NK maturation subsets within the bone marrow microenvironment of NBM, MDS, and AML cases. (A) Mean fluorescence intensity (MFI) of CD159a and KIR receptors on the surface of bone marrow CD56^{bright} CD94^{hi} CD16⁻ CD57⁻ immature NK cells in normal bone marrow (NBM, n = 30), myelodysplastic syndromes (MDS, n = 25), and acute myeloid leukemia (AML, n = 8) cases. Bars represent the mean \pm SEM (*P < 0.05; two-way ANOVA followed by Bonferroni post-test). (B) Mean fluorescence intensity (MFI) of CD159a and KIR receptors on the surface of marrow CD56^{dim} CD94^{med} CD16⁺ CD57⁻ mature NK cells in NBM (n = 30), MDS (n = 25), and AML (n = 8) cases. Bars represent the mean \pm SEM (ns, not significant; two-way ANOVA followed by Bonferroni post-test). (C) Mean fluorescence intensity (MFI) of CD159a and KIR receptors on the surface of bone marrow CD56^{dim} CD94^{low} CD16⁺ CD57⁺ hypermature NK cells in NBM (n = 30), MDS (n = 25), and AML (n = 8) cases. Bars represent the mean \pm SEM (*P < 0.05; two-way ANOVA followed by Bonferroni post-test).

2.1.4.5. Discussions

NK cells are effectors of utmost importance for the protection of an organism against malignantly transformed cells. Surprisingly, most studies have examined peripheral blood NK cells, whereas very few have explored the bone marrow when considering AML. In one such

study, Chretien et al. investigated the cryopreserved peripheral blood mononuclear cells and concluded that a correlation exists between NK cell maturation and the clinical outcomes of AML patients (Chretien et al., 2017). Our study targeted bone marrow NK cells in both normal settings and pathological conditions; therefore, the impacts of leukemic blasts and an altered microenvironment on the differentiation and maturation of NK cells should be accounted for in this study (Chretien et al., 2015; Williams et al., 2019). Leukemic blasts display antigen-presenting cell-like features, modulating T cell differentiation and further impacting the activation and differentiation of many other immune cells (Antohe et al., 2020; Fujisaki et al., 2011).

Unlike previously reported data (Hayakawa and Smyth, 2006), we were unable to identify any correlations between the percentages of bone marrow blasts and NK cells in MDS and AML samples. This might be explained by the relatively small number of MDS and AML patients included in this study, and by the clinically and biologically heterogeneity of MDS cases as reflected by WHO criteria and the Revised International Prognostic Scoring System.

In recent years, the unsupervised, automatic discrimination of NK subsets has largely been used to reduce the strong heterogeneity observed in NK cell maturation profiles among patients. In our study, the APS, a PCA based analysis, facilitated the fast and reliable identification of three distinct profiles: the immature $CD56^{\text{bright}} CD94^{\text{hi}} CD16^- CD57^-$ population, the mature $CD56^{\text{dim}} CD94^{\text{med}} CD16^+ CD57^-$ population, and the hypermature $CD56^{\text{dim}} CD94^{\text{low}} CD16^+ CD57^+$ population. Furthermore, similar to the results generated by the recently published FLOCK algorithm, developed for multidimensional cytometry data analysis (Chretien et al., 2015), we observed a rather heterogeneous expression of the investigated inhibitory receptors. This should be perhaps interpreted in the wider context of NK cells expressing as well other inhibitory molecules that were not analyzed in this study, such as LIR/ILT2, KIR2DL4, KIR2DL5, KIR3DL2, IRp60, and p75/AIRM1 (Siglec7) (Mamessier et al., 2011).

Our data illustrated no significant differences in the total percentages of NK cells between our three groups; only the in-depth analysis of AML cases revealed a heterogeneous distribution, with extreme values, as represented by the cases with FLT3-ITD, NPM1, and IDH2 mutations. However, should NK cells be investigated as a unique population, this data might offer different and erroneous conclusions.

Our study further aimed to quantify and compare the NK subpopulations in fresh bone marrow samples derived from normal individuals, AML patients, and patients with the MDS pre-malignant condition, which has been considered to represent an intermediate stage towards AML. Our data showed that although the percentage of immature NK cells in the bone marrow was significantly increased in the AML group compared with the NBM group, no such evolution could be observed for mature and hypermature NK cells. These rather unexpected results might support the conclusions reached by Chretien et al., in which the malignant bone marrow microenvironment, heavily influenced by the presence of leukemic blasts, determines whether a maturation blockade occurs (Chretien et al., 2017).

We also examined the expression patterns of several inhibitory receptors. Because MDS is viewed as an intermediate stage, a consistent pattern of evolution, starting with NBM, going through MDS, and culminating with AML, was expected. However, our data demonstrated that no such pattern emerged, and the inhibitory receptors (NKG2A and KIRs) appeared to follow distinctive evolutionary pathways depending on the NK subgroup and their presence in a normal or pathological setting.

For instance, in the NBM population, CD159a is expressed by a maximum number of cells belonging to the mature stage, but the percentage falls dramatically during the hypermature stage. In contrast, although the percentage of immature NK cells expressing KIR is extremely low (less than 1% of total NK cells), it increases markedly in the mature and

hypermature populations, with no significant differences between them (10% of total NK expressing CD158a/b and 5% being positive for CD158e1). CD159a-positive NK cells linearly increase among the immature population from NBM towards AML, while no statistically significant differences between the numbers of mature and hypermature effector NK cells expressing CD159a were observed between NBM and pathological conditions. However, AML cases showed increased heterogeneity of CD159a expression in the hypermature NK subset, with the highest values being attributed to cases with the FLT3-ITD and, respectively IDH2 mutations.

Interestingly, the two AML cases associated with the NPM1 genetic anomaly (deletion or recurrent mutations) presented a remarkable increase in the fraction of mature and hypermature NK cells in the detriment of immature cells, accompanied by the highest expressions of CD159a- and CD158a- positive hypermature NK cells. The two cases of AML associated with FLT3 genetic anomalies (deletion or mutation) phenocopied part of the NPM1-associated phenotype, presenting increased number of hypermature NK cells (if compared to the immature subset) with high expression of CD159a.

Final remarks

These data might suggest that variations in the number of NK cells expressing a particular KIR in normal bone marrow microenvironment conditions is accompanied by corresponding variations of receptor expression levels in the respective NK subpopulations. Additionally, the above-described pattern of immature NK cell percentages was similar to the MFI data of KIR receptors: increased expression in both MDS and AML compared to NBM. For the mature and hypermature NK subsets, a clear higher expression of KIR (similar to CD159a) was observed in AML compared to NBM, providing further evidence for an immune response that is hindered from acting against malignant cells. Interestingly, for the MDS cases, the cellular expression of CD159a and KIRs on mature NK cells was similar to NBM, despite a significant reduction in the respective cell percentages. Thus, we might conclude that MDS does not appear to represent a smooth transitional stage towards malignancy, but rather a decisive step for the evolution of the immune response to cancer cells as it struggles to choose an efficient path.

For further research, this study, in collaboration with the Oncology Department, should be extended to solid cancers (lung, renal, colorectal cancers) and investigate the maturation and senescence of NK cells in both peripheral blood and tumour tissue.

2.2. Biological consequences of targeted immune therapy in solid tumours

2.2.1. State of art

Monoclonal antibody (mAb)-based immunotherapy is now considered to be the central component of cancer therapy, alongside chemotherapy, surgery or radiation (reviewed in (Johnson et al., 2022; Zahavi and Weiner, 2020).

One of the main mechanisms of action for mAb therapy is that they directly target tumour cells while simultaneously promote the induction of long-lasting anti-tumour immune responses. A common direct mechanism by which mAb therapy induce tumour cell death is by blocking the growth factor receptor signalling. For instance, epidermal growth factor receptor (EGFR) is overexpressed by various types of cancers and signalling via EGFR leads to tumour cell proliferation, invasion and metastasis. In this context, Cetuximab, an anti-EGFR mAb,

block the ligand binding and subsequent signalling via EGFR, inducing tumour cell apoptosis (Li et al., 2005; Patel et al., 2009). The tumour microenvironment itself contains factors that promote angiogenesis and tumour growth at the expense of inhibiting the anti-tumour immune responses. For instance, targeting the vascular endothelial growth factor (VEGF), the factor which is abundant in the tumour microenvironment and stimulates the pro-tumorigenic angiogenesis process through VEGFR signalling, with mAb (Bevacizumab) proved to be clinically efficacious for many different solid cancers (Ellis and Hicklin, 2008).

Recently, the mAb therapy have move towards targeting immune cells (known as immune checkpoint inhibitors (ICI) therapy) instead of tumour antigens in order to potentiate the anti-tumour immune response. One of the challenges with this type of therapy is the fact that it is expensive and it can be ineffective in the presence of immunosenescence (IS) due to its mechanism of action linked to T cells. The main therapeutic effect of ICIs consists in disrupting the PD-1/PD-L1 axis or blocking CTLA-4, and thus, reactivating anergic lymphocytes and stimulating the cytotoxic potential of these cells. Unfortunately, the elderly population is generally less recruited in clinical trials, currently leading to insufficient data to conclude regarding the efficacy and safety of ICIs in geriatric subjects (Perrotta et al., 2019; Tagliamento et al., 2022). Interestingly, several clinical studies evaluating the efficacy of ICIs in elderly patients, in whom IS is more likely to be present, found that their survival rate was lower when compared to younger adults (Grossi et al., 2018).

Considering the general trend of applying the mAbs-based therapies for the treatment of many solid cancers, we found it important to investigate its off-target effects in colorectal cancers, and to review the role of IS in ceasing the ICI efficacy in metastatic lung cancers, while identifying the potential compounds that could overcome those negative effects.

This research direction has been achieved by publishing the following scientific articles:

ISI ARTICLES

Alexa-Stratulat T, **Pavel-Tanasa Mariana**[#], Cianga VA, Antoniu S. *Immune senescence in non-small cell lung cancer management: therapeutic relevance, biomarkers, and mitigating approaches*. *Expert Review of Anticancer Therapy* 2022; 22(11): 1197-1210. **IF: 3.627**
<https://doi.org/10.1080/14737140.2022.2139242> ([#] corresponding author)

Moisuc DC, Marinca MV, Gafton B, Alexa-Stratulat T, **Pavel-Tanasa Mariana**, Cianga P. *Antiangiogenic Drug-Induced Proteinuria as a Prognostic Factor in Metastatic Colorectal Cancer*. *Current Oncology* 2022; 29(6): 3996-4011. **IF: 3.109**
<https://doi.org/10.3390/curroncol29060319>.

2.2.2. Off-target effects of monoclonal antibodies-based therapy in metastatic colorectal cancer

2.2.2.1. Introduction

Colorectal cancer (CRC) has an increased incidence in both men and women (Siegel et al., 2014). If diagnosed at an early stage, it is associated with a good prognosis (Aguiar Junior et al., 2020). However, 20–25% of patients already have metastases at the time of diagnosis and about half of those diagnosed at an early stage will eventually develop metastatic disease (Van Cutsem et al., 2014). Surgery and fluoropyrimidine-based chemotherapy continue to represent the treatment backbone of CRC, but the advent of molecular-targeted therapies has

changed the treatment landscape and greatly influenced the prognosis of metastatic disease over the last 15 years (Piawah and Venook, 2019).

One of the major targets of the biological therapies is the cell proliferation pathway, which in CRC depends on Epidermal Growth Factor Receptor signaling. Monoclonal antibodies such as cetuximab or panitumumab have been successfully used, in conjunction with chemotherapy, for the treatment of patients not harboring mutations in the RAS oncogenes (i.e., wild-type KRAS and NRAS). Moreover, the BRAF mutations such as V600E or V600K have shown prognostic but not predictive significance for this group of patients in various studies (Grothey et al., 2021). Angiogenesis has an important role in tumour proliferation and metastasis. Vascular Endothelial Growth Factor (VEGF) is a key mediator of this process, and, as such, it is also a major target for many biological therapies. Inhibition of angiogenesis has become the standard approach in certain types of cancers such as colorectal, bronchopulmonary, ovarian, renal, breast, and cervical cancer (Ferrara and Adamis, 2016; Hegewisch-Becker et al., 2015). However, despite extensive research, one of the major drawbacks of antiangiogenic therapies continues to be the lack of predictive biomarkers.

A current global issue is the cost of anticancer drugs, for which more than USD 100 billion is spent annually worldwide (Prasad et al., 2017). The cost-effectiveness ratio of bevacizumab for mCRC is USD 571.240 per quality-adjusted life years in the first-line setting (Goldstein et al., 2016). Identifying a prognostic or predictive marker for bevacizumab therapy would help individualize treatment and alleviate the burden of increased cost.

In combination with chemotherapy, bevacizumab (a humanized IgG monoclonal antibody that binds to VEGF-A and prevents activation of the tyrosine kinase domain of its receptors VEGFR1 and VEGFR2) has been shown to be effective in clinical trials by increasing overall survival (OS), progression-free survival (PFS), and response rate (RR) (Bennouna et al., 2017; Khakoo et al., 2019; Ma et al., 2019). However, adverse events (AEs) of bevacizumab, in addition to those induced by chemotherapy, may negatively impact treatment outcomes. Hematological, digestive, and neurological toxicity have been reported in patients with CRC treated with chemotherapy (Botrel et al., 2016; Welch et al., 2010). Bevacizumab is also associated with several particular side events such as high blood pressure, risk of bleeding, proteinuria, fistulas, gastrointestinal perforations, thromboembolic events, impaired wound healing, and heart failure (Qu et al., 2015).

2.2.2.2. Aim

The aim of this retrospective study was to analyze the influence of proteinuria, hematological, hepatic, renal, digestive, and neurological toxicity on the results of treatment with bevacizumab plus chemotherapy in patients with mCRC. Identifying a biomarker may help to select the mCRC patient's subgroup that will have a favorable outcome following treatment with bevacizumab and chemotherapy.

2.2.2.3. Materials and methods

Patients' characteristics

We performed a retrospective analysis of patients diagnosed with mCRC treated with bevacizumab and chemotherapy in our center. Inclusion criteria were: age over 18 years, histologically confirmed colorectal cancer, first-line bevacizumab treatment, adequate baseline hematological, hepatic and renal function, and performed urinalysis before and during treatment. Patients with incomplete data were excluded.

Patients received bevacizumab 7.5 mg/kg every 3 weeks or 5 mg/kg every 2 weeks along with standard dose chemotherapy regimens: CapeOX (oxaliplatin 130 mg/m² iv and capecitabine 1000 mg/m² twice a day oral, day 1–14), mFOLFOX 6 (oxaliplatin 85 mg/m² iv,

fluorouracil 400 mg/m² bolus and 2400 mg/m² iv 46 h and leucovorin 400 mg/m² iv), CapeIRI (irinotecan 240 mg/m² iv and capecitabine 1000 mg/m² twice a day oral, day 1–14), FOLFIRI (irinotecan 180 mg/m² iv, fluorouracil 400 mg/m² bolus and 2400 mg/m² iv 46 h and leucovorin 400 mg/m² iv), de Gramont (fluorouracil 400 mg/m² bolus and 2400 mg/m² iv 46 h and leucovorin 200 mg/m² iv), or capecitabine monotherapy.

For each case, several types of data were collected by reviewing patients' medical records: demographic characteristics, types of chemotherapy, pre-existing comorbidities, treatment-related AEs (including the onset of proteinuria), PFS, and OS. Hematological (anemia, neutropenia, thrombocytopenia), hepatic, and renal toxicity were classified according to Common Terminology Criteria for Adverse Events (CTCAE) v4.0 by analysis of complete blood count (CBC), differential liver function (GGT, gamma-glutamyl transpeptidase; ASAT, aspartate-aminotransferase; ALAT, alanine-aminotransferase), and creatinine. Proteinuria was assessed in the summary urine test and was noted to be present or absent, with a cut-off level of 30 mg/dL. Tumour response was evaluated after at least 6 months of treatment and interpreted according to the Response Evaluation Criteria in Solid Tumours (RECIST) v1.1 provisions [33]: complete response (CR, disappearance of all lesions), partial response (PR, at least a 30% decrease in the sum of diameters of target lesions), stationary disease (SD, decrease by less than 30% or increase by less than 20%), progressive disease (PD, at least a 20% increase in the sum of diameters of target lesions or the occurrence of new lesions).

Statistical Analysis

For statistical analysis, we used the SPSS v.16.0 software (SPSS Inc., Chicago, IL, USA). The qualitative and quantitative variables were characterized by frequency, mean, median, and standard deviation to describe the basic characteristics of the studied population. The Chi-square test and Wilcoxon rank-sum test were used to compare median values and proportions. The Kaplan–Meier curve was used to estimate PFS and OS, and the log-rank test was used to compare groups, with a *p*-value of <0.05 indicating statistical significance. A logistic regression analysis was performed using the development of proteinuria as the dependent variable and the following factors as independent variables: previous hypertension, diabetes, other cardiovascular comorbidities, age, gender, and first-line chemotherapy regimen. To identify toxicities influencing OS, a univariate analysis was performed, and statistically significant factors were included in the multivariate Cox analysis using OS as the dependent variable. Other independent variables included were proteinuria, anemia, age groups (less or more than 65 years), comorbidities, stage at diagnosis (metastatic versus non-metastatic), number of metastatic sites (one versus more than one), and tumour location (left versus right).

2.2.2.4. Results

Baseline patient disposition and disease characteristics

A total of 150 mCRC patients undergoing first-line chemotherapy concomitant with bevacizumab between 2014 and 2019 were included in the analysis (Fig. 61). The median age of the patients was 64 ± 9.6 years. Most of the tumours (67%) were located on the descending colon. Mutations in the RAS (KRAS, NRAS) and BRAF (V600E) genes were present in 60 patients out of the 107 for whom these data were available. The most common site for metastasis was the liver (63%), followed by the lung (17%) and bone (5%), while 51 patients presented more than one site of metastasis. The median follow up was 27 months. There were no significant differences between groups in terms of gender (*p*=0.25), age (*p*=0.28), cardiovascular comorbidities (*p*=0.58), diabetes (*p*=0.47), primary tumour location (*p*=0.44), or associated chemotherapy regimen (*p*=0.97).

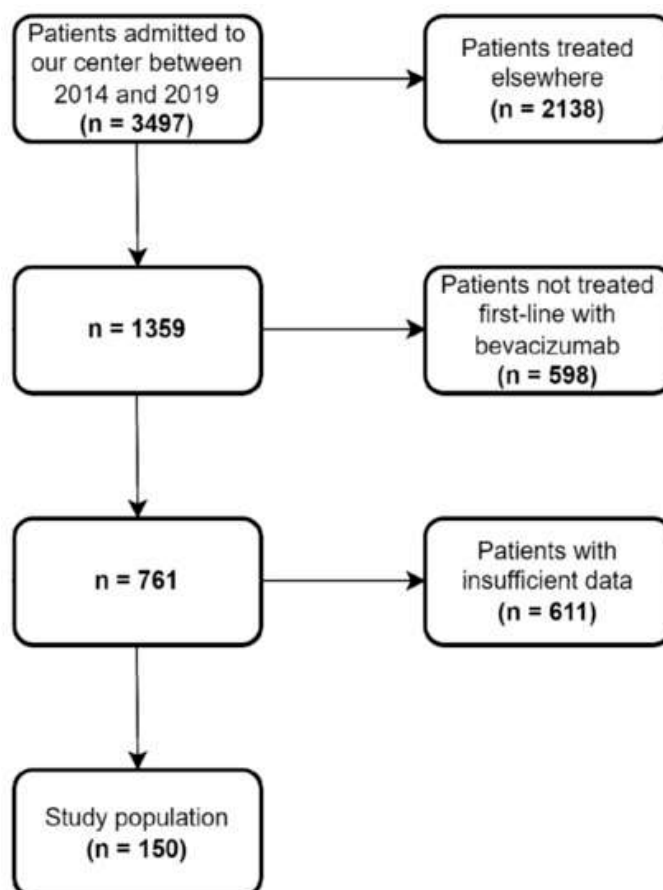


Figure 61. Flowchart detailing patient selection for the study.

Adverse events

We analyzed both bevacizumab- and chemotherapy-related toxicities. Hepatic toxicity and anemia were the most common AEs of any grade; hepatic toxicity and neutropenia were the most common grade 3 and 4 AEs. Grade 3 or higher oxaliplatin-related neurological toxicity (peripheral neuropathy) occurred in 11 patients.

Proteinuria

Proteinuria was present in 50.7% of patients. The median time to the onset of the proteinuria was 10 (range 1–32) months. None of the factors analyzed using the logistic regression method were related to the development of proteinuria: pre-existing hypertension ($p=0.08$), presence of diabetes ($p=0.477$), other cardiovascular comorbidities ($p=0.589$), gender ($p=0.259$), age ($p=0.383$), or chemotherapy regimen (oxaliplatin-based, $p=0.965$; irinotecan-based, $p=0.835$; fluorouracil/capecitabine-based, $p=0.976$). Median PFS was 13 months (95% CI 11.9–14.0) in the entire study population, and median OS was 35 months (95% CI 30.9–39.0). Patients who developed proteinuria during treatment had a longer PFS (15 versus 12 months, $p=0.039$) and OS (40 versus 25 months, $p=0.015$) compared with those without proteinuria (Fig. 62). The disease control rate (DCR) was also higher in patients with proteinuria (76.3% versus 68.9%), but the difference was not statistically significant ($p=0.309$).

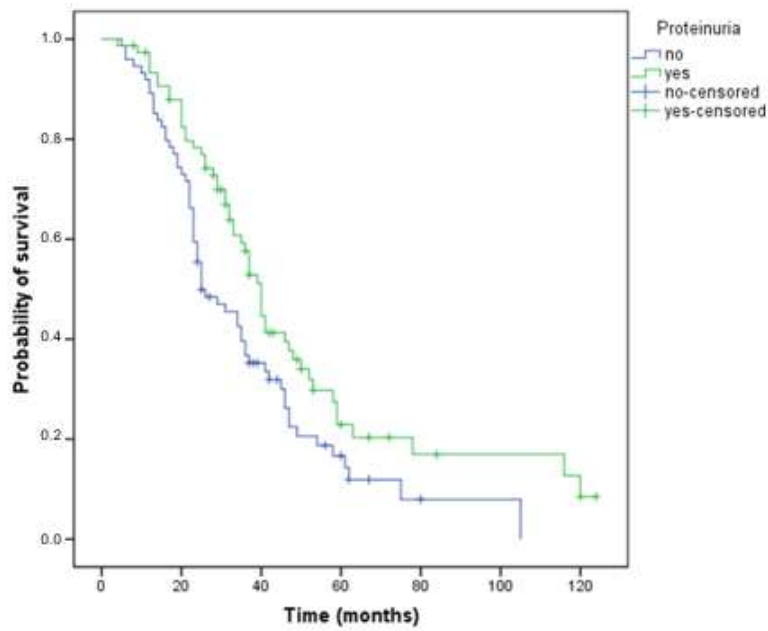


Figure 62. Kaplan–Meier curve of overall survival for patients who have or have not developed proteinuria during treatment (OS, 40 versus 25 months, $p=0.015$).

Anemia

Patients who had anemia during treatment, regardless of grade, had a 20-month shorter survival (Fig. 63) compared with those not experiencing this AE (32 versus 52 months, $p < 0.001$). The DCR was higher in patients without anemia (73.8% versus 72.2%), but the difference did not reach statistical significance ($p=0.84$).

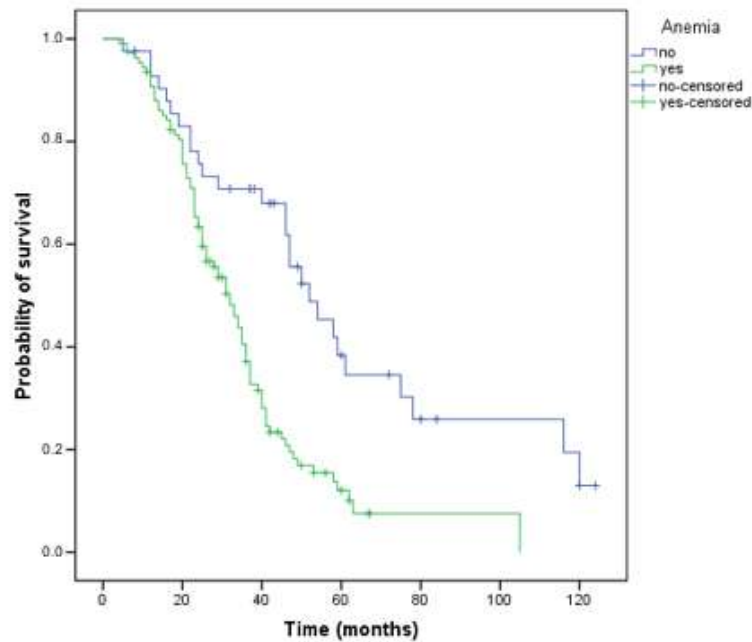


Figure 63. Kaplan–Meier curve of overall survival for patients who have or have not developed anemia during treatment (OS, 32 versus 52 months, $p < 0.001$).

Disease control achievement and stage at diagnosis

Patients who achieved disease control with first-line chemotherapy plus bevacizumab treatment had a significantly longer survival: 40 versus 23 months (Fig. 64) compared to those with progressive disease ($p < 0.001$).

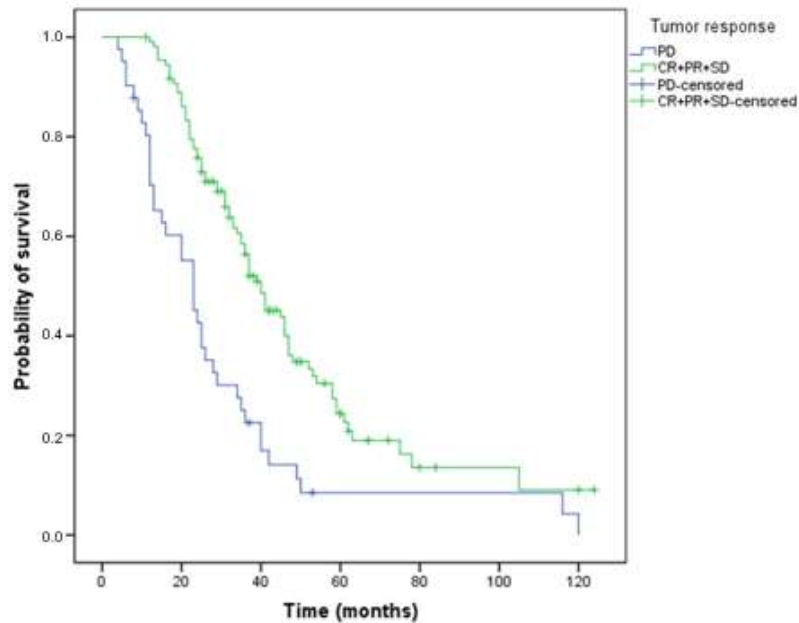


Figure 64. Kaplan–Meier curve of overall survival for patients who have or have not obtained a tumour response (OS, 40 versus 23 months, $p < 0.001$, PD—progressive disease, CR—complete response, PR—partial response, SD—stable disease).

Patients with the metastatic stage at diagnosis had a 31-month OS. Survival of those who had progressed in less than 12 months after completion of adjuvant chemotherapy was 37 months, while patients progressing after more than 12 months from completion of adjuvant treatment achieved the best OS, 50 months ($p=0.002$) (Fig. 65). Patients with a single metastatic site, regardless of location, had better survival rates compared to patients with at least two metastatic sites (39 versus 29 months, $p=0.017$).

Prognostic Factors

The following two toxicities were significantly associated with OS in the univariate analysis: proteinuria ($p=0.017$) and anemia ($p=0.001$). The other adverse events affected quality of life but not survival: neutropenia ($p=0.446$), thrombocytopenia ($p=0.259$), hepatic toxicity ($p=0.169$), renal toxicity ($p=0.164$), neurological toxicity ($p=0.364$), and digestive toxicity ($p=0.224$).

In the multivariate analysis, the following groups had a lower risk of death: patients with proteinuria (HR 0.589; 95% CI 0.402–0.863; $p=0.007$), one metastatic site (HR 0.533; 95% CI 0.363–0.783; $p=0.001$), and non-metastatic stage at diagnosis (HR 0.459; 95% CI 0.293–0.720; $p=0.001$). Patients with anemia (HR 2.437; 95% CI 1.531–3.881; $p < 0.001$) and diabetes (HR 1.828; 95% CI 1.002–3.337; $p=0.049$) had an increased risk of death.

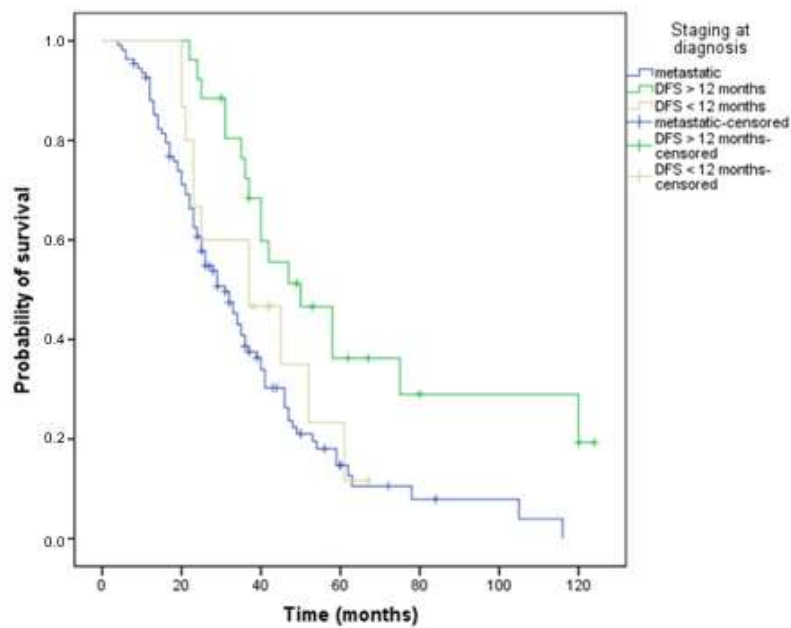


Figure 65. Kaplan–Meier curve of overall survival depending on the stage at diagnosis: metastatic or non-metastatic: DFS (disease-free survival) less or more than 12 months (OS, 31 versus 37 versus 50 months, $p=0.002$).

Propensity Score Matching

Additionally, the XLSTAT v.2022 version of the propensity score matching was employed to further minimize the case selection bias within the two groups (patients who have or have not developed proteinuria during treatment with bevacizumab). We have thus identified 64 pairs of patients, representing 85% of the total analyzed. In this context, patients who developed proteinuria had a longer OS (40 versus 25 months, $p=0.028$) as compared with those without proteinuria (Fig. 66A). Patients who maintained a normal hemoglobin value had a longer OS compared with anemic patients (54 versus 31 months, $p < 0.001$) (Fig. 66B). Moreover, patients who achieved disease control with first-line therapy had a longer OS (40 versus 23 months, $p < 0.001$) (Fig. 66C) compared to those with progressive disease. Patients with a metastatic stage at diagnosis had a 29-month OS, significantly shorter than those with a non-metastatic stage at diagnosis with DFS greater than 12 months or less than 12 months, respectively (29 versus 37 versus 50 months, $p=0.006$) (Fig. 66D). To further verify these results, we performed a multivariate Cox analysis for the above-mentioned subset of patients. All the parameters we have considered (proteinuria, anemia, diabetes, stage at diagnosis, and the number of metastatic sites) generated consistent significant results, thus strengthening our previous conclusions regarding their influence on OS.

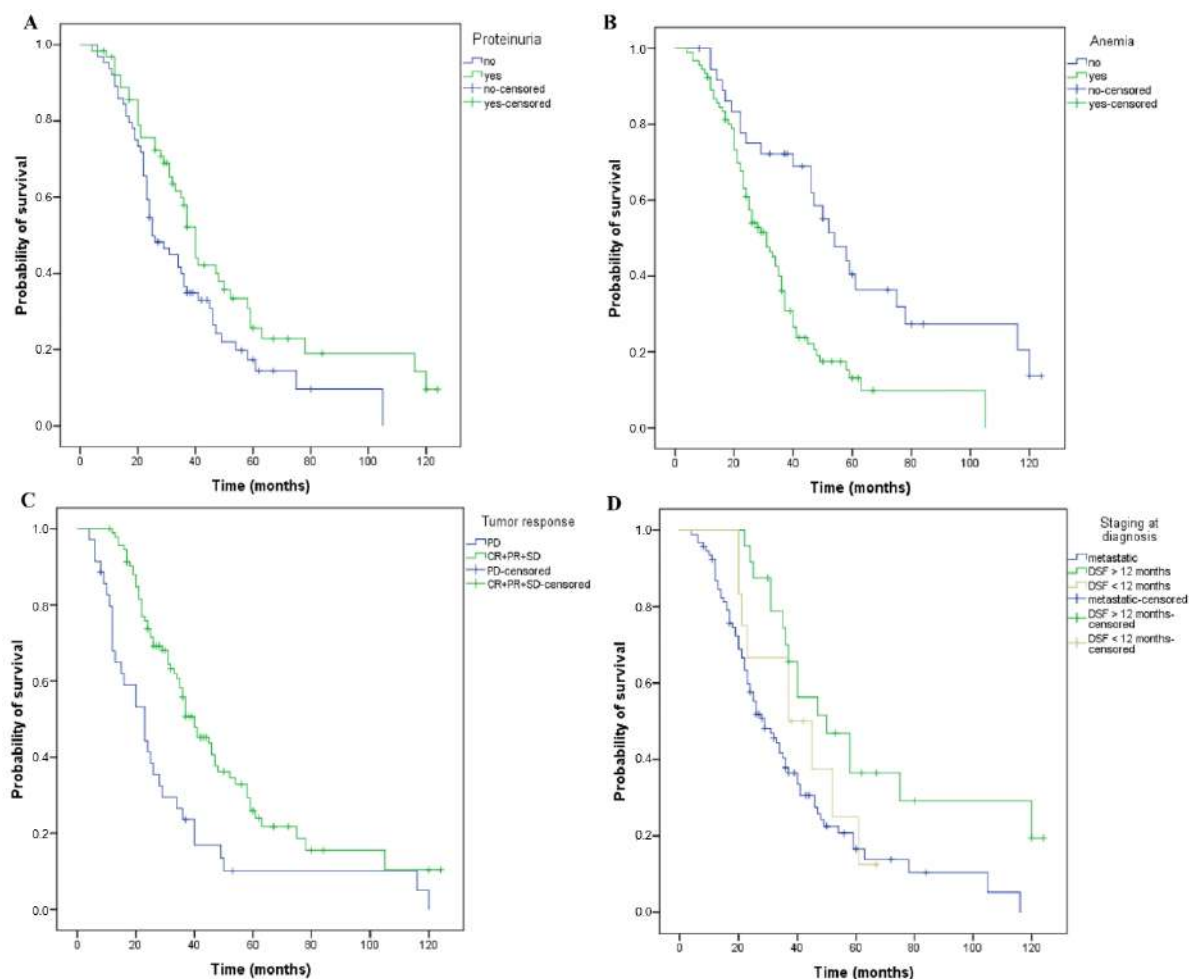


Figure 66. Kaplan–Meier curves of overall survival for matched patients using the propensity score matching method. The patients have or have not developed: **(A)** proteinuria (OS, 40 versus 25 months, $p=0.028$), and **(B)** anemia (OS, 31 versus 54 months, $p < 0.001$) during treatment. **(C)** The patients have or have not obtained a tumour response (OS, 40 versus 23 months, $p < 0.001$, PD—progressive disease, CR—complete response, PR—Partial response, SD-stabile disease). **(D)** The patients had or had no metastases at the stage of diagnosis, DFS=disease-free survival less or more than 12 months (OS, 29 versus 37 versus 50 months, $p=0.006$).

Table 2. Univariate and multivariate prognostic factors for longer OS in metastatic colorectal patients treated with bevacizumab and chemotherapy after performing propensity score matching.

Characteristics	Univariate Analysis			Multivariate Analysis		
	HR	95% CI	p-Value	HR	95% CI	p-Value
Proteinuria	0.637	0.423–0.960	0.031	0.592	0.391–0.896	0.013
Anemia	2.505	1.521–4.125	<0.001	2.599	1.569–4.306	<0.001
Age	0.764	0.510–1.145	0.192	-	-	-
Cardiovascular comorbidities	1.263	0.838–1.904	0.264	-	-	-
Diabetes	1.485	0.784–2.813	0.225	2.264	1.171–4.376	0.015
Staging at diagnosis	0.495	0.310–0.791	0.003	0.454	0.282–0.731	0.001
Number of metastatic sites	0.660	0.439–0.993	0.046	0.558	0.369–0.846	0.006
Tumor location	0.944	0.760–1.172	0.601	-	-	-

2.2.2.5. Discussions

Numerous studies and retrospective analyses have been performed to identify novel prognostic factors that could be readily used in the clinical setting for CRC patients. Factors such as the location of the primary tumour, histologic grade, history of primary surgery, metastasectomy, performance status, peritoneal metastases, lactate dehydrogenase, PFS interval prior to liver surgery, carcinoembryonic antigen levels, liver toxicity (transaminases), and the size of the two largest lesions on CT scans have been evaluated in several prospective and retrospective studies (Fendler et al., 2015; Shitara et al., 2011). However, no prognostic or predictive biomarkers specific to patients undergoing antiangiogenic systemic therapy have been identified to date. Although VEGF is one of the most studied biomarkers in clinical trials (Jubb et al., 2006; Kubisz et al., 2010), the data available so far are still contradictory.

The main purpose of this study was to analyze the putative relationship between the occurrence of treatment-related adverse events (proteinuria, hematological, hepatic, renal, digestive, and neurological toxicity) and OS. The most significant result showed that the category of patients who developed proteinuria had a significantly better OS and PFS compared to those who did not experience this AE.

Previous studies have shown a close correlation between the use of bevacizumab and the development of proteinuria (Zhao et al., 2017; Zhu et al., 2007). Proteinuria has also been studied as a predictive factor, but no consensus was reached. Zee et al. reported significantly lower survival rates in patients with colorectal cancer treated with antiangiogenic therapy if they developed proteinuria grade 2 or higher, as opposed to grade 0–1 (OS 4.2 months versus 23.9 months). In another study, no correlation was found between the severity of proteinuria and survival in patients with mCRC treated with bevacizumab (Iwasa et al., 2013). Feliu et al. demonstrated that the occurrence of proteinuria is correlated with the response rate. However, they included only elderly patients in the study. Patients with moderate and severe proteinuria had a response rate of 56% and an OS of 22 months compared to 37% and 20.1 months, respectively, in patients with grade 0–1 proteinuria, but the survival advantage was not statistically significant (Feliu et al., 2015). Another study showed that the early development of both hypertension and proteinuria after the initiation of bevacizumab in patients with breast cancer is associated with tumour response rate, and the authors suggested that these two side effects could be considered predictive (Tanaka et al., 2018).

Our results differ from the mentioned studies due in part to variations between target populations and also to differences in methods and parameter definitions. Another very important source of bias is the small patient numbers in all these studies, which we have also emphasized. For example, Zee et al. conclude that grade 2 proteinuria represents a pejorative factor for OS but not for PFS or RR in their subjects. In our slightly larger sample, we have found the presence of proteinuria to carry a better prognosis for both OS and PFS, and we hypothesized it might be regarded as a surrogate marker for higher efficacy of anti-angiogenic therapies. While qualitative analysis is definitely more error-prone, it offers a more affordable and feasible evaluation of proteinuria than quantitative methods. We only performed a qualitative evaluation (yes versus no) of proteinuria and identified it in 76 patients in our sample, while the more quantitative analysis of Zee et al. (though also based on dipstick urine protein level) found grade 1 proteinuria in 12 patients and grade 2 in only 4 of their patients, respectively. Further, they also noted that proteinuria (at any grade) has not been associated with kidney dysfunction, hence the grade 2 cut-off might indeed be considered somewhat arbitrary.

No guidelines are currently available for the management of bevacizumab-induced proteinuria, although there is general consensus on the necessity to prevent subsequent renal failure, cardiovascular complications, as well as tumour progression due to permanent

discontinuation of biologic therapy if proteinuria exceeds 2 g/24 h or nephrotic syndrome occurs, respectively.

In the present study, the occurrence of at least one episode of anemia during treatment was a negative prognostic factor for OS. Survival decreased significantly according to the grade of anemia (20 months for grade 3 versus 31 months for grade 2 versus 34 months for grade 1; no grade 4 or 5 anemia was reported). This is in accord with the conclusions of a meta-analysis reporting that anemia at any point during the course of the disease increases the risk of death in cancer patients. When presenting anemia, the relative risk of death was increased by 19% in lung cancer, by 75% in head and neck carcinomas, and by 47% in prostate cancer patients (Caro et al., 2001). Anemia during chemotherapy also affects OS by the deriving necessity to delay or reduce the dose of chemotherapy. In addition, anemia produces tumour hypoxia that reduces the effectiveness of chemotherapy and bevacizumab. Although anemia can be corrected, there is no evidence to improve long-term prognosis after performing therapeutic procedures (transfusions, stimulation of erythropoiesis).

Another factor influencing both OS and disease-free survival (DFS) is the tumour stage at diagnosis (Peng et al., 2014; Valentini et al., 2011). In multivariate analyses, we have split our study population into two groups (upfront metastatic, $n=109$; and non-metastatic, $n=41$) and found that initially non-metastatic patients had significantly better survival rates. Patients with a single metastatic site had a 10-month longer survival than patients with at least two metastatic sites. The present study also showed that tumour volume has a negative impact on the prognosis. Köhne et al. analyzed a panel of clinical, hematological, and biochemical factors to identify prognostic markers of CRC patients treated with fluorouracil-based chemotherapy, and the results showed that the number of metastatic sites, along with other factors, classified patients with mCRC into different risk categories. The most unfavorable risk was for patients with ECOG performance status 0–1, more than one metastatic site, and alkaline phosphatase over 300 U/L. Platelets ($>400 \times 10^9/L$), alkaline phosphatase level ($>300 IU/L$), WBC count ($>10 \times 10^9/L$), and hemoglobin ($<11 g/dL$) predicted an inferior survival probability. Lactate dehydrogenase, bilirubin, ALAT, ASAT, total protein, albumin, and carcinoembryonic antigen (CEA) levels were not significant (Kohne et al., 2002). The number of metastatic sites is considered a negative prognostic factor not only for CRC (Franko et al., 2016) but also for lung cancer (Oh et al., 2009), esogastric cancer (Chen et al., 2020), and for endometrial carcinoma (Jobsen et al., 2010).

Another multivariate analysis concluded that primary tumour location, performance status, number of metastatic sites, baseline CEA level, and platelets may be considered prognostic factors in patients with mCRC treated with oxaliplatin and bevacizumab (Hegewisch-Becker et al., 2018). In the current analysis, renal, hepatic, digestive, and neurological toxicities affected the quality of life to various degrees but did not influence OS.

Our research is subject to several limitations. We have included in our study 150 carefully chosen patients, a number that precludes definitive conclusions or recommendations based on the results above. However, our results provide additional data on the prognostic role of proteinuria and warrant more extensive prospective studies in order to validate the present findings. Another study limitation is the retrospective nature of the study and selection bias. For example, about 20% of patients present with de novo metastatic colon cancer. In the present study, the number of de novo metastatic diseases is $>70\%$, which suggests patients with a previous diagnosis of early-stage colorectal cancer are not reflecting the source population, and the finding that previous history of an early-stage disease has a better prognosis could merely be due to selection bias. In addition, some of the known prognostic factors including BRAF status, metastasectomy, subsequent line of chemotherapy, and baseline performance status were not examined in the analysis.

Final remarks

The results of our study suggest that, in addition to the non-metastatic stage at diagnosis and one metastatic site, the development of proteinuria during first-line treatment with bevacizumab and chemotherapy of patients with mCRC was an independent prognostic factor for OS and correlates with a better prognosis. Despite the fact that literature data are controversial in terms of the prognostic role of proteinuria, the results of our study argue in favor of it. The presence of diabetes, pre-existing hypertension, and other cardiovascular conditions did not increase proteinuria risk in the studied group. Neutropenia, thrombocytopenia, hepatic, renal, and neurological toxicity do not influence OS. The presence of anemia during treatment and diabetes were negative prognostic factors.

For future research directions, it is important to extend the study of various off-targets effects given by mAbs-based therapy seen in other types of solid cancers. Importantly, the efficiency and off-target effects of ICI therapy should be investigated rigorously to establish a well-grounded study.

2.3. The role of humoral immunity in COVID-19 and other inflammatory diseases

2.3.1. State of art

During the current COVID-19 pandemic, two questions have become central for settling the conditions required for an efficient immune protection against disease. Firstly, what is the durability of humoral immune responses after vaccination in infection-naïve or previously-infected individuals, and whether (or when) a vaccination boost is required for each of those, especially in the context of new up-coming variants? Of importance, there is increasing evidence that previously-infected individuals might have amplified antibody responses following vaccination that can be detected up to almost one year (Anand et al., 2021; Gaebler et al., 2021; Wajnberg et al., 2020). Secondly, how does age and underlying comorbidities influence the humoral immune responses and the durability of neutralizing antibody titres? As such, a recent study performed in the United Kingdom (UK) has identified reduced humoral and cellular responses in people aged 65 years or older not previously exposed to natural infection, when compared to younger subjects (Tut et al., 2022). However, more studies are required to understand how age can impact on the vaccine efficacy in other countries and nations.

These questions are important as the manifestations of SARS-CoV-2 infection can vary from asymptomatic or mild to critical and even fatal forms (Basheer et al., 2021). Thus far, there are several biological parameters that have been described to predict the fulminant evolution of the disease, such as increased C-reactive proteins (CRPs), lactate dehydrogenases (LDH) (Zhang et al., 2020b), the neutrophil/lymphocyte ratio (NLR), D-dimers and ferritin (Perreau et al., 2021). Some authors showed that the infected patient's response to SARS-CoV-2 is embodied by an innate immune response followed by neutrophilia, lymphocytes apoptosis, decrease in T cell numbers and increase in the serum levels of some specific pro-inflammatory cytokines (Zhang et al., 2020a). Consequently, the high concentrations of some pro-inflammatory factors were highlighted as pathogenic factors in COVID-19: interleukin 6 (IL-6); IL-10, IL-1, IL-1 β , IL-2, IL-4 and IL-5; IL-7, IL-12, tumour necrosis factor (TNF), interferon-gamma (INF- γ) and INF- β ; colony-stimulating factors (CSF) and macrophage inflammatory protein 1 alpha (MIP1 α); MIP-1B (Cardone et al., 2020; Huang et al., 2020;

Mehta et al., 2020; Rabaan et al., 2021). High levels of chemokines were also detected in severe forms of COVID-19: IFN-induced proteins-10 (IP-10/CXC-chemokine ligand 10 (CXCL10)), CXCL9, monocyte chemoattractant protein-1 (MCP1), chemokine ligand-2 (CCL)-2 and IL-8 (Rabaan et al., 2021).

In this context, many observational studies have augmented the evidence that deficient vitamin D serum levels are correlated with higher rate of incidence or severity of COVID-19 (De Smet et al., 2021; Dror et al., 2022; Merzon et al., 2020). Additional data has even implicated that supplementation with vitamin D could be critical in mitigating the COVID-19 progression to lessen its severity (Pilz et al., 2018). Therefore, various recent clinical trials also investigated whether supplementation with vitamin D could optimize the efficacy of COVID-19 vaccines (reviewed in (Chiu et al., 2021)). However, the new emerging data are showing little association between vitamin D status and antibody responses following anti-SARS-CoV-2 vaccination (Chillon et al., 2021; Inserra et al., 2021), suggesting that more studies are required for establishing the exact role of vitamin D in modulating the efficacy of severe acute respiratory syndrome coronavirus-2 (SARS-CoV-2) vaccines.

Another factor influencing the progression and mortality rate of COVID-19 infection was represented by the adipose tissue dysfunction. It is well established that adipose tissue is a major source of adipokines (adiponectin, leptin) and pro-inflammatory mediators (monocyte chemoattractant protein-1 (MCP-1), tumour necrosis factor (TNF- α), factor D, IL-6) which mitigate a long-lasting low-grade inflammation and a prothrombotic state which are exacerbated in the context of SARS-CoV-2 infection, predisposing to cardio-respiratory failure (reviewed in (Mery et al., 2020; Popkin et al., 2020)). Among adipokines, adiponectin circulating levels were showed to be significantly reduced in patients with COVID-19 respiratory failure in multiple studies (Blot et al., 2021; Kearns et al., 2021; Tonon et al., 2022). Moreover, leptin, which serum levels largely depends on the total adipose mass, also provides a high impact on the immune system, as it favors monocytes/ macrophages activation, pro-inflammatory cytokines release and a predominant Th-1 response, the three hallmarks of immune responses noticed in critical COVID-19 patients (Blot et al., 2021; Foldi et al., 2021).

This research direction has been achieved by publishing the following scientific articles:

ISI ARTICLES

- **Immunity in COVID-19**

Pavel-Tanasa Mariana[#], Constantinescu D, Cianga CM, Anisie E, Mereuta AI, Tuchilus CG, Cianga P. *Adipokines, and not vitamin D, associate with antibody immune responses following dual BNT162b2 vaccination within individuals younger than 60 years.* **Frontiers in Immunology** 2022; 13: 1000006. **IF: 8.787**

<https://doi.org/10.3389/fimmu.2022.1000006> ([#]corresponding author)

Trofin Felicia, Olivia Simona Dorneanu, Daniela Constantinescu, Eduard Vasile Nastase, Cătălina Luncă, Luminița Smaranda Iancu, Ioana-Maria Andrioaie, Alexandru Duhaniuc, Corina Maria Cianga, **Mariana Pavel-Tanasa**, Dana-Teodora Anton-Păduraru, and Petru Cianga. *Cytokines and Chemokines in Breastmilk of SARS-CoV-2 Infected or COVID-19 Vaccinated Mothers.* **Vaccines** 2022; 10(12):2001. **IF: 4.961**

<https://doi.org/10.3390/vaccines10122001>.

Miftode RS, Constantinescu D, Cianga CM, Petris AO, Timpau AS, Crisan A, Costache II, Mitu O, Anton-Paduraru DT, Miftode IL, **Pavel-Tanasa Mariana**, Cianga P, Serban IL. *A Novel Paradigm Based on ST2 and Its Contribution towards a Multimarker Approach in the Diagnosis and Prognosis of Heart Failure: A Prospective Study during the Pandemic Storm.* **Life (Basel)** 2021; 11(10): 1080. **IF: 3.253**

<https://doi.org/10.3390/life11101080>.

- **Immunity in other infectious and/or inflammatory conditions**

Obreja M, Miftode EG, Stoleriu I, Constantinescu D, Văță A, Leca D, Cianga CM, Dorneanu OS, **Pavel-Tanasa Mariana**, Cianga P. *Heparin-Binding Protein (HBP), Neutrophil Gelatinase-Associated Lipocalin (NGAL) and S100 Calcium-Binding Protein B (S100B) Can Confirm Bacterial Meningitis and Inform Adequate Antibiotic Treatment. *Antibiotics (Basel)* 2022; 11(6): 824. IF: 5.222 <https://doi.org/10.3390/antibiotics11060824>.*

Ioana-Andreea Sioustis, Maria-Alexandra Martu, Liana Aminov, **Mariana Pavel**; Petru Cianga, Diana C. Kappenberg-Nitescu, Ionut Luchian, Sorina M. Solomon, Silvia Martu. *Salivary Metalloproteinase-8 and Metalloproteinase-9 Evaluation in Patients Undergoing Fixed Orthodontic Treatment before and after Periodontal Therapy. *International Journal of Environmental Research and Public Health* 2021; 18(4):1583. IF: 4.614 <https://doi.org/10.3390/ijerph18041583>.*

Vlad CE*, Foia L, **Pavel-Tanasa Mariana***, Toma V, Florea L, Voroneanu L, Apetrii M, Dodi G, Covic A. *Evaluation of cardiovascular events and progression to end-stage renal disease in patients with dyslipidemia and chronic kidney disease from the North-Eastern area of Romania. *International Urology and Nephrology* 2022; 54(3): 647-659. IF: 2.266 <https://doi.org/10.1007/s11255-021-02919-2> (* equal contributions)*

Stefana Catalina Bilha, Anca Matei, Daniela Constantinescu, **Mariana Pavel Tanasa**, Raluca Mogos-Cioncu, Petru Cianga, Cristina Preda, Dumitru D. Branisteanu. *New insights into the metabolic-bone crosstalk in active acromegaly, *Endokrynologia Polska* 2021; 12: 665541. IF: 1.569 <https://doi.org/10.5603/EP.a2021.0028>.*

Anca Matei, Stefana Catalina Bilha, Daniela Constantinescu, **Mariana Pavel-Tanasa**, Petru Cianga, Adrian Covic, Dumitru D. Branisteanu. *Body composition, adipokines, FGF23-Klotho and bone in kidney transplantation: Is there a link? *Journal of Nephrology* 2021; 35: 293-304. IF: 4.406 <https://doi.org/10.1007/s40620-021-00972-9>.*

2.3.2. The role of adipokines and vitamin D in mediating the age-related antibody immune responses following dual anti-SARS-coV-2 vaccination

2.3.2.1. Introduction

Severe acute respiratory syndrome coronavirus-2 (SARS-CoV-2) led to a global health outbreak known as the COVID-19 pandemic which has been lasting since March 2020. Vaccine became accessible to people only in the beginning of 2021 which greatly helped reducing the mortality rate and severity of COVID-19 infection afterwards. The efficacy of vaccines was not fully known and studies documenting the immune responses following vaccination are continuing to emerge. Recent evidence indicate that natural infection prior vaccination may improve the antibody and cellular immune responses, while little is known about the factors influencing those processes, especially in the elderly. Several recent studies pointed out key candidates: vitamin D levels and obesity/adipose tissue mass.

2.3.2.2. Aim

For this study, we wondered what the antibody responses following dual BNT162b2 vaccination are in younger and older individuals from our population in relation to previous-infection status, and reveal, if any, the associations between the magnitude of RBD (Receptor-Binding Domain)-specific antibody titres and circulating levels of vitamin D and adipokines.

2.3.2.3. Materials and methods

Study participants and serum collection

Blood samples were collected at “St. Spiridon” County Clinical Emergency Hospital (Iasi, Romania) between April 2021 and August 2021 from presumably healthy individuals following dual BNT162b2 (BioNTech-Pfizer) vaccination (21 days interval between the two doses) at a mean of 67 days (SEM 1.88, IQR 47-91) after the second dose. The samples were next stratified according to previous exposure to natural SARS-CoV-2 infection based on anamnestic data. The vaccination for previously infected individuals was performed at least 90 days after infection, as recommended by our national authorities. This study has been reviewed and approved by the institutional ethics committees (St. Spiridon County Clinical Emergency Hospital of Iasi) and informed consent was obtained from participants in this study. More precisely, 192 participants agreed for antibody testing, of which 122 for both vitamin D (25OH) and adipokine assessment, and 14 only for vitamin D levels detection. The information related to age and gender were included in a database together with a unique identifier, in order to keep the sample’s identity unknown to the researcher. Around 9% of the subjects were obese and 1/5 of them were older than 60 years, and none of the participants was recorded with autoimmune diseases in our hospital database.

None of the subjects had vitamin D supplementation before the blood sampling. Blood samples were collected in vacutainers with no anticoagulant and processed within 6 hours of receipt at the Laboratory of Immunology. More precisely, blood was spun at 2000 G for 5 min, and the serum was separated and aliquoted for storage at -80°C until further analysis.

Sample processing for assessing the antibody responses and vitamin D levels

After thawing, the samples were centrifuged at 2000 G for 5 min. The assessment of antibody response against the spike-RBD (Receptor-Binding Domain) region of SARS-CoV-2 was performed using an electro-chemiluminescent microparticle immunoassay on cobas® automatic platforms. The limit of detection for our assay was 0.8 U/mL, and samples with values > 0.8 were classified as antibody-positive. For the detection of total vitamin D (25-Hydroxyvitamin D) levels, an electrochemiluminescence binding assay was also used on cobas® automatic platforms. The measuring range was 3.0-70.0 ng/mL (or 7.50-175 nmol/L), with a functional sensitivity of 4.01 ng/mL.

Quantification of adipokines and other cytokines

The concentration of various adipose tissue-related biomarkers was performed using a human obesity custom premixed kit from R&D systems and performed on a Luminex 100/200 platform. The samples were diluted 1:4 before being processed. The biomarkers included in the study were: monocyte chemoattractant protein-1 (MCP-1/CCL2), c-reactive protein (CRP), factor D, plasminogen activator inhibitor 1 (PAI-1/ SERPINE1), interleukins 6 (IL-6) and 10 (IL-10), adiponectin, leptin, resistin, and tumour necrosis factor (TNF- α). Briefly, 50 μ l of microparticle mixture were added to each well of the microplate and 50 μ l of standards and samples were added on top and left for 2 hours incubation at room temperature on a horizontal orbital microplate shaker set at 500 rpm. Following a washing procedure, 50 μ l of diluted biotin antibody cocktail were added to each well and the plate was incubated for 1 hour at room temperature on the shaker. After another wash step, the diluted streptavidin-PE solution was added for 30 min. The read of the plate was performed within 60 minutes.

Statistical analysis

Statistical analysis was performed using Graph Pad Prism, v5 (Graph Pad Software, San Diego, CA, USA) and SPSS, v25 (IBM SPSS Software, Chicago, IL, USA). Figures were created with Graph Pad Prism, v5. Data are presented as scatter dots or bars with information about the mean and SEM. Each figure legend contains the relevant statistical information: the

n, total number of participants, the significance p-value, and the statistical test used. All data were checked for both normality and variance using the Kolmogorov-Smirnov test. The parametric data were analyzed using the unpaired t-test and one-way ANOVA with Post-hoc Tukey's Multiple Comparison test. The majority of the data were non-parametric and the statistical tests applied were: Mann-Whitney test (the non-parametric counterpart to unpaired t-test), and Kruskal-Wallis with Dunn's Multiple Comparison test (the non-parametric counterpart to one-way ANOVA). Spearman's correlation coefficients (R) were used to assess positive or negative associations between measured variables. R values between 0.2-0.39 were treated as weak, between 0.4-0.59 as moderate, and between 0.6-0.79 as very strong correlation factors. The linear regression analyses related to main Figures 2 and 5 were performed using Graph Pad Prism v5 in order to identify the predictive value of factor X (independent variable plotted on the X axis) on factor Y (dependent variable plotted on the Y axis). Each linear regression graph shows the best-fit line with the 95% confidence band. The coefficient of determination R-squared (R^2) was used as a goodness-of-fit measure and the F-test to determine the level of significance. The linear regression models related to Figure 7 and Table 2 were generated using SPSS v25 for predicting the antibody response (the dependent variable) based on the serum concentrations of various independent variables (negative and positive factors). R^2 and adjusted R^2 were used as goodness-of-fit measures and ANOVA test was applied for assessing the statistical significance for the proposed predictive models. The dependent variable may be determined based on the expression of multiple independent variables (predictor, p): B_0 (constant) + B_1X_1 + B_2X_2 + ... + B_pX_p . The logistic regression analyses used for predicting the previous-infection status were performed using SPSS, v25. More precisely, receiver operating characteristic (ROC) curves were generated to compare the sensitivity (s_n) versus specificity (s_p) across a range of possible cut-off values, and the area under those curves (AUC) was used as a measure of test performance. The optimal cut-off values were determined by identifying the minimum distance from the ROC curve to the upper left corner point (where $s_n=1$ and $s_p=1$). The distance between this point ($s_n=1$, $s_p=1$) and any point on the ROC curve is $d = \sqrt{(1 - s_n)^2 - (1 - s_p)^2}$, which was calculated for each observed cut-off value in order to locate the minimum. The results for AUC are reported as area, standard error of the area (S.E.), 95% confidence interval of the area and P value (testing the null hypothesis that AUC=0.5). For negative predictors, the smaller values of the test result variables indicate stronger evidence for a positive actual state (previous infection), while for positive predictors, the larger values of the test variables suggest the previous infection status. The P values less than 0.05 was considered statistically significant.

2.3.2.4. Results

RBD-specific antibody responses following BNT162b2 dual vaccination are weaker in people over 60 years old

Blood samples were collected from 192 participants (149 [77.6%] were infection-naïve, while 43 [22.4%] declared previous natural infection) and who had completed the second vaccination with. Blood samples were collected a median of 74 (IQR 48-91) and 75 (IQR 43-91) days after the second vaccination for the infection-naïve and previously infected (also called infection-primed) groups of subjects, respectively. The previously infected group showed a significant 8.67-fold increase in the spike RBD-specific IgG titre compared to the infection-naïve group (mean values for the two groups: 12674 U/mL for infection-primed vs. 1462 for infection-naïve, $P < 0.0001$). Each group was further subdivided according to gender, and the female to male ratios were 2.7 and 2.3 for the infection-naïve and previously infected groups, respectively. Both females and males showed similar antibody titre in each main group

(Fig. 67A). When stratified by age, the subgroup of subjects older than 60 years showed significant reduction in the magnitude of the antibody response in both infection-naïve (2.24-fold difference between < 60 years old and > 60 years old) and – primed (2.92-fold difference between < 60 years old and > 60 years old) categories. Therefore, the fold increase in the previously-subjects was 8.82 for people < 60 years old, and to a less extent of 6.76 for people > 60 years old (Fig. 67B). Interestingly, the subjects showed a consistent trend of antibody titre decrease with age within the infection-naïve group. For instance, while individuals younger than 30 years had a mean titre value of 2042 U/mL, the population over 60 years had 3-times less, 668 U/mL ($P=0.0002$) – Fig. 67C-D. By contrast, within the previously infected group, the antibody titres were similar among the individuals younger than 60 years with a general mean of 13501 U/mL, however significantly higher than those seen in the subjects aged 60 years or older characterized by a titre mean of 4610 U/mL ($P=0.0032$). Our data clearly showed that across both main groups, infection-naïve and previously infected, there was a significant reduction in the antibody response following vaccination in older individuals.

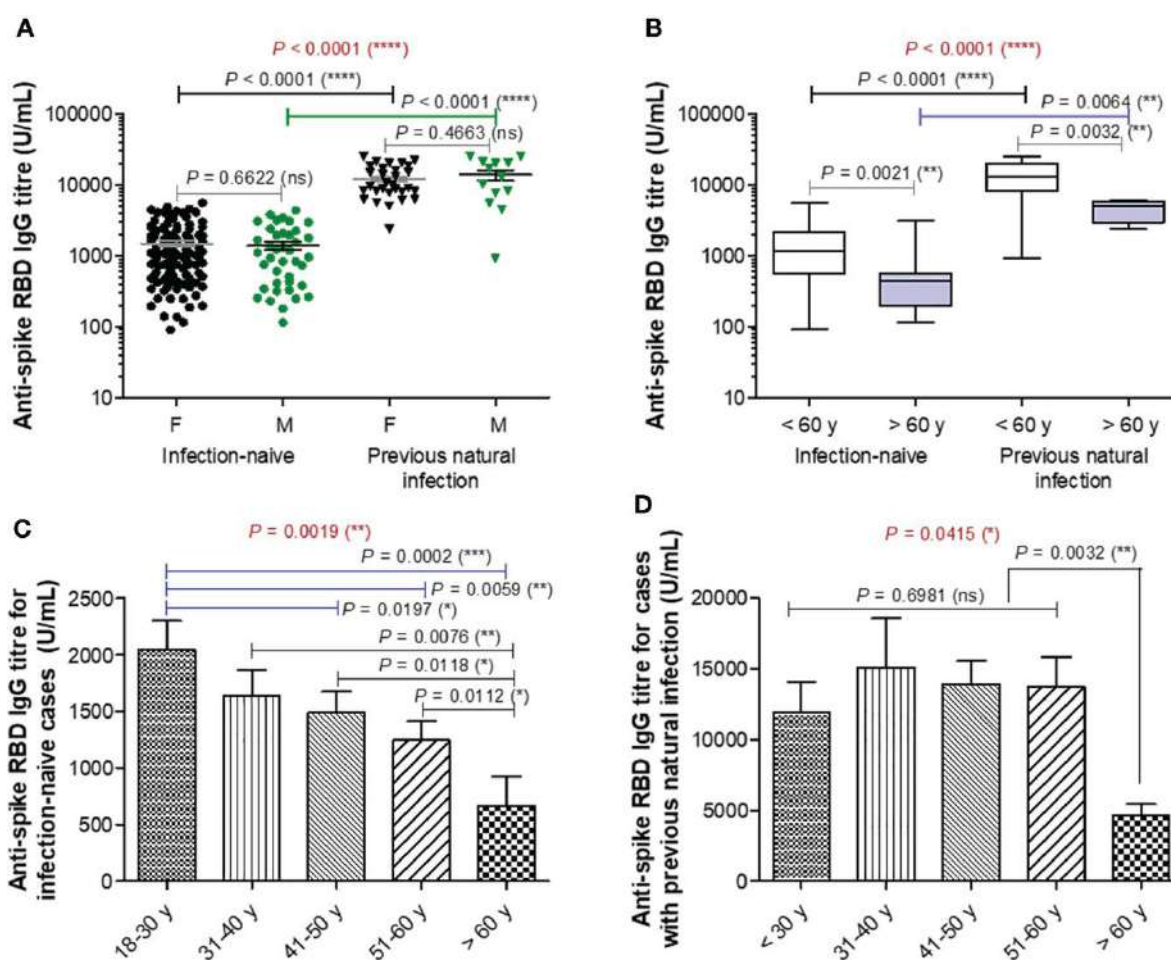


Figure 67. Spike RBD-specific IgG titre after two doses of BNT162b2 (BioNTech-Pfizer) vaccination. (A) Spike RBD-specific antibody titre after two doses of COVID-19 vaccination in both groups of subjects stratified by gender: infection-naïve (109 females, 40 males) and previously infected (30 females, 13 males) cases. The black and grey lines indicate the mean \pm SEM (**** $P < 0.0001$, ns, not significant; two-tailed Mann Whitney and Kruskal-Wallis followed by Dunn's Multiple Comparison tests). (B) Spike RBD-specific antibody titre after two doses of COVID-19 vaccination in both groups of subjects stratified by age: infection-naïve ($n = 149$) and previously infected ($n = 33$) cases. The black and grey lines indicate the mean \pm SEM (**** $P < 0.0001$, ** $P < 0.01$, ns, not significant; two-tailed Mann Whitney and Kruskal-Wallis followed by Dunn's Multiple Comparison tests). (C, D) Spike RBD-specific antibody titre in (C) infection-naïve and (D) infection-primed individuals stratified by

age. Bars indicate the mean \pm SEM (**** $P < 0.0001$, *** $P < 0.001$, ** $P < 0.01$, * $P < 0.05$, ns, not significant; two-tailed Mann Whitney and Kruskal-Wallis followed by Dunn's Multiple Comparison tests).

RBD-specific antibody responses following BNT162b2 dual vaccination do not depend on vitamin D levels

To further elucidate why this almost 2-3 times reduction in the spike RBD-specific antibody titre after vaccination in older subjects, we first investigated the role of vitamin D (25-OH) levels, if any, in controlling the antibody response. Surprisingly, there were no significant differences in the vitamin D serum levels between the two groups ($P=0.2544$, Fig. 68A) infection-naïve (mean value of 22.44 ng/mL) and infection-primed (mean value of 21.01 ng/mL), or between females and males (Fig. 68B).

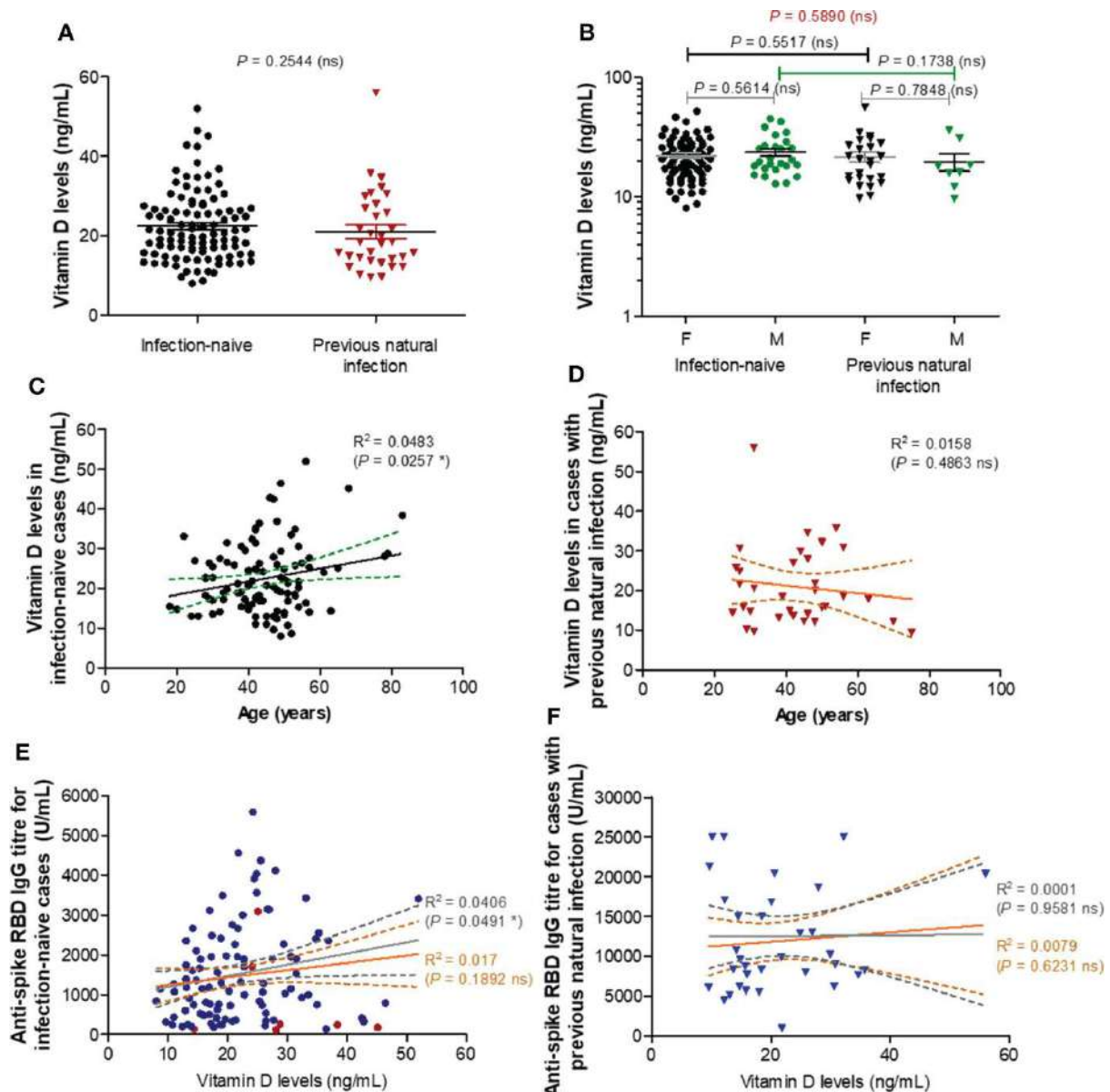


Figure 68. Vitamin D levels moderately correlate with RBD specific IgG antibody titres in individuals under 60 years. (A) Vitamin D levels in the serum collected from both groups of subjects: infection-naïve ($n = 103$) and previously infected ($n = 33$) cases. The black and red lines indicate the mean \pm SEM (ns, not significant; two-tailed Mann test). (B) Vitamin D levels according to gender in infection-naïve (77 females, 26 males) and previously infected (25 females, 8 males) cases. The black

and grey lines indicate the mean \pm SEM (ns, not significant; two-tailed Mann test). (C) The effect of age on vitamin D levels in infection-naïve subjects (R, correlation coefficient; * $P < 0.05$; F test). (D) The effect of age on vitamin D levels in infection-primed subjects (R, correlation coefficient; ns, not significant; F test). (E) The effect of vitamin D levels on the RBD-specific antibody response in infection-naïve subjects (R, correlation coefficient; * $P < 0.05$, ns, not significant; F test). The grey lines correspond to the group of individuals younger than 60 years, while the orange lines indicate the entire infection-naïve group. (F) The effect of vitamin D levels on the RBD-specific antibody response in infection-primed subjects (R, correlation coefficient; ns, not significant; F test). The grey lines correspond to the group of individuals younger than 60 years, while the orange lines indicate the entire infection-primed group.

Within the infection-naïve group, the vitamin D levels revealed a weak correlation with age ($R=0.220$ [95% CI 0.028 to 0.397], $P=0.0257$), as only one subject over 60 years had lower value than the general mean (Fig. 68C). However, this correlation was not seen in the previously-infected group (Fig. 68D). Further, no associations between vitamin D levels and antibody responses were identified in our study groups (Fig. 68E-F), except a weak, but significant correlation observed only among the infection-naïve individuals younger than 60 years ($R=0.201$ [95% CI 0.001-0.386], $P=0.0491$, Fig. 68E). These data clearly suggest that vitamin D levels do not play an important role in assessing the antibody response after BNT162b2 dual vaccination in both infection-naïve and previously-infected individuals.

Serum levels of pro-inflammatory biomarkers (MCP-1, CRP, factor D, PAI-1) decrease after previous infection and BNT162b2 vaccination compared to vaccination alone

As adipose tissue was recently shown to influence both the COVID-19 outcome and antibody generation targeting spike protein of SARS-CoV2 after vaccination or natural infection, we next explored the serum levels of ten well described adipose tissue-related factors: MCP-1/CCL2, CRP, factor D, PAI-1/ SERPINE1, interleukins 6 (IL-6) and 10 (IL-10), adiponectin, leptin, resistin, and TNF- α . Spike-specific antibody titres for cases included in this analysis are shown in Supplementary Figure 1. The first four listed factors (MCP-1, CRP, factor D, PAI-1) showed significant lower levels in the serum of previously infected individuals compared to the infection-naïve people with no significant differences according to gender. For MCP-1 levels within the infection-naïve group, the mean values were 397.5 pg/mL (95% CI 362.9-432.2) for females and 334.8 pg/mL (95% CI 305.1-364.5) for males. By comparison, the corresponding values within the infection-primed group showed an overall 2.3-fold significant decrease ($P < 0.0001$), of 156.4 pg/mL (95% CI 133.0-179.9) and 192.6 pg/mL (95% CI 122.0-263.3), respectively – Fig. 69A. Interestingly, the case with the highest MCP-1 serum levels (1024.96 pg/mL) also associated relatively higher values for the other pro-inflammatory molecules: CRP (2.20 mg/L), factor D (1.66 μ g/mL), PAI-1 (166.58 ng/mL), and antibody titre (3416 U/mL). Regarding the CRP serum levels, the differences were less pronounced, the overall fold-change being only 1.27 ($P=0.0035$, Fig. 69B). For Factor D and PAI-1 the values were reduced by 1.32 and respectively 1.64 times in the infection-primed group when compared to the infection-naïve individuals ($P < 0.0001$, Fig. 69C-D). As the values' distribution of those four biomarkers within the previously-infected group was clearly skewed to the right, we next investigated what those cases with extreme unexpected higher values had in common. Interestingly, those cases were the oldest in the group, being over 60 years. The general reduction of the four biomarkers' values seen in the infection-primed group was only visible within the people younger than 60 years ($P < 0.0001$), while the older group (over 60 years) did not show any change compared to the counterpart infection-naïve cases. Also, while within the infection-naïve group there were no significant differences among the two subgroups of individuals < 60 years old and > 60 years old, within the infection-primed

group the differences were indeed striking ($P < 0.01$). As those four biomarkers showed a consistent decrease in the infection-primed individuals (especially younger than 60 years), we called them as negative factors/ predictors for previous infection.

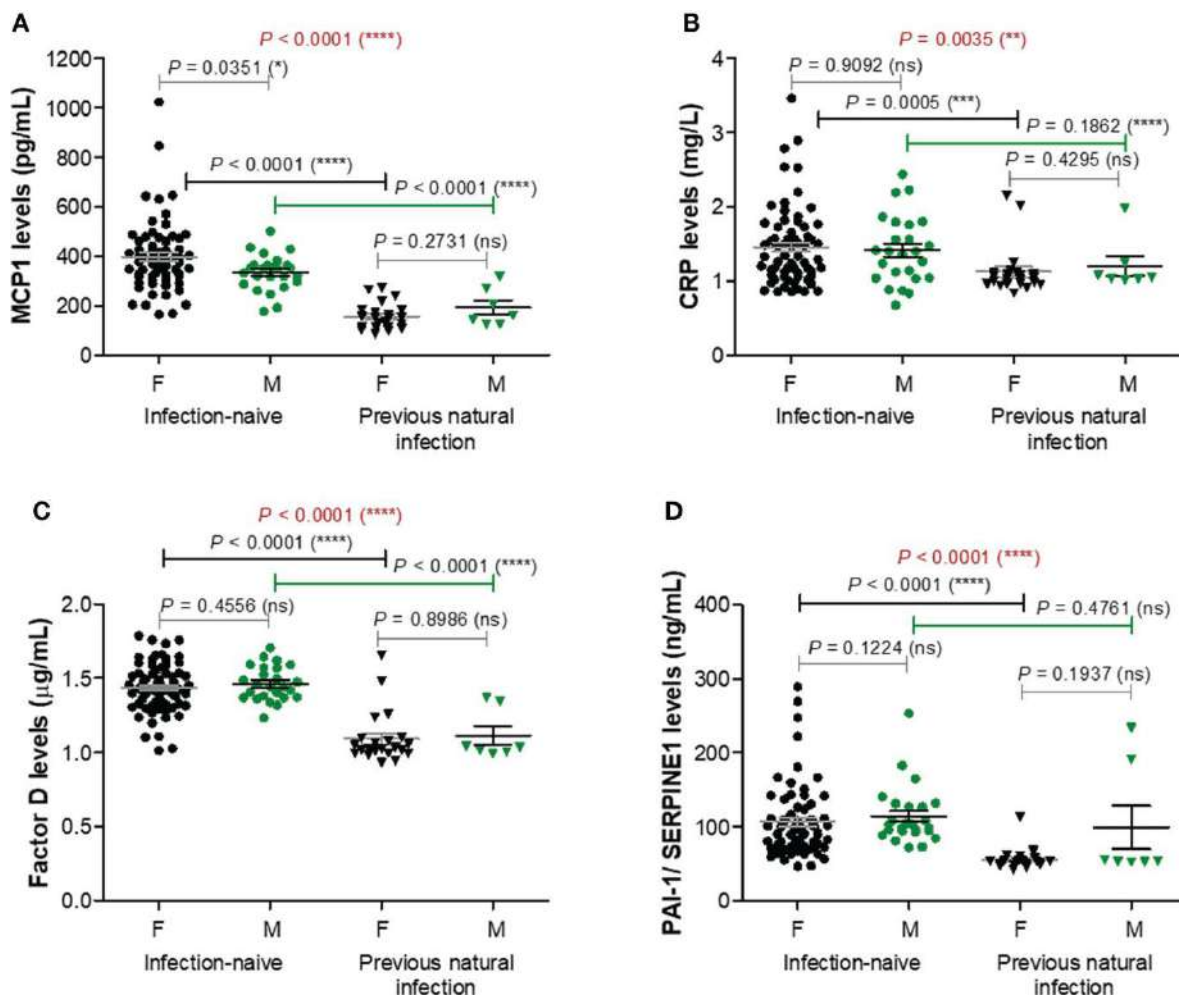


Figure 69. Plasma profile of pro-inflammatory molecules following BNT162b2 vaccination in previously infected or naïve individuals. (A) MCP-1 levels, (B) CRP levels, (C) Factor D levels, and (D) PAI-1/SERPINE1 levels in the serum samples collected from infection-naïve ($n = 92$, 67 females, 25 males) and previously infected ($n = 30$, 23 females, 7 males) cases. The black and grey lines indicate the mean \pm SEM (**** $P < 0.0001$, *** $P < 0.001$, ** $P < 0.01$, * $P < 0.05$, ns, not significant; two-tailed Mann Whitney and Kruskal-Wallis followed by Dunn's Multiple Comparison tests). F, females; M, males.

Serum levels of adipokines (adiponectin, leptin, IL-6, IL-10) increase after previous infection and BNT162b2 vaccination compared to vaccination alone

Among the next studied molecules, IL-6 and IL-10 concentrations were significantly increased ($P < 0.0001$) in the infection-primed group (11.82 pg/mL [95% CI 11.28-12.36] and 26.90 pg/mL [95% CI 25.79-28.01]), compared with the infection-naïve one (9.79 pg/mL [95% CI 9.61-9.97] and 23.30 pg/mL [95% CI 22.86-23.73]); however, IL-6 and IL-10 concentrations were not influenced by gender – Fig. 70A-B. Adipokines like adiponectin and leptin also increased in the infection-primed group. For instance, adiponectin levels were significantly higher by 1.57 times ($P < 0.0001$) in the infection-primed group (5.90 µg/mL [95% CI 5.34-6.47]) when compared to the infection-naïve cases (3.76 µg/mL [95% CI 3.63-3.89]). The adiponectin levels were slightly influenced by gender only in the infection-naïve group:

females had higher values than males (3.86 $\mu\text{g/mL}$ [95% CI 3.70-4.02]) vs. 3.50 $\mu\text{g/mL}$ [95% CI 3.28-3.73], $P=0.0051$, Fig. 70C). Leptin serum levels were also higher in the previously-infected individuals (45.31 ng/mL [95% CI 32.54-58.09]) compared to infection-naïve subjects (31.11 ng/mL [95% CI 25.55-36.67]) and higher in females compared to males within the last group (36.59 ng/mL [95% CI 29.56-43.63] vs. 16.43 ng/mL [95% CI 11.61-21.25, $P < 0.0001$], Fig. 70D). Considering the higher dispersion of values seen among the previously-infected individuals, we next stratified the cases by age. Similar to the case of the first four analyzed biomarkers, the overall increase seen in IL-6, IL-10, adiponectin or leptin serum levels were due to the increase only in the younger group (< 60 years old). The older infection-primed group did not show any change in those adipokines concentrations compared to the counterpart infection-naïve cases. Therefore, significant differences were detected among younger and older individuals within the infection-primed group for IL-6 (12.01 pg/mL [95% CI 11.42-12.60] for < 60 years old vs. 10.65 pg/mL [95% CI 9.53-11.78] for > 60 years old, $P=0.0387$) and adiponectin (6.32 $\mu\text{g/mL}$ [95% CI 5.86-6.77] for < 60 years old vs. 3.32 $\mu\text{g/mL}$ [95% CI 2.07-4.56] for > 60 years old) concentrations. As those four biomarkers increased in the infection-primed individuals (especially younger than 60 years), we called them as positive factors/ predictors for previous infection.

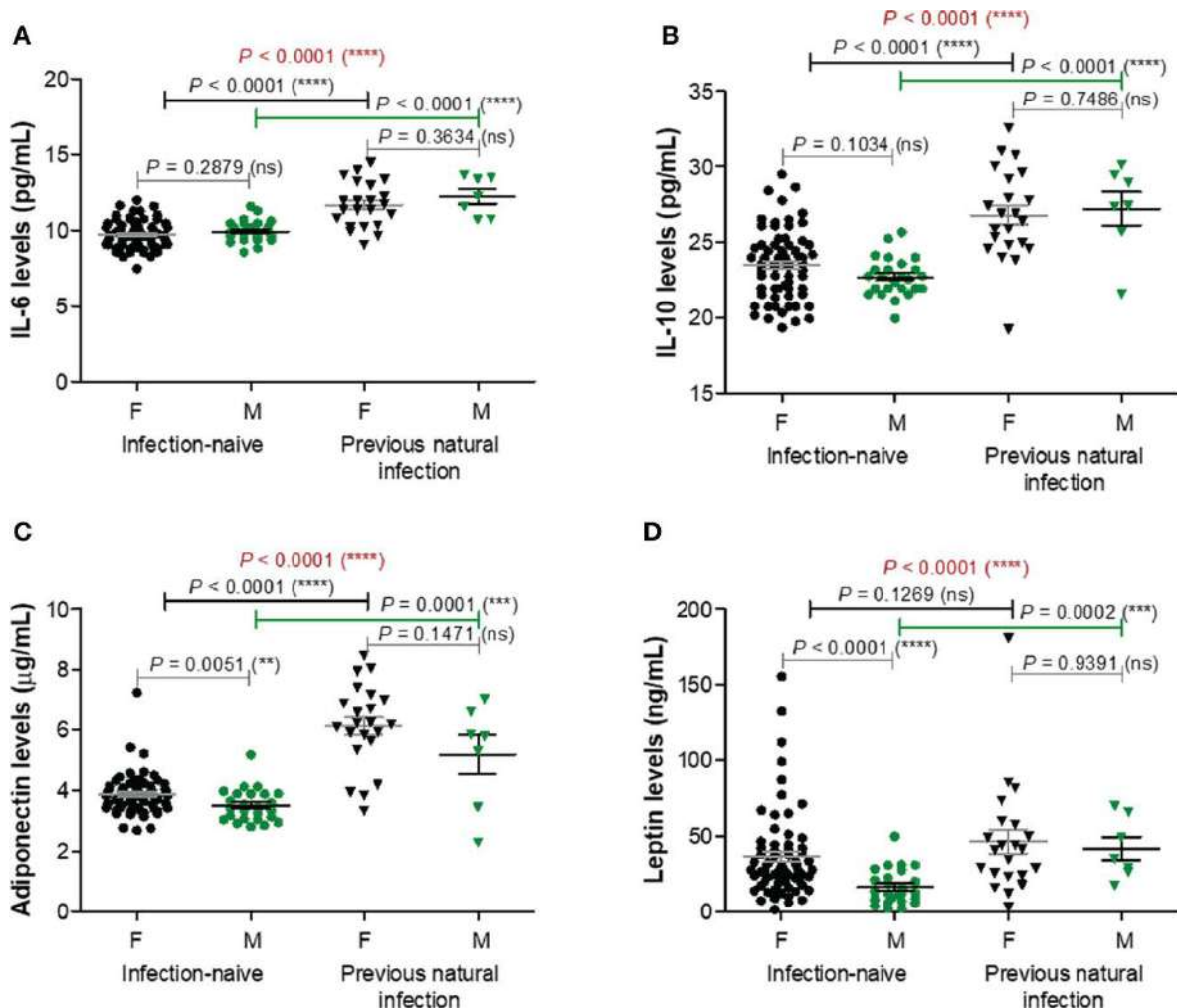


Figure 70. Plasma profile of adipokines following BNT162b2 vaccination in previously infected or naïve individuals. (A) IL-6 levels, (B) IL-10 levels, (C) Adiponectin levels, and (D) Leptin levels in the serum samples collected from infection-naïve (n = 92, 67 females, 25 males) and previously infected (n = 30, 23 females, 7 males) cases. The black and grey lines indicate the mean \pm SEM (** $P <$**

0.0001, ns, not significant; two-tailed Mann Whitney and Kruskal-Wallis followed by Dunn's Multiple Comparison tests). F, females; M, males.

TNF- α and resistin did not show any changes among different studied groups of subjects, except for TNF- α which was only influenced by gender irrespective of the infection status. Overall, these data suggest that the lower vaccination-induced antibody response seen in the older individuals who were previously exposed to natural infection is followed by no-change in adipokine biomarkers. Interestingly, in the case of previously-infected younger individuals, who showed at least 8.8-fold increase compared to their counterparts from the infection-naïve groups associated a significant reduction in the concentration of proinflammatory biomarkers (negative factors: MCP-1, CRP, factor D, PAI-1) concomitant with an increase in the serum levels of other adipokines, such as adiponectin, leptin, IL-6, and IL-10. These observations are important as they might also explain the discrepancies observed in the fold increase of anti-RBD antibody responses caused by previous infection and vaccination compared to vaccination alone in individuals younger than 60 years (8.82, $P=0.0021$) and older than 60 years (6.76, $P=0.0032$) – Fig. 67B.

Serum levels of adiponectin strongly correlate with RBD-specific antibody responses and negatively with age following BNT162b2 dual vaccination in previously-infected individuals

To further assess the association between age or spike RBD-specific antibody responses with various adipokines concentrations, we generated a regression statistical analysis depicted in Figure 5A. In the infection-naïve group, the strongest negative relationships were observed between age and Factor D levels or between age and anti-RBD titre, as expected. Interestingly, Factor D levels revealed a moderate negative dependency on the concentrations of distinct positive factors, while weak or moderate correlations were also noticed between any combinations of positive factors (top right corner in Fig. 71A). However, strong and very strong relationships were revealed between age, antibody response, positive and negative factors within the infection-primed group. While age positively correlated with negative factors and inversely associated with positive factors, the antibody titres mirrored those effects (positive correlations with positive factors and inverse correlations with negative factors). Interestingly the strongest relationship resulted from the inverse association of age with adiponectin levels ($R=-0.736$ [95% CI -0.868 to -0.506], $P < 0.0001$, Fig. 71B). As expected, a significant dependency of antibody response on adiponectin levels was confirmed ($P=0.0372$, Fig. 71B). All four negative factors (MCP-1, CRP, factor D, PAI-1) inversely correlated with adiponectin levels in previously-infected individuals following dual vaccination (Fig. 71C-F). Among them, CRP ($P=0.0009$), factor D ($P=0.0009$) and PAI-1 ($P=0.0005$) levels showed the highest inverse association with adiponectin concentrations. Importantly, while for adiponectin concentrations higher than 4.2 $\mu\text{g/mL}$ (corresponding to individuals younger than 56 years), the variation of CRP (mean 1.021 mg/L [95% CI 0.99-1.05]), factor D (mean 1.03 $\mu\text{g/mL}$ [95% CI 1.00-1.06]), PAI-1 (mean 52.63 ng/mL [95% CI 50.93-54.33]) levels were relatively reduced, adiponectin concentration lower than 5.3 $\mu\text{g/mL}$ (corresponding to individuals older than 56 years) associated an increase of 57.8% in CRP levels (mean 1.61 mg/L [95% CI 1.10-2.12], $P=0.0014$, Fig. 71D), 32.0% in factor D levels (mean 1.36 $\mu\text{g/mL}$ [95% CI 1.14-1.57], $P=0.0009$, Fig. 71E), and 126.3% in PAI-1 levels (mean 119.1 ng/mL [95% CI 57.53-199.7], $P=0.0123$, Fig. 71F). As expected, all four negative factors negatively correlated also with the spike RBD-specific antibody titres (Fig. 71C-F). Overall, these data clearly indicate that, among all investigated adipokines, adiponectin serum levels best correlate with age (negative association) and antibody titre (positive correlation). Our results also suggest that the reduced adiponectin levels seen in older individuals are associated with and might explain the lack of

reduction of the negative factors (MCP-1, CRP, factor D, PAI-1) after dual vaccination, reduction which was noticed only in people younger than 60 years.

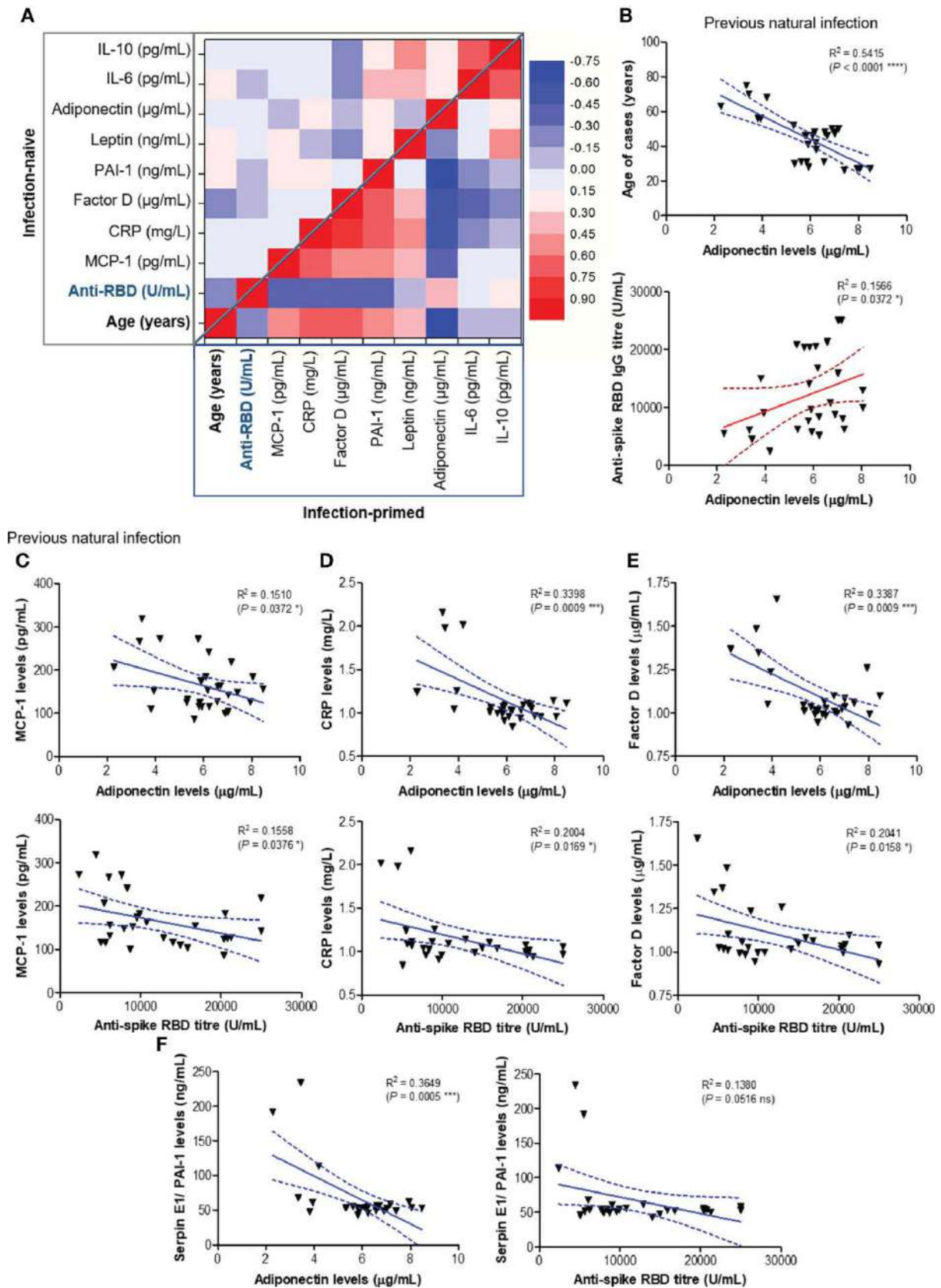


Figure 71. Regression statistics describing the relationship between age, antibody response and various adipokines within the two main study groups: infection-naïve and infection-primed.

Correlation coefficients (R) and statistical significances were computed for each pair of variables. (A) Heat map of R coefficients: left –upper corner corresponds to infection naïve cases, while the bottom-right corner corresponds to infection-primed cases. Linear regression analysis for (B) adiponectin levels and age (top) or adiponectin and RBD-specific antibody titre (bottom); (C) MCP-1 and adiponectin levels (top) or MCP-1 levels and antibody titre (bottom); (D) CRP and adiponectin levels (top) or CRP levels and antibody titre (bottom); (E) factor D and adiponectin levels (top) or factor D levels and antibody titre (bottom); (F) PAI-1/SERPINE1 and adiponectin levels (top) or PAI-1/SERPINE1 levels and antibody titre (bottom) in previously infected individuals. Data are presented as scatter plots with best-fit lines and 95% confidence bands (**** $P < 0.0001$, *** $P < 0.001$, * $P < 0.05$, ns, not significant; Spearman test).

Increased expression of proinflammatory biomarkers with age is associated with adiponectin reduction

At this point, combining those observations with the previous ones, where the antibody response in individuals over 60 years was much weaker and also, the magnitude of antibody increase in the infection-primed group was less than in the case of people younger than 60 years we concluded that the best factors identified to associate with age, showing either inverse (for adiponectin, IL-6, IL-10) or positive (for PAI-1, factor D, CRP) correlation are key in explaining the findings in older subjects, and probably, those relationships are normally present in the general population unexposed to infection or vaccine. Therefore, to validate this hypothesis, we investigated the expression of these factors using the normal tissue data from GTEx database generated before the pandemic. For instance, in fibroblasts, *SERPINE1* mRNA expression (encoding for PAI-1) significantly increased with age ($P=0.0398$, Fig. 72A), as well as in the subcutaneous adipose tissue ($P < 0.0001$), accompanied by a decrease in *ADIPOQ* mRNA expression (encoding for adiponectin, $P < 0.0001$, Fig. 72B). Consistently, in visceral adipose tissue, *CFD* expression (encoding for factor D) increased, while *ADIPOQ* and *IL6* expression diminished with age (Fig. 72C). Interestingly, in lung we only identified *SERPINE1* and *CFD* mRNA expression to change with age, as expected by increasing. All the other factors not shown in Fig. 72 did not significantly correlate with age. This data suggest that the baseline levels of positive factors decrease by age, while the baseline levels for negative factors (proinflammatory biomarkers) increase with age, thus making the older individuals to have an important delay (or blockage) in the dynamic response of key adipokines and consequently a lower antibody titre outcome.

Serum levels of MCP-1, factor D, adiponectin and IL-6 are good predictors for RBD-specific antibody responses within individuals younger than 60 years

We next aimed to define regression-based prediction models for antibody responses following dual BNT162b2 vaccination, starting from the serum concentrations of negative and positive factors (Table 3, Fig. 73). The first proposed model (Model 1-1) investigated the prediction strength of here-in identified negative factors: MCP-1, CRP, factor D and PAI-1. Among those, only MCP-1 and Factor D yielded significant contribution to the model, but only within the age group younger than 60 years (adj. $R^2=0.504$, $P < 0.001$, Table 3). Similarly, among positive predictors (Model 1-2: leptin, adiponectin, IL-6, IL-10), only adiponectin and IL-6 serum concentration proved to significantly contribute to the model within individuals < 60 years old (adj. $R^2=0.500$, $P < 0.001$, Table 3). The combined effect of both positive and negative factors provided only a modest improvement to the model (< 60 years: adj. $R^2=0.569$, $P < 0.001$, Table 3), suggesting that the serum concentration of either negative or positive factors is sufficient to predict the RBD-specific antibody responses within subjects younger than 60 years irrespective of the previous natural infection status.

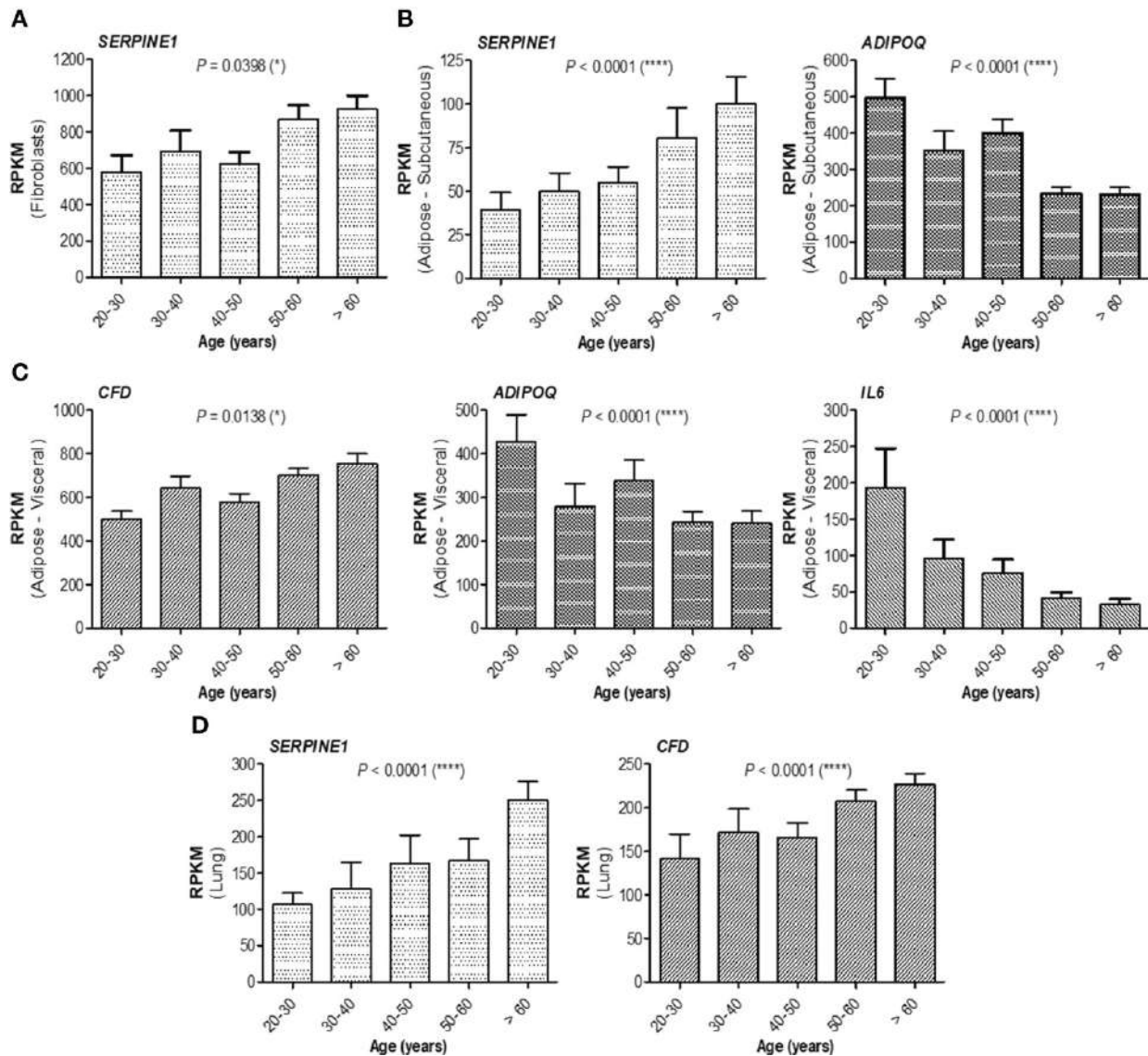


Figure 72. mRNA expression of adipokines collected from GTEx database. (A) mRNA expression of *SERPINE1* in fibroblasts, **(B)** mRNA expression of *SERPINE1* and *ADIPOQ* in subcutaneous adipose tissue, **(C)** mRNA expression of *CFD*, *ADIPOQ*, and *IL6* in visceral adipose tissue, and **(D)** mRNA expression of *SERPINE1* and *CFD* in the lung. The bars indicate the mean \pm SEM (**** $P < 0.0001$, * $P < 0.05$; Kruskal-Wallis test).

Table 3. Statistical evaluation for the indicated prediction models.

Model (linear regression)	R ²	Adjusted R ²	P value (ANOVA)
Negative factors (Model 1-1)			
MCP-1_CRP_Factor D_PA1-1	0.508	0.490	< 0.001
< 60 years	0.522	0.503	< 0.001
> 60 years	0.249	-0.251	0.740
MCP1_Factor D	0.500	0.491	< 0.001
< 60 years	0.513	0.504	< 0.001
> 60 years	0.153	-0.058	0.513
Positive factors (Model 1-2)			
Leptin_Adiponectin_IL-6_IL-10	0.486	0.468	< 0.001
< 60 years	0.510	0.491	< 0.001
> 60 years	0.373	-0.045	0.523

Adiponectin_IL-6	0.485	0.476	< 0.001
< 60 years	0.509	0.500	< 0.001
> 60 years	0.304	0.130	0.235
Combined factors (Model 1-3)			
MCP1_Factor D_ Adiponectin_IL-6	0.572	0.557	< 0.001
< 60 years	0.585	0.569	< 0.001
> 60 years	0.602	0.336	0.177
Factor D_Adiponectin	0.505	0.496	< 0.001
< 60 years	0.524	0.515	< 0.001
> 60 years	0.535	0.419	0.047

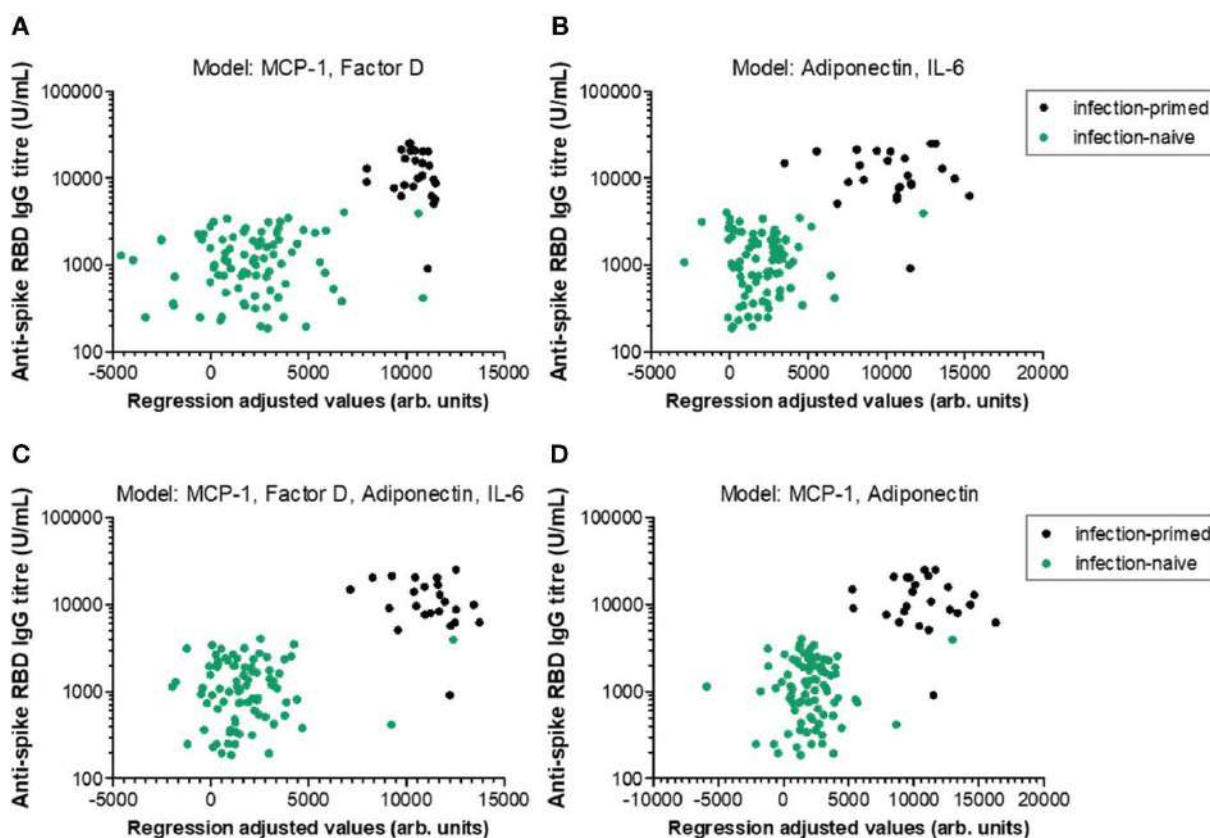


Figure 73. Linear regression models generated to predict the antibody response within individuals younger than 60 years. Antibody responses in relation to regression-adjusted predicted values generated by associating (A) negative factors such as MCP-1 and factor D, (B) positive factors such as adiponectin and IL-6, or (C) combined factors such as MCP-1, factor D, adiponectin, IL-6, or (D) MCP-1 and adiponectin. Infection-primed cases are depicted as black dots, while the infection-naïve cases are shown in green.

Serum concentrations of MCP-1, factor D, and PAI-1 are negative predictors for previous-infection

As the identified negative and positive factors changed significantly in cases with previous infection and vaccination compared to vaccination alone, we next wondered which of them would best predict the infection-primed status in the general population. For this we generated a Receiver Operating Characteristic (ROC) analysis for each negative and positive factor – Table 4. All four negative factors proved to be significant negative predictors for previous infection ($P < 0.0001$), however only MCP-1, factor D and PAI-1 yielded area under curve (AUC) values > 0.8 (MCP-1: 0.966 [95% CI 0.938-0.995]; factor D: 0.914 [95% CI

0.838-0.990]; PAI-1: 0.885 [95% CI 0.787-0.984], Table 4, Fig. 74A). For MCP-1 serum levels, a cut-off value of 272.76 pg/mL, was associated with 0.97 sensitivity and 0.87 specificity, and for factor D levels, a cut-off value of 1.26 µg/mL, was associated with 0.86 sensitivity and 0.90 specificity. However, at a cut-off value of 62.52 ng/mL for PAI-1, the assay achieved the highest specificity of 0.95 (sensitivity 0.86) (Table 4). All positive factors also proved to be good predictors for previous infection (Table 4, Fig. 74B). The highest AUC values were achieved for IL-6 (0.890 [95% CI 0.818-0.963], $P < 0.0001$) and adiponectin (0.876 [95% CI 0.779-0.972], $P < 0.0001$). For IL-6, at a cut-off of 10.67 pg/mL the sensitivity was 0.79 and the specificity was 0.82, while for adiponectin, a cut-off value of 5.26 µg/mL yielded a sensitivity of 0.79 and a high specificity of 0.98. To further validate these results, we next conducted a logistic regression analysis for defining various association models. As such, the association of either both selected negative predictors (model 1: MCP-1_FactorD) or both selected positive predictors (model 2: Adiponectin_IL-6) yielded to an outstanding discrimination for the subjects who had previous natural infection (Fig. 74C). As expected, the model 3 which comprised the first 2 models had the highest AUC value of 0.987 [95% CI 0.972-1.000]. Since age and gender are the most profound confounders in adipokine studies, we included them as covariates in our binary logistic regression models. Interestingly, age and gender provided a light improvement only to the adiponectin-based models (AUC varied from the initial value of 0.876 [95% CI 0.779-0.972] to 0.920 [95% CI 0.852-0.988]). Therefore, these data suggest that infection status may be indeed determined by the expression of negative factors (which is reduced in the infection-primed group) and positive factors (which is increased in the infection-primed group).

Table 4. Statistical evaluation of biomarkers for previous infection prediction.

Analyte	AUC	S.E.	P value	Confidence interval (CI)	Cut-off value	Sensitivity	Specificity
Negative factors							
MCP-1 (pg/mL)	0.966	0.014	< 0.001	0.938-0.995	272.76	0.966	0.870
CRP (mg/L)	0.725	0.053	< 0.001	0.621-0.828	1.11	0.793	0.739
Factor D (µg/mL)	0.914	0.039	< 0.001	0.838-0.990	1.26	0.862	0.902
PAI-1 (ng/mL)	0.885	0.050	< 0.001	0.787-0.984	62.52	0.862	0.946
Positive factors							
IL-6 (pg/mL)	0.890	0.037	< 0.001	0.818-0.963	10.67	0.793	0.826
IL-10 (pg/mL)	0.852	0.046	< 0.001	0.761-0.942	24.50	0.862	0.761
Leptin (ng/mL)	0.677	0.056	0.004	0.567-0.786	28.77	0.690	0.620
Adiponectin (µg/mL)	0.876	0.049	< 0.001	0.779-0.972	5.26	0.793	0.978

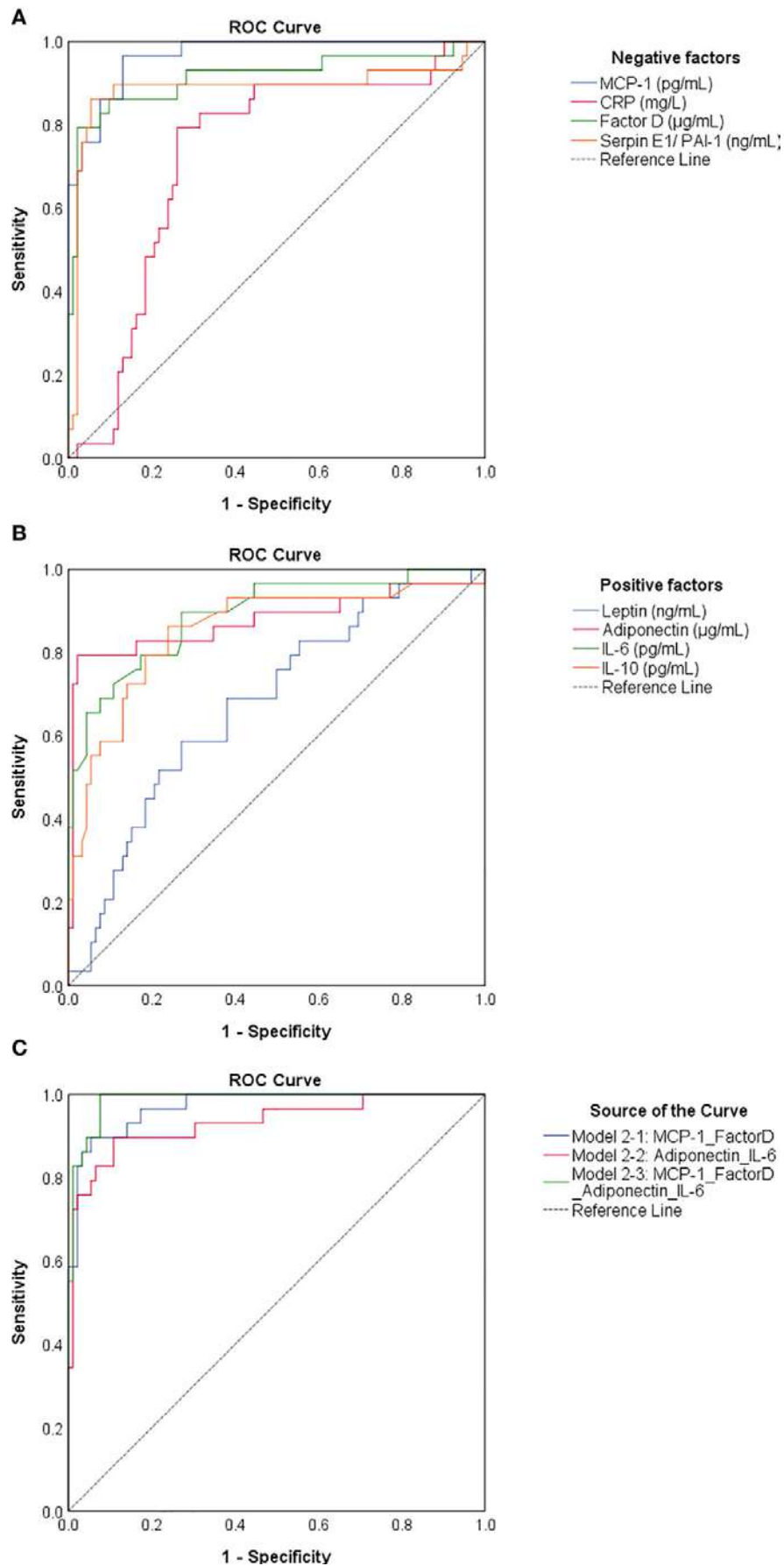


Figure 74. ROC curves generated for negative and positive determinants of previous natural infection. ROC curves for (A) negative and (B) positive determinants. (C) ROC curves related to

various associations of biomarkers. Model 2-1 comprises the values of MCP-1 and Factor D, model 2-2 comprises the values of adiponectin and IL-6, and model 2-3 comprises the biomarkers included in model 2-1 and 2-2. The AUC values between 0.8-0.9 define an excellent discrimination, while the AUC values > 0.9 denote an outstanding capacity of prediction.

2.3.2.5. Discussions

Here we have identified the antibody responses following dual BNT162b2 vaccination in infection-naïve or previously-infected individuals. Despite no significant influence of spike RBD-specific antibody titre by gender, we found a significant lower antibody response in individuals over 60 years, effect more pronounced within the previously-infected group of participants. A recent study performed in the United Kingdom (UK) reported an important impairment in the immune response among older people (> 65 years old) only in the infection-naïve group, while similar high antibody titres were noticed irrespective of age in the infection-primed group (Tut et al., 2022). These discrepancies seen between our results and the data from the UK population are very interesting and may be due to several reasons. First, the UK study included in the analysis only blood samples collected at 6 days after second vaccination, while in our study the samples were collected at a median of 75 [IQR 47-91] days. Second, the vaccination scheme differed between the two studies: in our research the second vaccination was performed at 21 days after the first dose as imposed by our national regulations, while in the UK, due to limited availability, the second dose's administration was delayed up to 3 months by the UK authorities (Azamgarhi et al., 2021). Nevertheless, any differences in the genetic background between UK and Romanian nationals may contribute to this outcome. Importantly, other studies also confirmed a higher magnitude of antibody response in previously-infected compared to naïve individuals after BNT162b2 vaccination (Eliakim-Raz et al., 2021; Muenza et al., 2022; Nomura et al., 2021).

To understand the differences in humoral immune responses between younger and older people, we next investigated the role of vitamin D. This was important, as vitamin D deficiency (< 20 ng/mL) was largely reported to influence the severity of COVID-19 (Alberca and Alberca, 2022; Kaya et al., 2021), as it is known to be associated with an increase in inflammatory cytokines (Peterson and Heffernan, 2008; Weir et al., 2020) and thrombotic episodes (Giannis et al., 2020; Mohammad et al., 2019). However, more recent studies performed on nationwide cohorts were not able to identify any association between vitamin D deficiency and hospitalization or mortality due to COVID-19, suggesting that is still insufficient scientific evidence for the role of vitamin D levels in COVID-19 infection (Lin et al., 2022; Tomaszewska et al., 2022). Other studies investigated the dependency of antibody response following vaccination with SARS-CoV-2 vaccines on vitamin D concentration and found no significant association (Chillon et al., 2021; Inserra et al., 2021). In our work, we only revealed a weak, but significant correlation between vitamin D serum levels and antibody titres following BNT162b2 vaccination in infection-naïve individuals younger than 60 years. Surprisingly, most of the individuals over 60 years included in our research had higher vitamin D concentrations than the general mean of 22.10 ng/mL [95% CI 20.56-23.63].

Little is known about the relationship between adipokines and humoral immune responses following vaccination with SRAS-CoV-2 vaccines. Adipokines are mainly produced by adipose tissues (subcutaneous and visceral) and are known to influence the immune system in multiple ways. For instance, adiponectin has anti-inflammatory actions as it suppresses the synthesis of pro-inflammatory cytokines (TNF- α , IL-6, and MCP-1) by monocytes/macrophages (Ohashi et al., 2010; Tsatsanis et al., 2005; Wulster-Radcliffe et al., 2004), while inducing the production of anti-inflammatory mediators like IL-1 receptor antagonist and IL-10 (Wolf et al., 2004). On the other hand, leptin, a pro-inflammatory adipokine induces the production of TNF- α , IL-6, and IL-10 by human B cells *in-vitro*

studies (Agrawal et al., 2011). There are also cross-regulations, as IL-6 acts on adipose tissue to promote leptin secretion (Han et al., 2020). PAI-1 is another adipokine with the main role in suppressing intravascular and tissue fibrinolysis, and such, high levels are associated with deregulated vascular coagulation and endothelial dysfunction (Sillen and Declerck, 2021). Elevated PAI-1 circulating concentration also causes insulin resistance contributing to developing a metabolic syndrome, and may, in turn, be influenced by multiple cytokines, growth factors and hormones (Birgel et al., 2000; Sillen and Declerck, 2021). Interestingly, it has been recently shown that PAI-1 also promotes a respiratory innate antiviral immunity (Dittmann et al., 2015; Zelaya et al., 2016). In our study we have identified several differences in the circulating levels of multiple adipose tissue-related factors between infection-naïve and infection-primed individuals. Of note, previously-infected subjects had higher levels of adiponectin and leptin which were correlated with higher IL-6 and IL-10, potentially reflecting polarization towards Th2 responses which rather boost the humoral immune responses (antibody production) and impede the cellular immunity. As such, IL-10 is a key cytokine involved in B cell activation, proliferation, antibody production, and class-switch towards IgG₁ and IgG₃ (Briere et al., 1994; Itoh and Hirohata, 1995; Moens and Tangye, 2014). However, these hypotheses require validation in future in-depth studies. Furthermore, increased adiponectin levels were also associated with a reduction in several pro-inflammatory molecules: MCP-1, factor D, CRP and PAI-1, indicating a potential suppression of innate immunity. In the UK study, the MCP-1 levels did not change, and only TNF- α and CXCL10 increased in infection-primed subjects at 6 days post-vaccination suggesting a potential polarization towards a Th1 phenotype (Tut et al., 2022). Interestingly, our observed changes were only present in individuals younger than 60 years. The older individuals might develop suboptimal immune responses as they seemed not to be responsive to those triggered molecular changes caused by previous infection and vaccination, and thus, explaining the relatively lower raise in antibody response observed in this category compared to the younger group. This observation might be important, also because it is known that adipokine dysfunction is another factor associated with aging and may induce various metabolic changes by promoting a low-grade inflammation (Cobos-Palacios et al., 2022; Mancuso and Bouchard, 2019). It has been shown that circulating concentrations of adiponectin either increase (Mancuso and Bouchard, 2019; Obata et al., 2013) or do not change with age (Coimbra et al., 2014). Surprisingly, the mRNA expression for adiponectin was reduced in the adipose tissue from the subjects included in the GTEx database. This observation might imply the fact that, despite a general lower synthesis of adiponectin by adipose tissues, there is less clearance due to adiponectin resistance. Of course, one of the important questions still remains to be addressed in future research in the context of COVID-19 infection: is it desirable an intense Th2 response with humoral immunity or a Th1 phenotype that augments the cellular immunity? Among all studied biomarkers, circulating MCP-1 and factor D acted as negative factors, while adiponectin and IL-6 as positive factors in predicting the magnitude of antibody response following dual BNT162b2 vaccination within individuals younger than 60 years. Interestingly, for determining the previous infection status, circulating MCP-1, factor D and PAI-1 proved to be excellent negative predictors. By contrast, adiponectin and IL-6 serum levels positively associated with the previous exposure status.

Our study has some limitations. Firstly, we did not have access to the information regarding the exact time or severity of the infection in the previously-infected individuals. However, the vaccination was performed at least 90 days post-disease as recommended by local authorities, and as the samples were collected at 2-3 months after dual BNT162b2 vaccination (performed at 21 days interval), we can argue that the RBD-specific antibody responses produced by vaccination did not confound with the antibody levels produced by infection. Secondly, we did not store the information about the body mass index or additional

comorbidities at the time of blood sample collection, information which is expected to impact on our analysis. Still, we had access to the retrospective hospital database, and identified that around 9% of included subjects were recorded with obesity, figure similar to the one reported recently (in 2019) for obesity prevalence in our country by the Eurostat data. Of note, the previously-infected individuals included in our research are those that survived to the primary exposure. Additionally, some subgroups included a limited number of individuals, as this study was designed as a retrospective analysis of prospectively collected samples.

Final remarks

Our data are of importance as they reveal the humoral immune responses following standard dual vaccination at a 2-3 months interval (median of 75 days). Here, we have identified that people over 60 years show lower antibody responses compared to the younger counterparts, irrespective of the infection status. Additionally, we show that vitamin D has a limited association with the amplitude of anti-RBD responses and only in younger infection-naïve individuals (not previously exposed to natural infection). Importantly, previously-infected individuals showed higher extent of antibody titres which were associated with higher levels of circulating adiponectin and lower concentrations of pro-inflammatory biomarkers (MCP-1, factor D, c-reactive protein (CRP), plasminogen activator inhibitor 1 (PAI-1)), but only in people younger than 60 years.

Older subjects had suboptimal antibody responses, suggesting that new vaccine designs might be required to offer a better protection for this category of individuals more susceptible to develop severe forms of COVID-19. Still, it might be necessary to even consider adjusting the vaccination scheme (only 21 days or more?) in order to achieve the desired protective immune responses. Nevertheless, this study was set as a starting point for defining the serum levels of various cytokines upon anti-SARS-CoV-2 vaccination or COVID-19 infection, and thus, it represented a good indicator when comparing the levels of cytokine secretion in the breastmilk of vaccinated or infected mothers with serum concentrations in the study of Trofin et al (Trofin et al., 2022).

SECTION II. FUTURE DIRECTIONS IN TEACHING, MEDICAL AND SCIENTIFIC ACTIVITIES

Perspectives in the teaching and medical activities

The medical academic activity requires a permanent training and continuous professional and didactic self-improvement by updating the knowledge in the field. Immunology, and also medicine in general, is a field of rapid expansion as many unknowns are still being discovered every day. Thus, I believe it is important for my future progress to stay current on both immunological and medical information, involving ongoing individual study and active participation to multiple national and international conferences and/or scientific meetings. Knowing the latest news in the field is mandatory for every medical teacher as this profession is constantly evolving and, therefore, we have the duty to prepare responsible and well-trained doctors for the future.

With respect to students, but also to this virtuous teaching profession, the quality of the training act has to be regularly improved and adjusted to the students' requirements. For this direction I plan to participate to post-graduate pedagogical/ educational courses and encourage the organization of academic exchanges between different national/ international universities. For receiving a feedback regarding the efficiency of my teaching act and also for improving the teaching-learning-evaluation process, I will perform periodic students' evaluation through tests that include key questions from the subjects learned during those classes.

As the information technology is now part of everyone's life, it is important to include it in our teaching strategies in order to attract the students' attention and raise their interest for the subject we are teaching them. Nevertheless, one should constantly integrate the novelties with the classical fundamental concepts in the field. Thus, I intend to extend the use of e-learning materials (illustrations, short-videos related to immunological information) in a dynamic classroom environment that promotes various discussions and debate between students, making them active participants in the teaching act. I also intend to develop an interactive specialized site with didactic purpose, which will allow access to various informative materials organized thematically and which would promote the individual study by daily/ weekly short queries.

Regardless of the studied field, encouraging critical thinking is a key component of the education process. It is our responsibility to identify the students that think out of the box, that show curiosity and constant self-improvement, and stimulate their knowledge and skills in solving various practical dilemmas. This is the first step in helping and promoting them to address various scientific questions from different perspectives, to critically read and interpret the scientific data presented in various manuscripts, and identify the missing spots that requires further research investigation. Further, they should be encouraged to actively attend students' scientific meetings and present their scientific questions and interest.

Teaching resident doctors from the Laboratory Medicine and Clinical Microbiology specialties is also part of my daily activities and a responsibility for properly training the next generation of doctors. The diagnosis tools are rapidly evolving and it is important to teach them to be prepared to successfully handle all the available techniques and treat every single case with responsibility and commitment, as often, the clinical diagnosis relies mainly on the laboratory tests. Also, as part of their training, apart from providing detailed explanations and guiding them step-by-step in the lab, we also consider it crucial to challenge them with individual study for preparing presentations on various subjects, and to encourage them to attend regular scientific meetings. We are also involving students and young doctors in the ongoing research projects and stimulate them to disseminate the achieved scientific results. As immunology and molecular biology are tightly linked to the others subdomains of Laboratory

Medicine (Virology, Microbiology, Biochemistry, Haematology) it is mandatory to collaborate with the other academics involved in the training process for the benefit of the forming doctors. This would promote a co-evolution of the academic teams involved in the teaching process, as well as providing opportunities for future common projects and collaborations.

The perspective directions outlined here are grounded on continuous professional and academic growth that can be achieved only by providing a strong support and valuable training to every generation of students and forming doctors, with the aim of setting-up excellent professionals.

Perspectives in the scientific activities

Scientific research activities are a must for any university which promotes excellence in education and training at graduate and post-graduate levels. My previous scientific expertise, research achievements and interests, as well as the well-established collaborations within the university and at the national/international level, form the foundation for my future research plans and directions. To begin with, I intend to continue and develop the research directions I have started during my postdoctoral time at Cambridge University and UMF Iasi in the fields of autophagy and immunobiology, and explore new and promising ones, while involving PhD students from various specialties.

Securing funds for research is an important component of the scientific activity. For assessing the necessary funds, I consider continuing to apply to the CNCS-UEFISCDI national competitions and to European grants specifically dedicated to young researchers, such as the Grants for Young Teams (TE), Exploratory Research Projects (PCE) or European Research Council Starting Grants (ERC). I also intend to apply, together with my future PhD students, to internal grants offered by *Grigore T. Popa* University of Medicine and Pharmacy Iasi, which would ensure the achievement of robust preliminary results required for funding competitions at national and international levels.

The main research directions will focus on the role of autophagy on regulating the functions/ activity of various immune cells in different physiological (e.g., ageing) or disease contexts (from haematological malignancies and solid cancers to autoimmunity or neurodegeneration) and are highlighted in the next paragraphs.

The role of autophagy in regulating the activity of NK cells in blood and solid cancers

The potential beneficial results of a new approach in blood cancers, by combining the conventional anti-tumour drugs with autophagy inhibitors have been recently released from phase I clinical trials (Rothe et al., 2019). For solid cancers, there is mounting preclinical evidence that targeting autophagy can enhance the efficacy of many anti-cancer therapies. Hydroxychloroquine (HCQ) is the first clinically-approved autophagy inhibitor, and preclinical trials have shown that HCQ alone and in combination therapy leads to enhancement of tumour shrinkage. Further phase II trials have shown promising effects for HCQ in Kras-mutated lung cancers, while chloroquine was associated with positive results in two out of three breast cancer trials (Mohsen et al., 2022).

Autophagy (literally “self-eating”) is an evolutionarily intracellular degradative pathway that is paramount to the cellular and organism homeostasis, as they promote adaptation to various adverse metabolic stresses, such as nutrient deprivation, hypoxia or increase in cell proliferation (Menzies et al., 2017a). This process requires the formation of double-membrane vesicles (autophagosomes) that engulf the cytoplasmic components and eventually fuse with late endosomes (to form amphisomes), and lysosomes (to form autolysosomes) - *2016 Nobel Prize in Physiology or Medicine*. The physiological relevance of autophagy is related to the

normal turnover of the cellular components and the clearance of misfolded long-lived proteins or damaged organelles (Pavel et al., 2016; Wu et al., 2016). In immunity, the relevance of autophagy in the development and functionality of the cellular components of the specific immune system (B and T cells) is well established (Munz, 2016b). Conversely, **whether autophagy also plays an important role in the homeostasis of nonspecific immune system cells, such as natural killer (NK) lymphocytes (a subset of innate lymphoid cells - ILC), has long remained elusive.** Recent studies suggest a protective role for autophagy in the development and maturation of NK cells, as genetic ablation of essential components of autophagic machinery (Atg5 – autophagy-related gene 5) in ILC populations (including NKs) results in progressive accumulation of damaged mitochondria and over-generation of reactive oxygen species (ROS), all leading to cell death (Lopez-Soto et al., 2017).

NK cells are defined as CD3⁻ CD56⁺ CD16^{+/-} cells and based on the membrane density of these molecules, the cells are divided in two subsets: *i*) the most prominent - the cytotoxic subset (90%), characterized by high CD16, low CD56 expressions (CD56^{low}CD16^{high}) and high levels of perforins and granzyme granules, and *ii*) the subset of smaller percentage (10%), characterized by low density or absence of CD16 molecule, high CD56 expression (CD56^{high}CD16^{low}) and increased capacity to produce and secrete cytokines, including interferon-gamma (IFN- γ), tumour necrosis factor (TNF- α), interleukins (IL-10, IL-13) and colony-stimulating factors (GM-CSF). While the CD56^{low}CD16^{high} cells are involved in NK-mediated cell lysis, the CD56^{high}CD16^{low} subset has a greater potential for migration and is recruited within the tumour tissue (Chiossone et al., 2018).

The main function of NK cells is to discriminate between normal and malignant cells based on the cell membrane expression of MHC (major histocompatibility complex) class I molecules. This process is consequent to the fact that NK cells are equipped with multiple activating and inhibitory receptors. Amongst them, the ones named KIR (Killer Immunoglobulin-like Receptors) play a key role in controlling tumour growth and metastasis (Gonzalez-Rodriguez et al., 2019). KIR is a family of 15 closely linked genes and highly polymorphic, organized into two major haplotypes, called AA and Bx and, thus, each individual inherits a combination of various KIR genes. Therefore, according to the "missing-self" hypothesis, NK cell activation occurs in contact with malignant transformed cells, which have lost the expression of MHC class I molecules and which, in addition, have acquired stress-induced ligands for NK-activating KIR receptors (Gonzalez-Rodriguez et al., 2019)..

Recent studies have reported that autophagy is involved in the degradation of cellular receptors *via* their interaction with autophagosomes, performed in a direct or adaptor-mediated manner (Pavel and Rubinsztein, 2017). The possibility of **manipulating the expression of KIR receptors** on the NK surface could, at least theoretically, **define novel strategies for amplifying the process of recognition and killing of malignant cells by NK.** However, strategies to improve the *in vivo* NK efficiency in recognizing malignant cells are still yet to be developed (Fang et al., 2018).

The general questions I intend to address for this research direction are: *What is the role of autophagy in regulating the membrane expression of KIR receptors and other regulatory molecules in NK cells? What are the implications of this regulation in cancer?*

This research study would involve two interconnected directions: computational/bioinformatics analysis together with experimental work.

- i) **Computational/bioinformatics analysis:** this work requires the identification of regulatory molecules (involved in controlling the lymphocyte activity) which may act as potential autophagy targets, by using various methods of structural biology analysis. Starting from the mathematical models presented in this thesis, I intend to build new

ones that would describe the complex interactions of activating and inhibitory signals that governs the general lymphocyte activity.

- ii) **Experimental work** would involve multiple techniques available in the Laboratory of Immunology through the CENEMED project. This would allow for the flow-cytometric analysis and sorting of various subsets of lymphocytes (NK, NKT, T cells) that can be further investigated for determining the basal and stimulated levels of autophagy and identify the differences between control and patient groups, or between various subgroups of patients (e.g. with favorable vs. poor clinical outcome) in terms of autophagy and receptors' expression under these circumstances. For this, we could use the digital droplet PCR technology to perform multiplexing for revealing the variations in autophagy gene expression at a single cell level, and flow-cytometric analysis for identifying the expression of the investigated molecules on immune cells.

The role of mechanical cues and YAP/TAZ mechanosensors in regulating cytokine secretion by immune cells

Mechanical cues and inflammation. Mechanical signal transduction underpins the activation and resolution of protective immune responses, as well as it plays a central role in the immune system dysfunction. Indeed, the importance of this research field started to be revealed recently, emerging from the concept that the immunological synapses take place in a dynamic environment: cellular motion, bulk fluid flow and the local ECM stiffness (Huse, 2017). In all tissues, inflammation can be initiated and propagated by ECM disruption. Firstly, molecules of ECM newly liberated by injury or inflammation include hyaluronan fragments, tenascins, and sulphated proteoglycans that act as “damage-associated molecular patterns” (DAMPs). Those DAMPs are recognized by specific PRRs on various inflammatory cells, which, activated, further damage the ECM by releasing cytokines, chemokines, proteolytic enzymes and oxidative metabolites. Nevertheless, the ECM can also regulate inflammation by sequestering the growth factors, cytokines, and chemokines, or affecting inflammatory cell migration.

It is now known that the lymphocyte activation, consequently to the immunological synapse formation, is a mechanosensitive process (Liu et al., 2014). Immune cells sense and exert force against their environment through dynamic cytoskeletal remodelling and, in most cases, the coupled action of the filamentous (F-actin) cytoskeleton and the myosin-II motors bears with the mechanical load. In line with this concept, experiments in which T cells were stimulated on deformable matrices coated with activating ligands revealed that lymphocytes exhibit stronger signalling and cytokine secretion on stiff surfaces compared to the soft ones (Wan et al., 2013).

However, while these studies focused on understanding the role of mechanical forces in mediating the intracellular signalling and cytokine production of immune cells (lymphocytes, antigen-presenting cells), the roles of applied forces in controlling the secretory output of tissue resident-cells (non-immune) are completely unknown.

Mechanical cues and cancer. The mechanism behind these mechanical signals (of contact inhibition or cell shape deformation generated by the pulling forces of the ECM) has only recently been linked to Hippo signalling (Aragona et al., 2013a; Zhao et al., 2007b), a pathway comprising two interconnected core modules: kinases (MST1/2, LATS1/2 kinases) and transcriptional regulators (YAP/TAZ co-transcriptional regulators and TEADs transcription factors). When cells are at low density and are flat/well-spread on a stiff extracellular matrix (ECM), YAP/TAZ localize in the nucleus and are active, while when the cells are round/compact at high cell density or plated on soft matrix with minimum adhesion area to the

ECM, YAP/TAZ are redistributed to the cytosol and are inactive (Aragona et al., 2013a; Dupont et al., 2011b). The activation of the Hippo transcriptional module is strongly associated with malignant transformation (epithelial-mesenchymal transition, loss of cell polarity) and cancer progression (Harvey et al., 2013; Yu et al., 2015).

Inflammation and cancer linked via intracellular signalling. Inflammation plays decisive roles at different stages of cancer development, from initiation, malignant transformation, to overgrowth, invasion and metastasis. For example, infections with hepatitis B (HBV) or C (HCV) viruses increase the risk of hepatocellular carcinoma (HCC) through establishing persistent infections associated with low-grade, but chronic inflammation. A completely different type of inflammation is the one intrinsic to solid tumours, when certain oncogenes, such as RAS or MYC family members, induce a transcriptional programme that leads to remodelling of the tumour microenvironment through recruitment of immune cells and expression of tumour –promoting chemokines and cytokines (Soucek et al., 2007; Sparmann and Bar-Sagi, 2004). Apart from the immune and cancer cells, the tissue-resident cells (including the mesenchymal, endothelial cells) also control and shape the tumour growth in autocrine and paracrine manners via direct cell-cell interaction and cytokine/ chemokine production. This is important, as the cytokines and chemokines expression profiles of the tumour microenvironments may be more relevant than its specific immune cells content. Different cytokines can either promote (IL-6, IL-8, IL-17, IL-23) or inhibit (IL-12, TRAIL, IFN γ) tumour development and progression, regardless of their source via various downstream effectors such as the NF-kB, AP-1, STAT, SMAD transcription factors and YAP/TAZ co-transcriptional regulators (West et al., 2015). In colorectal cancer and HCC, the tumour-promoting effect of IL-6 is mainly exerted via STAT3 activation (Park et al., 2010), but recent studies have shown that it also triggers activation of YAP/TAZ via a gp130-STAT3-independent mechanism to stimulate epithelial cell proliferation and aberrant differentiation (Taniguchi et al., 2015). Indeed, YAP depletion restores hepatocyte differentiation and causes pronounced tumour regression in a genetically engineered mouse HCC model. Paradoxically, YAP activation via LATS1/2 depletion can repress tumour growth by improving the anti-tumour immunity via a type I interferon-Toll-like receptors response in melanoma (B1), breast tumour (4T1) and head-neck carcinoma (SCC7) mouse models (Moroishi et al., 2016).

Considering the complexity of YAP/TAZ co-transcriptional regulators in promoting both the tumour growth and the anti-tumour immunity, it is important to clarify the role of tissue-resident and cancerous cells in modulating the expression and activity of these co-transcriptional factors: Are the cytokines and other soluble factors involved? What are the effects of ECM or cell-cell interactions on cytokine production?

Based on this scientific facts, my current hypothesis that requires further work for validation is that a prolonged applied mechanical stress promotes the production and secretion of various soluble factors such as cytokines and growth factors which in turn act via autocrine and paracrine signalling to reverse the normal contact inhibition state and up-regulate/activate the co-transcriptional regulators YAP and TAZ to induce cell proliferation and migration, key characteristics for malignant transformation. Therefore, these **specific research questions** need to be addressed:

1. *What is the role of mechanical stimuli in regulating cytokine transcription and secretion? If any, what are the intracellular mechanisms involved?*
2. *What are the paracrine/autocrine biological consequences of mechanical-induced cytokine production? What are the cytokines involved in the on-off switch of Hippo-YAP/TAZ signalling? Are these biological changes interconnected with alterations of other intracellular signalling pathways?*

This research work would involve a dual analysis of using invitro experimental setup with bioinformatics tools.

- i) The **experimental work** would involve the analysis of the role of various mechanical stress in regulating the cytokine production, while using various benign/ malignant cell lines or peripheral immune cells isolated from patients with solid cancers. The cytokine production could be determined either through serological methods (ELISA, Luminex) or by gene expression analysis using qRT-PCR. The cytokine secretion will be further correlated with YAP/TAZ expression identified by immunofluorescence experiments. If successful, co-culture experiments (isolated immune cells together with cancer cells) in a stiff 3D setup which mimics the tumour environment would be the next step in our research.
- ii) The **bioinformatics analysis** would allow defining the intracellular pathways that interconnect the identified hubs (cytokines, YAP-TAZ) and establish new links. This work would be further integrated into defining mathematical models that are able to dissect the dynamic non-linear nature of the living cells. The results will also be integrated using the already available data bases of single-cell RNA-Seq available for various cancer pathologies.

Overall, I intend to develop research activities that are lined up with the international standards and promote a valuable, robust and good science.

Final remarks

I finally believe that the most beautiful results in an academic career may be achieved only with a team effort and an endless scientific curiosity, dedication and professionalism. This habilitation thesis summarises the most fruitful professional, academic and scientific achievements during my postdoctoral period (2016-2023) that form the basis for the future projects.

Given the opportunity to select, instruct and coordinate talented PhD students during their journey into science, motivates me further to continue my dedication for research and academic career. Being a member of the *Grigore T Popa* University of Medicine and Pharmacy of Iasi is not only an honour, but also an important responsibility to increase the visibility and promote its value at the international levels by continuing my current collaborations and extending them in the future. These collaborations are not only beneficial to our discipline, department or faculty, but also to the future PhD students, as they are the best way to increase the chance in accessing various national and international funds, to participate in exchange programmes and achieve high visibility.

SECTION III. REFERENCES

- Aanei, C.M., Jacob, M.C., Veyrat-Masson, R., Picot, T., Rosenthal-Allieri, M.A., Lhoumeau, A.C., Ticchioni, M., Dumezy, F., and Campos Catafal, L. (2018). Database-guided Flow-cytometry for Evaluation of Bone Marrow Myeloid Cell Maturation. *Journal of visualized experiments : JoVE*.
- Ades, L., Itzykson, R., and Fenaux, P. (2014). Myelodysplastic syndromes. *Lancet* 383, 2239-2252.
- Agrawal, S., Gollapudi, S., Su, H., and Gupta, S. (2011). Leptin activates human B cells to secrete TNF- α , IL-6, and IL-10 via JAK2/STAT3 and p38MAPK/ERK1/2 signaling pathway. *J Clin Immunol* 31, 472-478.
- Aguiar Junior, S., Oliveira, M.M., Silva, D., Mello, C.A.L., Calsavara, V.F., and Curado, M.P. (2020). Survival of Patients with Colorectal Cancer in a Cancer Center. *Arq Gastroenterol* 57, 172-177.
- Alberca, G.G.F., and Alberca, R.W. (2022). Role of vitamin D deficiency and comorbidities in COVID-19. *World J Virol* 11, 85-89.
- Alemu, E.A., Lamark, T., Torgersen, K.M., Birgisdottir, A.B., Larsen, K.B., Jain, A., Olsvik, H., Overvatn, A., Kirkin, V., and Johansen, T. (2012). ATG8 family proteins act as scaffolds for assembly of the ULK complex: sequence requirements for LC3-interacting region (LIR) motifs. *The Journal of biological chemistry* 287, 39275-39290.
- Alizadeh, J., Glogowska, A., Thliveris, J., Kalantari, F., Shojaei, S., Hombach-Klonisch, S., Klonisch, T., and Ghavami, S. (2018). Autophagy modulates transforming growth factor beta 1 induced epithelial to mesenchymal transition in non-small cell lung cancer cells. *Biochim Biophys Acta Mol Cell Res* 1865, 749-768.
- Alvers, A.L., Fishwick, L.K., Wood, M.S., Hu, D., Chung, H.S., Dunn, W.A., Jr., and Aris, J.P. (2009). Autophagy and amino acid homeostasis are required for chronological longevity in *Saccharomyces cerevisiae*. *Aging Cell* 8, 353-369.
- Anand, S.P., Prevost, J., Nayrac, M., Beaudoin-Bussieres, G., Benlarbi, M., Gasser, R., Brassard, N., Laumaea, A., Gong, S.Y., Bourassa, C., *et al.* (2021). Longitudinal analysis of humoral immunity against SARS-CoV-2 Spike in convalescent individuals up to 8 months post-symptom onset. *Cell Rep Med* 2, 100290.
- Antohe, I., Dascalescu, A., Danaila, C., Titieanu, A., Zlei, M., Ivanov, I., Sireteanu, A., Pavel, M., and Cianga, P. (2020). B7-Positive and B7-Negative Acute Myeloid Leukemias Display Distinct T Cell Maturation Profiles, Immune Checkpoint Receptor Expression, and European Leukemia Net Risk Profiles. *Front Oncol* 10, 264.
- Aragona, M., Panciera, T., Manfrin, A., Giullitti, S., Michielin, F., Elvassore, N., Dupont, S., and Piccolo, S. (2013a). A Mechanical Checkpoint Controls Multicellular Growth through YAP/TAZ Regulation by Actin-Processing Factors. *Cell* 154, 1047-1059.
- Aragona, M., Panciera, T., Manfrin, A., Giullitti, S., Michielin, F., Elvassore, N., Dupont, S., and Piccolo, S. (2013b). A mechanical checkpoint controls multicellular growth through YAP/TAZ regulation by actin-processing factors. *Cell* 154, 1047-1059.
- Arber, D.A., Orazi, A., Hasserjian, R., Thiele, J., Borowitz, M.J., Le Beau, M.M., Bloomfield, C.D., Cazzola, M., and Vardiman, J.W. (2016). The 2016 revision to the World Health Organization classification of myeloid neoplasms and acute leukemia. *Blood* 127, 2391-2405.
- Arrasate, M., Mitra, S., Schweitzer, E.S., Segal, M.R., and Finkbeiner, S. (2004). Inclusion body formation reduces levels of mutant huntingtin and the risk of neuronal death. *Nature* 431, 805-810.
- Ashkenazi, A., Bento, C.F., Ricketts, T., Vicinanza, M., Siddiqi, F., Pavel, M., Squitieri, F., Hardenberg, M.C., Imarisio, S., and Menzies, F.M. (2017a). Polyglutamine tracts regulate beclin 1-dependent autophagy. *Nature* 545, 108.
- Ashkenazi, A., Bento, C.F., Ricketts, T., Vicinanza, M., Siddiqi, F., Pavel, M., Squitieri, F., Hardenberg, M.C., Imarisio, S., Menzies, F.M., *et al.* (2017b). Polyglutamine tracts regulate autophagy. *Autophagy* 13, 1613-1614.
- Axe, E.L., Walker, S.A., Manifava, M., Chandra, P., Roderick, H.L., Habermann, A., Griffiths, G., and Ktistakis, N.T. (2008). Autophagosome formation from membrane compartments enriched in phosphatidylinositol 3-phosphate and dynamically connected to the endoplasmic reticulum. *J Cell Biol* 182, 685-701.

- Azamgarhi, T., Hodgkinson, M., Shah, A., Skinner, J.A., Hauptmannova, I., Briggs, T.W.R., and Warren, S. (2021). BNT162b2 vaccine uptake and effectiveness in UK healthcare workers - a single centre cohort study. *Nature communications* 12, 3698.
- Babor, F., Fischer, J.C., and Uhrberg, M. (2013). The role of KIR genes and ligands in leukemia surveillance. *Front Immunol* 4, 27.
- Backues, S.K., Chen, D., Ruan, J., Xie, Z., and Klionsky, D.J. (2014). Estimating the size and number of autophagic bodies by electron microscopy. *Autophagy* 10, 155-164.
- Bai, H., Kang, P., Hernandez, A.M., and Tatar, M. (2013). Activin signaling targeted by insulin/dFOXO regulates aging and muscle proteostasis in *Drosophila*. *PLoS genetics* 9, e1003941.
- Baldwin, A.S. (2012). Regulation of cell death and autophagy by IKK and NF-kappaB: critical mechanisms in immune function and cancer. *Immunol Rev* 246, 327-345.
- Bandyopadhyay, U., and Cuervo, A.M. (2007). Chaperone-mediated autophagy in aging and neurodegeneration: lessons from alpha-synuclein. *Exp Gerontol* 42, 120-128.
- Barrett, A.J., and Le Blanc, K. (2010). Immunotherapy prospects for acute myeloid leukaemia. *Clinical and Experimental Immunology* 161, 223-232.
- Basheer, M., Saad, E., Shlezinger, D., and Assy, N. (2021). Convalescent Plasma Reduces Mortality and Decreases Hospitalization Stay in Patients with Moderate COVID-19 Pneumonia. *Metabolites* 11.
- Bavi, P., Uddin, S., Bu, R., Ahmed, M., Abubaker, J., Balde, V., Qadri, Z., Ajarim, D., Al-Dayel, F., Hussain, A.R., *et al.* (2011). The biological and clinical impact of inhibition of NF-kappaB-initiated apoptosis in diffuse large B cell lymphoma (DLBCL). *J Pathol* 224, 355-366.
- Behrends, C., Sowa, M.E., Gygi, S.P., and Harper, J.W. (2010). Network organization of the human autophagy system. *Nature* 466, 68-76.
- Bennouna, J., Phelip, J.M., Andre, T., Asselain, B., Sebastien, K., and Ducreux, M. (2017). Observational Cohort Study of Patients With Metastatic Colorectal Cancer Initiating Chemotherapy in Combination With Bevacizumab (CONCERT). *Clinical colorectal cancer* 16, 129-140 e124.
- Bento, C.F., Ashkenazi, A., Jimenez-Sanchez, M., and Rubinsztein, D.C. (2016a). The Parkinson's disease-associated genes ATP13A2 and SYT11 regulate autophagy via a common pathway. *Nature communications* 7, 11803.
- Bento, C.F., Renna, M., Ghislat, G., Puri, C., Ashkenazi, A., Vicinanza, M., Menzies, F.M., and Rubinsztein, D.C. (2016b). Mammalian autophagy: how does it work? *Annual Review of Biochemistry* 85, 685-713.
- Bento, C.F., Renna, M., Ghislat, G., Puri, C., Ashkenazi, A., Vicinanza, M., Menzies, F.M., and Rubinsztein, D.C. (2016c). Mammalian Autophagy: How Does It Work? *Annu Rev Biochem* 85, 685-713.
- Berthon, C., Driss, V., Liu, J., Kuranda, K., Leleu, X., Jouy, N., Hetuin, D., and Quesnel, B. (2010). In acute myeloid leukemia, B7-H1 (PD-L1) protection of blasts from cytotoxic T cells is induced by TLR ligands and interferon-gamma and can be reversed using MEK inhibitors. *Cancer Immunol Immunother* 59, 1839-1849.
- Biernacki, M.A., and Bleakley, M. (2020). Neoantigens in Hematologic Malignancies. *Front Immunol* 11, 121.
- Birgel, M., Gottschling-Zeller, H., Rohrig, K., and Hauner, H. (2000). Role of cytokines in the regulation of plasminogen activator inhibitor-1 expression and secretion in newly differentiated subcutaneous human adipocytes. *Arteriosclerosis, thrombosis, and vascular biology* 20, 1682-1687.
- Bjedov, I., Toivonen, J.M., Kerr, F., Slack, C., Jacobson, J., Foley, A., and Partridge, L. (2010). Mechanisms of life span extension by rapamycin in the fruit fly *Drosophila melanogaster*. *Cell Metab* 11, 35-46.
- Bjorkoy, G., Lamark, T., Brech, A., Outzen, H., Perander, M., Overvatn, A., Stenmark, H., and Johansen, T. (2005). p62/SQSTM1 forms protein aggregates degraded by autophagy and has a protective effect on huntingtin-induced cell death. *J Cell Biol* 171, 603-614.
- Bjorkstrom, N.K., Riese, P., Heuts, F., Andersson, S., Fauriat, C., Ivarsson, M.A., Bjorklund, A.T., Flodstrom-Tullberg, M., Michaelsson, J., Rottenberg, M.E., *et al.* (2010). Expression patterns of NKG2A, KIR, and CD57 define a process of CD56dim NK-cell differentiation uncoupled from NK-cell education. *Blood* 116, 3853-3864.

- Blot, M., David, M., Nguyen, M., Bourredjem, A., Group, L.S., Binquet, C., and Piroth, L. (2021). Are adipokines the missing link between obesity, immune response, and outcomes in severe COVID-19? *International journal of obesity* 45, 2126-2131.
- Botrel, T.E.A., Clark, L.G.O., Paladini, L., and Clark, O.A.C. (2016). Efficacy and safety of bevacizumab plus chemotherapy compared to chemotherapy alone in previously untreated advanced or metastatic colorectal cancer: a systematic review and meta-analysis. *BMC Cancer* 16, 677.
- Briere, F., Servet-Delprat, C., Bridon, J.M., Saint-Remy, J.M., and Banchereau, J. (1994). Human interleukin 10 induces naive surface immunoglobulin D+ (sIgD+) B cells to secrete IgG1 and IgG3. *The Journal of experimental medicine* 179, 757-762.
- Bullen, J.W., Balsbaugh, J.L., Chanda, D., Shabanowitz, J., Hunt, D.F., Neumann, D., and Hart, G.W. (2014). Cross-talk between two essential nutrient-sensitive enzymes: O-GlcNAc transferase (OGT) and AMP-activated protein kinase (AMPK). *J Biol Chem* 289, 10592-10606.
- Burnett, B., Li, F., and Pittman, R.N. (2003). The polyglutamine neurodegenerative protein ataxin-3 binds polyubiquitylated proteins and has ubiquitin protease activity. *Human molecular genetics* 12, 3195-3205.
- Cadwell, K., Liu, J.Y., Brown, S.L., Miyoshi, H., Loh, J., Lennerz, J.K., Kishi, C., Kc, W., Carrero, J.A., Hunt, S., *et al.* (2008). A key role for autophagy and the autophagy gene Atg16l1 in mouse and human intestinal Paneth cells. *Nature* 456, 259-263.
- Cancer Genome Atlas Research, N., Ley, T.J., Miller, C., Ding, L., Raphael, B.J., Mungall, A.J., Robertson, A., Hoadley, K., Triche, T.J., Jr., Laird, P.W., *et al.* (2013). Genomic and epigenomic landscapes of adult de novo acute myeloid leukemia. *N Engl J Med* 368, 2059-2074.
- Cardone, M., Yano, M., Rosenberg, A.S., and Puig, M. (2020). Lessons Learned to Date on COVID-19 Hyperinflammatory Syndrome: Considerations for Interventions to Mitigate SARS-CoV-2 Viral Infection and Detrimental Hyperinflammation. *Front Immunol* 11, 1131.
- Caro, J.J., Salas, M., Ward, A., and Goss, G. (2001). Anemia as an independent prognostic factor for survival in patients with cancer: a systemic, quantitative review. *Cancer* 91, 2214-2221.
- Carson, W.E., Fehniger, T.A., and Caligiuri, M.A. (1997). CD56bright natural killer cell subsets: characterization of distinct functional responses to interleukin-2 and the c-kit ligand. *Eur J Immunol* 27, 354-360.
- Castriconi, R., Carrega, P., Dondero, A., Bellora, F., Casu, B., Regis, S., Ferlazzo, G., and Bottino, C. (2018). Molecular Mechanisms Directing Migration and Retention of Natural Killer Cells in Human Tissues. *Front Immunol* 9, 2324.
- Catz, S.D., and Johnson, J.L. (2001). Transcriptional regulation of bcl-2 by nuclear factor kappa B and its significance in prostate cancer. *Oncogene* 20, 7342-7351.
- Cavallini, G., Donati, A., Gori, Z., Pollera, M., and Bergamini, E. (2001). The protection of rat liver autophagic proteolysis from the age-related decline co-varies with the duration of anti-ageing food restriction. *Exp Gerontol* 36, 497-506.
- Chai, Y., Berke, S.S., Cohen, R.E., and Paulson, H.L. (2004). Poly-ubiquitin binding by the polyglutamine disease protein ataxin-3 links its normal function to protein surveillance pathways. *The Journal of biological chemistry* 279, 3605-3611.
- Chamuleau, M.E., Souwer, Y., Van Ham, S.M., Zevenbergen, A., Westers, T.M., Berkhof, J., Meijer, C.J., van de Loosdrecht, A.A., and Ossenkoppele, G.J. (2004). Class II-associated invariant chain peptide expression on myeloid leukemic blasts predicts poor clinical outcome. *Cancer research* 64, 5546-5550.
- Chan, S.W., Lim, C.J., Chong, Y.F., Pobbati, A.V., Huang, C., and Hong, W. (2011). Hippo pathway-independent restriction of TAZ and YAP by angiotensin. *The Journal of biological chemistry* 286, 7018-7026.
- Chauhan, S., Goodwin, J.G., Chauhan, S., Manyam, G., Wang, J., Kamat, A.M., and Boyd, D.D. (2013). ZKSCAN3 is a master transcriptional repressor of autophagy. *Molecular cell* 50, 16-28.
- Chen, D.S., and Mellman, I. (2013). Oncology meets immunology: the cancer-immunity cycle. *Immunity* 39, 1-10.
- Chen, D.S., and Mellman, I. (2017). Elements of cancer immunity and the cancer-immune set point. *Nature* 541, 321-330.

- Chen, K., Deng, X., Yang, Z., Yu, D., Zhang, X., Li, W., Xie, D., He, Z., and Cheng, D. (2020). Sites of distant metastases and the cancer-specific survival of metastatic Siewert type II esophagogastric junction adenocarcinoma: a population-based study. *Expert Rev Gastroenterol Hepatol* *14*, 491-497.
- Chen, S.M., Li, Y.Y., Tu, C.H., Salazar, N., Tseng, Y.Y., Huang, S.F., Hsieh, L.L., and Lui, T.N. (2016). Blockade of Inhibitors of Apoptosis Proteins in Combination with Conventional Chemotherapy Leads to Synergistic Antitumor Activity in Medulloblastoma and Cancer Stem-Like Cells. *PLoS One* *11*, e0161299.
- Chen, W., Bai, Y., Patel, C., and Geng, F. (2019a). Autophagy promotes triple negative breast cancer metastasis via YAP nuclear localization. *Biochem Biophys Res Commun* *520*, 263-268.
- Chen, W., Bai, Y., Patel, C., and Geng, F. (2019b). Autophagy promotes triple negative breast cancer metastasis via YAP nuclear localization. *Biochemical and biophysical research communications*.
- Chen, X., Liu, S., Wang, L., Zhang, W., Ji, Y., and Ma, X. (2008). Clinical significance of B7-H1 (PD-L1) expression in human acute leukemia. *Cancer Biol Ther* *7*, 622-627.
- Cheon, S.Y., Kim, H., Rubinsztein, D.C., and Lee, J.E. (2019). Autophagy, Cellular Aging and Age-related Human Diseases. *Exp Neurobiol* *28*, 643-657.
- Chillon, T.S., Demircan, K., Heller, R.A., Hirschbil-Bremer, I.M., Diegmann, J., Bachmann, M., Moghaddam, A., and Schomburg, L. (2021). Relationship between Vitamin D Status and Antibody Response to COVID-19 mRNA Vaccination in Healthy Adults. *Biomedicines* *9*.
- Chiossone, L., Dumas, P.Y., Vienne, M., and Vivier, E. (2018). Natural killer cells and other innate lymphoid cells in cancer. *Nat Rev Immunol* *18*, 671-688.
- Chiu, S.K., Tsai, K.W., Wu, C.C., Zheng, C.M., Yang, C.H., Hu, W.C., Hou, Y.C., Lu, K.C., and Chao, Y.C. (2021). Putative Role of Vitamin D for COVID-19 Vaccination. *Int J Mol Sci* *22*.
- Choudhary, C., Kumar, C., Gnad, F., Nielsen, M.L., Rehman, M., Walther, T.C., Olsen, J.V., and Mann, M. (2009). Lysine acetylation targets protein complexes and co-regulates major cellular functions. *Science* *325*, 834-840.
- Chretien, A.S., Fauriat, C., Orlanducci, F., Galseran, C., Rey, J., Bouvier Borg, G., Gautherot, E., Granjeaud, S., Hamel-Broza, J.F., Demerle, C., *et al.* (2017). Natural Killer Defective Maturation Is Associated with Adverse Clinical Outcome in Patients with Acute Myeloid Leukemia. *Front Immunol* *8*, 573.
- Chretien, A.S., Granjeaud, S., Gondois-Rey, F., Harbi, S., Orlanducci, F., Blaise, D., Vey, N., Arnoulet, C., Fauriat, C., and Olive, D. (2015). Increased NK Cell Maturation in Patients with Acute Myeloid Leukemia. *Front Immunol* *6*, 564.
- Cicchini, M., Chakrabarti, R., Kongara, S., Price, S., Nahar, R., Lozy, F., Zhong, H., Vazquez, A., Kang, Y., and Karantza, V. (2014). Autophagy regulator BECN1 suppresses mammary tumorigenesis driven by WNT1 activation and following parity. *Autophagy* *10*, 2036-2052.
- Cobos-Palacios, L., Ruiz-Moreno, M.I., Vilches-Perez, A., Vargas-Candela, A., Munoz-Ubeda, M., Benitez Porres, J., Navarro-Sanz, A., Lopez-Carmona, M.D., Sanz-Canovas, J., Perez-Belmonte, L.M., *et al.* (2022). Metabolically healthy obesity: Inflammatory biomarkers and adipokines in elderly population. *PLoS one* *17*, e0265362.
- Coimbra, S., Brandao Proenca, J., Santos-Silva, A., and Neuparth, M.J. (2014). Adiponectin, leptin, and chemerin in elderly patients with type 2 diabetes mellitus: a close linkage with obesity and length of the disease. *BioMed research international* *2014*, 701915.
- Colleran, A., Ryan, A., O'Gorman, A., Mureau, C., Liptrot, C., Dockery, P., Fearnhead, H., and Egan, L.J. (2011). Autophagosomal IkappaB alpha degradation plays a role in the long term control of tumor necrosis factor-alpha-induced nuclear factor-kappaB (NF-kappaB) activity. *J Biol Chem* *286*, 22886-22893.
- Comb, W.C., Cogswell, P., Sitcheran, R., and Baldwin, A.S. (2011). IKK-dependent, NF-kappaB-independent control of autophagic gene expression. *Oncogene* *30*, 1727-1732.
- Comet, I., Riising, E.M., Leblanc, B., and Helin, K. (2016). Maintaining cell identity: PRC2-mediated regulation of transcription and cancer. *Nature reviews Cancer* *16*, 803-810.
- Costello, R.T., Sivori, S., Marcenaro, E., Lafage-Pochitaloff, M., Mozziconacci, M.J., Reviron, D., Gastaut, J.A., Pende, D., Olive, D., and Moretta, A. (2002). Defective expression and function of natural killer cell-triggering receptors in patients with acute myeloid leukemia. *Blood* *99*, 3661-3667.

- Coue, M., Brenner, S.L., Spector, I., and Korn, E.D. (1987). Inhibition of actin polymerization by latrunculin A. *FEBS Lett* 213, 316-318.
- Curran, E.K., Godfrey, J., and Kline, J. (2017). Mechanisms of Immune Tolerance in Leukemia and Lymphoma. *Trends in Immunology* 38, 513-525.
- Dada, R. (2018). Program death inhibitors in classical Hodgkin's lymphoma: a comprehensive review. *Ann Hematol* 97, 555-561.
- Davidson-Moncada, J., Viboch, E., Church, S.E., Warren, S.E., and Rutella, S. (2018). Dissecting the Immune Landscape of Acute Myeloid Leukemia. *Biomedicines* 6.
- de Pillis, L., Fister, K.R., Gu, W.Q., Collins, C., Daub, M., Gross, D., Moore, J., and Preskill, B. (2009). Mathematical model creation for cancer chemo-immunotherapy. *Comput Math Method M* 10, 165-184.
- De Smet, D., De Smet, K., Herroelen, P., Gryspeerdt, S., and Martens, G.A. (2021). Serum 25(OH)D Level on Hospital Admission Associated With COVID-19 Stage and Mortality. *Am J Clin Pathol* 155, 381-388.
- Del Roso, A., Vittorini, S., Cavallini, G., Donati, A., Gori, Z., Masini, M., Pollera, M., and Bergamini, E. (2003). Ageing-related changes in the in vivo function of rat liver macroautophagy and proteolysis. *Exp Gerontol* 38, 519-527.
- Delorme-Axford, E., Guimaraes, R.S., Reggiori, F., and Klionsky, D.J. (2015). The yeast *Saccharomyces cerevisiae*: an overview of methods to study autophagy progression. *Methods* 75, 3-12.
- Deng, Z., Zhao, J., Cai, S., Qi, Y., Yu, Q., Martin, M.P., Gao, X., Chen, R., Zhuo, J., Zhen, J., *et al.* (2019). Natural Killer Cells Offer Differential Protection From Leukemia in Chinese Southern Han. *Front Immunol* 10, 1646.
- Denton, D., and Kumar, S. (2019). Autophagy-dependent cell death. *Cell Death Differ* 26, 605-616.
- Di Vito, C., Mikulak, J., and Mavilio, D. (2019). On the Way to Become a Natural Killer Cell. *Front Immunol* 10, 1812.
- DiFiglia, M., Sapp, E., Chase, K.O., Davies, S.W., Bates, G.P., Vonsattel, J.P., and Aronin, N. (1997). Aggregation of huntingtin in neuronal intranuclear inclusions and dystrophic neurites in brain. *Science* 277, 1990-1993.
- Ding, Y., Kim, S., Lee, S.Y., Koo, J.K., Wang, Z., and Choi, M.E. (2014). Autophagy regulates TGF-beta expression and suppresses kidney fibrosis induced by unilateral ureteral obstruction. *J Am Soc Nephrol* 25, 2835-2846.
- Dittmann, M., Hoffmann, H.H., Scull, M.A., Gilmore, R.H., Bell, K.L., Ciancanelli, M., Wilson, S.J., Crotta, S., Yu, Y., Flatley, B., *et al.* (2015). A serpin shapes the extracellular environment to prevent influenza A virus maturation. *Cell* 160, 631-643.
- Djajadikerta, A., Keshri, S., Pavel, M., Prestil, R., Ryan, L., and Rubinsztein, D.C. (2020). Autophagy Induction as a Therapeutic Strategy for Neurodegenerative Diseases. *Journal of molecular biology* 432, 2799-2821.
- Djavaheri-Mergny, M., Amelotti, M., Mathieu, J., Besancon, F., Bauvy, C., Souquere, S., Pierron, G., and Codogno, P. (2006). NF-kappaB activation represses tumor necrosis factor-alpha-induced autophagy. *J Biol Chem* 281, 30373-30382.
- Dohner, H., Estey, E., Grimwade, D., Amadori, S., Appelbaum, F.R., Buchner, T., Dombret, H., Ebert, B.L., Fenaux, P., Larson, R.A., *et al.* (2017). Diagnosis and management of AML in adults: 2017 ELN recommendations from an international expert panel. *Blood* 129, 424-447.
- Dolen, Y., and Esendagli, G. (2013). Myeloid leukemia cells with a B7-2(+) subpopulation provoke Th-cell responses and become immuno-suppressive through the modulation of B7 ligands. *European Journal of Immunology* 43, 747-757.
- Donati, A., Cavallini, G., Paradiso, C., Vittorini, S., Pollera, M., Gori, Z., and Bergamini, E. (2001). Age-related changes in the regulation of autophagic proteolysis in rat isolated hepatocytes. *J Gerontol A Biol Sci Med Sci* 56, B288-293.
- Donati, A., Ventruti, A., Cavallini, G., Masini, M., Vittorini, S., Chantret, I., Codogno, P., and Bergamini, E. (2008). In vivo effect of an antilipolytic drug (3,5'-dimethylpyrazole) on autophagic proteolysis and autophagy-related gene expression in rat liver. *Biochemical and biophysical research communications* 366, 786-792.

- Dooley, H.C., Razi, M., Polson, H.E., Girardin, S.E., Wilson, M.I., and Tooze, S.A. (2014). WIPI2 links LC3 conjugation with PI3P, autophagosome formation, and pathogen clearance by recruiting Atg12-5-16L1. *Molecular cell* 55, 238-252.
- Dror, A.A., Morozov, N., Daoud, A., Namir, Y., Yakir, O., Shachar, Y., Lifshitz, M., Segal, E., Fisher, L., Mizrachi, M., *et al.* (2022). Pre-infection 25-hydroxyvitamin D3 levels and association with severity of COVID-19 illness. *PloS one* 17, e0263069.
- Dudenhoffer-Pfeifer, M., and Bryder, D. (2018). Immunoediting is not a primary transformation event in a murine model of MLL-ENL AML. *Life Sci Alliance* 1, e201800079.
- Dulphy, N., Chretien, A.S., Khaznadar, Z., Fauriat, C., Nanbakhsh, A., Caignard, A., Chouaib, S., Olive, D., and Toubert, A. (2016). Underground Adaptation to a Hostile Environment: Acute Myeloid Leukemia vs. Natural Killer Cells. *Front Immunol* 7, 94.
- Dupont, S., Morsut, L., Aragona, M., Enzo, E., Giulitti, S., Cordenonsi, M., Zanconato, F., Le Digabel, J., Forcato, M., Bicciato, S., *et al.* (2011a). Role of YAP/TAZ in mechanotransduction. *Nature* 474, 179-183.
- Dupont, S., Morsut, L., Aragona, M., Enzo, E., Giulitti, S., Cordenonsi, M., Zanconato, F., Le Digabel, J., Forcato, M., Bicciato, S., *et al.* (2011b). Role of YAP/TAZ in mechanotransduction. *Nature* 474, 179-U212.
- Dutta, J., Fan, Y., Gupta, N., Fan, G., and Gelinas, C. (2006). Current insights into the regulation of programmed cell death by NF-kappaB. *Oncogene* 25, 6800-6816.
- Egan, D., Kim, J., Shaw, R.J., and Guan, K.L. (2011). The autophagy initiating kinase ULK1 is regulated via opposing phosphorylation by AMPK and mTOR. *Autophagy* 7, 643-644.
- Elena, S.F., and Sanjuán, R. (2003). Evolution. Climb every mountain? *Science* 302, 2074-2075.
- Eliakim-Raz, N., Leibovici-Weisman, Y., Stemmer, A., Ness, A., Awwad, M., Ghantous, N., and Stemmer, S.M. (2021). Antibody Titers Before and After a Third Dose of the SARS-CoV-2 BNT162b2 Vaccine in Adults Aged ≥ 60 Years. *Jama-J Am Med Assoc* 326, 2203-2204.
- Ellis, L.M., and Hicklin, D.J. (2008). VEGF-targeted therapy: mechanisms of anti-tumour activity. *Nature reviews Cancer* 8, 579-591.
- Epling-Burnette, P.K., Bai, F., Painter, J.S., Rollison, D.E., Salih, H.R., Krusch, M., Zou, J., Ku, E., Zhong, B., Boulware, D., *et al.* (2007). Reduced natural killer (NK) function associated with high-risk myelodysplastic syndrome (MDS) and reduced expression of activating NK receptors. *Blood* 109, 4816-4824.
- Esendagli, G. (2013). A co-stimulatory trap set by myeloid leukemia cells. *Oncoimmunology* 2.
- Fan, Q., Yang, L., Zhang, X., Ma, Y., Li, Y., Dong, L., Zong, Z., Hua, X., Su, D., Li, H., *et al.* (2018). Autophagy promotes metastasis and glycolysis by upregulating MCT1 expression and Wnt/beta-catenin signaling pathway activation in hepatocellular carcinoma cells. *J Exp Clin Cancer Res* 37, 9.
- Fang, F., Xiao, W., and Tian, Z. (2018). Challenges of NK cell-based immunotherapy in the new era. *Front Med* 12, 440-450.
- Fauriat, C., Just-Landi, S., Mallet, F., Arnoulet, C., Sainty, D., Olive, D., and Costello, R.T. (2007). Deficient expression of NCR in NK cells from acute myeloid leukemia: Evolution during leukemia treatment and impact of leukemia cells in NCRdull phenotype induction. *Blood* 109, 323-330.
- Feliu, J., Salud, A., Safont, M.J., Garcia-Giron, C., Aparicio, J., Losa, F., Bosch, C., Escudero, P., Casado, E., Jorge, M., *et al.* (2015). Correlation of hypertension and proteinuria with outcome in elderly bevacizumab-treated patients with metastatic colorectal cancer. *PloS one* 10, e0116527.
- Feller, N., van der Velden, V.H., Brooimans, R.A., Boeckx, N., Preijers, F., Kelder, A., de Greef, I., Westra, G., Te Marvelde, J.G., Aerts, P., *et al.* (2013). Defining consensus leukemia-associated immunophenotypes for detection of minimal residual disease in acute myeloid leukemia in a multicenter setting. *Blood Cancer J* 3, e129.
- Fendler, W.P., Ilhan, H., Paprottka, P.M., Jakobs, T.F., Heinemann, V., Bartenstein, P., Khalaf, F., Ezziddin, S., Hacker, M., and Haug, A.R. (2015). Nomogram including pretherapeutic parameters for prediction of survival after SIRT of hepatic metastases from colorectal cancer. *European radiology* 25, 2693-2700.
- Fernández Á, F., Sebti, S., Wei, Y., Zou, Z., Shi, M., McMillan, K.L., He, C., Ting, T., Liu, Y., Chiang, W.C., *et al.* (2018). Disruption of the beclin 1-BCL2 autophagy regulatory complex promotes longevity in mice. *Nature* 558, 136-140.

- Fernandez, A.F., Sebti, S., Wei, Y., Zou, Z., Shi, M., McMillan, K.L., He, C., Ting, T., Liu, Y., Chiang, W.C., *et al.* (2018). Disruption of the beclin 1-BCL2 autophagy regulatory complex promotes longevity in mice. *Nature* 558, 136-140.
- Ferrara, N., and Adamis, A.P. (2016). Ten years of anti-vascular endothelial growth factor therapy. *Nature reviews Drug discovery* 15, 385-403.
- Fleming, A., Bourdenx, M., Fujimaki, M., Karabiyik, C., Krause, G.J., Lopez, A., Martin-Segura, A., Puri, C., Scrivo, A., Skidmore, J., *et al.* (2022). The different autophagy degradation pathways and neurodegeneration. *Neuron* 110, 935-966.
- Folcarelli, R., van Staveren, S., Bouman, R., Hilvering, B., Tinnevelt, G.H., Postma, G., van den Brink, O.F., Buydens, L.M.C., Vrisekoop, N., Koenderman, L., *et al.* (2018). Automated flow cytometric identification of disease-specific cells by the ECLIPSE algorithm. *Scientific reports* 8, 10907.
- Foldi, M., Farkas, N., Kiss, S., Dembrovszky, F., Szakacs, Z., Balasko, M., Eross, B., Hegyi, P., and Szentesi, A. (2021). Visceral Adiposity Elevates the Risk of Critical Condition in COVID-19: A Systematic Review and Meta-Analysis. *Obesity (Silver Spring)* 29, 521-528.
- Franko, J., Shi, Q., Meyers, J.P., Maughan, T.S., Adams, R.A., Seymour, M.T., Saltz, L., Punt, C.J.A., Koopman, M., Tournigand, C., *et al.* (2016). Prognosis of patients with peritoneal metastatic colorectal cancer given systemic therapy: an analysis of individual patient data from prospective randomised trials from the Analysis and Research in Cancers of the Digestive System (ARCAD) database. *Lancet Oncol* 17, 1709-1719.
- Freud, A.G., Yokohama, A., Becknell, B., Lee, M.T., Mao, H.C., Ferketich, A.K., and Caligiuri, M.A. (2006). Evidence for discrete stages of human natural killer cell differentiation in vivo. *The Journal of experimental medicine* 203, 1033-1043.
- Fujisaki, J., Wu, J., Carlson, A.L., Silberstein, L., Putheti, P., Larocca, R., Gao, W., Saito, T.I., Lo Celso, C., Tsuyuzaki, H., *et al.* (2011). In vivo imaging of Treg cells providing immune privilege to the haematopoietic stem-cell niche. *Nature* 474, 216-219.
- Fullgrabe, J., Klionsky, D.J., and Joseph, B. (2014). The return of the nucleus: transcriptional and epigenetic control of autophagy. *Nature reviews Molecular cell biology* 15, 65-74.
- Gaebler, C., Wang, Z., Lorenzi, J.C.C., Muecksch, F., Finkin, S., Tokuyama, M., Cho, A., Jankovic, M., Schaefer-Babajew, D., Oliveira, T.Y., *et al.* (2021). Evolution of antibody immunity to SARS-CoV-2. *Nature* 591, 639-644.
- Gajewska, M., Gajkowska, B., and Motyl, T. (2005). Apoptosis and autophagy induced by TGF- β 1 in bovine mammary epithelial BME-UV1 cells. *J Physiol Pharmacol* 56 Suppl 3, 143-157.
- Ganley, I.G., Lam du, H., Wang, J., Ding, X., Chen, S., and Jiang, X. (2009). ULK1.ATG13.FIP200 complex mediates mTOR signaling and is essential for autophagy. *The Journal of biological chemistry* 284, 12297-12305.
- Gao, C., Cao, W., Bao, L., Zuo, W., Xie, G., Cai, T., Fu, W., Zhang, J., Wu, W., Zhang, X., *et al.* (2010). Autophagy negatively regulates Wnt signalling by promoting Dishevelled degradation. *Nature cell biology* 12, 781-790.
- Garcia-Arencibia, M., Hochfeld, W.E., Toh, P.P., and Rubinsztein, D.C. (2010). Autophagy, a guardian against neurodegeneration. *Semin Cell Dev Biol* 21, 691-698.
- Ge, L., Melville, D., Zhang, M., and Schekman, R. (2013). The ER-Golgi intermediate compartment is a key membrane source for the LC3 lipidation step of autophagosome biogenesis. *eLife* 2, e00947.
- Ge, L., Zhang, M., and Schekman, R. (2014). Phosphatidylinositol 3-kinase and COPII generate LC3 lipidation vesicles from the ER-Golgi intermediate compartment. *eLife* 3, e04135.
- Geiger, T.L., and Sun, J.C. (2016). Development and maturation of natural killer cells. *Curr Opin Immunol* 39, 82-89.
- Gerstung, M., Papaemmanuil, E., Martincorena, I., Bullinger, L., Gaidzik, V.I., Paschka, P., Heuser, M., Thol, F., Bolli, N., Ganly, P., *et al.* (2017). Precision oncology for acute myeloid leukemia using a knowledge bank approach. *Nature genetics* 49, 332-340.
- Ghavami, S., Cunnington, R.H., Gupta, S., Yeganeh, B., Filomeno, K.L., Freed, D.H., Chen, S., Klonsch, T., Halayko, A.J., Ambrose, E., *et al.* (2015). Autophagy is a regulator of TGF- β 1-induced fibrogenesis in primary human atrial myofibroblasts. *Cell Death Dis* 6, e1696.
- Giannis, D., Ziogas, I.A., and Gianni, P. (2020). Coagulation disorders in coronavirus infected patients: COVID-19, SARS-CoV-1, MERS-CoV and lessons from the past. *J Clin Virol* 127, 104362.

- Goldstein, D.A., Zeichner, S.B., Bartnik, C.M., Neustadter, E., and Flowers, C.R. (2016). Metastatic Colorectal Cancer: A Systematic Review of the Value of Current Therapies. *Clinical colorectal cancer* 15, 1-6.
- Gonzalez-Rodriguez, A.P., Villa-Alvarez, M., Sordo-Bahamonde, C., Lorenzo-Herrero, S., and Gonzalez, S. (2019). NK Cells in the Treatment of Hematological Malignancies. *J Clin Med* 8.
- Gradzka, S., Thomas, O.S., Kretz, O., Haimovici, A., Vasilikos, L., Wong, W.W., Hacker, G., and Gentle, I.E. (2018). Inhibitor of apoptosis proteins are required for effective fusion of autophagosomes with lysosomes. *Cell Death Dis* 9, 529.
- Greaves, P., and Gribben, J.G. (2013). The role of B7 family molecules in hematologic malignancy. *Blood* 121, 734-744.
- Green, D.R., Galluzzi, L., and Kroemer, G. (2011). Mitochondria and the autophagy-inflammation-cell death axis in organismal aging. *Science* 333, 1109-1112.
- Greenwood, E.J.D., Matheson, N.J., Wals, K., van den Boomen, D.J.H., Antrobus, R., Williamson, J.C., and Lehner, P.J. (2016). Temporal proteomic analysis of HIV infection reveals remodelling of the host phosphoproteome by lentiviral Vif variants. *eLife* 5.
- Greenwood, E.J.D., Williamson, J.C., Sienkiewicz, A., Naamati, A., Matheson, N.J., and Lehner, P.J. (2019). Promiscuous Targeting of Cellular Proteins by Vpr Drives Systems-Level Proteomic Remodeling in HIV-1 Infection. *Cell reports* 27, 1579-+.
- Greiner, J., Hofmann, S., Schmitt, M., Gotz, M., Wiesneth, M., Schrezenmeier, H., Bunjes, D., Dohner, H., and Bullinger, L. (2017). Acute myeloid leukemia with mutated nucleophosmin 1: an immunogenic acute myeloid leukemia subtype and potential candidate for immune checkpoint inhibition. *Haematologica* 102, e499-e501.
- Grossi, F., Crinò, L., Logroscino, A., Canova, S., Delmonte, A., Melotti, B., Proto, C., Gelibter, A., Cappuzzo, F., Turci, D., *et al.* (2018). Use of nivolumab in elderly patients with advanced squamous non-small-cell lung cancer: results from the Italian cohort of an expanded access programme. *Eur J Cancer* 100, 126-134.
- Grothey, A., Fakih, M., and Tabernero, J. (2021). Management of BRAF-mutant metastatic colorectal cancer: a review of treatment options and evidence-based guidelines. *Ann Oncol* 32, 959-967.
- GTEX Consortium (2013). The Genotype-Tissue Expression (GTEx) project. *Nat Genet* 45, 580-585.
- Guo, Y., Chang, C., Huang, R., Liu, B., Bao, L., and Liu, W. (2012). AP1 is essential for generation of autophagosomes from the trans-Golgi network. *J Cell Sci* 125, 1706-1715.
- Hamasaki, M., Furuta, N., Matsuda, A., Nezu, A., Yamamoto, A., Fujita, N., Oomori, H., Noda, T., Haraguchi, T., Hiraoka, Y., *et al.* (2013). Autophagosomes form at ER-mitochondria contact sites. *Nature* 495, 389-393.
- Han, K., Kim, J., and Choi, M. (2014). Quantitative indices of autophagy activity from minimal models. *Theor Biol Med Model* 11, 31.
- Han, M.S., White, A., Perry, R.J., Camporez, J.P., Hidalgo, J., Shulman, G.I., and Davis, R.J. (2020). Regulation of adipose tissue inflammation by interleukin 6. *Proceedings of the National Academy of Sciences of the United States of America* 117, 2751-2760.
- Hara, T., Nakamura, K., Matsui, M., Yamamoto, A., Nakahara, Y., Suzuki-Migishima, R., Yokoyama, M., Mishima, K., Saito, I., Okano, H., *et al.* (2006). Suppression of basal autophagy in neural cells causes neurodegenerative disease in mice. *Nature* 441, 885-889.
- Harrison, D.E., Strong, R., Sharp, Z.D., Nelson, J.F., Astle, C.M., Flurkey, K., Nadon, N.L., Wilkinson, J.E., Frenkel, K., Carter, C.S., *et al.* (2009). Rapamycin fed late in life extends lifespan in genetically heterogeneous mice. *Nature* 460, 392-395.
- Hars, E.S., Qi, H., Ryazanov, A.G., Jin, S., Cai, L., Hu, C., and Liu, L.F. (2007). Autophagy regulates ageing in *C. elegans*. *Autophagy* 3, 93-95.
- Harvey, K.F., Zhang, X.M., and Thomas, D.M. (2013). The Hippo pathway and human cancer. *Nature Reviews Cancer* 13, 246-257.
- Hayakawa, Y., and Smyth, M.J. (2006). CD27 dissects mature NK cells into two subsets with distinct responsiveness and migratory capacity. *Journal of immunology* 176, 1517-1524.
- Hayashi-Nishino, M., Fujita, N., Noda, T., Yamaguchi, A., Yoshimori, T., and Yamamoto, A. (2009). A subdomain of the endoplasmic reticulum forms a cradle for autophagosome formation. *Nature cell biology* 11, 1433-1437.

- He, R., Peng, J., Yuan, P., Xu, F., and Wei, W. (2015). Divergent roles of BECN1 in LC3 lipidation and autophagosomal function. *Autophagy* *11*, 740-747.
- He, R., Wang, M., Zhao, C., Shen, M., Yu, Y., He, L., Zhao, Y., Chen, H., Shi, X., Zhou, M., *et al.* (2019). TFEB-driven autophagy potentiates TGF-beta induced migration in pancreatic cancer cells. *J Exp Clin Cancer Res* *38*, 340.
- Hegewisch-Becker, S., Graeven, U., Lerchenmuller, C.A., Killing, B., Depenbusch, R., Steffens, C.C., Al-Batran, S.E., Lange, T., Dietrich, G., Stoehmacher, J., *et al.* (2015). Maintenance strategies after first-line oxaliplatin plus fluoropyrimidine plus bevacizumab for patients with metastatic colorectal cancer (AIO 0207): a randomised, non-inferiority, open-label, phase 3 trial. *Lancet Oncol* *16*, 1355-1369.
- Hegewisch-Becker, S., Nopel-Dunnebacke, S., Hinke, A., Graeven, U., Reinacher-Schick, A., Hertel, J., Lerchenmuller, C.A., Killing, B., Depenbusch, R., Al-Batran, S.E., *et al.* (2018). Impact of primary tumour location and RAS/BRAF mutational status in metastatic colorectal cancer treated with first-line regimens containing oxaliplatin and bevacizumab: Prognostic factors from the AIO KRK0207 first-line and maintenance therapy trial. *European journal of cancer* *101*, 105-113.
- Hill, S.M., Wrobel, L., Ashkenazi, A., Fernandez-Estevéz, M., Tan, K., Burli, R.W., and Rubinsztein, D.C. (2021). VCP/p97 regulates Beclin-1-dependent autophagy initiation. *Nature chemical biology* *17*, 448-455.
- Horton, R., Wilming, L., Rand, V., Lovering, R.C., Bruford, E.A., Khodiyar, V.K., Lush, M.J., Povey, S., Talbot, C.C., Jr., Wright, M.W., *et al.* (2004). Gene map of the extended human MHC. *Nat Rev Genet* *5*, 889-899.
- Hosokawa, N., Hara, T., Kaizuka, T., Kishi, C., Takamura, A., Miura, Y., Iemura, S.-i., Natsume, T., Takehana, K., and Yamada, N. (2009a). Nutrient-dependent mTORC1 association with the ULK1-Atg13-FIP200 complex required for autophagy. *Molecular biology of the cell* *20*, 1981-1991.
- Hosokawa, N., Hara, T., Kaizuka, T., Kishi, C., Takamura, A., Miura, Y., Iemura, S., Natsume, T., Takehana, K., Yamada, N., *et al.* (2009b). Nutrient-dependent mTORC1 association with the ULK1-Atg13-FIP200 complex required for autophagy. *Mol Biol Cell* *20*, 1981-1991.
- Hsu, K.C., Keever-Taylor, C.A., Wilton, A., Pinto, C., Heller, G., Arkun, K., O'Reilly, R.J., Horowitz, M.M., and Dupont, B. (2005). Improved outcome in HLA-identical sibling hematopoietic stem-cell transplantation for acute myelogenous leukemia predicted by KIR and HLA genotypes. *Blood* *105*, 4878-4884.
- Hu, Y., Lv, X., Wu, Y., Xu, J., Wang, L., Chen, W., Zhang, W., Li, J., Zhang, S., and Qiu, H. (2015). Expression of costimulatory molecule B7-H3 and its prognostic implications in human acute leukemia. *Hematology* *20*, 187-195.
- Huang, C., Wang, Y., Li, X., Ren, L., Zhao, J., Hu, Y., Zhang, L., Fan, G., Xu, J., Gu, X., *et al.* (2020). Clinical features of patients infected with 2019 novel coronavirus in Wuhan, China. *Lancet* *395*, 497-506.
- Huang, X., Wang, X.N., Yuan, X.D., Wu, W.Y., Lobie, P.E., and Wu, Z. (2019). XIAP facilitates breast and colon carcinoma growth via promotion of p62 depletion through ubiquitination-dependent proteasomal degradation. *Oncogene* *38*, 1448-1460.
- Huang, X., Wu, Z., Mei, Y., and Wu, M. (2013). XIAP inhibits autophagy via XIAP-Mdm2-p53 signalling. *EMBO J* *32*, 2204-2216.
- Huntington, N.D., Voshchenrich, C.A., and Di Santo, J.P. (2007). Developmental pathways that generate natural-killer-cell diversity in mice and humans. *Nat Rev Immunol* *7*, 703-714.
- Huse, M. (2017). Mechanical forces in the immune system. *Nat Rev Immunol*.
- Ikeda, S., Nah, J., Shirakabe, A., Zhai, P., Oka, S.I., Sciarretta, S., Guan, K.L., Shimokawa, H., and Sadoshima, J. (2021). YAP plays a crucial role in the development of cardiomyopathy in lysosomal storage diseases. *J Clin Invest* *131*.
- Imarisio, S., Carmichael, J., Korolchuk, V., Chen, C.W., Saiki, S., Rose, C., Krishna, G., Davies, J.E., Ttofi, E., Underwood, B.R., *et al.* (2008). Huntington's disease: from pathology and genetics to potential therapies. *The Biochemical journal* *412*, 191-209.
- Insera, F., Tاجر, C., Antonietti, L., Mariani, J., Ferder, L., and Manucha, W. (2021). Vitamin D supplementation: An alternative to enhance the effectiveness of vaccines against SARS-CoV-2? *Vaccine* *39*, 4930-4931.

- Itakura, E., and Mizushima, N. (2011). p62 Targeting to the autophagosome formation site requires self-oligomerization but not LC3 binding. *J Cell Biol* 192, 17-27.
- Itoh, K., and Hirohata, S. (1995). The role of IL-10 in human B cell activation, proliferation, and differentiation. *Journal of immunology* 154, 4341-4350.
- Iwasa, S., Nakajima, T.E., Nagashima, K., Honma, Y., Kato, K., Hamaguchi, T., Yamada, Y., and Shimada, Y. (2013). Lack of association of proteinuria and clinical outcome in patients treated with bevacizumab for metastatic colorectal cancer. *Anticancer Res* 33, 309-316.
- Jacomin, A.C., Samavedam, S., Promponas, V., and Nezis, I.P. (2016). iLIR database: A web resource for LIR motif-containing proteins in eukaryotes. *Autophagy* 12, 1945-1953.
- Jin, M., and Klionsky, D.J. (2014). Regulation of autophagy: modulation of the size and number of autophagosomes. *FEBS letters* 588, 2457-2463.
- Jing, Q., Li, G., Chen, X., Liu, C., Lu, S., Zheng, H., Ma, H., Qin, Y., Zhang, D., Zhang, S., *et al.* (2019). Wnt3a promotes radioresistance via autophagy in squamous cell carcinoma of the head and neck. *J Cell Mol Med* 23, 4711-4722.
- Jobsen, J.J., ten Cate, L.N., Lybeert, M.L., van der Steen-Banasik, E.M., Scholten, A., van der Palen, J., Slot, A., Kroese, M.C., Schutter, E.M., and Siesling, S. (2010). The number of metastatic sites for stage IIIA endometrial carcinoma, endometrioid cell type, is a strong negative prognostic factor. *Gynecol Oncol* 117, 32-36.
- Johnson, D.B., Nebhan, C.A., Moslehi, J.J., and Balko, J.M. (2022). Immune-checkpoint inhibitors: long-term implications of toxicity. *Nat Rev Clin Oncol* 19, 254-267.
- Johnson, R., and Halder, G. (2014). The two faces of Hippo: targeting the Hippo pathway for regenerative medicine and cancer treatment. *Nature Reviews Drug Discovery* 13, 63-79.
- Jubb, A.M., Hurwitz, H.I., Bai, W., Holmgren, E.B., Tobin, P., Guerrero, A.S., Kabbinavar, F., Holden, S.N., Novotny, W.F., Frantz, G.D., *et al.* (2006). Impact of vascular endothelial growth factor-A expression, thrombospondin-2 expression, and microvessel density on the treatment effect of bevacizumab in metastatic colorectal cancer. *J Clin Oncol* 24, 217-227.
- Juhász, G., Erdi, B., Sass, M., and Neufeld, T.P. (2007). Atg7-dependent autophagy promotes neuronal health, stress tolerance, and longevity but is dispensable for metamorphosis in *Drosophila*. *Genes & development* 21, 3061-3066.
- Jung, C.H., Jun, C.B., Ro, S.H., Kim, Y.M., Otto, N.M., Cao, J., Kundu, M., and Kim, D.H. (2009). ULK-Atg13-FIP200 complexes mediate mTOR signaling to the autophagy machinery. *Mol Biol Cell* 20, 1992-2003.
- Kabeya, Y., Mizushima, N., Ueno, T., Yamamoto, A., Kirisako, T., Noda, T., Kominami, E., Ohsumi, Y., and Yoshimori, T. (2000). LC3, a mammalian homologue of yeast Apg8p, is localized in autophagosome membranes after processing. *The EMBO journal* 19, 5720-5728.
- Kapuy, O., Holczer, M., Marton, M., and Korcsmaros, T. (2021). Autophagy-dependent survival is controlled with a unique regulatory network upon various cellular stress events. *Cell Death Dis* 12, 309.
- Kapuy, O., Vinod, P.K., Mandl, J., and Banhegyi, G. (2013). A cellular stress-directed bistable switch controls the crosstalk between autophagy and apoptosis. *Mol Biosyst* 9, 296-306.
- Karin, M. (2006). Nuclear factor-kappaB in cancer development and progression. *Nature* 441, 431-436.
- Karin, M., and Lin, A. (2002). NF-kappaB at the crossroads of life and death. *Nat Immunol* 3, 221-227.
- Kaya, M.O., Pamukcu, E., and Yakar, B. (2021). The role of vitamin D deficiency on COVID-19: a systematic review and meta-analysis of observational studies. *Epidemiol Health* 43, e2021074.
- Kearns, S.M., Ahern, K.W., Patrie, J.T., Horton, W.B., Harris, T.E., and Kadl, A. (2021). Reduced adiponectin levels in patients with COVID-19 acute respiratory failure: A case-control study. *Physiol Rep* 9, e14843.
- Kenific, C.M., and Debnath, J. (2015). Cellular and metabolic functions for autophagy in cancer cells. *Trends in cell biology* 25, 37-45.
- Kenzelmann Broz, D., and Attardi, L.D. (2013). TRP53 activates a global autophagy program to promote tumor suppression. *Autophagy* 9, 1440-1442.
- Khakoo, S., Chau, I., Pedley, I., Ellis, R., Steward, W., Harrison, M., Baijal, S., Tahir, S., Ross, P., Raouf, S., *et al.* (2019). ACORN: Observational Study of Bevacizumab in Combination With First-Line Chemotherapy for Treatment of Metastatic Colorectal Cancer in the UK. *Clinical colorectal cancer* 18, 280-291 e285.

- Khaminets, A., Behl, C., and Dikic, I. (2016). Ubiquitin-Dependent And Independent Signals In Selective Autophagy. *Trends in cell biology* 26, 6-16.
- Kim, J., Kundu, M., Viollet, B., and Guan, K.L. (2011a). AMPK and mTOR regulate autophagy through direct phosphorylation of Ulk1. *Nat Cell Biol* 13, 132-141.
- Kim, J.E., You, D.J., Lee, C., Ahn, C., Seong, J.Y., and Hwang, J.I. (2010). Suppression of NF-kappaB signaling by KEAP1 regulation of IKKbeta activity through autophagic degradation and inhibition of phosphorylation. *Cell Signal* 22, 1645-1654.
- Kim, W., Bennett, E.J., Huttlin, E.L., Guo, A., Li, J., Possemato, A., Sowa, M.E., Rad, R., Rush, J., Comb, M.J., *et al.* (2011b). Systematic and quantitative assessment of the ubiquitin-modified proteome. *Molecular cell* 44, 325-340.
- Kimura, S., Noda, T., and Yoshimori, T. (2007). Dissection of the autophagosome maturation process by a novel reporter protein, tandem fluorescent-tagged LC3. *Autophagy* 3, 452-460.
- Kioka, N., Sakata, S., Kawauchi, T., Amachi, T., Akiyama, S.K., Okazaki, K., Yaen, C., Yamada, K.M., and Aota, S. (1999). Vinexin: a novel vinculin-binding protein with multiple SH3 domains enhances actin cytoskeletal organization. *J Cell Biol* 144, 59-69.
- Kirkin, V., Lamark, T., Sou, Y.S., Bjorkoy, G., Nunn, J.L., Bruun, J.A., Shvets, E., McEwan, D.G., Clausen, T.H., Wild, P., *et al.* (2009a). A role for NBR1 in autophagosomal degradation of ubiquitinated substrates. *Mol Cell* 33, 505-516.
- Kirkin, V., McEwan, D.G., Novak, I., and Dikic, I. (2009b). A role for ubiquitin in selective autophagy. *Mol Cell* 34, 259-269.
- Kiyono, K., Suzuki, H.I., Matsuyama, H., Morishita, Y., Komuro, A., Kano, M.R., Sugimoto, K., and Miyazono, K. (2009). Autophagy is activated by TGF-beta and potentiates TGF-beta-mediated growth inhibition in human hepatocellular carcinoma cells. *Cancer Res* 69, 8844-8852.
- Klionsky, D.J. (2006). Neurodegeneration: good riddance to bad rubbish. *Nature* 441, 819-820.
- Klionsky, D.J., Abdalla, F.C., Abeliovich, H., Abraham, R.T., Acevedo-Arozena, A., Adeli, K., Agholme, L., Agnello, M., Agostinis, P., Aguirre-Ghiso, J.A., *et al.* (2012). Guidelines for the use and interpretation of assays for monitoring autophagy. *Autophagy* 8, 445-544.
- Klionsky, D.J., Abdel-Aziz, A.K., Abdelfatah, S., Abdellatif, M., Abdoli, A., Abel, S., Abeliovich, H., Abildgaard, M.H., Abudu, Y.P., Acevedo-Arozena, A., *et al.* (2021). Guidelines for the use and interpretation of assays for monitoring autophagy (4th edition)(1). *Autophagy* 17, 1-382.
- Knaevelsrud, H., Soreng, K., Raiborg, C., Haberg, K., Rasmuson, F., Brech, A., Liestol, K., Rusten, T.E., Stenmark, H., Neufeld, T.P., *et al.* (2013). Membrane remodeling by the PX-BAR protein SNX18 promotes autophagosome formation. *J Cell Biol* 202, 331-349.
- Knorr, R.L., Lipowsky, R., and Dimova, R. (2015). Autophagosome closure requires membrane scission. *Autophagy* 11, 2134-2137.
- Kohne, C.H., Cunningham, D., Di Costanzo, F., Glimelius, B., Blijham, G., Aranda, E., Scheithauer, W., Rougier, P., Palmer, M., Wils, J., *et al.* (2002). Clinical determinants of survival in patients with 5-fluorouracil-based treatment for metastatic colorectal cancer: results of a multivariate analysis of 3825 patients. *Ann Oncol* 13, 308-317.
- Komatsu, M., Waguri, S., Chiba, T., Murata, S., Iwata, J., Tanida, I., Ueno, T., Koike, M., Uchiyama, Y., Kominami, E., *et al.* (2006). Loss of autophagy in the central nervous system causes neurodegeneration in mice. *Nature* 441, 880-884.
- Kondo, A., Yamashita, T., Tamura, H., Zhao, W., Tsuji, T., Shimizu, M., Shinya, E., Takahashi, H., Tamada, K., Chen, L., *et al.* (2010). Interferon-gamma and tumor necrosis factor-alpha induce an immunoinhibitory molecule, B7-H1, via nuclear factor-kappaB activation in blasts in myelodysplastic syndromes. *Blood* 116, 1124-1131.
- Kremer, A.N., van der Meijden, E.D., Honders, M.W., Goeman, J.J., Wiertz, E.J., Falkenburg, J.H., and Griffioen, M. (2012). Endogenous HLA class II epitopes that are immunogenic in vivo show distinct behavior toward HLA-DM and its natural inhibitor HLA-DO. *Blood* 120, 3246-3255.
- Kremer, A.N., van der Meijden, E.D., Honders, M.W., Pont, M.J., Goeman, J.J., Falkenburg, J.H., and Griffioen, M. (2014). Human leukocyte antigen-DO regulates surface presentation of human leukocyte antigen class II-restricted antigens on B cell malignancies. *Biology of blood and marrow transplantation : journal of the American Society for Blood and Marrow Transplantation* 20, 742-747.

- Kriegl, J., and Loos, B. (2019). The good, the bad and the autophagosome: exploring unanswered questions of autophagy-dependent cell death. *Cell Death Differ* 26, 640-652.
- Kronig, H., Kremmler, L., Haller, B., Englert, C., Peschel, C., Andreesen, R., and Blank, C.U. (2014). Interferon-induced programmed death-ligand 1 (PD-L1/B7-H1) expression increases on human acute myeloid leukemia blast cells during treatment. *Eur J Haematol* 92, 195-203.
- Kubisz, P., Chudy, P., Stasko, J., Galajda, P., Holly, P., Vysehradsky, R., and Mokaň, M. (2010). Circulating vascular endothelial growth factor in the normo- and/or microalbuminuric patients with type 2 diabetes mellitus. *Acta Diabetol* 47, 119-124.
- Kyi, C., and Postow, M.A. (2016). Immune checkpoint inhibitor combinations in solid tumors: opportunities and challenges. *Immunotherapy-Uk* 8, 821-837.
- Lamb, C.A., Nuhlen, S., Judith, D., Frith, D., Snijders, A.P., Behrends, C., and Tooze, S.A. (2016). TBC1D14 regulates autophagy via the TRAPP complex and ATG9 traffic. *The EMBO journal* 35, 281-301.
- Lapierre, L.R., De Magalhaes Filho, C.D., McQuary, P.R., Chu, C.C., Visvikis, O., Chang, J.T., Gelino, S., Ong, B., Davis, A.E., Irazoqui, J.E., *et al.* (2013). The TFEB orthologue HLH-30 regulates autophagy and modulates longevity in *Caenorhabditis elegans*. *Nature communications* 4, 2267.
- Laplante, M., and Sabatini, D.M. (2012). mTOR signaling in growth control and disease. *Cell* 149, 274-293.
- Lee, Y.A., Noon, L.A., Akat, K.M., Ybanez, M.D., Lee, T.F., Berres, M.L., Fujiwara, N., Goossens, N., Chou, H.I., Parvin-Nejad, F.P., *et al.* (2018). Autophagy is a gatekeeper of hepatic differentiation and carcinogenesis by controlling the degradation of Yap. *Nature communications* 9, 4962.
- Leerberg, J.M., Gomez, G.A., Verma, S., Moussa, E.J., Wu, S.K., Priya, R., Hoffman, B.D., Grashoff, C., Schwartz, M.A., and Yap, A.S. (2014). Tension-sensitive actin assembly supports contractility at the epithelial zonula adherens. *Current biology : CB* 24, 1689-1699.
- Levine, B., Liu, R., Dong, X., and Zhong, Q. (2015). Beclin orthologs: integrative hubs of cell signaling, membrane trafficking, and physiology. *Trends in cell biology* 25, 533-544.
- Li, S., Schmitz, K.R., Jeffrey, P.D., Wiltzius, J.J., Kussie, P., and Ferguson, K.M. (2005). Structural basis for inhibition of the epidermal growth factor receptor by cetuximab. *Cancer Cell* 7, 301-311.
- Liang, N., Zhang, C., Dill, P., Panasyuk, G., Pion, D., Koka, V., Gallazzini, M., Olson, E.N., Lam, H., Henske, E.P., *et al.* (2014). Regulation of YAP by mTOR and autophagy reveals a therapeutic target of tuberous sclerosis complex. *J Exp Med* 211, 2249-2263.
- Liang, X.H., Jackson, S., Seaman, M., Brown, K., Kempkes, B., Hibshoosh, H., and Levine, B. (1999). Induction of autophagy and inhibition of tumorigenesis by beclin 1. *Nature* 402, 672-676.
- Lim, M.S., and Elenitoba-Johnson, K.S. (2004). The molecular pathology of primary immunodeficiencies. *J Mol Diagn* 6, 59-83.
- Lin, F., Ghislat, G., Luo, S., Renna, M., Siddiqi, F., and Rubinsztein, D.C. (2015). XIAP and cIAP1 amplifications induce Beclin 1-dependent autophagy through NFkappaB activation. *Hum Mol Genet* 24, 2899-2913.
- Lin, L.Y., Mulick, A., Mathur, R., Smeeth, L., Warren-Gash, C., and Langan, S.M. (2022). The association between vitamin D status and COVID-19 in England: A cohort study using UK Biobank. *PloS one* 17, e0269064.
- Lipinski, M.M., Hoffman, G., Ng, A., Zhou, W., Py, B.F., Hsu, E., Liu, X., Eisenberg, J., Liu, J., Blenis, J., *et al.* (2010a). A genome-wide siRNA screen reveals multiple mTORC1 independent signaling pathways regulating autophagy under normal nutritional conditions. In *Dev Cell (United States: 2010 Elsevier Inc)*, pp. 1041-1052.
- Lipinski, M.M., Zheng, B., Lu, T., Yan, Z., Py, B.F., Ng, A., Xavier, R.J., Li, C., Yankner, B.A., Scherzer, C.R., *et al.* (2010b). Genome-wide analysis reveals mechanisms modulating autophagy in normal brain aging and in Alzheimer's disease. *Proceedings of the National Academy of Sciences of the United States of America* 107, 14164-14169.
- Lippai, M., and Low, P. (2014). The role of the selective adaptor p62 and ubiquitin-like proteins in autophagy. *BioMed research international* 2014, 832704.
- Liu, B., Chen, W., Evavold, B.D., and Zhu, C. (2014). Accumulation of dynamic catch bonds between TCR and agonist peptide-MHC triggers T cell signaling. *Cell* 157, 357-368.
- Liu, K., Zhang, L., Zhao, Q., Zhao, Z., Zhi, F., Qin, Y., and Cui, J. (2018). SKP2 attenuates NF-kappaB signaling by mediating IKKbeta degradation through autophagy. *J Mol Cell Biol* 10, 205-215.

- Loerch, P.M., Lu, T., Dakin, K.A., Vann, J.M., Isaacs, A., Geula, C., Wang, J., Pan, Y., Gabuzda, D.H., Li, C., *et al.* (2008). Evolution of the aging brain transcriptome and synaptic regulation. *PLoS One* 3, e3329.
- Loke, P., and Allison, J.P. (2004). Emerging mechanisms of immune regulation: the extended B7 family and regulatory T cells. *Arthritis Res Ther* 6, 208-214.
- Loken, M.R., Chu, S.C., Fritschle, W., Kalnoski, M., and Wells, D.A. (2009). Normalization of bone marrow aspirates for hemodilution in flow cytometric analyses. *Cytometry B Clin Cytom* 76, 27-36.
- Long, E.O., Kim, H.S., Liu, D., Peterson, M.E., and Rajagopalan, S. (2013). Controlling natural killer cell responses: integration of signals for activation and inhibition. *Annu Rev Immunol* 31, 227-258.
- Longatti, A., Lamb, C.A., Razi, M., Yoshimura, S., Barr, F.A., and Tooze, S.A. (2012). TBC1D14 regulates autophagosome formation via Rab11- and ULK1-positive recycling endosomes. *J Cell Biol* 197, 659-675.
- Loos, B., du Toit, A., and Hofmeyr, J.H. (2014). Defining and measuring autophagosome flux-concept and reality. *Autophagy* 10, 2087-2096.
- Loos, B., Klionsky, D.J., Du Toit, A., and Hofmeyr, J.S. (2020). On the relevance of precision autophagy flux control in vivo - Points of departure for clinical translation. *Autophagy* 16, 750-762.
- López-Otín, C., Blasco, M.A., Partridge, L., Serrano, M., and Kroemer, G. (2013). The hallmarks of aging. *Cell* 153, 1194-1217.
- Lopez-Soto, A., Bravo-San Pedro, J.M., Kroemer, G., Galluzzi, L., and Gonzalez, S. (2017). Involvement of autophagy in NK cell development and function. *Autophagy* 13, 633-636.
- Lopez-Verges, S., Milush, J.M., Pandey, S., York, V.A., Arakawa-Hoyt, J., Pircher, H., Norris, P.J., Nixon, D.F., and Lanier, L.L. (2010). CD57 defines a functionally distinct population of mature NK cells in the human CD56dimCD16+ NK-cell subset. *Blood* 116, 3865-3874.
- Luo, J.L., Kamata, H., and Karin, M. (2005). IKK/NF-kappaB signaling: balancing life and death--a new approach to cancer therapy. *J Clin Invest* 115, 2625-2632.
- Ma, H., Wu, X., Tao, M., Tang, N., Li, Y., Zhang, X., and Zhou, Q. (2019). Efficacy and safety of bevacizumab-based maintenance therapy in metastatic colorectal cancer: A meta-analysis. *Medicine (Baltimore)* 98, e18227.
- Ma, Q., Qiang, J., Gu, P., Wang, Y., Geng, Y., and Wang, M. (2011). Age-related autophagy alterations in the brain of senescence accelerated mouse prone 8 (SAMP8) mice. *Exp Gerontol* 46, 533-541.
- Maeda, A., Yamamoto, K., Yamashita, K., Asagoe, K., Nohgawa, M., Kita, K., Iwasaki, H., Ueda, T., Takahashi, A., and Sasada, M. (1998). The expression of co-stimulatory molecules and their relationship to the prognosis of human acute myeloid leukaemia: poor prognosis of B7-2-positive leukaemia. *British journal of haematology* 102, 1257-1262.
- Mahnke, Y.D., Brodie, T.M., Sallusto, F., Roederer, M., and Lugli, E. (2013). The who's who of T-cell differentiation: human memory T-cell subsets. *Eur J Immunol* 43, 2797-2809.
- Makita, M., Azuma, T., Hamaguchi, H., Niiya, H., Kojima, K., Fujita, S., Tanimoto, M., Harada, M., and Yasukawa, M. (2002). Leukemia-associated fusion proteins, dek-can and bcr-abl, represent immunogenic HLA-DR-restricted epitopes recognized by fusion peptide-specific CD4+ T lymphocytes. *Leukemia* 16, 2400-2407.
- Mamessier, E., Sylvain, A., Thibault, M.L., Houvenaeghel, G., Jacquemier, J., Castellano, R., Goncalves, A., Andre, P., Romagne, F., Thibault, G., *et al.* (2011). Human breast cancer cells enhance self tolerance by promoting evasion from NK cell antitumor immunity. *J Clin Invest* 121, 3609-3622.
- Mammucari, C., Milan, G., Romanello, V., Masiero, E., Rudolf, R., Del Piccolo, P., Burden, S.J., Di Lisi, R., Sandri, C., Zhao, J., *et al.* (2007). FoxO3 controls autophagy in skeletal muscle in vivo. *Cell Metab* 6, 458-471.
- Mana-Capelli, S., Paramasivam, M., Dutta, S., and McCollum, D. (2014). Angiomotins link F-actin architecture to Hippo pathway signaling. *Mol Biol Cell* 25, 1676-1685.
- Mancuso, P., and Bouchard, B. (2019). The Impact of Aging on Adipose Function and Adipokine Synthesis. *Front Endocrinol (Lausanne)* 10, 137.
- Marsh, S.A., Powell, P.C., Dell'italia, L.J., and Chatham, J.C. (2013). Cardiac O-GlcNAcylation blunts autophagic signaling in the diabetic heart. *Life Sci* 92, 648-656.
- Martina, J.A., Diab, H.I., Li, H., and Puertollano, R. (2014). Novel roles for the MiTF/TFE family of transcription factors in organelle biogenesis, nutrient sensing, and energy homeostasis. *Cell Mol Life Sci* 71, 2483-2497.

- Martner, A., Rydstrom, A., Riise, R.E., Aurelius, J., Anderson, H., Brune, M., Foa, R., Hellstrand, K., and Thoren, F.B. (2016). Role of natural killer cell subsets and natural cytotoxicity receptors for the outcome of immunotherapy in acute myeloid leukemia. *Oncoimmunology* 5, e1041701.
- Masarova, L., Kantarjian, H., Garcia-Mannero, G., Ravandi, F., Sharma, P., and Daver, N. (2017). Harnessing the Immune System Against Leukemia: Monoclonal Antibodies and Checkpoint Strategies for AML. *Immunotherapy-Uk* 995, 73-95.
- Massey, A.C., Kiffin, R., and Cuervo, A.M. (2006). Autophagic defects in aging: looking for an "emergency exit"? *Cell Cycle* 5, 1292-1296.
- Maticic, M., Smith, D.L., Pan, X., Maqani, N., Bekiranov, S., Boeke, J.D., and Smith, J.S. (2010). A microarray-based genetic screen for yeast chronological aging factors. *PLoS genetics* 6, e1000921.
- Matsumoto, G., Wada, K., Okuno, M., Kurosawa, M., and Nukina, N. (2011). Serine 403 phosphorylation of p62/SQSTM1 regulates selective autophagic clearance of ubiquitinated proteins. *Mol Cell* 44, 279-289.
- Maude, S.L., Frey, N., Shaw, P.A., Aplenc, R., Barrett, D.M., Bunin, N.J., Chew, A., Gonzalez, V.E., Zheng, Z., Lacey, S.F., *et al.* (2014). Chimeric antigen receptor T cells for sustained remissions in leukemia. *N Engl J Med* 371, 1507-1517.
- Mehta, P., McAuley, D.F., Brown, M., Sanchez, E., Tattersall, R.S., Manson, J.J., and Hlh Across Speciality Collaboration, U.K. (2020). COVID-19: consider cytokine storm syndromes and immunosuppression. *Lancet* 395, 1033-1034.
- Mei, J., Jiang, G., Chen, Y., Xu, Y., Wan, Y., Chen, R., Liu, F., Mao, W., Zheng, M., and Xu, J. (2022). HLA class II molecule HLA-DRA identifies immuno-hot tumors and predicts the therapeutic response to anti-PD-1 immunotherapy in NSCLC. *BMC Cancer* 22, 738.
- Melendez, A., Tallozy, Z., Seaman, M., Eskelinen, E.L., Hall, D.H., and Levine, B. (2003). Autophagy genes are essential for dauer development and life-span extension in *C. elegans*. *Science* 301, 1387-1391.
- Menzies, F.M., Fleming, A., Caricasole, A., Bento, C.F., Andrews, S.P., Ashkenazi, A., Fullgrabe, J., Jackson, A., Jimenez Sanchez, M., Karabiyik, C., *et al.* (2017a). Autophagy and Neurodegeneration: Pathogenic Mechanisms and Therapeutic Opportunities. *Neuron* 93, 1015-1034.
- Menzies, F.M., Fleming, A., Caricasole, A., Bento, C.F., Andrews, S.P., Ashkenazi, A., Fullgrabe, J., Jackson, A., Jimenez Sanchez, M., Karabiyik, C., *et al.* (2017b). Autophagy and Neurodegeneration: Pathogenic Mechanisms and Therapeutic Opportunities. *Neuron* 93, 1015-1034.
- Menzies, F.M., Huebener, J., Renna, M., Bonin, M., Riess, O., and Rubinsztein, D.C. (2010). Autophagy induction reduces mutant ataxin-3 levels and toxicity in a mouse model of spinocerebellar ataxia type 3. *Brain* 133, 93-104.
- Mery, G., Epaulard, O., Borel, A.L., Toussaint, B., and Le Gouellec, A. (2020). COVID-19: Underlying Adipokine Storm and Angiotensin 1-7 Umbrella. *Front Immunol* 11, 1714.
- Merzon, E., Tworowski, D., Gorohovski, A., Vinker, S., Golan Cohen, A., Green, I., and Frenkel-Morgenstern, M. (2020). Low plasma 25(OH) vitamin D level is associated with increased risk of COVID-19 infection: an Israeli population-based study. *The FEBS journal* 287, 3693-3702.
- Mincarelli, L., Lister, A., Lipscombe, J., and Macaulay, I.C. (2018). Defining Cell Identity with Single-Cell Omics. *Proteomics* 18, e1700312.
- Mizushima, N., and Levine, B. (2010). Autophagy in mammalian development and differentiation. *Nature cell biology* 12, 823-830.
- Moens, L., and Tangye, S.G. (2014). Cytokine-Mediated Regulation of Plasma Cell Generation: IL-21 Takes Center Stage. *Front Immunol* 5, 65.
- Mohammad, S., Mishra, A., and Ashraf, M.Z. (2019). Emerging Role of Vitamin D and its Associated Molecules in Pathways Related to Pathogenesis of Thrombosis. *Biomolecules* 9.
- Mohsen, S., Sobash, P.T., Algwaiz, G.F., Nasef, N., Al-Zeidaneen, S.A., and Karim, N.A. (2022). Autophagy Agents in Clinical Trials for Cancer Therapy: A Brief Review. *Curr Oncol* 29, 1695-1708.
- Moldovan, M., Rosberg, M.R., Alvarez, S., Klein, D., Martini, R., and Krarup, C. (2016). Aging-associated changes in motor axon voltage-gated Na(+) channel function in mice. *Neurobiol Aging* 39, 128-139.
- Moreau, K., Ravikumar, B., Renna, M., Puri, C., and Rubinsztein, D.C. (2011). Autophagosome precursor maturation requires homotypic fusion. *Cell* 146, 303-317.

- Moroishi, T., Hansen, C.G., and Guan, K.L. (2015). The emerging roles of YAP and TAZ in cancer. *Nature Reviews Cancer* 15, 73-79.
- Moroishi, T., Hayashi, T., Pan, W.W., Fujita, Y., Holt, M.V., Qin, J., Carson, D.A., and Guan, K.L. (2016). The Hippo Pathway Kinases LATS1/2 Suppress Cancer Immunity. *Cell* 167, 1525-1539 e1517.
- Mortenson, J.B., Heppler, L.N., Banks, C.J., Weerasekara, V.K., Whited, M.D., Piccolo, S.R., Johnson, W.E., Thompson, J.W., and Andersen, J.L. (2015). Histone deacetylase 6 (HDAC6) promotes the pro-survival activity of 14-3-3zeta via deacetylation of lysines within the 14-3-3zeta binding pocket. *J Biol Chem* 290, 12487-12496.
- Muena, N.A., Garcia-Salum, T., Pardo-Roa, C., Avendano, M.J., Serrano, E.F., Levican, J., Almonacid, L.I., Valenzuela, G., Poblete, E., Strohmeier, S., *et al.* (2022). Induction of SARS-CoV-2 neutralizing antibodies by CoronaVac and BNT162b2 vaccines in naive and previously infected individuals. *Ebiomedicine* 78, 103972.
- Muers, M. (2011). Complex disease: ups and downs at the MHC. *Nat Rev Genet* 12, 456-457.
- Munz, C. (2016a). Autophagy Beyond Intracellular MHC Class II Antigen Presentation. *Trends Immunol* 37, 755-763.
- Munz, C. (2016b). Autophagy proteins in antigen processing for presentation on MHC molecules. *Immunol Rev* 272, 17-27.
- Nager, M., Sallan, M.C., Visa, A., Pushparaj, C., Santacana, M., Macia, A., Yeramian, A., Canti, C., and Herreros, J. (2018). Inhibition of WNT-CTNNB1 signaling upregulates SQSTM1 and sensitizes glioblastoma cells to autophagy blockers. *Autophagy* 14, 619-636.
- Nascimento-Ferreira, I., Santos-Ferreira, T., Sousa-Ferreira, L., Auregan, G., Onofre, I., Alves, S., Dufour, N., Colomer Gould, V.F., Koeppen, A., Deglon, N., *et al.* (2011). Overexpression of the autophagic beclin-1 protein clears mutant ataxin-3 and alleviates Machado-Joseph disease. *Brain : a journal of neurology* 134, 1400-1415.
- Nettesheim, A., Shim, M.S., Hirt, J., and Liton, P.B. (2019). Transcriptome analysis reveals autophagy as regulator of TGFbeta/Smad-induced fibrogenesis in trabecular meshwork cells. *Sci Rep* 9, 16092.
- Niida, M., Tanaka, M., and Kamitani, T. (2010). Downregulation of active IKK beta by Ro52-mediated autophagy. *Mol Immunol* 47, 2378-2387.
- Nomura, Y., Sawahata, M., Nakamura, Y., Kurihara, M., Koike, R., Katsube, O., Hagiwara, K., Niho, S., Masuda, N., Tanaka, T., *et al.* (2021). Age and Smoking Predict Antibody Titres at 3 Months after the Second Dose of the BNT162b2 COVID-19 Vaccine. *Vaccines (Basel)* 9.
- Obata, Y., Yamada, Y., Takahi, Y., Baden, M.Y., Saisho, K., Tamba, S., Yamamoto, K., Umeda, M., Furubayashi, A., and Matsuzawa, Y. (2013). Relationship between serum adiponectin levels and age in healthy subjects and patients with type 2 diabetes. *Clinical endocrinology* 79, 204-210.
- Oh, Y., Taylor, S., Bekele, B.N., Debnam, J.M., Allen, P.K., Suki, D., Sawaya, R., Komaki, R., Stewart, D.J., and Karp, D.D. (2009). Number of metastatic sites is a strong predictor of survival in patients with nonsmall cell lung cancer with or without brain metastases. *Cancer* 115, 2930-2938.
- Ohashi, K., Parker, J.L., Ouchi, N., Higuchi, A., Vita, J.A., Gokce, N., Pedersen, A.A., Kalthoff, C., Tullin, S., Sams, A., *et al.* (2010). Adiponectin promotes macrophage polarization toward an anti-inflammatory phenotype. *The Journal of biological chemistry* 285, 6153-6160.
- Orsi, A., Razi, M., Dooley, H.C., Robinson, D., Weston, A.E., Collinson, L.M., and Tooze, S.A. (2012). Dynamic and transient interactions of Atg9 with autophagosomes, but not membrane integration, are required for autophagy. *Molecular biology of the cell* 23, 1860-1873.
- Ostroumov, D., Fekete-Drimusz, N., Saborowski, M., Kuhnelt, F., and Woller, N. (2018). CD4 and CD8 T lymphocyte interplay in controlling tumor growth. *Cell Mol Life Sci* 75, 689-713.
- Panciera, T., Azzolin, L., Cordenonsi, M., and Piccolo, S. (2017). Mechanobiology of YAP and TAZ in physiology and disease. *Nature reviews Molecular cell biology* 18, 758-770.
- Pankiv, S., Clausen, T.H., Lamark, T., Brech, A., Bruun, J.A., Outzen, H., Overvatn, A., Bjorkoy, G., and Johansen, T. (2007). p62/SQSTM1 binds directly to Atg8/LC3 to facilitate degradation of ubiquitinated protein aggregates by autophagy. *The Journal of biological chemistry* 282, 24131-24145.
- Papaemmanuil, E., Gerstung, M., Bullinger, L., Gaidzik, V.I., Paschka, P., Roberts, N.D., Potter, N.E., Heuser, M., Thol, F., Bolli, N., *et al.* (2016). Genomic Classification and Prognosis in Acute Myeloid Leukemia. *N Engl J Med* 374, 2209-2221.

- Papinski, D., Schuschnig, M., Reiter, W., Wilhelm, L., Barnes, C.A., Maiolica, A., Hansmann, I., Pfaffenwimmer, T., Kijanska, M., Stoffel, I., *et al.* (2014). Early steps in autophagy depend on direct phosphorylation of Atg9 by the Atg1 kinase. *Mol Cell* 53, 471-483.
- Park, E.J., Lee, J.H., Yu, G.Y., He, G., Ali, S.R., Holzer, R.G., Osterreicher, C.H., Takahashi, H., and Karin, M. (2010). Dietary and genetic obesity promote liver inflammation and tumorigenesis by enhancing IL-6 and TNF expression. *Cell* 140, 197-208.
- Patel, D., Bassi, R., Hooper, A., Prewett, M., Hicklin, D.J., and Kang, X. (2009). Anti-epidermal growth factor receptor monoclonal antibody cetuximab inhibits EGFR/HER-2 heterodimerization and activation. *International journal of oncology* 34, 25-32.
- Paulson, H.L., Das, S.S., Crino, P.B., Perez, M.K., Patel, S.C., Gotsdiner, D., Fischbeck, K.H., and Pittman, R.N. (1997). Machado-Joseph disease gene product is a cytoplasmic protein widely expressed in brain. *Annals of neurology* 41, 453-462.
- Pavel, M., Imarisio, S., Menzies, F.M., Jimenez-Sanchez, M., Siddiqi, F.H., Wu, X., Renna, M., O'Kane, C.J., Crowther, D.C., and Rubinsztein, D.C. (2016). CCT complex restricts neuropathogenic protein aggregation via autophagy. *Nat Commun* 7, 13821.
- Pavel, M., Park, S.J., Frake, R.A., Son, S.M., Manni, M.M., Bento, C.F., Renna, M., Ricketts, T., Menzies, F.M., Tanasa, R., *et al.* (2021a). alpha-Catenin levels determine direction of YAP/TAZ response to autophagy perturbation. *Nature communications* 12, 1703.
- Pavel, M., Park, S.J., Tanasa, R., and Rubinsztein, D.C. (2021b). Cell type-specific YAP1-WWTR1/TAZ transcriptional responses after autophagy perturbations are determined by levels of alpha-catenins (CTNNA1 and CTNNA3). *Autophagy* 17, 1788-1790.
- Pavel, M., Renna, M., Park, S.J., Menzies, F.M., Ricketts, T., Fullgrabe, J., Ashkenazi, A., Frake, R.A., Lombarte, A.C., Bento, C.F., *et al.* (2018a). Contact inhibition controls cell survival and proliferation via YAP/TAZ-autophagy axis. *Nat Commun* 9, 2961.
- Pavel, M., Renna, M., Park, S.J., Menzies, F.M., Ricketts, T., Fullgrabe, J., Ashkenazi, A., Frake, R.A., Lombarte, A.C., Bento, C.F., *et al.* (2018b). Contact inhibition controls cell survival and proliferation via YAP/TAZ-autophagy axis. *Nat Commun* 9, 2961.
- Pavel, M., and Rubinsztein, D.C. (2013). Autophagy Upregulation as a Therapeutic Strategy for Neurodegenerative Diseases. In *Antitumor Potential and other Emerging Medicinal Properties of Natural Compounds*, F.E. Fang, and B.T. Ng, eds. (Dordrecht: Springer Netherlands), pp. 227-238.
- Pavel, M., and Rubinsztein, D.C. (2017). Mammalian autophagy and the plasma membrane. *The FEBS journal* 284, 672-679.
- Peng, J., Ding, Y., Tu, S., Shi, D., Sun, L., Li, X., Wu, H., and Cai, S. (2014). Prognostic nomograms for predicting survival and distant metastases in locally advanced rectal cancers. *PloS one* 9, e106344.
- Peng, X., Wang, Y., Li, H., Fan, J., Shen, J., Yu, X., Zhou, Y., and Mao, H. (2019). ATG5-mediated autophagy suppresses NF-kappaB signaling to limit epithelial inflammatory response to kidney injury. *Cell Death Dis* 10, 253.
- Perez Gonzalez, N., Tao, J., Rochman, N.D., Vig, D., Chiu, E., Wirtz, D., and Sun, S.X. (2018). Cell tension and mechanical regulation of cell volume. *Molecular biology of the cell* 29, 0.
- Perreau, M., Suffiotti, M., Marques-Vidal, P., Wiedemann, A., Levy, Y., Laouenan, C., Ghosn, J., Fenwick, C., Comte, D., Roger, T., *et al.* (2021). The cytokines HGF and CXCL13 predict the severity and the mortality in COVID-19 patients. *Nature communications* 12, 4888.
- Perrotta, F., Rocco, D., Vitiello, F., De Palma, R., Guerra, G., De Luca, A., Navani, N., and Bianco, A. (2019). Immune Checkpoint Blockade for Advanced NSCLC: A New Landscape for Elderly Patients. *Int J Mol Sci* 20.
- Peterson, C.A., and Heffernan, M.E. (2008). Serum tumor necrosis factor-alpha concentrations are negatively correlated with serum 25(OH)D concentrations in healthy women. *J Inflamm (Lond)* 5, 10.
- Petherick, K.J., Williams, A.C., Lane, J.D., Ordonez-Moran, P., Huelsken, J., Collard, T.J., Smartt, H.J., Batson, J., Malik, K., Paraskeva, C., *et al.* (2013). Autolysosomal beta-catenin degradation regulates Wnt-autophagy-p62 crosstalk. *EMBO J* 32, 1903-1916.
- Piawah, S., and Venook, A.P. (2019). Targeted therapy for colorectal cancer metastases: A review of current methods of molecularly targeted therapy and the use of tumor biomarkers in the treatment of metastatic colorectal cancer. *Cancer* 125, 4139-4147.

- Pilz, S., Marz, W., Cashman, K.D., Kiely, M.E., Whiting, S.J., Holick, M.F., Grant, W.B., Pludowski, P., Hilgsmann, M., Trummer, C., *et al.* (2018). Rationale and Plan for Vitamin D Food Fortification: A Review and Guidance Paper. *Front Endocrinol (Lausanne)* 9, 373.
- Ploeger, C., Waldburger, N., Fraas, A., Goepfert, B., Pusch, S., Breuhahn, K., Wang, X.W., Schirmacher, P., and Roessler, S. (2016). Chromosome 8p tumor suppressor genes SH2D4A and SORBS3 cooperate to inhibit interleukin-6 signaling in hepatocellular carcinoma. *Hepatology* 64, 828-842.
- Pokharel, S.M., Shil, N.K., and Bose, S. (2016). Autophagy, TGF-beta, and SMAD-2/3 Signaling Regulates Interferon-beta Response in Respiratory Syncytial Virus Infected Macrophages. *Front Cell Infect Microbiol* 6, 174.
- Polymeropoulos, M.H., Lavedan, C., Leroy, E., Ide, S.E., Dehejia, A., Dutra, A., Pike, B., Root, H., Rubenstein, J., Boyer, R., *et al.* (1997). Mutation in the alpha-synuclein gene identified in families with Parkinson's disease. *Science* 276, 2045-2047.
- Popkin, B.M., Du, S., Green, W.D., Beck, M.A., Algaith, T., Herbst, C.H., Alsukait, R.F., Alluhidan, M., Alazemi, N., and Shekar, M. (2020). Individuals with obesity and COVID-19: A global perspective on the epidemiology and biological relationships. *Obes Rev* 21, e13128.
- Prasad, V., De Jesus, K., and Mailankody, S. (2017). The high price of anticancer drugs: origins, implications, barriers, solutions. *Nat Rev Clin Oncol* 14, 381-390.
- Puri, C., Manni, M.M., Vicinanza, M., Hilcenko, C., Zhu, Y., Runwal, G., Stamatakou, E., Menzies, F.M., Mamchaoui, K., Bitoun, M., *et al.* (2020). A DNMT2 Centronuclear Myopathy Mutation Reveals a Link between Recycling Endosome Scission and Autophagy. *Developmental cell* 53, 154-168 e156.
- Puri, C., Renna, M., Bento, C.F., Moreau, K., and Rubinsztein, D.C. (2013). Diverse autophagosome membrane sources coalesce in recycling endosomes. *Cell* 154, 1285-1299.
- Pyo, J.O., Yoo, S.M., Ahn, H.H., Nah, J., Hong, S.H., Kam, T.I., Jung, S., and Jung, Y.K. (2013). Overexpression of Atg5 in mice activates autophagy and extends lifespan. *Nat Commun* 4, 2300.
- Qing, G., Yan, P., and Xiao, G. (2006). Hsp90 inhibition results in autophagy-mediated proteasome-independent degradation of I κ B kinase (IKK). *Cell Res* 16, 895-901.
- Qu, C.Y., Zheng, Y., Zhou, M., Zhang, Y., Shen, F., Cao, J., and Xu, L.M. (2015). Value of bevacizumab in treatment of colorectal cancer: A meta-analysis. *World J Gastroenterol* 21, 5072-5080.
- Rabaan, A.A., Al-Ahmed, S.H., Muhammad, J., Khan, A., Sule, A.A., Tirupathi, R., Mutair, A.A., Alhumaid, S., Al-Omari, A., Dhawan, M., *et al.* (2021). Role of Inflammatory Cytokines in COVID-19 Patients: A Review on Molecular Mechanisms, Immune Functions, Immunopathology and Immunomodulatory Drugs to Counter Cytokine Storm. *Vaccines (Basel)* 9.
- Rabanal-Ruiz, Y., and Korolchuk, V.I. (2018). mTORC1 and Nutrient Homeostasis: The Central Role of the Lysosome. *Int J Mol Sci* 19.
- Rana, A., Oliveira, M.P., Khamoui, A.V., Aparicio, R., Rera, M., Rossiter, H.B., and Walker, D.W. (2017). Promoting Drp1-mediated mitochondrial fission in midlife prolongs healthy lifespan of *Drosophila melanogaster*. *Nature communications* 8, 448.
- Rangarajan, E.S., and Izard, T. (2013). Dimer asymmetry defines alpha-catenin interactions. *Nature structural & molecular biology* 20, 188-193.
- Ravikumar, B., Duden, R., and Rubinsztein, D.C. (2002). Aggregate-prone proteins with polyglutamine and polyalanine expansions are degraded by autophagy. *Hum Mol Genet* 11, 1107-1117.
- Ravikumar, B., Moreau, K., Jahreiss, L., Puri, C., and Rubinsztein, D.C. (2010a). Plasma membrane contributes to the formation of pre-autophagosomal structures. *Nat Cell Biol* 12, 747-757.
- Ravikumar, B., Sarkar, S., Davies, J.E., Futter, M., Garcia-Arencibia, M., Green-Thompson, Z.W., Jimenez-Sanchez, M., Korolchuk, V.I., Lichtenberg, M., Luo, S., *et al.* (2010b). Regulation of mammalian autophagy in physiology and pathophysiology. *Physiological reviews* 90, 1383-1435.
- Ravikumar, B., Vacher, C., Berger, Z., Davies, J.E., Luo, S., Oroz, L.G., Scaravilli, F., Easton, D.F., Duden, R., and O'Kane, C.J. (2004a). Inhibition of mTOR induces autophagy and reduces toxicity of polyglutamine expansions in fly and mouse models of Huntington disease. *Nature genetics* 36, 585.
- Ravikumar, B., Vacher, C., Berger, Z., Davies, J.E., Luo, S., Oroz, L.G., Scaravilli, F., Easton, D.F., Duden, R., O'Kane, C.J., *et al.* (2004b). Inhibition of mTOR induces autophagy and reduces toxicity

- of polyglutamine expansions in fly and mouse models of Huntington disease. *Nature genetics* 36, 585-595.
- Riess, O., Rub, U., Pastore, A., Bauer, P., and Schols, L. (2008). SCA3: neurological features, pathogenesis and animal models. *Cerebellum* 7, 125-137.
- Roberts, Z.J., Better, M., Bot, A., Roberts, M.R., and Ribas, A. (2018). Axicabtagene ciloleucel, a first-in-class CAR T cell therapy for aggressive NHL. *Leuk Lymphoma* 59, 1785-1796.
- Roche, P.A., and Furuta, K. (2015). The ins and outs of MHC class II-mediated antigen processing and presentation. *Nat Rev Immunol* 15, 203-216.
- Roczniak-Ferguson, A., Petit, C.S., Froehlich, F., Qian, S., Ky, J., Angarola, B., Walther, T.C., and Ferguson, S.M. (2012). The transcription factor TFEB links mTORC1 signaling to transcriptional control of lysosome homeostasis. *Science signaling* 5, ra42.
- Roessler, S., Long, E.L., Budhu, A., Chen, Y., Zhao, X., Ji, J., Walker, R., Jia, H.L., Ye, Q.H., Qin, L.X., *et al.* (2012). Integrative genomic identification of genes on 8p associated with hepatocellular carcinoma progression and patient survival. *Gastroenterology* 142, 957-966.e912.
- Rothe, K., Porter, V., and Jiang, X. (2019). Current Outlook on Autophagy in Human Leukemia: Foe in Cancer Stem Cells and Drug Resistance, Friend in New Therapeutic Interventions. *Int J Mol Sci* 20.
- Rubinsztein, D.C. (2006). The roles of intracellular protein-degradation pathways in neurodegeneration. *Nature* 443, 780-786.
- Rubinsztein, D.C. (2012). Autophagy—alias self-eating—appetite and ageing. *EMBO reports* 13, 173-174.
- Rubinsztein, D.C., Codogno, P., and Levine, B. (2012). Autophagy modulation as a potential therapeutic target for diverse diseases. *Nature Reviews Drug Discovery* 11, 709-U784.
- Ruggeri, L., Capanni, M., Urbani, E., Perruccio, K., Shlomchik, W.D., Tosti, A., Posati, S., Rogaia, D., Frassoni, F., Aversa, F., *et al.* (2002). Effectiveness of donor natural killer cell alloreactivity in mismatched hematopoietic transplants. *Science* 295, 2097-2100.
- Rui, Y.N., Xu, Z., Patel, B., Chen, Z., Chen, D., Tito, A., David, G., Sun, Y., Stimming, E.F., Bellen, H.J., *et al.* (2015). Huntingtin functions as a scaffold for selective macroautophagy. *Nature cell biology* 17, 262-275.
- Ryu, D., Mouchiroud, L., Andreux, P.A., Katsyuba, E., Moullan, N., Nicolet-Dit-Felix, A.A., Williams, E.G., Jha, P., Lo Sasso, G., Huzard, D., *et al.* (2016). Urolithin A induces mitophagy and prolongs lifespan in *C. elegans* and increases muscle function in rodents. *Nature medicine* 22, 879-888.
- Sardiello, M., Palmieri, M., di Ronza, A., Medina, D.L., Valenza, M., Gennarino, V.A., Di Malta, C., Donaudo, F., Embrione, V., Polishchuk, R.S., *et al.* (2009). A gene network regulating lysosomal biogenesis and function. *Science* 325, 473-477.
- Sarkar, S., Korolchuk, V.I., Renna, M., Imarisio, S., Fleming, A., Williams, A., Garcia-Arencibia, M., Rose, C., Luo, S., Underwood, B.R., *et al.* (2011). Complex inhibitory effects of nitric oxide on autophagy. *Mol Cell* 43, 19-32.
- Sarpal, R., Yan, V., Kazakova, L., Sheppard, L., Yu, J.C., Fernandez-Gonzalez, R., and Tepass, U. (2019). Role of alpha-Catenin and its mechanosensing properties in regulating Hippo/YAP-dependent tissue growth. *PLoS Genet* 15, e1008454.
- Schiavi, A., Maglioni, S., Palikaras, K., Shaik, A., Strappazzon, F., Brinkmann, V., Torgovnick, A., Castelein, N., De Henau, S., Braeckman, B.P., *et al.* (2015). Iron-Starvation-Induced Mitophagy Mediates Lifespan Extension upon Mitochondrial Stress in *C. elegans*. *Current biology : CB* 25, 1810-1822.
- Schlegelmilch, K., Mohseni, M., Kirak, O., Pruszk, J., Rodriguez, J.R., Zhou, D., Kreger, B.T., Vasioukhin, V., Avruch, J., Brummelkamp, T.R., *et al.* (2011). Yap1 acts downstream of alpha-catenin to control epidermal proliferation. *Cell* 144, 782-795.
- Settembre, C., Di Malta, C., Polito, V.A., Garcia Arcencibia, M., Vetrini, F., Erdin, S., Erdin, S.U., Huynh, T., Medina, D., Colella, P., *et al.* (2011). TFEB links autophagy to lysosomal biogenesis. *Science* 332, 1429-1433.
- Settembre, C., Zoncu, R., Medina, D.L., Vetrini, F., Erdin, S., Erdin, S., Huynh, T., Ferron, M., Karsenty, G., Vellard, M.C., *et al.* (2012). A lysosome-to-nucleus signalling mechanism senses and regulates the lysosome via mTOR and TFEB. *The EMBO journal* 31, 1095-1108.

- Shibata, M., Lu, T., Furuya, T., Degterev, A., Mizushima, N., Yoshimori, T., MacDonald, M., Yankner, B., and Yuan, J. (2006). Regulation of intracellular accumulation of mutant Huntingtin by Beclin 1. *J Biol Chem* *281*, 14474-14485.
- Shitara, K., Matsuo, K., Yokota, T., Takahari, D., Shibata, T., Ura, T., Inaba, Y., Yamaura, H., Sato, Y., Najima, M., *et al.* (2011). Prognostic factors for metastatic colorectal cancer patients undergoing irinotecan-based second-line chemotherapy. *Gastrointest Cancer Res* *4*, 168-172.
- Siegel, R., Desantis, C., and Jemal, A. (2014). Colorectal cancer statistics, 2014. *CA Cancer J Clin* *64*, 104-117.
- Sillen, M., and Declerck, P.J. (2021). A Narrative Review on Plasminogen Activator Inhibitor-1 and Its (Patho)Physiological Role: To Target or Not to Target? *Int J Mol Sci* *22*.
- Simonsen, A., Cumming, R.C., Brech, A., Isakson, P., Schubert, D.R., and Finley, K.D. (2008). Promoting basal levels of autophagy in the nervous system enhances longevity and oxidant resistance in adult *Drosophila*. *Autophagy* *4*, 176-184.
- Singh, B.N., Kumar, D., Shankar, S., and Srivastava, R.K. (2012). Rottlerin induces autophagy which leads to apoptotic cell death through inhibition of PI3K/Akt/mTOR pathway in human pancreatic cancer stem cells. *Biochem Pharmacol* *84*, 1154-1163.
- Singh, R., and Cuervo, A.M. (2011). Autophagy in the cellular energetic balance. *Cell Metab* *13*, 495-504.
- Son, S.M., Park, S.J., Fernandez-Estevez, M., and Rubinsztein, D.C. (2021). Autophagy regulation by acetylation-implications for neurodegenerative diseases. *Exp Mol Med* *53*, 30-41.
- Son, S.M., Park, S.J., Lee, H., Siddiqi, F., Lee, J.E., Menzies, F.M., and Rubinsztein, D.C. (2019). Leucine Signals to mTORC1 via Its Metabolite Acetyl-Coenzyme A. *Cell Metab* *29*, 192-201 e197.
- Son, S.M., Park, S.J., Stamatakou, E., Vicinanza, M., Menzies, F.M., and Rubinsztein, D.C. (2020). Leucine regulates autophagy via acetylation of the mTORC1 component raptor. *Nat Commun* *11*, 3148.
- Song, Q., Mao, B., Cheng, J., Gao, Y., Jiang, K., Chen, J., Yuan, Z., and Meng, S. (2015). YAP enhances autophagic flux to promote breast cancer cell survival in response to nutrient deprivation. *PLoS one* *10*, e0120790.
- Soucek, L., Lawlor, E.R., Soto, D., Shchors, K., Swigart, L.B., and Evan, G.I. (2007). Mast cells are required for angiogenesis and macroscopic expansion of Myc-induced pancreatic islet tumors. *Nature medicine* *13*, 1211-1218.
- Sparmann, A., and Bar-Sagi, D. (2004). Ras-induced interleukin-8 expression plays a critical role in tumor growth and angiogenesis. *Cancer Cell* *6*, 447-458.
- Sridhar, S., Botbol, Y., Macian, F., and Cuervo, A.M. (2012). Autophagy and disease: always two sides to a problem. *The Journal of pathology* *226*, 255-273.
- Stabile, H., Fionda, C., Gismondi, A., and Santoni, A. (2017). Role of Distinct Natural Killer Cell Subsets in Anticancer Response. *Front Immunol* *8*, 293.
- Stadhouders, R., Fillion, G.J., and Graf, T. (2019). Transcription factors and 3D genome conformation in cell-fate decisions. *Nature* *569*, 345-354.
- Stolz, A., Ernst, A., and Dikic, I. (2014). Cargo recognition and trafficking in selective autophagy. *Nat Cell Biol* *16*, 495-501.
- Su, N., Wang, P., and Li, Y. (2016). Role of Wnt/beta-catenin pathway in inducing autophagy and apoptosis in multiple myeloma cells. *Oncol Lett* *12*, 4623-4629.
- Sun, N., Youle, R.J., and Finkel, T. (2016). The Mitochondrial Basis of Aging. *Molecular cell* *61*, 654-666.
- Sun, X., and Tang, D. (2014). HMGB1-dependent and -independent autophagy. *Autophagy* *10*, 1873-1876.
- Sun, Y., Xiong, L., Wang, X., Wang, L., Chen, B., Huang, J., Huang, M., Chen, J., Wu, J., Huang, S., *et al.* (2021). Autophagy inhibition attenuates TGF-beta2-induced epithelial-mesenchymal transition in lens epithelial cells. *Life Sci* *265*, 118741.
- Tagliamento, M., Frelaut, M., Baldini, C., Naigeon, M., Nencioni, A., Chaput, N., and Besse, B. (2022). The use of immunotherapy in older patients with advanced non-small cell lung cancer. *Cancer treatment reviews* *106*, 102394.
- Talati, C., and Sweet, K. (2018). Recently approved therapies in acute myeloid leukemia: A complex treatment landscape. *Leuk Res* *73*, 58-66.

- Tamura, H., Dan, K., Tamada, K., Nakamura, K., Shioi, Y., Hyodo, H., Wang, S.D., Dong, H.D., Chen, L.P., and Ogata, K. (2005). Expression of functional B7-H2 and B7.2 costimulatory molecules and their prognostic implications in de novo acute myeloid leukemia. *Clinical Cancer Research* *11*, 5708-5717.
- Tanaka, H., Takahashi, K., Yamaguchi, K., Kontani, K., Motoki, T., Asakura, M., Kosaka, S., Yokomise, H., and Houchi, H. (2018). Hypertension and Proteinuria as Predictive Factors of Effects of Bevacizumab on Advanced Breast Cancer in Japan. *Biol Pharm Bull* *41*, 644-648.
- Tang, D., Kang, R., Livesey, K.M., Cheh, C.W., Farkas, A., Loughran, P., Hoppe, G., Bianchi, M.E., Tracey, K.J., Zeh, H.J., 3rd, *et al.* (2010). Endogenous HMGB1 regulates autophagy. *J Cell Biol* *190*, 881-892.
- Taniguchi, K., Wu, L.W., Grivennikov, S.I., de Jong, P.R., Lian, I., Yu, F.X., Wang, K., Ho, S.B., Boland, B.S., Chang, J.T., *et al.* (2015). A gp130-Src-YAP module links inflammation to epithelial regeneration. *Nature* *519*, 57-62.
- Tassa, A., Roux, M.P., Attaix, D., and Bechet, D.M. (2003). Class III phosphoinositide 3-kinase--Beclin1 complex mediates the amino acid-dependent regulation of autophagy in C2C12 myotubes. *The Biochemical journal* *376*, 577-586.
- Tavassoly, I., Parmar, J., Shajahan-Haq, A.N., Clarke, R., Baumann, W.T., and Tyson, J.J. (2015). Dynamic Modeling of the Interaction Between Autophagy and Apoptosis in Mammalian Cells. *CPT Pharmacometrics Syst Pharmacol* *4*, 263-272.
- Team, R.C. (2020). R: A language and environment for statistical computing. (R Foundation for Statistical Computing.).
- Tefferi, A., and Vardiman, J.W. (2009). Myelodysplastic syndromes. *N Engl J Med* *361*, 1872-1885.
- Terman, A. (1995). The effect of age on formation and elimination of autophagic vacuoles in mouse hepatocytes. *Gerontology* *41 Suppl 2*, 319-326.
- Thompson, R.H., Gillett, M.D., Chevillat, J.C., Lohse, C.M., Dong, H., Webster, W.S., Chen, L., Zinke, H., Blute, M.L., Leibovich, B.C., *et al.* (2005). Costimulatory molecule B7-H1 in primary and metastatic clear cell renal cell carcinoma. *Cancer* *104*, 2084-2091.
- Thorsson, V., Gibbs, D.L., Brown, S.D., Wolf, D., Bortone, D.S., Ou Yang, T.H., Porta-Pardo, E., Gao, G.F., Plaisier, C.L., Eddy, J.A., *et al.* (2018). The Immune Landscape of Cancer. *Immunity* *48*, 812-830 e814.
- Toit, A.D., Loos, B., and Hofmeyr, J.H.S. (2020). Supply and Demand Analysis of Autophagy. *Methods Mol Biol* *2088*, 345-357.
- Tomaszewska, A., Rustecka, A., Lipinska-Opalka, A., Piprek, R.P., Kloc, M., Kalicki, B., and Kubiak, J.Z. (2022). The Role of Vitamin D in COVID-19 and the Impact of Pandemic Restrictions on Vitamin D Blood Content. *Front Pharmacol* *13*, 836738.
- Tonon, F., Di Bella, S., Giudici, F., Zerbato, V., Segat, L., Koncan, R., Misin, A., Toffoli, B., D'Agaro, P., Luzzati, R., *et al.* (2022). Discriminatory Value of Adiponectin to Leptin Ratio for COVID-19 Pneumonia. *Int J Endocrinol* *2022*, 9908450.
- Topp, M.S., Gokbuget, N., Zugmaier, G., Klappers, P., Stelljes, M., Neumann, S., Viardot, A., Marks, R., Diedrich, H., Faul, C., *et al.* (2014). Phase II trial of the anti-CD19 bispecific T cell-engager blinatumomab shows hematologic and molecular remissions in patients with relapsed or refractory B-precursor acute lymphoblastic leukemia. *J Clin Oncol* *32*, 4134-4140.
- Totaro, A., Panciera, T., and Piccolo, S. (2018). YAP/TAZ upstream signals and downstream responses. *Nature cell biology* *20*, 888-899.
- Totaro, A., Zhuang, Q., Panciera, T., Battilana, G., Azzolin, L., Brumana, G., Gandin, A., Brusatin, G., Cordenonsi, M., and Piccolo, S. (2019). Cell phenotypic plasticity requires autophagic flux driven by YAP/TAZ mechanotransduction. *Proceedings of the National Academy of Sciences of the United States of America* *116*, 17848-17857.
- Trettel, F., Rigamonti, D., Hilditch-Maguire, P., Wheeler, V.C., Sharp, A.H., Persichetti, F., Cattaneo, E., and MacDonald, M.E. (2000). Dominant phenotypes produced by the HD mutation in STHdh(Q111) striatal cells. *Human molecular genetics* *9*, 2799-2809.
- Trofin, F., Dorneanu, O.S., Constantinescu, D., Nastase, E.V., Lunca, C., Iancu, L.S., Andrioaie, I.M., Duhaniuc, A., Cianga, C.M., Pavel-Tanasa, M., *et al.* (2022). Cytokines and Chemokines in Breastmilk of SARS-CoV-2 Infected or COVID-19 Vaccinated Mothers. *Vaccines (Basel)* *10*.

- Trottier, Y., Cancel, G., An-Gourfinkel, I., Lutz, Y., Weber, C., Brice, A., Hirsch, E., and Mandel, J.L. (1998). Heterogeneous intracellular localization and expression of ataxin-3. *Neurobiology of disease* 5, 335-347.
- Tsatsanis, C., Zacharioudaki, V., Androulidaki, A., Dermitzaki, E., Charalampopoulos, I., Minas, V., Gravanis, A., and Margioris, A.N. (2005). Adiponectin induces TNF-alpha and IL-6 in macrophages and promotes tolerance to itself and other pro-inflammatory stimuli. *Biochemical and biophysical research communications* 335, 1254-1263.
- Tsuboi, Y., Kurimoto, M., Nagai, S., Hayakawa, Y., Kamiyama, H., Hayashi, N., Kitajima, I., and Endo, S. (2009). Induction of autophagic cell death and radiosensitization by the pharmacological inhibition of nuclear factor-kappa B activation in human glioma cell lines. *J Neurosurg* 110, 594-604.
- Tsukamoto, S., Kuma, A., Murakami, M., Kishi, C., Yamamoto, A., and Mizushima, N. (2008). Autophagy is essential for preimplantation development of mouse embryos. *Science* 321, 117-120.
- Tumaneng, K., Schlegelmilch, K., Russell, R.C., Yimlamai, D., Basnet, H., Mahadevan, N., Fitamant, J., Bardeesy, N., Camargo, F.D., and Guan, K.L. (2012). YAP mediates crosstalk between the Hippo and PI(3)K-TOR pathways by suppressing PTEN via miR-29. *Nature cell biology* 14, 1322-1329.
- Tut, G., Lancaster, T., Sylla, P., Butler, M.S., Kaur, N., Spalkova, E., Bentley, C., Amin, U., Jadir, A., Hulme, S., *et al.* (2022). Antibody and cellular immune responses following dual COVID-19 vaccination within infection-naïve residents of long-term care facilities: an observational cohort study. *Lancet Healthy Longev* 3, e461-e469.
- Tyagi, A., Ly, S., El-Dana, F., Yuan, B., Jaggupilli, A., Grimm, S., Konopleva, M., Buhring, H.J., and Battula, V.L. (2022). Evidence supporting a role for the immune checkpoint protein B7-H3 in NK cell-mediated cytotoxicity against AML. *Blood* 139, 2782-2796.
- Uckun, F.M., Lin, T.L., Mims, A.S., Patel, P., Lee, C., Shahidzadeh, A., Shami, P.J., Cull, E., Cogle, C.R., and Watts, J. (2021). A Clinical Phase 1B Study of the CD3xCD123 Bispecific Antibody APVO436 in Patients with Relapsed/Refractory Acute Myeloid Leukemia or Myelodysplastic Syndrome. *Cancers (Basel)* 13.
- Unanue, E.R., Turk, V., and Neefjes, J. (2016). Variations in MHC Class II Antigen Processing and Presentation in Health and Disease. *Annu Rev Immunol* 34, 265-297.
- Valentini, V., van Stiphout, R.G., Lammering, G., Gambacorta, M.A., Barba, M.C., Bebenek, M., Bonnetain, F., Bosset, J.F., Bujko, K., Cionini, L., *et al.* (2011). Nomograms for predicting local recurrence, distant metastases, and overall survival for patients with locally advanced rectal cancer on the basis of European randomized clinical trials. *J Clin Oncol* 29, 3163-3172.
- Van Cutsem, E., Cervantes, A., Nordlinger, B., Arnold, D., and Group, E.G.W. (2014). Metastatic colorectal cancer: ESMO Clinical Practice Guidelines for diagnosis, treatment and follow-up. *Ann Oncol* 25 Suppl 3, iii1-9.
- van den Ancker, W., van Luijn, M.M., Chamuleau, M.E., Kelder, A., Feller, N., Terwijn, M., Zevenbergen, A., Schuurhuis, G.J., van Ham, S.M., Westers, T.M., *et al.* (2014). High class II-associated invariant chain peptide expression on residual leukemic cells is associated with increased relapse risk in acute myeloid leukemia. *Leuk Res* 38, 691-693.
- van Dongen, J.J., Lhermitte, L., Bottcher, S., Almeida, J., van der Velden, V.H., Flores-Montero, J., Rawstron, A., Asnafi, V., Lecomte, Q., Lucio, P., *et al.* (2012). EuroFlow antibody panels for standardized n-dimensional flow cytometric immunophenotyping of normal, reactive and malignant leukocytes. *Leukemia* 26, 1908-1975.
- van Luijn, M.M., Chamuleau, M.E., Ossenkuppele, G.J., van de Loosdrecht, A.A., and Marieke van Ham, S. (2012). Tumor immune escape in acute myeloid leukemia: Class II-associated invariant chain peptide expression as result of deficient antigen presentation. *Oncoimmunology* 1, 211-213.
- van Luijn, M.M., Chamuleau, M.E., Rensing, M.E., Wiertz, E.J., Ostrand-Rosenberg, S., Souwer, Y., Zevenbergen, A., Ossenkuppele, G.J., van de Loosdrecht, A.A., and van Ham, S.M. (2010a). Alternative Ii-independent antigen-processing pathway in leukemic blasts involves TAP-dependent peptide loading of HLA class II complexes. *Cancer Immunol Immunother* 59, 1825-1838.
- van Luijn, M.M., Chamuleau, M.E., Thompson, J.A., Ostrand-Rosenberg, S., Westers, T.M., Souwer, Y., Ossenkuppele, G.J., van Ham, S.M., and van de Loosdrecht, A.A. (2010b). Class II-associated invariant chain peptide down-modulation enhances the immunogenicity of myeloid leukemic blasts resulting in increased CD4+ T-cell responses. *Haematologica* 95, 485-493.

- van Luijn, M.M., van den Ancker, W., Chamuleau, M.E., Zevenbergen, A., Westers, T.M., Ossenkoppele, G.J., van Ham, S.M., and van de Loosdrecht, A.A. (2011). Absence of class II-associated invariant chain peptide on leukemic blasts of patients promotes activation of autologous leukemia-reactive CD4⁺ T cells. *Cancer research* *71*, 2507-2517.
- van Luijn, M.M., van den Ancker, W., van Ham, S.M., and van de Loosdrecht, A.A. (2014). Class II-associated invariant chain peptide as predictive immune marker in minimal residual disease in acute myeloid leukemia. *Oncoimmunology* *3*.
- Varelas, X. (2014). The Hippo pathway effectors TAZ and YAP in development, homeostasis and disease. *Development* *141*, 1614-1626.
- Velikkakath, A.K., Nishimura, T., Oita, E., Ishihara, N., and Mizushima, N. (2012). Mammalian Atg2 proteins are essential for autophagosome formation and important for regulation of size and distribution of lipid droplets. *Molecular biology of the cell* *23*, 896-909.
- Verzella, D., Pescatore, A., Capece, D., Vecchiotti, D., Ursini, M.V., Franzoso, G., Alesse, E., and Zazzeroni, F. (2020). Life, death, and autophagy in cancer: NF-kappaB turns up everywhere. *Cell Death Dis* *11*, 210.
- Vicinanza, M., Korolchuk, V.I., Ashkenazi, A., Puri, C., Menzies, F.M., Clarke, J.H., and Rubinsztein, D.C. (2015). PI(5)P regulates autophagosome biogenesis. *Molecular cell* *57*, 219-234.
- Vilchez, D., Saez, I., and Dillin, A. (2014). The role of protein clearance mechanisms in organismal ageing and age-related diseases. *Nat Commun* *5*, 5659.
- Vite, A., Zhang, C., Yi, R., Emms, S., and Radice, G.L. (2018). alpha-Catenin-dependent cytoskeletal tension controls Yap activity in the heart. *Development* *145*.
- Wajnberg, A., Amanat, F., Firpo, A., Altman, D.R., Bailey, M.J., Mansour, M., McMahon, M., Meade, P., Mendu, D.R., Muellers, K., *et al.* (2020). Robust neutralizing antibodies to SARS-CoV-2 infection persist for months. *Science* *370*, 1227-1230.
- Wan, Z., Zhang, S., Fan, Y., Liu, K., Du, F., Davey, A.M., Zhang, H., Han, W., Xiong, C., and Liu, W. (2013). B cell activation is regulated by the stiffness properties of the substrate presenting the antigens. *Journal of immunology* *190*, 4661-4675.
- Wang, C.Y., Mayo, M.W., Korneluk, R.G., Goeddel, D.V., and Baldwin, A.S., Jr. (1998). NF-kappaB antiapoptosis: induction of TRAF1 and TRAF2 and c-IAP1 and c-IAP2 to suppress caspase-8 activation. *Science* *281*, 1680-1683.
- Wang, N., Feng, Y., Zhu, M., Siu, F.M., Ng, K.M., and Che, C.M. (2013). A novel mechanism of XIAP degradation induced by timosaponin AIII in hepatocellular carcinoma. *Biochimica et biophysica acta* *1833*, 2890-2899.
- Wang, P., Gong, Y., Guo, T., Li, M., Fang, L., Yin, S., Kamran, M., Liu, Y., Xu, J., Xu, L., *et al.* (2019). Activation of Aurora A kinase increases YAP stability via blockage of autophagy. *Cell Death Dis* *10*, 432.
- Wang, R.C., Wei, Y., An, Z., Zou, Z., Xiao, G., Bhagat, G., White, M., Reichelt, J., and Levine, B. (2012a). Akt-mediated regulation of autophagy and tumorigenesis through Beclin 1 phosphorylation. *Science* *338*, 956-959.
- Wang, R.F. (2001). The role of MHC class II-restricted tumor antigens and CD4⁺ T cells in antitumor immunity. *Trends Immunol* *22*, 269-276.
- Wang, W., Huang, J., and Chen, J. (2011). Angiotensin-like proteins associate with and negatively regulate YAP1. *J Biol Chem* *286*, 4364-4370.
- Wang, Y.J., Yang, T.Y., Ma, Y.G., Halade, G.V., Zhang, J.Q., Lindsey, M.L., and Jin, Y.F. (2012b). Mathematical modeling and stability analysis of macrophage activation in left ventricular remodeling post-myocardial infarction. *Bmc Genomics* *13*.
- Wani, W.Y., Boyer-Guittaut, M., Dodson, M., Chatham, J., Darley-Usmar, V., and Zhang, J. (2015). Regulation of autophagy by protein post-translational modification. *Laboratory investigation; a journal of technical methods and pathology* *95*, 14-25.
- Webb, J.L., Ravikumar, B., Atkins, J., Skepper, J.N., and Rubinsztein, D.C. (2003). Alpha-Synuclein is degraded by both autophagy and the proteasome. *J Biol Chem* *278*, 25009-25013.
- Weidberg, H., Shvets, E., and Elazar, Z. (2011). Biogenesis and cargo selectivity of autophagosomes. *Annual review of biochemistry* *80*, 125-156.
- Weir, E.K., Thenappan, T., Bhargava, M., and Chen, Y. (2020). Does vitamin D deficiency increase the severity of COVID-19? *Clin Med (Lond)* *20*, e107-e108.

- Welch, S., Spithoff, K., Rumble, R.B., Maroun, J., and Gastrointestinal Cancer Disease Site, G. (2010). Bevacizumab combined with chemotherapy for patients with advanced colorectal cancer: a systematic review. *Ann Oncol* 21, 1152-1162.
- Wen, X., and Klionsky, D.J. (2019). At a Glance: A History of Autophagy and Cancer. *Semin Cancer Biol.*
- West, N.R., McCuaig, S., Franchini, F., and Powrie, F. (2015). Emerging cytokine networks in colorectal cancer. *Nat Rev Immunol* 15, 615-629.
- White, E. (2012). Deconvoluting the context-dependent role for autophagy in cancer. *Nature Reviews Cancer* 12, 401-410.
- White, E. (2015). The role for autophagy in cancer. *J Clin Invest* 125, 42-46.
- Whiteway, A., Corbett, T., Anderson, R., Macdonald, I., and Prentice, H.G. (2003). Expression of co-stimulatory molecules on acute myeloid leukaemia blasts may effect duration of first remission. *British journal of haematology* 120, 442-451.
- Wilhelm, T., Byrne, J., Medina, R., Kolundzic, E., Geisinger, J., Hajduskova, M., Tursun, B., and Richly, H. (2017). Neuronal inhibition of the autophagy nucleation complex extends life span in post-reproductive *C. elegans*. *Genes & development* 31, 1561-1572.
- Williams, P., Basu, S., Garcia-Manero, G., Hourigan, C.S., Oetjen, K.A., Cortes, J.E., Ravandi, F., Jabbour, E.J., Al-Hamal, Z., Konopleva, M., *et al.* (2019). The distribution of T-cell subsets and the expression of immune checkpoint receptors and ligands in patients with newly diagnosed and relapsed acute myeloid leukemia. *Cancer* 125, 1470-1481.
- Winslow, A.R., and Rubinsztein, D.C. (2008). Autophagy in neurodegeneration and development. *Biochim Biophys Acta* 1782, 723-729.
- Winslow, A.R., and Rubinsztein, D.C. (2011). The Parkinson disease protein α -synuclein inhibits autophagy. *Autophagy* 7, 429-431.
- Wolf, A.M., Wolf, D., Rumpold, H., Enrich, B., and Tilg, H. (2004). Adiponectin induces the anti-inflammatory cytokines IL-10 and IL-1RA in human leukocytes. *Biochemical and biophysical research communications* 323, 630-635.
- Wong, S.Q., Kumar, A.V., Mills, J., and Lapierre, L.R. (2020). Autophagy in aging and longevity. *Hum Genet* 139, 277-290.
- Wu, X., Fleming, A., Ricketts, T., Pavel, M., Virgin, H., Menzies, F.M., and Rubinsztein, D.C. (2016). Autophagy regulates Notch degradation and modulates stem cell development and neurogenesis. *Nature communications* 7, 10533.
- Wulster-Radcliffe, M.C., Ajuwon, K.M., Wang, J., Christian, J.A., and Spurlock, M.E. (2004). Adiponectin differentially regulates cytokines in porcine macrophages. *Biochemical and biophysical research communications* 316, 924-929.
- Xie, Y., Kang, R., Sun, X., Zhong, M., Huang, J., Klionsky, D.J., and Tang, D. (2015). Posttranslational modification of autophagy-related proteins in macroautophagy. *Autophagy* 11, 28-45.
- Xie, Z., and Klionsky, D.J. (2007). Autophagosome formation: core machinery and adaptations. *Nature cell biology* 9, 1102-1109.
- Xu, L., Zhang, Y., Luo, G., and Li, Y. (2015). The roles of stem cell memory T cells in hematological malignancies. *J Hematol Oncol* 8, 113.
- Xu, Y., Xia, X., and Pan, H. (2013). Active autophagy in the tumor microenvironment: A novel mechanism for cancer metastasis. *Oncol Lett* 5, 411-416.
- Yadav, T., Quivy, J.P., and Almouzni, G. (2018). Chromatin plasticity: A versatile landscape that underlies cell fate and identity. *Science* 361, 1332-1336.
- Yamamoto, A., Tagawa, Y., Yoshimori, T., Moriyama, Y., Masaki, R., and Tashiro, Y. (1998). Bafilomycin A1 prevents maturation of autophagic vacuoles by inhibiting fusion between autophagosomes and lysosomes in rat hepatoma cell line, H-4-II-E cells. *Cell structure and function* 23, 33-42.
- Ye, Y., Tan, S., Zhou, X., Li, X., Jundt, M.C., Lichter, N., Hidebrand, A., Dhasarathy, A., and Wu, M. (2015). Inhibition of p-IkappaBalpha Ubiquitylation by Autophagy-Related Gene 7 to Regulate Inflammatory Responses to Bacterial Infection. *J Infect Dis* 212, 1816-1826.
- Young, A.R., Chan, E.Y., Hu, X.W., Kochl, R., Crawshaw, S.G., High, S., Hailey, D.W., Lippincott-Schwartz, J., and Tooze, S.A. (2006). Starvation and ULK1-dependent cycling of mammalian Atg9 between the TGN and endosomes. *J Cell Sci* 119, 3888-3900.

- Young, M.D., Mitchell, T.J., Vieira Braga, F.A., Tran, M.G.B., Stewart, B.J., Ferdinand, J.R., Collord, G., Botting, R.A., Popescu, D.M., Loudon, K.W., *et al.* (2018). Single-cell transcriptomes from human kidneys reveal the cellular identity of renal tumors. *Science* 361, 594-599.
- Yu, F.X., Zhao, B., and Guan, K.L. (2015). Hippo Pathway in Organ Size Control, Tissue Homeostasis, and Cancer. *Cell* 163, 811-828.
- Yu, N., Li, X., Song, W., Li, D., Yu, D., Zeng, X., Li, M., Leng, X., and Li, X. (2012). CD4(+)CD25(+)CD127 (low/-) T cells: a more specific Treg population in human peripheral blood. *Inflammation* 35, 1773-1780.
- Yuan, P., Hu, Q., He, X., Long, Y., Song, X., Wu, F., He, Y., and Zhou, X. (2020). Laminar flow inhibits the Hippo/YAP pathway via autophagy and SIRT1-mediated deacetylation against atherosclerosis. *Cell Death Dis* 11, 141.
- Zahavi, D., and Weiner, L. (2020). Monoclonal Antibodies in Cancer Therapy. *Antibodies (Basel)* 9.
- Zelaya, H., Alvarez, S., Kitazawa, H., and Villena, J. (2016). Respiratory Antiviral Immunity and Immunobiotics: Beneficial Effects on Inflammation-Coagulation Interaction during Influenza Virus Infection. *Front Immunol* 7, 633.
- Zhang, L., Chen, X., Liu, X., Kline, D.E., Teague, R.M., Gajewski, T.F., and Kline, J. (2013). CD40 ligation reverses T cell tolerance in acute myeloid leukemia. *J Clin Invest* 123, 1999-2010.
- Zhang, Q., Bastard, P., Liu, Z., Le Pen, J., Moncada-Velez, M., Chen, J., Ogishi, M., Sabli, I.K.D., Hodeib, S., Korol, C., *et al.* (2020a). Inborn errors of type I IFN immunity in patients with life-threatening COVID-19. *Science* 370.
- Zhang, X., Qiao, Y., Wu, Q., Chen, Y., Zou, S., Liu, X., Zhu, G., Zhao, Y., Chen, Y., Yu, Y., *et al.* (2017). The essential role of YAP O-GlcNAcylation in high-glucose-stimulated liver tumorigenesis. *Nat Commun* 8, 15280.
- Zhang, Z.L., Hou, Y.L., Li, D.T., and Li, F.Z. (2020b). Laboratory findings of COVID-19: a systematic review and meta-analysis. *Scand J Clin Lab Invest* 80, 441-447.
- Zhao, B., Li, L., Lu, Q., Wang, L.H., Liu, C.Y., Lei, Q., and Guan, K.L. (2011). Angiomotin is a novel Hippo pathway component that inhibits YAP oncoprotein. *Genes & development* 25, 51-63.
- Zhao, B., Wei, X., Li, W., Udan, R.S., Yang, Q., Kim, J., Xie, J., Ikenoue, T., Yu, J., Li, L., *et al.* (2007a). Inactivation of YAP oncoprotein by the Hippo pathway is involved in cell contact inhibition and tissue growth control. *Genes & development* 21, 2747-2761.
- Zhao, B., Wei, X., Li, W., Udan, R.S., Yang, Q., Kim, J., Xie, J., Ikenoue, T., Yu, J., Li, L., *et al.* (2007b). Inactivation of YAP oncoprotein by the Hippo pathway is involved in cell contact inhibition and tissue growth control. *Genes & development* 21, 2747-2761.
- Zhao, M., Zhang, Y., Jiang, Y., Wang, K., Wang, X., Zhou, D., Wang, Y., Yu, R., and Zhou, X. (2021). YAP promotes autophagy and progression of gliomas via upregulating HMGB1. *J Exp Clin Cancer Res* 40, 99.
- Zhao, T., Wang, X., Xu, T., Xu, X., and Liu, Z. (2017). Bevacizumab significantly increases the risks of hypertension and proteinuria in cancer patients: A systematic review and comprehensive meta-analysis. *Oncotarget* 8, 51492-51506.
- Zhong, C., and Zhu, J. (2017). Transcriptional regulators dictate innate lymphoid cell fates. *Protein Cell* 8, 242-254.
- Zhu, X., Wu, S., Dahut, W.L., and Parikh, C.R. (2007). Risks of proteinuria and hypertension with bevacizumab, an antibody against vascular endothelial growth factor: systematic review and meta-analysis. *Am J Kidney Dis* 49, 186-193.